Universitat
de les Illes Balears

DOCTORAL THESIS

2021

SEDIMENT FINGERPRINTING AND HYDRO-SEDIMENTARY MONITORING AS TOOLS FOR CATCHMENT MANAGEMENT IN MEDITERRANEAN ENVIRONMENTS

Julián García Comendador

Universitat
de les Illes Balears

MEDhyCON
Mediterranean Ecogeomorphological and Hydrological Connectivity Research Team

DOCTORAL THESIS

2021

Doctoral Programme of History, History of Art and Geography

SEDIMENT FINGERPRINTING AND HYDRO-SEDIMENTARY MONITORING AS TOOLS FOR CATCHMENT MANAGEMENT IN MEDITERRANEAN ENVIRONMENTS

Julián García Comendador

Supervisor and Tutor: Dr. Joan Estrany Bertos

Co-supervisor: Dr. Núria Martínez Carreras

Doctor by the Universitat de les Illes Balears

Note:

This file contains scientific articles that have been revised and modified according to the comments made by recognized referees. Despite some slight modifications have been made in order to correct spelling or other small errors, as well as to homogenise the style of the text and the numbering of tables and figures, no changes have been made to the published contents and results.

Agradecimientos:

Hace diez años era una persona muy diferente a la que soy ahora. Era impresor, oficial offset de 3ª. Mi trayectoria académica había sido un fracaso absoluto, ni me planteaba poner un pie en la universidad. Hoy estoy redactando los agradecimientos de mi tesis doctoral, mi tesis doctoral. Esta tesis es el reflejo de más de diez años de cambios drásticos en mi vida.

Quiero agradecerle a mi director de tesis, Joan Estrany, su confianza en mí. El darme la oportunidad de vivir una aventura de semejante envergadura. Enseñarme qué es la ciencia, el valor del esfuerzo y que el trabajo bien hecho es una recompensa en sí mismo. Empecé a trabajar contigo como alumno colaborador en 2012. Desde entonces han pasado 9 años geniales. He podido viajar por el mundo, exponer en congresos, publicar en revistas científicas, trabajar en el Atlas, la inundación de Sant Llorenç des Cardassar, el incendio de Andratx, he impartido clases en la universidad y, finalmente, redactado una tesis. Por todo ello, muchísimas gracias Joan.

Agradecer Núria Martínez Carreras, mi codirectora de tesis, su esfuerzo, dedicación y paciencia. Me acogiste en Luxemburgo y me enseñaste una manera muy diferente de trabajar. Ir siempre un poco más allá, la relevancia de la reflexión antes de escribir la primera línea, el cómo plantearse preguntas clave y como plasmar ideas en papel. Muchísimas gracias Núria.

Quiero extender los agradecimientos a todos los que me han acompañado o apoyado durante este viaje. A Josep Fortesa, Aleix Calsamiglia y Jaume Company. Hemos compartido muchísimas horas en el despacho y el campo. Tengo muchos momentos grabados en la memoria, instalando sondas, recogiendo muestras, saltado vallas, metiéndonos en los torrentes, empujando el todoterreno... No me olvidaré nunca de nuestras surrealistas aventuras en Tánger, las asistencias a congresos, vuelos de drone y cafés en el bar. Ha sido un placer estar a vuestro lado. También a todos los miembros y colaboradores del equipo MEDhyCON, Tomeu Alorda, Maurici Ruíz, Xurxo Gago, José A. López Tarazón, Adolfo Calvo Cases, Bartomeu Sastre, Hannane Reddad, Manuel E. Lucas Borja, Laura Ferrer, Jérôme Latron, Monserrat Ferrer, Raquel Vaquer y Miquel Tomàs. Muchas gracias.

Gracias también a los miembros del Laboratorio de Radiología Ambiental de la UIB. Toni Borràs, Edwin Palacio y de nuevo Laura Ferrer por su trabajo imprescindible para esta tesis y su amabilidad. A Joana María Petrus por sus consejos y asesoramiento. A todo el equipo del Catchment and Eco-Hydrology Research Group (CAT) del Luxembourg Institute of Science and Technology (LIST) por acogerme y permitirme usar sus instalaciones. A los miembros del Laboratorio de Paisaje y Geografía Física de la Université Sultan Moulay Slimane, gracias Hanane Reddad, Hassan Ouakhir, Nadia Ennaji, Abdelatif Essanbri y Mohamed Kharize, gracias.

Gracias a mis amigos, especialmente a los que me han acompañado en tantas horas de ensayo y conciertos. Ha sido mi terapia psicológica durante todos estos años. Gracias Albert, Javi, Narci, Chano, Miki, Alex, Sanse, Edu y Cardo. Nos queda aún mucho rock and roll. Gracias a Alex Molins, Albert Santos Y Marina Torrens por los buenos momentos que hemos pasado todos estos años.

Muchísimas gracias a Narcís Rodrígez y a Alexandre Coll por el diseño y collage de la portada.

Finalmente, quiero agradecerle de todo corazón a mi pareja su confianza, sus constantes palabras de ánimo y por supuesto su paciencia durante la etapa de doctorado. Susana Soto, sin tu apoyo y consejo nunca habría llegado hasta aquí. Por supuesto también a nuestros hijos, Marc y Ariadna, por hacerme la persona más feliz del mundo. Os quiero.

Funding of the thesis

This thesis was supported through the pre-doctoral contract (FPU15/05239) funded by the Spanish Ministry of Education and Vocational Training and by the research project CGL2017-88200-R "Functional hydrological and sediment connectivity at Mediterranean catchments: global change scenarios –MEDhyCON2" funded by the Spanish Ministry of Science and Innovation, the Spanish Agency of Research (AEI) and the European Regional Development Funds (ERDF).

Thesis as compendium of research papers

Published:

García-Comendador, J., Fortesa, J., Calsamiglia, A., Calvo-Cases, A., Estrany, J. 2017. Post-fire hydrological response and suspended sediment transport of a terraced Mediterranean catchment. Earth Surf. Process. Landforms, 42: 2254– 2265. doi: 10.1002/esp.4181.

García-Comendador, J., Fortesa, J., Calsamiglia, A., Garcias, F., Estrany, J. 2017. Source ascription in bed sediments of a Mediterranean temporary stream after the first post-fire flush. J Soils Sediments 17, 2582–2595. doi: 10.1007/s11368-017-1806-1.

García-Comendador, J., Martínez-Carreras, N., Fortesa, J., Borràs, A., Calsamiglia, A., Estrany, J. 2020. Analysis of post-fire suspended sediment sources by using colour parameters. Geoderma, 379, 114638. doi: 10.1016/j.geoderma.2020.114638.

Unpublished:

García-Comendador, J., Martínez-Carreras, N., Fortesa, J., Company, J., Borràs, A., Estrany, J. 2021. Combining sediment fingerprinting and hydro-sedimentary monitoring to assess suspended sediment provenance in a mid-mountainous Mediterranean catchment. Journal of Environmental Management. **Under review**.

Preliminary results:

In-channel alterations of the most common soil properties used as tracers in sediment fingerprinting studies. **Paper in preparation**.

Contents

List of figures

List of tables

List of acronyms

AR1d - One-day

AR3d - Three days antecedent rainfall

AR7d - Seven days antecedent rainfall

BNDVI - Blue Normalized Difference Vegetation Index

CV - Coefficient of variation

DEM - Digital Elevation Model

DFA - Discriminant Function Analysis

dNBR - differenced Normalized Burn Ratio

DOD - DEM of Difference

DS - Downstream Site

DTM - Digital Terrain Model

EMMA - End Member Mixing Models

FRNs - Fallout Radionuclides

GOF – Goodness of Fit

I30 – Rainfall intensity in 30 minutes

IPmax-30 - Maximum rainfall intensity in 30 min

LFF - Large Forest Fires

LIST - Luxembourg Institute of Science and Technology

Load - Total sediment load

nRMSE - normalized Root Mean Square Error

P.tot - Total rainfall

PCA - Principal Component Analysis

PSD - Particle Size Distribution

Q - Stream discharge

Qmax - Maximum discharge peak

Qmean - average discharge

Rtot – Total rainfall

SfM - Structure from Motion

SS - Suspended Sediment

SS peak - Maximum Sediment Concentration

SSA – Specific Surface Area

SSC - Suspended Sediment Concentrations

SSCmax - Maximum suspended sediment concentration

SSCmean - Mean suspended sediment concentration

SSload - Total suspended sediment load

US - Upstream Site

Wvol - Total water volume

Abstract

Soil erosion is a natural process that encompasses weathering, transport and deposition of soil particles. These processes are essential in terrestrial geochemical cycles. However, the on- and off-site erosion effects are considered to be one of the most important causes of terrestrial and aquatic ecosystems degradation. The characteristics of the Mediterranean region are marked by complex relationships between natural, human, biotic and abiotic variables. In addition, an irregular rainfall distribution, strong seasonality and the physiographic landscape characteristics promote divergent responses in erosion rates and sediment yields. In this context, the Mediterranean basin has the highest sediment yields in all of Europe. In addition, it is emerging as a hot spot point in Global Change dynamics, especially with reference to climate and land use change, which could generate an increase in erosive and sediment transport processes. At the catchment scale, sediment transfer occurs in hill slopes, between hill slopes and channels or within channels. Information on the nature and relative contribution of sediment sources is a key aspect with regard to designing and implementing erosion control strategies in catchments.

The main objective of this thesis is to identify erosion and sediment transport processes in two Mediterranean catchments affected by different global change processes at different spatio-temporal scales, improving current techniques for sediment origin determination (i.e., reducing uncertainties, time and cost) so it can better implemented in catchment management plans. For this purpose, the hydro-sedimentary dynamics and the origin of the sediments has been investigated on the island of Mallorca (Spain), in two small catchments; the Sa Font de la Vila catchment - 4.8 km^2, affected by wildfires - and the Es Fangar catchment (3.4 km^2), affected by land use changes. The combination of sediment fingerprinting and hydro-sedimentary monitoring made it possible to assess its hydro-sedimentary dynamics during the study period. In Sa Font de la Vila, results showed a gradual decrease in contribution from burned sources over time, while in Es Fangar the contributions from crops dominated throughout the study period, without substantial changes. Sediment yields were 6.3 t km^2 yr^{-1} and 4.5 t km^2 yr^{-1} for Sa Font de la Vila and Es Fangar respectively, low results in comparison with other Mediterranean catchments. This was mainly attributed to the calcareous lithology, land uses (in Es Fangar catchment), vegetation recovery (in Sa Font de la Vila catchment) and agricultural terraces.

The use of soil colour parameters as tracers was successfully evaluated in the two catchments, confirming its suitability as a fast and inexpensive tracer, even in fire-affected catchments. Furthermore, the strong correlations between the measurements made with a spectro-radiometer and a scanner make colour even more accessible for its implementation in catchment management plans. The experiment on tracer conservatism confirmed that in-channel changes suffered by all the analysed tracers (coefficient of variation $\bar{x}$ 8.1 ± 8.8%) were generally lower than their spatial variability within the catchment (coefficient of variation $\bar{x}$ 16.3 ± 18.5%). Furthermore, the colour parameters were the least variable tracers (i.e. the most conservative). with a coefficient of variation of 2.6 ± 2.2%.

Finally, it was not possible to identify the activation patterns of different sediment sources combining hydro-sedimentary monitoring and sediment fingerprinting. This was probably caused by Es Fangar's catchment stability in terms of the origin of the suspended sediment. Es Fangar catchment sediment source stability is attributed to lithological characteristics, land uses and the presence of agricultural terraces in the study area. However, events of higher magnitude could exceed the sedimentary (dis)connectivity thresholds of the rest of the sources, promoting a sediment cascade effect.

The results presented in this thesis are relevant and represent an advance in the optimization of the sediment fingerprinting technique. Despite some limitations that need to be further investigated, hydro-sedimentary monitoring and sediment fingerprinting used in combination was shown to be very useful for integrated catchment management plans in Mediterranean environments.

Key words: Sediment fingerprinting, Mediterranean catchments, hydro-sedimentary monitoring, catchment management.

Resumen

La erosión es un proceso natural que comprende la meteorización, transporte y depósito de partículas del suelo. Estos procesos son esenciales dentro de los ciclos geoquímicos terrestres. Sin embargo, los efectos *in situ* y *ex situ* de la erosión se consideran una de las causas más importantes de la degradación de la calidad en ecosistemas terrestres y acuáticos. Las características de la región mediterránea están marcadas por relaciones complejas entre variables naturales, humanas, bióticas y abióticas. Además, una distribución irregular de las lluvias, una marcada estacionalidad y las características fisiográficas del paisaje promueven respuestas divergentes en las tasas de erosión y producción de sedimentos. En este contexto, la cuenca Mediterránea presenta los rendimientos de sedimento más altos de toda Europa. Además, se perfila como un punto crítico de la dinámica del Cambio Global, especialmente en lo que respecta al Cambio Climático y de uso del suelo, lo que podría generar un aumento de los procesos erosivos y de transporte de sedimento. A escala de cuenca de drenaje, la transferencia de sedimentos ocurre en laderas, entre laderas y canales o dentro de canales. La información sobre la naturaleza y contribución relativa de las fuentes de sedimento es un aspecto clave para diseñar e implementar estrategias de control de la erosión en cuencas de drenaje.

El objetivo principal de esta tesis es identificar procesos de erosión y transporte de sedimentos en dos cuencas mediterráneas afectadas por diferentes procesos de cambio global a diferentes escalas espacio-temporales, mejorando las técnicas actuales para la determinación del origen de los sedimentos (es decir, reducir incertidumbres, tiempo y costo) para su mejor implementación en planes de gestión de cuencas de drenaje. Para ello, se investigó la dinámica hidro-sedimentaria y el origen de los sedimentos en dos pequeñas cuencas de drenaje de la isla de Mallorca (España); Sa Font de la Vila -4,8 km^2, afectada por incendios forestales - y Es Fangar (3,4 km^2), afectada por cambios de usos del suelo. La combinación de la técnica sediment fingerprinting y monitoreo hidro-sedimentario continuo permitió evaluar su dinámica hidro-sedimentaria durante el período de estudio. En Sa Font de la Vila, los resultados mostraron una disminución paulatina de las aportaciones de fuentes quemadas a lo largo del tiempo, mientras que en Es Fangar las aportaciones de las zonas de cultivos dominaron durante todo el período de estudio sin cambios sustanciales. Los rendimientos de sedimentos fueron 6,3 t km^2 a^{-1} y 4,5 t km^2 a^{-1} para Sa Font de la Vila y Es Fangar respectivamente, bajos en comparación con otras cuencas mediterráneas. Esto se atribuyó principalmente a la litología calcárea de las cuencas, los usos del suelo (en Es Fangar), la recuperación de la vegetación (en Sa Font de la Vila) y la presencia de terrazas agrícolas.

El uso de parámetros de color como trazadores se evaluó con éxito en las dos cuencas, lo que confirma su idoneidad para su uso como un trazador rápido y económico, incluso en cuencas afectadas por incendios. Además, las fuertes correlaciones entre las medidas tomadas con un espectro-radiómetro y un escáner, hacen del color un trazador muy accesible para su implementación en planes gestión. El experimento sobre conservación de las propiedades de los trazadores mostró variaciones bajas en la mayoría de los trazadores analizados (coeficiente de variación $\bar{x}$ 8,1 ± 8,8%). Estas fueron generalmente menores que su propia variabilidad espacial dentro de la cuenca

(coeficiente de variación $\bar{x}$ 16,3 ± 18,5%). Además, los parámetros de color fueron los trazadores menos variables (i.e. más conservadores) con un coeficiente de variación de 2,6 ± 2,2%.

Finalmente, no fue posible identificar los patrones de activación de diferentes fuentes de sedimentos combinando el monitoreo hidro-sedimentario y sediment fingerprinting. Esto fue causado principalmente por la estabilidad de la cuenca de Es Fangar en términos de origen de sedimentos en suspensión. La estabilidad de las fuentes de sedimentos se atribuyó a las características litológicas, usos del suelo y la presencia de terrazas agrícolas en el área de estudio. Sin embargo, eventos de mayor magnitud podrían superar los umbrales de (des)conectividad sedimentaria del resto de fuentes consideradas y activarlas.

Los resultados que presenta esta tesis son relevantes y suponen un avance en la optimización de la técnica sediment fingerprinting. Pese a algunas limitaciones que se han de seguir investigando, se demostró que la combinación de monitoreo hidro-sedimentario y sediment fingerprinting es de gran utilidad para los planes de gestión integrada de cuencas de drenaje Mediterráneas.

Palabras clave: Sediment fingerprinting, Cuencas mediterráneas, monitoreo hidro-sedimentario, Gestión de cuencas de drenaje.

Resum

L'erosió és un procés natural que comprèn la meteorització, transport i dipòsit de partícules sòl. Aquests processos són essencials dins dels cicles geoquímics terrestres. No obstant això, els efectes *in situ* i *ex situ* de l'erosió es consideren una de les causes més importants de la degradació de la qualitat en ecosistemes terrestres i aquàtics. Les característiques de la regió mediterrània estan marcades per relacions complexes entre variables naturals, humanes, biòtiques i abiòtiques. A més, una distribució irregular de les pluges, una marcada estacionalitat i les característiques fisiogràfiques del paisatge promouen respostes divergents en les taxes d'erosió i la producció de sediments. En aquest context, la conca Mediterrània presenta els rendiments de sediment més alts de tot Europa. A més, es perfila com un punt crític de la dinàmica del Canvi Global, especialment pel que fa a el Canvi Climàtic i usos del sòl, la qual cosa podria generar un augment dels processos erosius i de transport de sediment. A escala de conca de drenatge, la transferència de sediments es dona en vessants, entre vessants i canals o dins els canals. La informació sobre la naturalesa i contribució relativa de les fonts de sediment és un aspecte clau per dissenyar i implementar estratègies de control de l'erosió en conques de drenatge.

L'objectiu principal d'aquesta tesi és identificar processos d'erosió i transport de sediments en dues conques mediterrànies afectades per diferents processos de Canvi Global a diferents escales espai-temporals, millorant les tècniques actuals per a la determinació de l'origen dels sediments (és a dir, reduir incerteses, temps i cost) per a la seva millor implementació en plans de gestió de conques de drenatge. Per a això, es va investigar la dinàmica hidro-sedimentària i l'origen dels sediments en dos petites conques de drenatge de l'illa de Mallorca (Espanya); Sa Font de la Vila -4,8 km^2, afectada per incendis forestals - i Es Fangar (3,4 km^2), afectada per canvis d'usos del sòl. La combinació de la tècnica sediment fingerprinting i monitoratge hidro-sedimentari va permetre avaluar la seva dinàmica hidro-sedimentària durant el període d'estudi. A Sa Font de la Vila, els resultats van mostrar una disminució gradual de les aportacions de fonts cremades al llarg del temps, mentre que a Es Fangar les aportacions de fonts de cultius van dominar durant tot el període d'estudi sense canvis substancials. Els rendiments de sediments van ser 6,3 t km^2 a^{-1} i 4,5 t km^2 a^{-1} per a Sa Font de la Vila i Es Fangar respectivament, baixos en comparació amb altres conques mediterrànies. Això es va atribuir principalment a la litologia calcària de les conques hidrogràfiques, els usos de terra (a Es Fangar), la recuperació de la vegetació (a Sa Font de la Vila) i la presència de terrasses agrícoles.

L'ús de paràmetres de color com a traçadors es va avaluar amb èxit en les dues conques, la qual cosa confirma la seva idoneïtat per al seu ús com un traçador ràpid i econòmic, fins i tot en conques afectades per incendis. A més, les fortes correlacions entre les mesures preses amb un espectre-radiòmetre i un escàner, fan del color un traçador molt accessible per a la seva implementació en plans gestió. L'experiment sobre conservació de les propietats dels traçadors, va mostrar variacions baixes en la majoria dels traçadors analitzats (coeficient de variació $\bar{x}$ 8,1 ± 8,8%). Aquestes van ser generalment menors que la seva pròpia variabilitat espacial dins de la conca (coeficient de variació $\bar{x}$ 16,3 ± 18,5%). A més, els paràmetres de color van ser els traçadors menys variables (i.e. més conservadors) amb un coeficient de variació de 2,6 ± 2,2%.

Finalment, no va ser possible identificar els patrons d'activació de diferents fonts de sediments combinant el monitoratge hidro-sedimentari i sediment fingerprinting. Això va ser causa principalment a l'estabilitat de la conca d'Es Fangar en termes d'origen de sediments en suspensió. L'estabilitat de les fonts de sediments s'atribueix a les característiques litològiques, usos de sòl i la presència de terrasses agrícoles en l'àrea d'estudi. No obstant això, esdeveniments de major magnitud podrien superar els llindars de (des)connectivitat sedimentària de la resta de fonts considerades i activar-les.

Els resultats que presenta aquesta tesi són rellevants i suposen un avanç en l'optimització de la tècnica sediment fingerprinting. Malgrat algunes limitacions que s'han de seguir investigant, es va demostrar que la combinació de monitorització hidro-sedimentari i sediment fingerprinting és de gran utilitat per als plans de gestió integrada de conques de drenatge Mediterrànies.

Paraules clau: Sediment fingerprinting, conques mediterrànies, monitorització hidro-sedimentària, gestió de conques de drenatge.

1. Introduction

1.1. Soil erosion and sediment transport processes in drainage catchments

Soil erosion is a natural process that encompasses the detachment, transport and deposition of soil particles driven by a specific force (i.e. water, wind, etc.). Thus, soil erosion plays a key role in the geological cycle (e.g. Garrels and Mackenzie, 1971; Wold and Hay, 1990), terrestrial geochemical cycles (e.g. Berhe et al., 2007; López-Bermúdez, 1990; Ludwig and Probst, 1996), aquatic ecosystems (e.g. Kjelland et al., 2015; Newcombe and Macdonald, 1991) as well as coastal areas and delta evolution (e.g. McLaughlin et al., 2003). However, erosion on-site effects are considered to be one of the most significant causes of soil quality degradation in natural, agricultural, and forest ecosystems and, therefore, in crop yield reduction (Pimentel and Kounang, 1998). Erosion global predictions, based in high spatial resolution Revised Universal Soil Loss Equation (RUSLE)-based semi-empirical modelling approach (GloSEM), determined global erosion in potential soil erosion rates of $43^{+9.2}_{-7}$ Pg yr^{-1} for 2015 (Borrelli et al., 2020). In addition, climatic predictions indicate an evolution of the hydrological cycle that can promote an increase of global water erosion processes around 30 to 66% (Borrelli et al., 2020). These trends in terrestrial systems, combined with an accelerated population growth, point erosion as a serious worldwide environmental and a human health issue (Pimentel, 2006).

The term Catchment is used in British English as a synonym for a river basin, whereas watershed is more associated with the line dividing two river basins. Therefore, a catchment is a topographical unit delimited by drainage divide watershed that isolates a stream system. All the surface area of a catchment drains to the same point, and it works as a "*hydrological response unit, a biophysical unit, and a holistic ecosystem in terms of the materials, energy, and information that flow through it*" (Wang et al., 2016). Drainage catchments integrate all aspects of the hydrological cycle as well as erosion and sediment transport processes from sources to sinks within a defined area (Sivapalan, 2005). Therefore, catchments are the fundamental landscape unit when it

comes to the study of the cycling of water, sediments, and dissolved geochemical and biogeochemical constituents.

The sediment connectivity concept was defined by Bracken et al. (2015) as "*the connected transfer of sediment from a source to a sink in a system via sediment detachment and sediment transport, which is controlled by how the sediment moves between all geomorphic zones: on hill slopes, between hill slopes and channels and within channels*". Sediment connectivity is ruled by catchment structural features (i.e. structural connectivity), determined by its physical characteristics (e.g. morphology) and functional features, related with how the structural features interact through runoff processes (e.g. runoff generation, sediment transference between catchment compartments; i.e. functional connectivity) (Bracken et al., 2015; Najafi et al., 2021; Turnbull et al., 2008; Wainwright et al., 2011). Structural connectivity can be assessed by applying contiguity indexes, as indices of connectivity (e.g. Borselli et al., 2008; Cavalli et al., 2013; Heckmann et al., 2018). However, functional connectivity (or process-based connectivity; Bracken et al., 2015) is generally more difficult to measure (Calsamiglia et al., 2020; Wainwright et al., 2011). The complexity of the latter lies in the fact that it is dependent on the characteristics of the processes that connect the different structural catchment units, and therefore, on the magnitude of the events and their spatio-temporal distribution. An effective hillslope-to-channel connectivity generates a transference of eroded soil particles to the river network, introducing sediment into the river system. Size, mass and shape of the sediment particles, in combination with flow characteristics determine its transport. Within the channel system, coarse sediment particles (i.e. boulders to sand fraction) are transported in the lower part of the water column through rolling or saltation mechanisms, whereas, finer fractions (i.e. clay and silt) and dissolved sediment are transported in suspension within the turbulent flow (Hjulström, 1936). Fluxes altered by fine sediment particles transported downstream might modify physical, chemical and biotic processes in water bodies as, for example, altering light penetration and temperature, inducing siltation processes or increasing concentrations of nutrient, heavy metals or pesticides (Bilotta and Brazier, 2008; Collins and Walling, 2007). Similarly, altered fluxes can negatively affect aquatic ecosystems status (Newcombe and Macdonald, 1991; Verkaik

et al., 2013), water quality (Horowitz et al., 2007), induce dam siltation and reduce the capacity of water reservoirs (Navas et al., 2004; Vörösmarty et al., 2003).

It is estimated that 95% of the sediment reaching oceans is transported by rivers (Syvitski, 2003) and suspended sediment equals 70% of the of the total sediment load (Morgan, 2005). Suspended sediment in many rivers normally encompass <2 mm fraction, with most of the load being <63 µm (Droppo, 2001; Phillips and Walling, 1995; Walling et al., 2000; Walling and Moorehead, 1989). The latest fraction (i.e. <63 µm) is considered the most chemically active component of the whole solid load (Foster and Charlesworth, 1996; Horowitz et al., 1993). In addition, suspended sediment is mainly transported in aggregate/flocculate form (Droppo et al., 1997; Droppo and Ongley, 1994). Flocs represent a complex interaction between water, inorganic particles, organic particles and pores that can exhibit heterogeneous behaviour. Therefore, flocculation, with autonomous and interactive physical, chemical and biological complex reactions, has significant implications for sediment and sediment-associated contaminants transport (Droppo, 2001). Accordingly, increase in the knowledge related to the fine sediment transportation related processes is essential to the overall understanding of sediment transport and its consequences, and therefore, to attempts to mitigate the negative effects derived therefrom.

Catchment sediment yield (t km^{-2} yr^{-1}) is "the integrated result of all erosion and sediment transporting processes operating in a catchment" (Vanmaercke et al., 2011b). However, the extrapolation of soil erosion rates to catchment sediment yields does not accurately represent the complexity and spatial variations between upstream erosive processes and sediment mobilization through hillslopes and channels (de Vente et al., 2007; Vanmaercke et al., 2011a; Walling, 1983). The difficulties of linking on-site erosion processes with sediment loss through catchment outlet was defined by Walling (1983) as the sediment delivery problem. Only a fraction of the upstream reaches the outlet in sediment form.

The sediment delivery ratio, is the proportion of sediment that reaches the catchment outlet (sediment yield) in relation to the quantified erosion within the catchment (gross erosion; t km^2 yr^{-1}) (de Vente et al., 2007; Maner, 1958; Walling, 1983) as:

$$Sediment\ delivery\ ratio = \frac{Sediment\ yield}{Gross\ erosion}$$

Nevertheless, the nature of the catchment, i.e. sediment source location, topographical features, channel condition and drainage patterns, vegetation type status, land use and soil texture influence the sediment delivery ratio. The influence differs for every individual catchment and results in temporal discontinuity and spatial heterogeneity in sediment transfer, generating discrepancies between the amount of soil eroded and exported at the catchment outlet. This in turn hinders the conception of a simple relationship between sediment yield and gross erosion, because the spatial and temporal lumping and its black box nature prevent the generation of generally applicable predictive rules (Walling, 1983). Technical advances (e.g. sediment tracing, connectivity indexes) in the study of geomorphological processes made possible a better understanding of source-sink relationships, the role of catchment configuration and the influence of natural (e.g. vegetation, soil texture) and human (e.g. agricultural terraces, land uses) features. For instance, sediment tracing techniques (e.g. sediment fingerprinting) and soil redistribution investigations using environmental radionuclides (e.g. ^{137}Cs, $^{210}Pb_{ex}$ and ^{7}Be) used in combination with traditional hydro-sedimentary monitoring can be used to establish integrated sediment budgets (Collins et al., 2001; Navas et al., 2014; Porto et al., 2011; Walling, 1999; Walling and Collins, 2008).

Integrated sediment budgets are represented in the form of flow diagrams that represent the eroded input/output of sediment from different defined catchment compartments to try to elucidate where the sediment is coming from, its transport pathways and transported and stored storage zones (e.g. Dietrich and Dunne, 1978; Estrany et al., 2012; Slaymaker, 2003). River systems act as “jerky conveyor belts” (Ferguson, 1981), where sediment transfer from sources to sinks is irregular over time and space. Sediment may be lost and stored in a sink or new eroded sediment may be

added to the transfer process. The sediment budget construction requires a deep understanding of the four main parts of the conveyor belt: (1) sediment delivered from sources, (2) entrainment at critical shear stress, (3) transport downstream, and (4) deposition in temporary or permanent sinks (Fryirs, 2013). However, although integrated sediment budgets have been proved useful to understand erosion/deposition dynamics within catchments, they also have some limitations, as the temporal and spatial lumping of sediments (Fryirs, 2013; Walling, 1983). In a nutshell, the temporal lumping problem refers to the time resolution of the sediment balance. If the sediment budget is constructed using a long time period dataset, results integrating sediment delivery processes occurred during different events of different magnitude. It is thus not possible to elucidate if the activation of sediment transfer within a catchment is associated with low frequency and high magnitude rainfall events that cause huge erosive processes (e.g. rill gully erosion) or by lower magnitude rain events with a lesser energy processes but continuous, i.e. sheet erosion. Conversely, spatial lumping refers to the fact that total erosion and storage processes are expressed using a single number (i.e. the sediment delivery ratio). Hence, sediment budgets do not account for spatial heterogeneity in a catchment's physical configuration, which results in significantly different sediment delivery responses within a catchment (i.e. inputs, outputs and storage). Therefore, each sediment source has a unique delivery potential, and its position relative to the channel and catchment division determines the probability that the sediment contained by a specific source will be delivered to the river system.

In this context, different sediment sources within a catchment can be activated depending on predominant hydro-sedimentary drivers (Misset et al., 2019). For example, channel actuates as the main sediment source in a catchment when slope-to-channel connectivity is not effective. The reactivation of fine sediment deposited in riverbeds, sediment bars or channel banks is governed by flow rate, shear stress, or stream power (Park and Hunt, 2017). Conversely, sediment transfer can also control erosion processes on catchment hillslopes. The precipitation intensity, runoff, or mass movements drive its effectiveness. However, vegetation changes, mass movements, sediment supply exhaustion or human disturbances (e.g. check dams, agricultural

terraces) can drastically alter sediment origin (Belmont et al., 2011; Grabowski and Gurnell, 2016; Vanmaercke et al., 2017).

Identification of dominant sediment sources, quantification of their relative contributions to suspended sediment loads, as well as the determination of the resistance thresholds on the driving forces that activate them, can be an essential part of assessing the factors controlling suspended sediment transport as a surrogate of erosion problems in river catchments.

1.2. Sediment delivery in Mediterranean catchments

In Europe, crop yield reduction caused by soil erosion is estimated as non-significant in global terms (Bakker et al., 2007). However, results presented considerable spatial variability between northern and southern Europe, the Mediterranean Region being considered as the most vulnerable area (Bakker et al., 2007). The Mediterranean Region has unique characteristics worldwide, strongly marked by complex relationships between natural and human, biotic and abiotic variables (Wainwright, 2009). An irregular distribution of rainfall and the hot and dry character of summers, in combination with lithological, and physiographic characteristics promote divergent responses in erosion rates and sediment yields over time and space (García-Ruiz et al., 2013; Kosmas et al., 1997; Peña-Angulo et al., 2019). In this context, a compilation of sediment yield data from 1,794 different locations throughout Europe showed that ca. 85% of the data from the Mediterranean region exceeded 40 t km^{-2} yr^{-1}, and more than 50% exceeded 200 t km^{-2} yr^{-1}, these being the highest rates in Europe together with those of mountainous areas (Vanmaercke et al., 2011b).

The Mediterranean region has been singled out as a hotspot of Global Change dynamics, especially referring to the climate and land-use change (Gates and Ließ, 2001; Paeth et al., 2017). Climate change and land-use change are stated to be the major potential drivers of erosion processes through a more intense hydrological cycle (Borrelli et al., 2020; Luetzenburg et al., 2020; O'Neal et al., 2005). Climate projections for southern Europe predict decreases in rainfall amounts, in combination with rising temperatures and high intensity rainfall episodes (Giorgi and Lionello, 2008; Stojković

et al., 2014). It is estimated that rainfall erosivity is more closely related to rainfall intensity than to rainfall volume (Borrelli et al., 2020). A change in rainfall amounts, combined with dryer conditions and an increase of the intermittency and magnitude of rainfall episodes and floods associated can eventually disturb ecosystem equilibrium. As a result, geomorphological cycles could be altered, probably increasing erosive and land degradation processes (Favis-Mortlock and Guerra, 1999; Olesen and Bindi, 2002). As a result of depth economic changes, land cover changes in Mediterranean Europe are marked principally by a dichotomous increase of urban and forested areas (Catalán et al., 2008; Gates and Ließ, 2001; Pons and Rullan, 2014; Tomaz et al., 2013). Urbanization results in a reduction of soil permeability, often resulting in increased runoff ratios, higher discharge peaks and lower lag times (Sala and Inbar, 1992). Conversely, the increase in forest coverage could lead to opposite effects. Forests mainly appeared in abandoned and marginal croplands and agricultural areas, which are more prone to high erosion rates (Poesen and Hooke, 1997; Serrat and Ludwig, 2004). The growth of forest cover generates major soil protection, increasing the infiltration capacity, decreasing surface runoff generation and erosive processes (Hooke, 2006). However, the combination of forest mass growth, rising temperatures, high intensity storms and a lack of forest management can intensify wildfire risk, one of the major causes of erosion and soil degradation in Mediterranean environments (Shakesby, 2011). Denser vegetation cover and fuel accumulation can produce flammable connectivity patches in large areas along the landscapes (Moreira et al., 2011), with higher occurrence risk of Large Forest Fires (i.e. >500 ha) in fire-prone environments. The Mediterranean basin is a fire-prone environment (Pausas et al., 2008), as evidenced by the strong forest fire regime during the mid and late Holocene (Carrión et al., 2003). The climate, characterized by a hot dry summer season, is the main control factor of the pyrogeography of the Mediterranean landscapes. The native vegetation was adapted to a particular fire regime through mechanisms of regrowth and germination (Pausas and Verdú, 2005). Furthermore, some characteristics (e.g. volatile compounds, branch and leaves accumulation) of many Mediterranean pyrophyte species (e.g. *Pinus halepensis*) promote the fast spreading of wildfires to ensure their community permanence against non-adapted species (Pausas and Verdú, 2005).

The complete or partial removal of the vegetation and litter cover cause a reduction in the interception, infiltration, evapotranspiration and sediment trapping. This combined with the alteration of some physicochemical soil properties such as water repellence, structure stability, texture and particle size distribution (Certini, 2005) can disrupt channel-slope connectivity, overland flow generation and sediment yields. Many studies have also documented the increase of overland flow generation in post-fire environments (Cosandey et al., 2005; Ferreira et al., 2005; Scott and Van Wyk, 1990; Stoof et al., 2015). This is caused mainly by the reduction in vegetation cover and the increasing of soil hydrophobicity which drastically reduces the response time during rainfall-runoff events, especially during the first post-fire year (Candela et al., 2005). This scenario, together with a lower aggregate stability, increases the sediment yield in hillslopes, as well as the sediment delivery to, and sediment fluxes within river channels, which can result in irreversible soil degradation.

Under the current context of Global Change, it becomes important to implement catchment management plans so as to protect this vulnerable environment and prevent or diminish modification of its geomorphological cycles. To this end, it is necessary to monitor erosive processes and sediment transport, as well as to detect erosion hotspots.

1.3. Catchment hydro-sedimentary monitoring

Continuous monitoring of water and sediment at catchment scale makes possible the quantification of sediment loads, sediment yields, stationary patterns and assessment flood event response to different driving forces thresholds or natural and human perturbations. At catchment scale, on-site erosion effects have a measurable off-site response (i.e. sediment and water yields). Therefore, reliable long- and short-term data is essential to assess on- and off-site effects of different erosion processes (Phillips, 2010; Walling, 1983).

Traditionally, manual sampling strategies were used to estimate sediment yields. However, continuous electronic monitoring to collect high-resolution and long term data replaced these traditional techniques, allowing a more accurate characterization

of hydro-sedimentary dynamics (Walling, 1988; Wass and Leeks, 1999). The continuous water and sediment monitoring makes possible the analysis of hysteretic patterns in the relationship between discharge (Q) and suspended sediment concentrations (SSC). Hysteresis in geomorphic systems is defined as a loop-like non-linear behaviour where at least two values of a dependent variable are associated with a single value of an independent variable (Phillips, 2003; Zuecco et al., 2016). A non-linear behaviour between Q and SSC is normally related with runoff generation process at hillslope and catchment scales (Camporese et al., 2014; Dooge, 2005). Hysteretic patterns change when a driving variable (e.g. rainfall, soil moisture) exceed a certain threshold. As a result, abrupt changes can occur in a response variable (e.g. Q, SSC) because different hydrological processes may become dominant. Therefore "hysteresis is the dependence of a response variable not only on the current value of a driving variable but on its past history as well" (Camporese et al., 2014). Many works analyse the hysteretic relations between two variables in hydrology: discharge is related with rainfall (e.g. Andermann et al., 2012), groundwater (e.g. Fovet et al., 2015), soil moisture (e.g. Fortesa et al., 2020), solute concentrations (e.g. Burt et al., 2015), water temperature (e.g. Blaen et al., 2012) and suspended sediment concentrations (e.g. Fortesa et al., 2021). Between Q and SSC, hysteretic analysis can reveal different patterns on sediment connectivity, indicating the activation of different catchment compartments and relating it to driving force thresholds. Likewise, changes in sediment sources can be performed in the relationship Q and SSC, providing information about its foreseeable distance from the measurement point according to the rotation direction, the shape of the loop and its area (Williams, 1989). Hysteretic clockwise loops are associated with the activation of sediment sources that are close to the measurement point, while counter-clockwise loops are associated to sediment mobilization from remote sites within a catchment (Giménez et al., 2012; López-Tarazón and Estrany, 2017; Rovira and Batalla, 2006). Several quantitative indexes have been developed to improve hysteretic classification (e.g. Aich et al., 2014; Langlois et al., 2005; Lawler et al., 2006; Lloyd et al., 2016). These indexes provide quantitative data about hysteretic loops features, allowing the comparisons at different spatio-temporal scales, detection in pattern changes, as well as correlation with other hydro-meteorological variables such as rainfall, discharge or suspended

sediment concentration. However, the evaluation of hysteretic behaviour between Q and SSC has been scarcely integrated in catchment management strategies, partially due to the differential relationship between sediment and runoff depending on the scale of study (de Boer and Campbell, 1989) and the difficult interpretation of complex hysteretic loop patterns (Sherriff et al., 2016).

1.4. Sediment source fingerprinting

To reduce the negative on- and off-site effects derived from erosion and sediment transport processes and apply correct management practices, it is necessary to detect erosion hotspots within a catchment. The EU Water Framework Directive (European Community, 2000) developed an implicit assumption about the relevance of sediment monitoring to assess the role of sediments in the ecological status of water bodies (Collins and Anthony, 2008; Perks et al., 2017). Therefore, information on the nature and relative contribution of sediment sources in river systems is emerging as a key aspect when designing and implementing specific erosion control strategies.

A methodology for determining the sediment origin that has become very relevant in the last 20 years is the sediment source fingerprinting approach also known simply as sediment fingerprinting. It has been applied at different temporal scales: from the flood event (Gaspar et al., 2019; Martínez-Carreras et al., 2010b) up to determining the origin of historically deposited sediments (e.g. over the last ca. 100 years; Pulley et al., 2018). The first references using tracers to quantify and model sediment origin in catchments date back to the 1970s (Klages and Hsieh, 1975; Wall and Wilding, 1976; Walling et al., 1979). However, the incorporation of new statistic methodologies, the implementation of un-mixing models to quantify the sediment apportion and the use of new tracers has increased its use, which is reflected in the increasing number of publications every year (Collins et al., 2020; Davis and Fox, 2009; Walling, 2013).

The technique relies on the comparison of different soil properties (i.e. tracers) between samples collected in potential erosion areas and targeted suspended sediment samples collected within the fluvial network (Figure 1.1; Haddadchi et al., 2013; Walling, 2013). In an idealized conceptual framework, (1) soil particles –

comprising potential source areas within a catchment– are detached and transported during rainfall events, (2) the eroded particles are mixed during subsequent transportation to and through the fluvial system, (3) the resultant mixture is transported by rivers in form of sediment load, (4) the soil properties used as sediment tracers reflect the spatio-temporal variations of eroding source sediment contributions and (5) source and sediment tracers can be compared in order to quantitatively estimate the apportionment of sediment provenance. Thus, a required consideration when it comes to correctly apply sediment fingerprinting is that soil and sediment properties used as tracers should be representative of the main erosion sources, must be measurable and remain stable or vary in a predictable way over time and space (Motha et al., 2002).

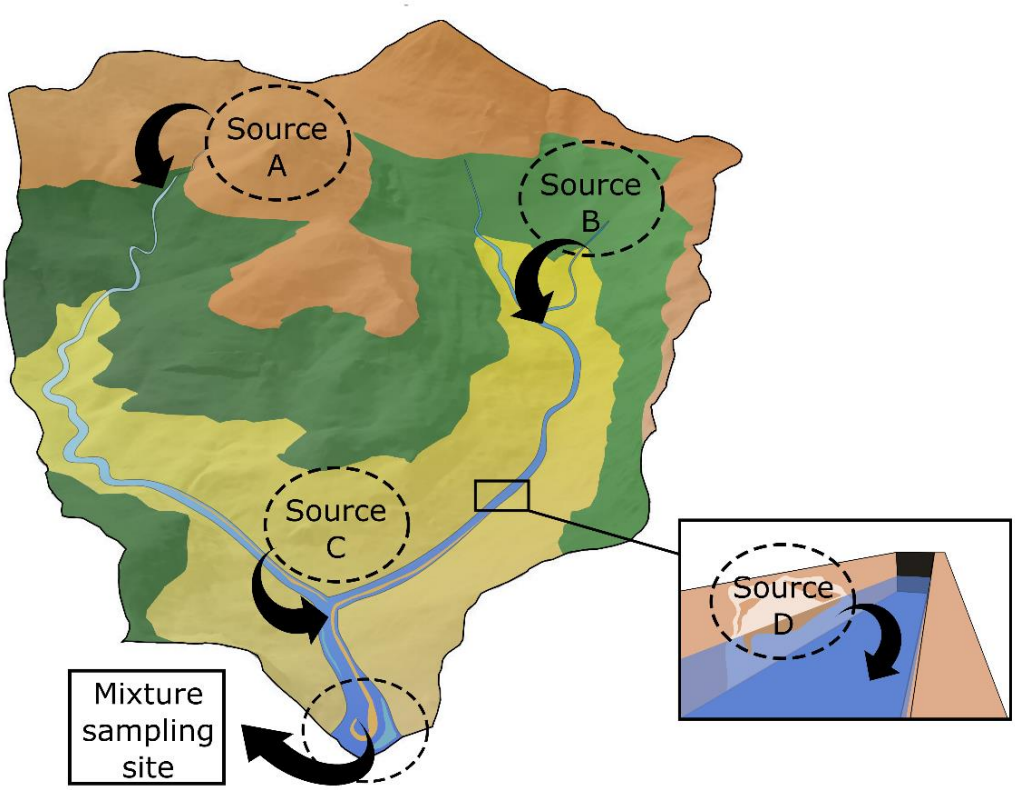

Figure 1.1. A simplified conceptual model of the sediment source fingerprinting technique based in 3 different surface sources (A, B and C; e.g. land uses, lithology) and one subsurface source (D; channel banks).

Tracers can be categorized in three different groups: (1) geochemical (e.g. inorganic elements, radionuclides and mineral magnetism), (2) biochemical (e.g. organic elements, stable isotopes, biomarkers, organic chemicals and DNA) and (3) physical (e.g. spectrometry, particle size characteristic) (Koiter et al., 2013). Therefore, several

properties have been used as sediment tracers (Collins et al., 2017; Haddadchi et al., 2013), including colour parameters (e.g. Barthod et al., 2015; Grimshaw and Lewin, 1980; Martínez-Carreras et al., 2010a), grain size distribution (e.g. Kurashige and Fusejima, 1997; Weltje and Prins, 2007), clay mineralogy (e.g. Eberl, 2004; Gingele and De Deckker, 2005), mineral magnetic properties (e.g. Pulley and Collins, 2018; Yu and Oldfield, 1993), geochemistry (e.g. Chen et al., 2019; Collins and Walling, 2002), fallout radionuclide activities (e.g. Estrany et al., 2016; Evrard et al., 2020; Evrard et al., 2016; Wallbrink and Murray, 1993), cosmogenic radionuclides (e.g. Perg et al., 2003), stable isotopes (e.g. Fox and Papanicolaou, 2008), biomarkers (e.g. Reiffarth et al., 2016), pollen (e.g. Brown, 1985); and enzymatic activity (Nosrati et al., 2011).

In general, there are four key stages in the application of the sediment fingerprinting approach (Figure 1.2). The first step, sampling, encompasses the source classification and the source and design of the sediment sampling strategy (Figure 1.2A). There is no general protocol for soil and sediment sampling. However, a prior knowledge is required of the catchment through field observation, sediment connectivity indexes, interviews with local people or aerial photographs analysis to define erosion problem areas (Koiter et al., 2013; Krause et al., 2003; Paolo et al., 2004; Upadhayay et al., 2020). Source classification is normally done according to spatial provenance (e.g. tributary sub catchments or geological units) or source typology (e.g. surface vs. subsurface sources, land uses) depending on the objectives (Collins et al., 2017). Usually, sediment source sampling is carried out following a stratified strategy in a single field campaign. Here, it is important to collect representative samples of the source groups in areas showing evidence of slope-to-channel connectivity or erosion scars for channel bank sampling. On the other hand, the target sediment sampling for contemporary studies is usually based on suspended sediment (e.g. Navratil et al., 2012) or bed sediment (e.g. Collins and Walling, 2007) sampling. Many methods have been used to collect suspended sediment samples at the catchment outlets. Submersible pumps, auto samplers, portable continuous-flow centrifuge or manual sampling using bottles were the most common for sediment sampling during flood events (Collins et al., 2017; Davis and Fox, 2009). However, in numerous studies (Ankers et al., 2003; Estrany et al., 2016; Evans et al., 2006; Koiter et al., 2013; Laceby

et al., 2015; Martínez-Carreras et al., 2010c) the authors opted to collect time-integrated sediment samples using time-integrated sediment traps (Phillips et al., 2000). For bed sediment sampling, re-suspension techniques were the most common (Duerdoth et al., 2015; Estrany et al., 2011; Lambert and Walling, 1988). Conversely, for long-term scales or historical sediment sampling, authors usually extract sediment cores from depositional zones, floodplains, reservoirs, wetlands or lake deposits (Foster et al., 2006; Li et al., 2020; Miller et al., 2005; Navas et al., 2011; Pulley et al., 2015).

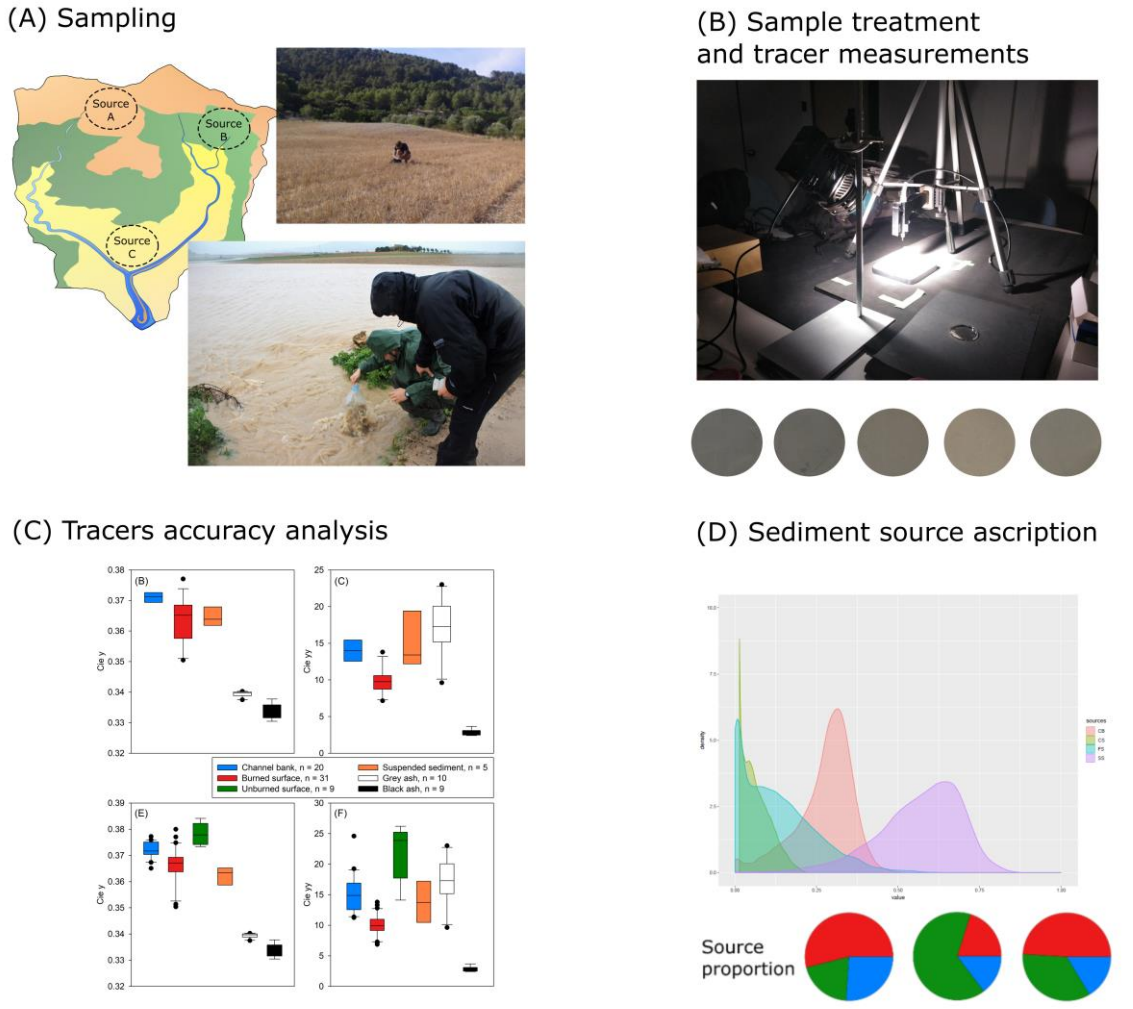

Figure 1.2. General four key steps in the application of sediment source fingerprinting

The second step is the pre-processing of sediment and source samples and tracer measurements (Figure 1.2B). Samples might be treated to eventually solve some issues that influence a tracer's conservativeness (e.g. sieving at different fractions). In this stage, researches largely addressed the influence of particle size and organic matter on

tracer values (e.g. Crockford and Olley, 1998; Hill et al., 1998; Koiter et al., 2018; Laceby et al., 2017). Several ways to address particle size and organic matter differences between sources and sediment are: sieving to a specific size (e.g. He and Walling, 1996), removing the organic content (e.g. Pulley and Rowntree, 2016) and using correction factors (e.g. Collins et al., 1997). However, there may be processes relevant to a tracer's concentration stability that are independent of particle size or organic content, which need to be further investigated. Measurement techniques depend on the budget available and the tracer set selection. Although the technique has evolved with advances in computing technology and the inclusion of new tracers, some of the most used methods are the following: gamma spectrometry to measure fallout radionuclides activity (e.g. Owens and Walling., 1996), microwave digestion coupled with inductively coupled plasma mass spectrometry (ICP-MS) analysis for geochemical elements (e.g. Estrany et al., 2011), magnetic susceptibility sensors for mineral magnetics (e.g. Ramon et al., 2020) and diffuse reflectance spectrometers for colour measurements (e.g. Martínez-Carreras et al., 2010c).

At the third stage, tracer accuracy analysis (Figure 1.2C), is mainly focused on tracer conservative behaviour and its ability to discriminate between source categories. To deal with these two issues, the statistical procedure used most often was described by Collins and Walling (2002). This two-step process involves the performing of a Kruskal-Wallis *H* test to assess if the selected tracers discriminate between the different source categories, and a Discriminant Function Analysis (DFA) so as to select the optimum tracer set. However, other static procedures have been used such as Principal Component Analysis (PCA; e.g. Walling, 2005), the Mann–Whitney *U* test (e.g. Carter et al., 2003), Wilcoxon rank-sum test (e.g. Juracek and Ziegler, 2009), the Tukey test (e.g. Motha et al., 2003), *t* test (e.g. Hancock and Revill, 2013), conservativeness index and a ranking based on consensus (Lizaga et al., 2020a) or tracer-particle size relationships and source mixing polygons (Smith et al., 2018). More recently, the use of artificial mixtures with known source proportions has been introduced in fingerprint researches (e.g. Brosinsky et al., 2014) to investigate the linear additivity behaviour of tracers by comparing measured and predicted values using a mass balance approach.

Finally, step 4 is the sediment source ascription (Figure 1.2D). Quantitative estimations of the relative contributions of each source to sediment samples are assessed mathematically by using unmixing models (Collins et al., 1997; Walling and Woodward, 1995; Yu and Oldfield, 1993, 1989). Recently, Lizaga et al. (2020b) developed the FingerPro mixing model as R package, incorporating statistical and graphical tools for the selection of unmixing dataset to optimize results. Frequentist linear mixing models are normally based on the solving of a system of linear equations based on chemical mass conservation. Models are normally constrained as source type contributions sum to unity. Solutions are usually obtained by minimizing the errors associated with the system of equations, so that the differences between estimated and measured tracer values in the target samples are minimised. Additionally, other types of statistical models have expanded greatly. Bayesian mixing models (e.g. Abban et al., 2016; Blake et al., 2018; Massoudieh et al., 2013; Nosrati et al., 2014; Stock et al., 2018; Stock and Semmens, 2016), which allow a better representation of the natural variability in sources and sediment data due to their flexible likelihood-based structure. To a lesser extent, End Member Mixing Models (EMMA; Mukundan et al., 2010; Rose et al., 2018) based on performing a principal component analysis (PCA) with the tracer data measured on the sediment samples collected at the outlet, have also been used.

Despite the constant evolution and improvement of the sediment source fingerprinting approach, there are still a number of challenges to be addressed to reduce the uncertainties inherent in the technique. These uncertainties are mainly associated with sampling methodologies (e.g. Manjoro et al., 2017), spatial variability of source material properties (e.g. Du and Walling, 2017), statistical models selection and optimization (e.g. Haddadchi et al., 2014; Nosrati et al., 2014; Palazón and Navas, 2017), and alteration of soil properties during conveyance or temporal deposition within the river channel (e.g. Koiter et al., 2013). These aspects warrant further research in order to assess the degree to which the assumptions of the sediment fingerprinting approach are met. Similarly, land-use managers/regulators have a relatively poor understanding of fingerprinting techniques, and therefore do not necessarily understand the benefits of incorporating such methods into their management framework (Miller et al., 2015). In this respect, the development of

economic and rapid methodologies might be essential for its application as a catchment management tool.

1.5. Sediment fingerprinting and hydro-sedimentary monitoring as tools for catchment management

Catchment/watershed management involves all human actions aimed at the manipulation of resources so as to provide goods and services without adversely affecting the ecosystem status (FAO, 1998). Catchment management has evolved into integrated catchment management, which assimilates social, technical and institutional dimensions. It can be defined as a "process that recognises the catchment as the appropriate organising unit for understanding and managing ecosystem processes in a context that includes social, economic and political considerations, and guides communities towards an agreed vision of sustainable natural resource management in their catchment" (Fenemor et al., 2011).

Earth science research is essential for catchment management. The best management practices require an understanding of how the different elements of the landscape (e.g. soil, water, land uses, human structures) interact, and recognition of the linkages between upstream and downstream processes. Source control practices are essential in catchment management. The empirically-based Universal Soil Loss Equation (USLE) and other related models (i.e. Revised Universal Soil Loss Equation [RUSLE], Modified Universal Soil Loss Equation [MUSLE], Chemicals, Runoff, and Erosion from Agricultural Management Systems [CREAMS], Groundwater Loading Effects of Agricultural Management Systems [GLEAMS] and the Water Erosion Prediction Project [WEPP]) are often used to predict erosion (Drake and Hogan, 2013). However, despite the usefulness of models, a good understanding of physical processes occurring on the soil surface and interactions between the different catchment components and sediment delivery driving forces is crucial for the development and application of the optimal erosion control measures. Therefore, it is necessary to collect reliable information about sediment mobilization through hillslopes and within the channel, and downstream sediment yields. However, a widespread adoption of standard methodologies to evaluate sediment transport dynamics and identify major sediment

production areas is still missing (Du and Walling, 2017; McCarney-Castle et al., 2017; Walling and Collins, 2008). Information about spatiotemporal variation in suspended sediment sources, concentrations and loads can be assessed by a combined approach of continuous monitoring of water and sediment fluxes with sediment sources fingerprinting. In a highly variable environment such as the Mediterranean Region, collecting constant information about sediment delivery throughout the year should be considered. Furthermore, long datasets (e.g. several years) are needed in order to compute past trends and eventually account for global change. In addition, this information is essential for the development of sediment transport models that integrate information on sediment origin (Owens et al., 2005; Perks et al., 2017; Vercruysse et al., 2019).

1.6. Hypothesis and objectives

The working **hypothesis** of this thesis are:

H1: *Optimization of the sediment fingerprinting technique through research on the conservative behaviour of soil parameters and the use of low-cost and fast-to-measure tracers allowing evaluation of some of the assumptions underlying the technique, improvement of its applicability and the reduction of uncertainties.*

H2: *Hydro-sedimentary monitoring combined with sediment fingerprinting makes possible a better identification of the activation patterns of the different sediment sources within a catchment, resulting in a useful tool for catchment management.*

One general objective is proposed:

GO1: *To identify erosion and sediment transport processes (functional connectivity) in two Mediterranean catchments affected by different global change processes at different spatio-temporal scales, by improving current techniques for sediment origin determination (i.e., reducing uncertainties, time and cost) for its better implementation in catchment management plans.*

The general objective is developed within the five core chapters through the following specific objectives:

SO1: *To assess the water and suspended sediment yields and their dynamics in a Mediterranean catchment representative of terraced landscapes affected by afforestation and recurrent wildfires during the first three post-fire hydrological years (2013–2016.*

SO2: *To use ^{137}Cs and $^{210}Pb_{ex}$ radioisotopes as tracers to recognise the effect of fire on sediment sources during the first post-fire flush in a Mediterranean temporary stream three months after a severe wildfire.*

SO3: *To evaluate sediment colour parameters for predicting relative contributions of burned and unburned sources in fire-affected catchments.*

SO4: *To analyse and link sediment sources contributions with the hydro-sedimentary response of a catchment, thus determining the main factors regulating sediment source contributions and evaluating the potential of hydro-sedimentary monitoring combined with sediment fingerprinting as a catchment management tool.*

SO5: *To investigate eventual changes occurring within the most common soil properties used as tracers in sediment fingerprinting studies due to submersion and in-channel storage.*

1.7. Thesis structure

The thesis *corpus* is composed of a paper compendium divided into 9 chapters. Chapters 4, 5, and 6 correspond to research articles published in scientific journals, Chapter 7 to a manuscript under review for publication, and Chapter 8 to a manuscript in preparation for submission (Table 1.1, Figure 1.3.).

Table 1.1. Title, keywords, journal and status of the research articles of the thesis.

Chapter	Title	Keywords	Journal	Status
Chapter 4	Post-fire hydrological response and suspended sediment transport of a terraced Mediterranean catchment	Sediment delivery processes, wildfires, terraces, nested catchments, Mediterranean fluvial systems	Earth Surface Processes and Landforms	Published
Chapter 5	Source ascription in bed sediments of a Mediterranean temporary stream after the first post-fire flush	First flush sediment sources, wildfire disturbances, fingerprinting technique, fallout radionuclides, Mediterranean fluvial systems	Journal of Soils and Sediments	Published
Chapter 6	Analysis of post-fire suspended sediment sources by using colour parameters	Sediment fingerprinting, colour, fallout radionuclides, wildfire, ash, suspended sediment sources	Geoderma	Published
Chapter 7	Combining sediment fingerprinting and hydro-sedimentary monitoring to assess suspended sediment provenance in a mid-mountainous Mediterranean catchment	Sediment fingerprinting, End Member Mixing Analysis, hysteresis, hydro-sedimentary dynamics, sediment sources, Mediterranean catchments	Journal of Environmental Management	Under review
Chapter 8	Preliminary results: In-channel alterations of soil properties used as tracers in sediment fingerprinting studies	-	-	In preparation

Chapter 1 is a general introduction that briefly reviews the state of the art of erosion processes, the role of hydro-sedimentary monitoring and sediment fingerprinting to mitigate negative impacts promoted by the soil loss and sediment transport and their potential as management tools.

Chapter 2 is an overall description of the thesis study areas.

Chapter 3 details the methods mainly used to achieve the established scientific objectives.

Chapter 4 is related to the specific objective 1. Runoff and suspended sediment transport dynamics and its post-fire evolution are analysed in a fire affected Mediterranean catchment.

Chapter 5 is related to the specific objective 2. In this chapter ^{137}Cs and $^{210}Pb_{ex}$ were used to quantify the relative contribution of different sediment sources to the fine bed sediment temporarily stored on the riverbed surface during the first post-fire flush.

Chapter 6 is related to the specific objective 3. Here, sediment colour and fallout radionuclides are used to distinguish between burned and unburned sources in a fire affected catchment.

Chapter 7 is related to the specific objective 4. In this chapter, two different source apportion models were evaluated. After that, changes in source contributions were linked to the hydro-sedimentary response of different magnitude flood events to determine the main factors regulating sediment contributions.

Chapter 8 is related to the specific objective 5. Here the conservative behaviour of different properties of the sediment was evaluated after a one-year experiment.

Chapter 9 contains a general discussion and conclusions.

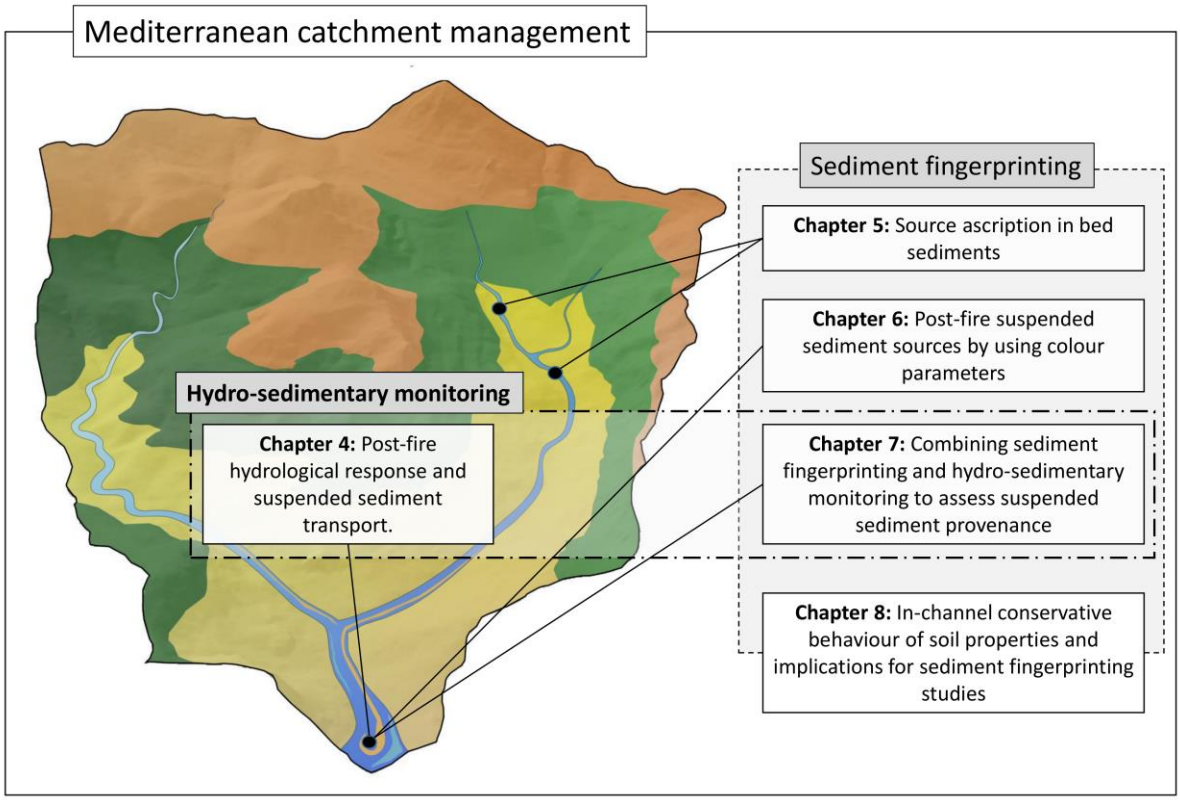

Figure 1.3. Links between chapters that compose the thesis paper compendium. The chapter titles have been shortened for clarity in the figure.

1.8. References

Abban, B., Thanos Papanicolaou, A.N., Cowles, M.K., Wilson, C.G., Abaci, O., Wacha, K., Schilling, K., Schnoebelen, D., 2016. An enhanced Bayesian fingerprinting framework for studying sediment source dynamics in intensively managed landscapes. Water Resour. Res. 52, 4646–4673. https://doi.org/10.1002/2015WR018030

Aich, V., Zimmermann, A., Elsenbeer, H., 2014. Quantification and interpretation of suspended-sediment discharge hysteresis patterns: How much data do we need? Catena 122, 120–129. https://doi.org/10.1016/j.catena.2014.06.020

Andermann, C., Longuevergne, L., Bonnet, S., Crave, A., Davy, P., Gloaguen, R., 2012. Impact of transient groundwater storage on the discharge of Himalayan rivers. Nat. Geosci. 5. https://doi.org/10.1038/ngeo1356

Ankers, C., Walling, D.E., Smith, R.P., 2003. The influence of catchment characteristics on suspended sediment properties. Hydrobiologia 494, 159–167. https://doi.org/10.1023/A:1025458114068

Bakker, M.M., Govers, G., Jones, R.A., Rounsevell, M.D.A., 2007. The effect of soil erosion on Europe's crop yields. Ecosystems 10, 1209–1219. https://doi.org/10.1007/s10021-007-9090-3

Barthod, L.R.M., Liu, K., Lobb, D.A., Owens, P.N., Martínez-Carreras, N., Koiter, A.J., Petticrew, E.L., McCullough, G.K., Liu, C., Gaspar, L., 2015. Selecting Color-based Tracers and Classifying Sediment Sources in the Assessment of Sediment Dynamics Using Sediment Source Fingerprinting. J. Environ. Qual. 44, 1605–1616. https://doi.org/10.2134/jeq2015.01.0043

Belmont, P., Gran, K.B., Schottler, S.P., Wilcock, P.R., Day, S.S., Jennings, C., Lauer, J.W., Viparelli, E., Willenbring, J.K., Engstrom, D.R., Parker, G., 2011. Large shift in source of fine sediment in the upper Mississippi River. Environ. Sci. Technol. 45, 8804–8810. https://doi.org/10.1021/es2019109

Berhe, A.A., Harte, J., Harden, J.W., Torn, M.S., 2007. The significance of the erosion-induced terrestrial carbon sink. Bioscience. https://doi.org/10.1641/B570408

Bilotta, G.S., Brazier, R.E., 2008. Understanding the influence of suspended solids on water quality and aquatic biota. Water Res. 42, 2849–2861. https://doi.org/10.1016/j.watres.2008.03.018

Blaen, P.J., Hannah, D.M., Brown, L.E., Milner, A.M., 2012. Water temperature dynamics in High Arctic river basins. Hydrol. Process. 27, n/a-n/a. https://doi.org/10.1002/hyp.9431

Blake, W.H., Boeckx, P., Stock, B.C., Smith, H.G., Bodé, S., Upadhayay, H.R., Gaspar, L., Goddard, R., Lennard, A.T., Lizaga, I., Lobb, D.A., Owens, P.N., Petticrew, E.L., Kuzyk, Z.Z.A., Gari, B.D., Munishi, L., Mtei, K., Nebiyu, A., Mabit, L., Navas, A., Semmens, B.X., 2018. A deconvolutional Bayesian mixing model approach for river basin sediment source apportionment. Sci. Rep. 8, 1–12. https://doi.org/10.1038/s41598-018-30905-9

Borrelli, P., Robinson, D.A., Panagos, P., Lugato, E., Yang, J.E., Alewell, C., Wuepper, D., Montanarella, L., Ballabio, C., 2020. Land use and climate change impacts on global soil erosion by water (2015-2070). Proc. Natl. Acad. Sci. U. S. A. 117, 21994–22001. https://doi.org/10.1073/pnas.2001403117

Borselli, L., Cassi, P., Torri, D., 2008. Prolegomena to sediment and flow connectivity in the

landscape: A GIS and field numerical assessment. Catena 75, 268–277. https://doi.org/10.1016/j.catena.2008.07.006

Bracken, L.J., Turnbull, L., Wainwright, J., Bogaart, P., 2015. Sediment connectivity: A framework for understanding sediment transfer at multiple scales. Earth Surf. Process. Landforms 40, 177–188. https://doi.org/10.1002/esp.3635

Brosinsky, A., Foerster, S., Segl, K., Kaufmann, H., 2014. Spectral fingerprinting: sediment source discrimination and contribution modelling of artificial mixtures based on VNIR-SWIR spectral properties. J. Soils Sediments 14, 1949–1964. https://doi.org/10.1007/s11368-014-0925-1

Brown, A.G., 1985. The potential use of pollen in the identification of suspended sediment sources. Earth Surf. Process. Landforms 10, 27–32. https://doi.org/10.1002/esp.3290100106

Burt, T.P., Worrall, F., Howden, N.J.K., Anderson, M.G., 2015. Shifts in discharge-concentration relationships as a small catchment recover from severe drought. Hydrol. Process. 29, 498–507. https://doi.org/10.1002/hyp.10169

Calsamiglia, A., Gago, J., Garcia-Comendador, J., Bernat, J.F., Calvo-Cases, A., Estrany, J., 2020. Evaluating functional connectivity in a small agricultural catchment under contrasting flood events by using UAV. Earth Surf. Process. Landforms 45, 800–815. https://doi.org/10.1002/esp.4769

Camporese, M., Penna, D., Borga, M., Paniconi, C., 2014. A field and modeling study of nonlinear storage-discharge dynamics for an Alpine headwater catchment. Water Resour. Res. 50, 806–822. https://doi.org/10.1002/2013WR013604

Candela, A., Aronica, G., Santoro, M., 2005. Effects of Forest Fires on Flood Frequency Curves in a Mediterranean Catchment/Effets d'incendies de forêt sur les courbes de fréquence de crue dans un bassin versant Méditerranéen. Hydrol. Sci. J. 50, 206. https://doi.org/10.1623/hysj.50.2.193.61795

Carrión, J.S., Sánchez-Gómez, P., Mota, J.F., Yll, R., Chaín, C., 2003. Holocene vegetation dynamics, fire and grazing in the Sierra de Gádor, southern Spain. The Holocene 13, 839–849. https://doi.org/10.1191/0959683603hl662rp

Carter, J., Owens, P.N., Walling, D.E., Leeks, G.J.L., 2003. Fingerprinting suspended sediment sources in a large urban river system, in: Science of the Total Environment. Elsevier, pp. 513–534. https://doi.org/10.1016/S0048-9697(03)00071-8

Catalán, B., Saurí, D., Serra, P., 2008. Urban sprawl in the Mediterranean?. Patterns of growth and change in the Barcelona Metropolitan Region 1993-2000. Landsc. Urban Plan. 85, 174–184. https://doi.org/10.1016/j.landurbplan.2007.11.004

Cavalli, M., Trevisani, S., Comiti, F., Marchi, L., 2013. Geomorphometric assessment of spatial sediment connectivity in small Alpine catchments. Geomorphology 188, 31–41. https://doi.org/10.1016/j.geomorph.2012.05.007

Certini, G., 2005. Effects of fire on properties of forest soils: A review. Oecologia. https://doi.org/10.1007/s00442-004-1788-8

Chen, F., Wang, X., Li, X., Wang, J., Xie, D., Ni, J., Liu, Y., 2019. Using the sediment fingerprinting method to identify the sediment sources in small catchments with similar geological conditions. Agric. Ecosyst. Environ. 286, 106655. https://doi.org/10.1016/j.agee.2019.106655

Collins, A.. L., Walling, D.. E., 2002. Selecting fingerprint properties for discriminating potential suspended sediment sources in river basins. J. Hydrol. 261, 218–244. https://doi.org/10.1016/S0022-1694(02)00011-2

Collins, A.L., Anthony, S.G., 2008. Assessing the likelihood of catchments across England and Wales meeting "good ecological status" due to sediment contributions from agricultural sources. Environ. Sci. Policy 11, 163–170. https://doi.org/10.1016/j.envsci.2007.07.008

Collins, A.L., Blackwell, M., Boeckx, P., Chivers, C.A., Emelko, M., Evrard, O., Foster, I., Gellis, A., Gholami, H., Granger, S., Harris, P., Horowitz, A.J., Laceby, J.P., Martinez-Carreras, N., Minella, J., Mol, L., Nosrati, K., Pulley, S., Silins, U., da Silva, Y.J., Stone, M., Tiecher, T., Upadhayay, H.R., Zhang, Y., 2020. Sediment source fingerprinting: benchmarking recent outputs, remaining challenges and emerging themes. J. Soils Sediments 20, 1–34. https://doi.org/10.1007/s11368-020-02755-4

Collins, A.L., Walling, D.E., 2007. The storage and provenance of fine sediment on the channel bed of two contrasting lowland permeable catchments, UK. River Res. Appl. 23, 429–450. https://doi.org/10.1002/rra.992

Collins, A.L., Walling, D.E., Leeks, G.J.L., 1997. Source type ascription for fluvial suspended sediment based on a quantitative composite fingerprinting technique. Catena 29, 1–27. https://doi.org/10.1016/S0341-8162(96)00064-1

Collins, A.L., Walling, D.E., Sichingabula, H.M., Leeks, G.J.L., 2001. Using ^{137}Cs measurements to quantify soil erosion and redistribution rates for areas under different land use in the Upper Kaleya River basin, southern Zambia. Geoderma 104, 299–323. https://doi.org/10.1016/S0016-7061(01)00087-8

Collins, A.L.L., Pulley, S., Foster, I.D.L.D.L., Gellis, A., Porto, P., Horowitz, A.J.J., 2017. Sediment source fingerprinting as an aid to catchment management: A review of the current state of knowledge and a methodological decision-tree for end-users. J. Environ. Manage. 194, 86–108. https://doi.org/10.1016/j.jenvman.2016.09.075

Cosandey, C., Andréassian, V., Martin, C., Didon-Lescot, J.F., Lavabre, J., Folton, N., Mathys, N., Richard, D., 2005. The hydrological impact of the mediterranean forest: A review of French research. J. Hydrol. 301, 235–249. https://doi.org/10.1016/j.jhydrol.2004.06.040

Crockford, R.H., Olley, J.M., 1998. The effects of particle breakage and abrasion on the magnetic properties of two soils. Hydrol. Process. 12, 1495–1505. https://doi.org/10.1002/(SICI)1099-1085(199807)12:9<1495::AID-HYP652>3.0.CO;2-M

Davis, C.M., Fox, J.F., 2009. Sediment Fingerprinting: Review of the Method and Future Improvements for Allocating Nonpoint Source Pollution. J. Environ. Eng. 135, 490–504. https://doi.org/10.1061/(ASCE)0733-9372(2009)135:7(490)

de Boer, D.H., Campbell, I.A., 1989. Spatial scale dependence of sediment dynamics in a semi-arid badland drainage basin. Catena 16, 277–290. https://doi.org/10.1016/0341-8162(89)90014-3

de Vente, J., Poesen, J., Arabkhedri, M., Verstraeten, G., 2007. The sediment delivery problem revisited. Prog. Phys. Geogr. 31, 155–178. https://doi.org/10.1177/0309133307076485

Dietrich, W.E., Dunne, T., 1978. Sediment budget for a small catchment in mountainous terrain. Z. Geomorph. N. F., Suppl. Bd. 29.

Dooge, J.C.I., 2005. Bringing it all together. Hydrol. Earth Syst. Sci. 9, 3–14. https://doi.org/10.5194/hess-9-3-2005

Drake, K., Hogan, M., 2013. Watershed Management Guidebook: A Guide to Outcome-Based Watershed Management. Integrated Environmental Restoration Services, Inc. in collaboration with the Lahontan Regional Water Quality Control Board and the District, Tahoe Resource Conservation.

Droppo, I.G., 2001. Rethinking what constitutes suspended sediment. Hydrol. Process. 15, 1551–1564. https://doi.org/10.1002/hyp.228

Droppo, I.G., Leppard, G.G., Flannigan, D.T., Liss, S.N., 1997. The freshwater floc: A functional relationship of water and organic and inorganic floc constituents affecting suspended sediment properties. Water, Air, Soil Pollut. 99, 43–53. https://doi.org/10.1007/bf02406843

Droppo, I.G., Ongley, E.D., 1994. Flocculation of suspended sediment in rivers of southeastern Canada. Water Res. 28, 1799–1809. https://doi.org/10.1016/0043-1354(94)90253-4

Du, P., Walling, D.E., 2017. Fingerprinting surficial sediment sources: Exploring some potential problems associated with the spatial variability of source material properties. J. Environ. Manage. 194, 4–15. https://doi.org/10.1016/j.jenvman.2016.05.066

Duerdoth, C.P., Arnold, A., Murphy, J.F., Naden, P.S., Scarlett, P., Collins, A.L., Sear, D.A., Jones, J.I., 2015. Assessment of a rapid method for quantitative reach-scale estimates of deposited fine sediment in rivers. Geomorphology 230, 37–50. https://doi.org/10.1016/j.geomorph.2014.11.003

Eberl, D.D., 2004. Quantitative mineralogy of the Yukon River system: Changes with reach and season, and determining sediment provenance. Am. Mineral. 89, 1784–1794. https://doi.org/10.2138/am-2004-11-1225

Estrany, J., Garcia, C., Martínez-Carreras, N., Walling, D.E., 2012. A suspended sediment budget for the agricultural can Revull catchment (Mallorca, Spain). Zeitschrift fur Geomorphol. 56, 169–193. https://doi.org/10.1127/0372-8854/2012/S-00110

Estrany, J., Garcia, C., Walling, D.E.D.E.D.E., Ferrer, L., 2011. Fluxes and storage of fine-grained sediment and associated contaminants in the Na Borges River (Mallorca, Spain). Catena 87, 291–305. https://doi.org/10.1016/j.catena.2011.06.009

Estrany, J., López-Tarazón, J.A., Smith, H.G., 2016. Wildfire Effects on Suspended Sediment Delivery Quantified Using Fallout Radionuclide Tracers in a Mediterranean Catchment. L. Degrad. Dev. 27, 1501–1512. https://doi.org/10.1002/ldr.2462

European Community, 2000. Directive 2000/60/EC of the European Parliament and of the Council of 23 October 2000 Establishing a Framework for Community Action in the Field of Water Policy. Off. J. Eur. Communities L 327, 1–72.

Evans, D.J., Gibson, C.E., Rossell, R.S., 2006. Sediment loads and sources in heavily modified Irish catchments: A move towards informed management strategies. Geomorphology 79, 93–113. https://doi.org/10.1016/j.geomorph.2005.09.018

Evrard, O., Chaboche, P.-A., Ramon, R., Foucher, A., Laceby, J.P., 2020. A global review of sediment source fingerprinting research incorporating fallout radiocesium (^{137}Cs). Geomorphology 107103. https://doi.org/10.1016/j.geomorph.2020.107103

Evrard, O., Laceby, J.P., Huon, S., Lefèvre, I., Sengtaheuanghoung, O., Ribolzi, O., 2016. Combining multiple fallout radionuclides (137Cs, 7Be, 210Pbxs) to investigate temporal sediment source dynamics in tropical, ephemeral riverine systems. J. Soils Sediments 16, 1130–1144. https://doi.org/10.1007/s11368-015-1316-y

FAO, 1998. Watershed management field manual [WWW Document]. FAO Conserv. Guid. 13/5. URL http://www.fao.org/docrep/006/t0099e/t0099e00.HTM

Favis-Mortlock, D.T., Guerra, A.J.T., 1999. The implications of general circulation model estimates of rainfall for future erosion: A case study from Brazil. Catena 37, 329–354. https://doi.org/10.1016/S0341-8162(99)00025-9

Fenemor, A., Phillips, C., Allen, W., Young, R.G., Harmsworth, G., Bowden, B., Basher, L., Gillespie, P.A., Kilvington, M., Davies-Colley, R., Dymond, J., Cole, A., Lauder, G., Davie, T., Smith, R., Markham, S., Deans, N., Stuart, B., Atkinson, M., Collins, A., 2011. Integrated catchment management-interweaving social process and science knowledge. New Zeal. J. Mar. Freshw. Res. https://doi.org/10.1080/00288330.2011.593529

Ferguson, R.I., 1981. Channel form and channel changes (Britain)., in: (ed), L.J. (Ed.), British Rivers. Allen and Unwin, London, pp. 90–125.

Ferreira, A.J.D., Coelho, C.O.A., Boulet, A.K., Leighton-Boyce, G., Keizer, J.J., Ritsema, C.J., 2005. Influence of burning intensity on water repellency and hydrological processes at forest and shrub sites in Portugal. Soil Res. 43, 327. https://doi.org/10.1071/SR04084

Fortesa, J., Latron, J., García-Comendador, J., Company, J., Estrany, J., 2020. Runoff and soil moisture as driving factors in suspended sediment transport of a small mid-mountain Mediterranean catchment. Geomorphology 368, 107349. https://doi.org/10.1016/j.geomorph.2020.107349

Fortesa, J., Ricci, G.F., García-Comendador, J., Gentile, F., Estrany, J., Sauquet, E., Datry, T., De Girolamo, A.M., 2021. Analysing hydrological and sediment transport regime in two Mediterranean intermittent rivers. Catena 196, 104865. https://doi.org/10.1016/j.catena.2020.104865

Foster, I.D.L., Charlesworth, S.M., 1996. Heavy metals in the hydrological cycle: Trends and explanation. Hydrol. Process. 10, 227–261. https://doi.org/10.1002/(SICI)1099-1085(199602)10:2<227::AID-HYP357>3.0.CO;2-X

Foster, I.D.L., Mighall, T.M., Proffitt, H., Walling, D.E., Owens, P.N., 2006. Post-depositional ^{137}Cs mobility in the sediments of three shallow coastal lagoons, SW England. J. Paleolimnol. 35, 881–895. https://doi.org/10.1007/s10933-005-6187-6

Fovet, O., Ruiz, L., Hrachowitz, M., Faucheux, M., Gascuel-Odoux, C., 2015. Hydrological hysteresis and its value for assessing process consistency in catchment conceptual models. Hydrol. Earth Syst. Sci. 19, 105–123. https://doi.org/10.5194/hess-19-105-2015

Fox, J.F., Papanicolaou, A.N., 2008. Application of the spatial distribution of nitrogen stable isotopes for sediment tracing at the watershed scale. J. Hydrol. 358, 46–55. https://doi.org/10.1016/j.jhydrol.2008.05.032

Fryirs, K., 2013. (Dis)Connectivity in catchment sediment cascades: A fresh look at the sediment delivery problem. Earth Surf. Process. Landforms 38, 30–46. https://doi.org/10.1002/esp.3242

García-Ruiz, J.M., Nadal-Romero, E., Lana-Renault, N., Beguería, S., 2013. Erosion in Mediterranean landscapes: Changes and future challenges. Geomorphology 198, 20–36. https://doi.org/10.1016/j.geomorph.2013.05.023

Garrels, R.M., Mackenzie, F.T., 1971. Gregor's denudation of the continents. Nature 231. https://doi.org/10.1038/231382a0

Gaspar, L., Lizaga, I., Blake, W.H., Latorre, B., Quijano, L., Navas, A., 2019. Fingerprinting changes in source contribution for evaluating soil response during an exceptional rainfall in Spanish pre-pyrenees. J. Environ. Manage. 240, 136–148

Gates, L.D., Ließ, S., 2001. Impacts of deforestation and afforestation in the Mediterranean region as simulated by the MPI atmospheric GCM. Glob. Planet. Change 30, 309–328. https://doi.org/10.1016/S0921-8181(00)00091-6

Giménez, R., Casalí, J., Grande, I., Díez, J., Campo, M.A., Álvarez-Mozos, J., Goñi, M., 2012. Factors controlling sediment export in a small agricultural watershed in Navarre (Spain). Agric. Water Manag. 110, 1–8. https://doi.org/10.1016/j.agwat.2012.03.007

Gingele, F.X., De Deckker, P., 2005. Clay mineral, geochemical and Sr-Nd isotopic fingerprinting of sediments in the Murray-Darling fluvial system, southeast Australia. Aust. J. Earth Sci. 52, 965–974. https://doi.org/10.1080/08120090500302301

Giorgi, F., Lionello, P., 2008. Climate change projections for the Mediterranean region. Glob. Planet. Change 63, 90–104. https://doi.org/10.1016/j.gloplacha.2007.09.005

Grabowski, R.C., Gurnell, A.M., 2016. Diagnosing problems of fine sediment delivery and transfer in a lowland catchment. Aquat. Sci. 78, 95–106. https://doi.org/10.1007/s00027-015-0426-3

Grimshaw, D.L., Lewin, J., 1980. Source identification for suspended sediments. J. Hydrol. 47, 151–162. https://doi.org/10.1016/0022-1694(80)90053-0

Haddadchi, A., Olley, J., Laceby, P., 2014. Accuracy of mixing models in predicting sediment source contributions. Sci. Total Environ. 497–498, 139–152. https://doi.org/10.1016/j.scitotenv.2014.07.105

Haddadchi, A., Ryder, D.S., Evrard, O., Olley, J., 2013. Sediment fingerprinting in fluvial systems: review of tracers, sediment sources and mixing models. Int. J. Sediment Res. 28, 560–578. https://doi.org/10.1016/S1001-6279(14)60013-5

Hancock, G.J., Revill, A.T., 2013. Erosion source discrimination in a rural Australian catchment using compound-specific isotope analysis (CSIA). Hydrol. Process. 27, 923–932. https://doi.org/10.1002/hyp.9466

He, Q., Walling, D.E., 1996. Interpreting particle size effects in the adsorption of ^{137}Cs and unsupported ^{210}Pb by mineral soils and sediments. J. Environ. Radioact. 30, 117–137. https://doi.org/10.1016/0265-931X(96)89275-7

Heckmann, T., Cavalli, M., Cerdan, O., Foerster, S., Javaux, M., Lode, E., Smetanová, A., Vericat, D., Brardinoni, F., 2018. Indices of sediment connectivity: opportunities, challenges and limitations. Earth-Science Rev. https://doi.org/10.1016/j.earscirev.2018.08.004

Hill, B.R., DeCarlo, E.H., Fuller, C.C., Wong, M.F., 1998. Using sediment 'fingerprints' to assess sediment-budget errors, North Halawa Valley, Oahu, Hawaii, 1991–92. Earth Surf. Process. Landforms 23, 493–508. https://doi.org/10.1002/(SICI)1096-9837(199806)23:6<493::AID-ESP862>3.0.CO;2-V

Hjulström, F., 1936. Studies of the Morphological Activity of Rivers as Illustrated by the River Fyris. Geogr. Ann. 18, 121. https://doi.org/10.2307/519824

Hooke, J.M., 2006. Human impacts on fluvial systems in the Mediterranean region. Geomorphology 79, 311–335. https://doi.org/10.1016/j.geomorph.2006.06.036

Horowitz, A.J., Elrick, K.A., Cook, R.B., 1993. Effect of mining and related activities on the

sediment trace element geochemistry of lake coeur D'Alene, idaho, USA. Part I: Surface sediments. Hydrol. Process. 7, 403–423. https://doi.org/10.1002/hyp.3360070406

Horowitz, A.J., Elrick, K.A., Smith, J.J., 2007. Measuring the fluxes of suspended sediment, trace elements and nutrients for the city of atlanta, USA: Insights on the global water quality impacts of increasing urbanization. IAHS-AISH Publ. 314, 57–70.

Juracek, K.E., Ziegler, A.C., 2009. Estimation of sediment sources using selected chemical tracers in the Perry lake basin, Kansas, USA. Int. J. Sediment Res. 24, 108–125. https://doi.org/10.1016/S1001-6279(09)60020-2

Kjelland, M.E., Woodley, C.M., Swannack, T.M., Smith, D.L., 2015. A review of the potential effects of suspended sediment on fishes: potential dredging-related physiological, behavioral, and transgenerational implications. Environ. Syst. Decis. https://doi.org/10.1007/s10669-015-9557-2

Klages, M.G., Hsieh, Y.P., 1975. Suspended Solids Carried by the Gallatin River of Southwestern Montana: II. Using Mineralogy for Inferring Sources. J. Environ. Qual. 4, 68–73. https://doi.org/10.2134/jeq1975.00472425000400010016x

Koiter, A.J., Lobb, D.A., Owens, P.N., Petticrew, E.L., Tiessen, K.H.D., Li, S., 2013. Investigating the role of connectivity and scale in assessing the sources of sediment in an agricultural watershed in the Canadian prairies using sediment source fingerprinting. J. Soils Sediments 13, 1676–1691. https://doi.org/10.1007/s11368-013-0762-7

Koiter, A.J., Owens, P.N., Petticrew, E.L., Lobb, D.A., 2018. Assessment of particle size and organic matter correction factors in sediment source fingerprinting investigations: An example of two contrasting watersheds in Canada. Geoderma 325, 195–207. https://doi.org/10.1016/j.geoderma.2018.02.044

Koiter, A.J.J., Owens, P.N.N., Petticrew, E.L.L., Lobb, D.A.A., 2013. The behavioural characteristics of sediment properties and their implications for sediment fingerprinting as an approach for identifying sediment sources in river basins. Earth-Science Rev. 125, 24–42. https://doi.org/10.1016/j.earscirev.2013.05.009

Kosmas, C., Danalatos, N., Cammeraat, L.H., Chabart, M., Diamantopoulos, J., Farand, R., Gutierrez, L., Jacob, A., Marques, H., Martinez-Fernandez, J., Mizara, A., Moustakas, N., Nicolau, J.M., Oliveros, C., Pinna, G., Puddu, R., Puigdefabregas, J., Roxo, M., Simao, A., Stamou, G., Tomasi, N., Usai, D., Vacca, A., 1997. The effect of land use on runoff and soil erosion rates under Mediterranean conditions. Catena 29, 45–59. https://doi.org/10.1016/S0341-8162(96)00062-8

Krause, A.K., Franks, S.W., Kalma, J.D., Loughran, R.J., Rowan, J.S., 2003. Multi-parameter fingerprinting of sediment deposition in a small gullied catchment in SE Australia. Catena 53, 327–348. https://doi.org/10.1016/S0341-8162(03)00085-7

Kurashige, Y., Fusejima, Y., 1997. Source identification of suspended sediment from grain-size distributions: I. Application of nonparametric statistical tests. Catena 31, 39–52. https://doi.org/10.1016/S0341-8162(97)00033-7

Laceby, J.P., Evrard, O., Smith, H.G., Blake, W.H., Olley, J.M., Minella, J.P.G., Owens, P.N., 2017. The challenges and opportunities of addressing particle size effects in sediment source fingerprinting: A review, Earth-Science Reviews. Elsevier. https://doi.org/10.1016/j.earscirev.2017.04.009

Laceby, J.P., McMahon, J., Evrard, O., Olley, J., 2015. A comparison of geological and statistical

approaches to element selection for sediment fingerprinting. J. Soils Sediments 15, 2117–2131. https://doi.org/10.1007/s11368-015-1111-9

Lambert, C.P., Walling, D.E., 1988. Measurement of channel storage of suspended sediment in a gravel-bed river. Catena 15, 65–80. https://doi.org/10.1016/0341-8162(88)90017-3

Langlois, J.L., Johnson, D.W., Mehuys, G.R., 2005. Suspended sediment dynamics associated with snowmelt runoff in a small mountain stream of Lake Tahoe (Nevada). Hydrol. Process. 19, 3569–3580. https://doi.org/10.1002/hyp.5844

Lawler, D.M., Petts, G.E., Foster, I.D.L., Harper, S., 2006. Turbidity dynamics during spring storm events in an urban headwater river system: The Upper Tame, West Midlands, UK. Sci. Total Environ. 360, 109–126. https://doi.org/10.1016/j.scitotenv.2005.08.032

Li, Z., Xu, X., Zhang, Y., Wang, K., 2020. Fingerprinting sediment sources in a typical karst catchment of southwest China. Int. Soil Water Conserv. Res. https://doi.org/10.1016/j.iswcr.2020.06.005

Lizaga, I., Latorre, B., Gaspar, L., Navas, A., 2020a. Consensus ranking as a method to identify non-conservative and dissenting tracers in fingerprinting studies. Sci. Total Environ. 720, 137537. https://doi.org/10.1016/j.scitotenv.2020.137537

Lizaga, I., Latorre, B., Gaspar, L., Navas, A., 2020b. FingerPro: an R Package for Tracking the Provenance of Sediment. Water Resour. Manag. 34, 3879–3894. https://doi.org/10.1007/s11269-020-02650-0

Lloyd, C.E.M., Freer, J.E., Johnes, P.J., Collins, A.L., 2016. Using hysteresis analysis of high-resolution water quality monitoring data, including uncertainty, to infer controls on nutrient and sediment transfer in catchments. Sci. Total Environ. 543, 388–404. https://doi.org/10.1016/j.scitotenv.2015.11.028

López-Bermúdez, F., 1990. Soil erosion by water on the desertification of a semi-arid Mediterranean fluvial basin: the Segura basin, Spain. Agric. Ecosyst. Environ. 33, 129–145. https://doi.org/10.1016/0167-8809(90)90238-9

López-Tarazón, J.A., Estrany, J., 2017. Exploring suspended sediment delivery dynamics of two Mediterranean nested catchments. Hydrol. Process. 31, 698–715. https://doi.org/10.1002/hyp.11069

Ludwig, W., Probst, J.L., 1996. Predicting the oceanic input of organic carbon by continental erosion. Global Biogeochem. Cycles 10, 23–41. https://doi.org/10.1029/95GB02925

Luetzenburg, G., Bittner, M.J., Calsamiglia, A., Renschler, C.S., Estrany, J., Poeppl, R., 2020. Climate and land use change effects on soil erosion in two small agricultural catchment systems Fugnitz – Austria, Can Revull – Spain. Sci. Total Environ. 704, 135389. https://doi.org/10.1016/j.scitotenv.2019.135389

Maner, S.B., 1958. Factors affecting sediment delivery rates in the red hills physiographic area. Trans. Am. Geophys. Union 39, 669. https://doi.org/10.1029/TR039i004p00669

Manjoro, M., Rowntree, K., Kakembo, V., Collins, A.L., 2017. Use of sediment source fingerprinting to assess the role of subsurface erosion in the supply of fine sediment in a degraded catchment in the Eastern Cape, South Africa. J. Environ. Manage. 194, 27–41. https://doi.org/10.1016/J.JENVMAN.2016.07.019

Martínez-Carreras, N., Krein, A., Gallart, F., Iffly, J.F., Pfister, L., Hoffmann, L., Owens, P.N., 2010a. Assessment of different colour parameters for discriminating potential suspended

sediment sources and provenance: A multi-scale study in Luxembourg. Geomorphology 118, 118–129. https://doi.org/10.1016/j.geomorph.2009.12.013

Martínez-Carreras, N., Krein, A., Udelhoven, T., Gallart, F., Iffly, J.F., Hoffmann, L., Pfister, L., Walling, D.E., 2010b. A rapid spectral-reflectance-based fingerprinting approach for documenting suspended sediment sources during storm runoff events. J. Soils Sediments 10, 400–413. https://doi.org/10.1007/s11368-009-0162-1

Martínez-Carreras, N., Udelhoven, T., Krein, A., Gallart, F., Iffly, J.F., Ziebel, J., Hoffmann, L., Pfister, L., Walling, D.E., 2010c. The use of sediment colour measured by diffuse reflectance spectrometry to determine sediment sources: Application to the Attert River catchment (Luxembourg). J. Hydrol. 382, 49–63. https://doi.org/10.1016/j.jhydrol.2009.12.017

Massoudieh, A., Gellis, A., Banks, W.S., Wieczorek, M.E., 2013. Suspended sediment source apportionment in Chesapeake Bay watershed using Bayesian chemical mass balance receptor modeling. Hydrol. Process. 27, 3363–3374. https://doi.org/10.1002/hyp.9429

McCarney-Castle, K., Childress, T.M., Heaton, C.R., 2017. Sediment source identification and load prediction in a mixed-use Piedmont watershed, South Carolina. J. Environ. Manage. 185, 60–69. https://doi.org/10.1016/j.jenvman.2016.10.036

McLaughlin, C.J., Smith, C.A., Buddemeier, R.W., Bartley, J.D., Maxwell, B.A., 2003. Rivers, runoff, and reefs. Glob. Planet. Change 39. https://doi.org/10.1016/S0921-8181(03)00024-9

Miller, J., Mackin, G., Miller, S.M.O., 2015. Application of Geochemical Tracers to Fluvial Sediment. Springer International Publishing, Dordrecht.

Miller, J.R., Lord, M., Yurkovich, S., Mackin, G., Kolenbrander, L., 2005. Historical trends in sedimentation rates and sediment provenance, Fairfield Lake, Western North Carolina. J. Am. Water Resour. Assoc. 41, 1053–1075. https://doi.org/10.1111/j.1752-1688.2005.tb03785.x

Misset, C., Recking, A., Legout, C., Poirel, A., Cazilhac, M., Esteves, M., Bertrand, M., 2019. An attempt to link suspended load hysteresis patterns and sediment sources configuration in alpine catchments. J. Hydrol. 576, 72–84. https://doi.org/10.1016/j.jhydrol.2019.06.039

Moreira, F., Viedma, O., Arianoutsou, M., Curt, T., Koutsias, N., Rigolot, E., Barbati, A., Corona, P., Vaz, P., Xanthopoulos, G., Mouillot, F., Bilgili, E., 2011. Landscape - wildfire interactions in southern Europe: Implications for landscape management. J. Environ. Manage. https://doi.org/10.1016/j.jenvman.2011.06.028

Morgan, R.P.., 2005. Soil Erosion and Conservation, 3rd edition, European Journal of Soil Science.

Motha, J.A., Wallbrink, P.J., Hairsine, P.B., Grayson, R.B., 2002. Tracer properties of eroded sediment and source material. Hydrol. Process. 16, 1983–2000. https://doi.org/10.1002/hyp.397

Motha, J.A., Wallbrink, P.J., Hairsine, P.B., Grayson, R.B., 2003. Determining the sources of suspended sediment in a forested catchment in southeastern Australia. Water Resour. Res. 39, 1056. https://doi.org/10.1029/2001WR000794

Mukundan, R., Radcliffe, D.E., Ritchie, J.C., Risse, L.M., McKinley, R.A., 2010. Sediment Fingerprinting to Determine the Source of Suspended Sediment in a Southern Piedmont Stream. J. Environ. Qual. 39, 1328–1337. https://doi.org/10.2134/jeq2009.0405

Najafi, S., Dragovich, D., Heckmann, T., Sadeghi, S.H., 2021. Sediment connectivity concepts and approaches. Catena. https://doi.org/10.1016/j.catena.2020.104880

Navas, A., Garcés, B.V., Machín, J., 2004. An approach to integrated assessement of reservoir siltation : the Joaquín Costa reservoir as a case study. Hydrol. Easrt Syst. Sci. 8, 1193–1199. https://doi.org/10.5194/hess-8-1193-2004

Navas, A., López-Vicente, M., Gaspar, L., Palazón, L., Quijano, L., 2014. Establishing a tracer-based sediment budget to preserve wetlands in Mediterranean mountain agroecosystems (NE Spain). Sci. Total Environ. 496, 132–143. https://doi.org/10.1016/j.scitotenv.2014.07.026

Navas, A., Valero-Garcés, B., Gaspar, L., Palazón, L., 2011. Radionuclides and stable elements in the sediments of the Yesa Reservoir, Central Spanish Pyrenees. J. Soils Sediments 11, 1082–1098. https://doi.org/10.1007/s11368-011-0401-0

Navratil, O., Evrard, O., Esteves, M., Legout, C., Ayrault, S., Némery, J., Mate-Marin, A., Ahmadi, M., Lefèvre, I., Poirel, A., Bonté, P., 2012. Temporal variability of suspended sediment sources in an alpine catchment combining river/rainfall monitoring and sediment fingerprinting. Earth Surf. Process. Landforms 37, 828–846. https://doi.org/10.1002/esp.3201

Newcombe, C.P., Macdonald, D.D., 1991. Effects of Suspended Sediments on Aquatic Ecosystems. North Am. J. Fish. Manag. 11, 72–82. https://doi.org/10.1577/1548-8675(1991)011<0072:EOSSOA>2.3.CO;2

Nosrati, K., Govers, G., Ahmadi, H., Sharifi, F., Amoozegar, M.A., Merckx, R., Vanmaercke, M., 2011. An exploratory study on the use of enzyme activities as sediment tracers: Biochemical fingerprints? Int. J. Sediment Res. 26, 136–151. https://doi.org/10.1016/S1001-6279(11)60082-6

Nosrati, K., Govers, G., Semmens, B.X., Ward, E.J., 2014. A mixing model to incorporate uncertainty in sediment fingerprinting. Geoderma 217–218, 173–180. https://doi.org/10.1016/j.geoderma.2013.12.002

O'Neal, M.R., Nearing, M.A., Vining, R.C., Southworth, J., Pfeifer, R.A., 2005. Climate change impacts on soil erosion in Midwest United States with changes in crop management, in: Catena. Elsevier, pp. 165–184. https://doi.org/10.1016/j.catena.2005.03.003

Olesen, J.E., Bindi, M., 2002. Consequences of climate change for European agricultural productivity, land use and policy. Eur. J. Agron. https://doi.org/10.1016/S1161-0301(02)00004-7

Owens, P.N., Batalla, R.J., Collins, A.J., Gomez, B., Hicks, D.M., Horowitz, A.J., Kondolf, G.M., Marden, M., Page, M.J., Peacock, D.H., Petticrew, E.L., Salomons, W., Trustrum, N.A., 2005. Fine-grained sediment in river systems: Environmental significance and management issues. River Res. Appl. 21, 693–717. https://doi.org/10.1002/rra.878

Owens, P.N., Walling, D.E., He, Q., 1996. The behaviour of bomb-derived caesium-137 fallout in catchment soils. J. Environ. Radioact. 32, 169–191. https://doi.org/10.1016/0265-931X(96)84941-1

Paeth, H., Vogt, G., Paxian, A., Hertig, E., Seubert, S., Jacobeit, J., 2017. Quantifying the evidence of climate change in the light of uncertainty exemplified by the Mediterranean hot spot region. Glob. Planet. Change 151, 144–151. https://doi.org/10.1016/j.gloplacha.2016.03.003

Palazón, L., Navas, A., 2017. Variability in source sediment contributions by applying different statistic test for a Pyrenean catchment. J. Environ. Manage. 194, 42–53. https://doi.org/10.1016/j.jenvman.2016.07.058

Paolo, J., Minella, G., Henrique Merten, G., Clarke, R.T., 2004. Identification of sediment sources in a small rural drainage basin. IAHS Publ.

Park, J., Hunt, J.R., 2017. Coupling fine particle and bedload transport in gravel-bedded streams. J. Hydrol. 552, 532–543. https://doi.org/10.1016/j.jhydrol.2017.07.023

Pausas, J.G., Llovet, J., Rodrigo, A., Vallejo, R., 2008. Are wildfires a disaster in the Mediterranean basin? A review. Int. J. Wildl. Fire 17, 713–723. https://doi.org/10.1071/WF07151

Pausas, J.G., Verdú, M., 2005. Plant persistence traits in fire-prone ecosystems of the Mediterranean basin: A phylogenetic approach. Oikos 109, 196–202. https://doi.org/10.1111/j.0030-1299.2005.13596.x

Peña-Angulo, D., Nadal-Romero, E., González-Hidalgo, J.C., Albaladejo, J., Andreu, V., Bagarello, V., Barhi, H., Batalla, R.J., Bernal, S., Bienes, R., Campo, J., Campo-Bescós, M.A., Canatario-Duarte, A., Cantón, Y., Casali, J., Castillo, V., Cerdà, A., Cheggour, A., Cid, P., Cortesi, N., Desir, G., Díaz-Pereira, E., Espigares, T., Estrany, J., Fernández-Raga, M., Ferreira, C.S.S., Ferro, V., Gallart, F., Giménez, R., Gimeno, E., Gómez, J.A., Gómez-Gutiérrez, A., Gómez-Macpherson, H., González-Pelayo, O., Hueso-González, P., Kairis, O., Karatzas, G.P., Klotz, S., Kosmas, C., Lana-Renault, N., Lasanta, T., Latron, J., Lázaro, R., Le Bissonnais, Y., Le Bouteiller, C., Licciardello, F., López-Tarazón, J.A., Lucía, A., Marín, C., Marqués, M.J., Martínez-Fernández, J., Martínez-Mena, M., Martínez-Murillo, J.F., Mateos, L., Mathys, N., Merino-Martín, L., Moreno-de las Heras, M., Moustakas, N., Nicolau, J.M., Novara, A., Pampalone, V., Raclot, D., Rodríguez-Blanco, M.L., Rodrigo-Comino, J., Romero-Díaz, A., Roose, E., Rubio, J.L., Ruiz-Sinoga, J.D., Schnabel, S., Senciales-González, J.M., Simonneaux, V., Solé-Benet, A., Taguas, E. V., Taboada-Castro, M.T.M., Taboada-Castro, M.T.M., Todisco, F., Úbeda, X., Varouchakis, E.A., Vericat, D., Wittenberg, L., Zabaleta, A., Zorn, M., 2019. Spatial variability of the relationships of runoff and sediment yield with weather types throughout the Mediterranean basin. J. Hydrol. 571, 390–405. https://doi.org/10.1016/j.jhydrol.2019.01.059

Perg, L.A., Anderson, R.S., Finkel, R.C., 2003. Use of cosmogenic radionuclides as a sediment tracer in the Santa Cruz littoral cell, California, United States, Geology.

Perks, M.T., Warburton, J., Bracken, L.J., Reaney, S.M., Emery, S.B., Hirst, S., 2017. Use of spatially distributed time-integrated sediment sampling networks and distributed fine sediment modelling to inform catchment management. J. Environ. Manage. 202, 469–478. https://doi.org/10.1016/j.jenvman.2017.01.045

Phillips, J.D., 2003. Sources of nonlinearity and complexity in geomorphic systems. Prog. Phys. Geogr. Earth Environ. 27, 1–23. https://doi.org/10.1191/0309133303pp340ra

Phillips, J.D., 2010. Sediment Storage, Sediment Yield, and Time Scales in Landscape Denudation Studies. Geogr. Anal. 18, 161–167. https://doi.org/10.1111/j.1538-4632.1986.tb00089.x

Phillips, J.M., Russell, M.A., Walling, D.E., 2000. Time-integrated sampling of fluvial suspended sediment: A simple methodology for small catchments. Hydrol. Process. 14, 2589–2602. https://doi.org/10.1002/1099-1085(20001015)14:14<2589::AID-HYP94>3.0.CO;2-D

Phillips, J.M., Walling, D.E., 1995. An assessment of the effects of sample collection, storage

and resuspension on the representativeness of measurements of the effective particle size distribution of fluvial suspended sediment. Water Res. 29, 2498–2508. https://doi.org/10.1016/0043-1354(95)00087-2

Pimentel, D., Kounang, N., 1998. Ecology of soil erosion in ecosystems. Ecosystems 1, 416–426. https://doi.org/10.1007/s100219900035

Poesen, J.W.A.W.A., Hooke, J.M.M., 1997. Erosion, flooding and channel management in Mediterranean environments of southern Europe. Prog. Phys. Geogr. 21, 157–199. https://doi.org/10.1177/030913339702100201

Pons, A., Rullan, O., 2014. The expansion of urbanisation in the Balearic Islands (1956-2006). J. Mar. Isl. Cult. https://doi.org/10.1016/j.imic.2014.11.004

Porto, P., Walling, D.E., Callegari, G., 2011. Using 137Cs measurements to establish catchment sediment budgets and explore scale effects. Hydrol. Process. 25, 886–900. https://doi.org/10.1002/hyp.7874

Pulley, S., Collins, A.L., 2018. Tracing catchment fine sediment sources using the new SIFT (SedIment Fingerprinting Tool) open source software. Sci. Total Environ. 635, 838–858. https://doi.org/10.1016/j.scitotenv.2018.04.126

Pulley, S., Foster, I., Antunes, P., 2015. The application of sediment fingerprinting to floodplain and lake sediment cores: assumptions and uncertainties evaluated through case studies in the Nene Basin, UK. J. Soils Sediments 15, 2132–2154. https://doi.org/10.1007/s11368-015-1136-0

Pulley, S., Rowntree, K., 2016. The use of an ordinary colour scanner to fingerprint sediment sources in the South African Karoo. J. Environ. Manage. 165, 253–262. https://doi.org/10.1016/j.jenvman.2015.09.037

Pulley, S., Van der Waal, B., Rowntree, K., Collins, A.L., 2018. Colour as reliable tracer to identify the sources of historically deposited flood bench sediment in the Transkei, South Africa: A comparison with mineral magnetic tracers before and after hydrogen peroxide pre-treatment. Catena 160, 242–251. https://doi.org/10.1016/j.catena.2017.09.018

Ramon, R., Evrard, O., Laceby, J.P., Caner, L., Inda, A. V., Barros, C.A.P. d., Minella, J.P.G., Tiecher, T., 2020. Combining spectroscopy and magnetism with geochemical tracers to improve the discrimination of sediment sources in a homogeneous subtropical catchment. Catena 195, 104800. https://doi.org/10.1016/j.catena.2020.104800

Reiffarth, D.G., Petticrew, E.L., Owens, P.N., Lobb, D.A., 2016. Sources of variability in fatty acid (FA) biomarkers in the application of compound-specific stable isotopes (CSSIs) to soil and sediment fingerprinting and tracing: A review. Sci. Total Environ. 565, 8–27. https://doi.org/10.1016/j.scitotenv.2016.04.137

Rose, L.A., Karwan, D.L., Aufdenkampe, A.K., 2018. Sediment Fingerprinting Suggests Differential Suspended Particulate Matter Formation and Transport Processes Across Hydrologic Regimes. J. Geophys. Res. Biogeosciences 123, 1213–1229. https://doi.org/10.1002/2017JG004210

Rovira, A., Batalla, R.J., 2006. Temporal distribution of suspended sediment transport in a Mediterranean basin: The Lower Tordera (NE SPAIN). Geomorphology 79, 58–71. https://doi.org/10.1016/j.geomorph.2005.09.016

Sala, M., Inbar, M., 1992. Some hydrologic effects of urbanization in Catalan rivers. Catena 19, 363–378. https://doi.org/10.1016/0341-8162(92)90009-Z

Scott, D.F., Van Wyk, D.B., 1990. The effects of wildfire on soil wettability and hydrological behaviour of an afforested catchment. J. Hydrol. 121, 239–256. https://doi.org/10.1016/0022-1694(90)90234-O

Serrat, P., Ludwig, W., 2004. Erosion and fluvial sediment supply in undisturbed and cultivated basins: The case of the Desix and Maury river basins (western Mediterranean area), in: IAHS-AISH Publication.

Shakesby, R.A. a., 2011. Post-wildfire soil erosion in the Mediterranean: Review and future research directions. Earth-Science Rev. 105, 71–100. https://doi.org/10.1016/j.earscirev.2011.01.001

Sherriff, S.C., Rowan, J.S., Fenton, O., Jordan, P., Melland, A.R., Mellander, P.E., Huallacháin, D., 2016. Storm Event Suspended Sediment-Discharge Hysteresis and Controls in Agricultural Watersheds: Implications for Watershed Scale Sediment Management. Environ. Sci. Technol. 50, 1769–1778. https://doi.org/10.1021/acs.est.5b04573

Sivapalan, M., 2005. Pattern, Process and Function: Elements of a Unified Theory of Hydrology at the Catchment Scale, in: Anderson, M. (Ed.), Encyclopedia of Hydrological Sciences. John Wiley & Sons, Ltd, Chichester, UK, pp. 193–219. https://doi.org/10.1002/0470848944.hsa012

Slaymaker, O., 2003. The sediment budget as conceptual framework and management tool, in: Hydrobiologia. https://doi.org/10.1023/A:1025437509525

Smith, H.G., Karam, D.S., Lennard, A.T., 2018. Evaluating tracer selection for catchment sediment fingerprinting. J. Soils Sediments 18, 3005–3019. https://doi.org/10.1007/s11368-018-1990-7

Stock, B.C., Jackson, A.L., Ward, E.J., Parnell, A.C., Phillips, D.L., Semmens, B.X., 2018. Analyzing mixing systems using a new generation of Bayesian tracer mixing models. PeerJ 6, e5096. https://doi.org/10.7717/peerj.5096

Stock, B.C., Semmens, B.X., 2016. Unifying error structures in commonly used biotracer mixing models. Ecology 97, 2562–2569. https://doi.org/10.1002/ecy.1517

Stojković, M., Ilić, A., Prohaska, S., Plavšić, J., 2014. Multi-temporal analysis of mean annual and seasonal stream flow trends, including periodicity and multiple non-linear regression. Water Resour. Manag. 28, 4319–4335. https://doi.org/10.1007/s11269-014-0753-5

Stoof, C.R., Ferreira, A.J.D., Mol, W., Van den Berg, J., De Kort, A., Drooger, S., Slingerland, E.C., Mansholt, A.U., Ferreira, C.S.S., Ritsema, C.J., 2015. Soil surface changes increase runoff and erosion risk after a low-moderate severity fire. Geoderma 239, 58–67. https://doi.org/10.1016/j.geoderma.2014.09.020

Syvitski, J.P.M., 2003. Supply and flux of sediment along hydrological pathways: Research for the 21st century. Glob. Planet. Change 39, 1–11. https://doi.org/10.1016/S0921-8181(03)00008-0

Tomaz, C., Alegria, C., Monteiro, J.M., Teixeira, M.C., 2013. Land cover change and afforestation of marginal and abandoned agricultural land: A 10year analysis in a Mediterranean region. For. Ecol. Manage. 308, 40–49. https://doi.org/10.1016/j.foreco.2013.07.044

Turnbull, L., Wainwright, J., Brazier, R.E., 2008. A conceptual framework for understanding semi-arid land degradation: ecohydrological interactions across multiple-space and time scales. Ecohydrology 1, 23–34. https://doi.org/10.1002/eco.4

Upadhayay, H.R., Lamichhane, S., Bajracharya, R.M., Cornelis, W., Collins, A.L., Boeckx, P., 2020. Sensitivity of source apportionment predicted by a Bayesian tracer mixing model to the inclusion of a sediment connectivity index as an informative prior: Illustration using the Kharka catchment (Nepal). Sci. Total Environ. 713, 136703. https://doi.org/10.1016/j.scitotenv.2020.136703

Vanmaercke, M., Ardizzone, F., Rossi, M., Guzzetti, F., 2017. Exploring the effects of seismicity on landslides and catchment sediment yield: An Italian case study. Geomorphology 278, 171–183. https://doi.org/10.1016/j.geomorph.2016.11.010

Vanmaercke, M., Poesen, J., Maetens, W., de Vente, J., Verstraeten, G., 2011a. Sediment yield as a desertification risk indicator. Sci. Total Environ. 409, 1715–1725. https://doi.org/10.1016/j.scitotenv.2011.01.034

Vanmaercke, M., Poesen, J., Verstraeten, G., de Vente, J., Ocakoglu, F., 2011b. Sediment yield in Europe: Spatial patterns and scale dependency. Geomorphology 130, 142–161. https://doi.org/10.1016/j.geomorph.2011.03.010

Vercruysse, K., Dawson, D.A., Glenis, V., Bertsch, R., Wright, N., Kilsby, C., 2019. Developing spatial prioritization criteria for integrated urban flood management based on a source-to-impact flood analysis. J. Hydrol. 578, 124038. https://doi.org/10.1016/j.jhydrol.2019.124038

Verkaik, I., Vila-Escalé, M., Rieradevall, M., Prat, N., 2013. Seasonal drought plays a stronger role than wildfire in shaping macroinvertebrate communities of Mediterranean streams. Int. Rev. Hydrobiol. 98, 271–283. https://doi.org/10.1002/iroh.201201618

Vörösmarty, C.J., Meybeck, M., Fekete, B., Sharma, K., Green, P., Syvitski, J.P.M., 2003. Anthropogenic sediment retention: Major global impact from registered river impoundments. Glob. Planet. Change 39, 169–190. https://doi.org/10.1016/S0921-8181(03)00023-7

Wainwright, J., 2009. Weathering, Soils, and Slope Processes, in: Woodward, J. (Ed.), The Physical Geography of the Mediterranean. Oxford University Press, Oxford, pp. 169–202. https://doi.org/10.1093/oso/9780199268030.003.0018

Wainwright, J., Turnbull, L., Ibrahim, T.G., Lexartza-Artza, I., Thornton, S.F., Brazier, R.E., 2011. Linking environmental régimes, space and time: Interpretations of structural and functional connectivity. Geomorphology 126, 387–404. https://doi.org/10.1016/j.geomorph.2010.07.027

Wall, G.J., Wilding, L.P., 1976. Mineralogy and Related Parameters of Fluvial Suspended Sediments in Northwestern Ohio. J. Environ. Qual. 5, 168–173. https://doi.org/10.2134/jeq1976.00472425000500020012x

Wallbrink, P.J., Murray, A.S., 1993. Use of fallout radionuclides as indicators of erosion processes. Hydrol. Process. 7, 297–304. https://doi.org/10.1002/hyp.3360070307

Walling, D.E., 1983. The sediment delivery problem. J. Hydrol. 65, 209–237. https://doi.org/10.1016/0022-1694(83)90217-2

Walling, D.E., 1988. Measuring sediment yield from river basins, in: Lal, R. (Ed.), Soil Erosion Research Methods. Soil and Water Conservation Society, USA, pp. 39–73. https://doi.org/10.1201/9780203739358-3

Walling, D.E., 1999. Linking land use, erosion and sediment yields in river basins. Hydrobiologia 410, 223–240. https://doi.org/10.1023/A:1003825813091

Walling, D.E., 2013. The evolution of sediment source fingerprinting investigations in fluvial systems. J. Soils Sediments 13, 1658–1675. https://doi.org/10.1007/s11368-013-0767-2

Walling, D.E., Collins, A.L., 2008. The catchment sediment budget as a management tool, Environmental Science and Policy. Elsevier. https://doi.org/10.1016/j.envsci.2007.10.004

Walling, D.E., Moorehead, P.W., 1989. The particle size characteristics of fluvial suspended sediment: an overview. Hydrobiologia 176–177, 125–149. https://doi.org/10.1007/BF00026549

Walling, D.E., Owens, P.N., Waterfall, B.D., Leeks, G.J.L., Wass, P.D., 2000. The particle size characteristics of fluvial suspended sediment in the Humber and Tweed catchments, UK. Sci. Total Environ. 251–252, 205–222. https://doi.org/10.1016/S0048-9697(00)00384-3

Walling, D.E., Peart, M.R., Oldfield, F., Thompson, R., 1979. Suspended sediment sources identified by magnetic measurements. Nature 281, 110–113. https://doi.org/10.1038/281110a0

Walling, D.E., Woodward, J.C., 1995. Tracing sources of suspended sediment in river basins: a case study of the River Culm, Devon, UK. Mar. Freshw. Res. 46, 327–336. https://doi.org/10.1071/mf9950327

Walling, D.E.E., 2005. Tracing suspended sediment sources in catchments and river systems 344, 159–184.

Wang, G., Mang, S., Cai, H., Liu, S., Zhang, Z., Wang, L., Innes, J.L., 2016. Integrated watershed management: evolution, development and emerging trends. J. For. Res. 27, 967–994. https://doi.org/10.1007/s11676-016-0293-3

Wass, P.D., Leeks, G.J.L., 1999. Suspended sediment fluxes in the Humber catchment, UK. Hydrol. Process. 13, 935–953. https://doi.org/10.1002/(SICI)1099-1085(199905)13:7<935::AID-HYP783>3.0.CO;2-L

Weltje, G.J., Prins, M.A., 2007. Genetically meaningful decomposition of grain-size distributions. Sediment. Geol. 202, 409–424. https://doi.org/10.1016/j.sedgeo.2007.03.007

Williams, G.P.G.., 1989. Sediment concentration versus water discharge during single hydrologic events in rivers. J. Hydrol. 111, 89–106. https://doi.org/10.1016/0022-1694(89)90254-0

Wold, C.N., Hay, W.W., 1990. Estimating ancient sediment fluxes. Am. J. Sci. 290, 1069–1089. https://doi.org/10.2475/ajs.290.9.1069

Yu, L., Oldfield, F., 1989. A multivariate mixing model for identifying sediment source from magnetic measurements. Quat. Res. 32, 168–181. https://doi.org/10.1016/0033-5894(89)90073-2

Yu, L., Oldfield, F., 1993. Quantitative sediment source ascription using magnetic measurements in a reservoir-catchment system near Nijar, S.E. Spain. Earth Surf. Process. Landforms 18, 441–454. https://doi.org/10.1002/esp.3290180506

Zuecco, G., Penna, D., Borga, M., van Meerveld, H.J., 2016. A versatile index to characterize hysteresis between hydrological variables at the runoff event timescale. Hydrol. Process. 30, 1449–1466. https://doi.org/10.1002/hyp.10681

2. Study areas

2.1. Overview

Located in the western Mediterranean Sea, Mallorca is the largest island of the Balearic archipelago with an area of 3620 km^2 (Figure 2.1A). The island's morphological structure was determined by its genesis, generated by the compressive stresses which occurred during Alpine orogeny in the Upper Cretaceous. Materials from the Carboniferous to the Middle Miocene were raised above sea level forming the principal mountainous reliefs, while Pliocene and Quaternary materials filled the distensile trenches of the Central Plain and the south-eastern coast (Álvaro et al., 1989). As a consequence, the island is dominated by a SE to NW horst-graben structure that compose its principal structural units: the Llevant Ranges, the Campos and Manacor basins, the Central Ranges, the Palma, Inca and Sa Pobla basins, and the Tramuntana Range (Figure 2.1B).

This thesis is focused on two small catchments < 5 km^2 (the Sa Font de la Vila and Es Fangar creek catchments) located in the Tramuntana Range. The study areas are representative of the natural and human Mediterranean mountainous landscapes, where the complex reliefs strongly determined human occupation, land uses and land management practices. In addition, the Sa Font de la Vila catchment was affected recurrently by forest fires, including the largest fire registered in the Balearic Islands.

The Tramuntana Range is the most abrupt horst of the island of Mallorca. It is located along the NW coast of the island, in a SE-NW direction (Figure 2.1B). It has a total length of ca. 90 km and a maximum width of ca. 20 km, occupying approximately an area of 1,000 km^2. Its highest point is the Puig Major peak with an altitude of 1,445 m.a.s.l. The Tramuntana Range structure is mainly composed of Mesozoic materials in the form of thrusts on Tertiary deposits. The predominant lithologies were Jurassic micrite limestone's, limestone conglomerates and calcarenites of the Lower Miocene superimposed on clays of the Upper Triassic (Keuper; Figure 2.1C). According to the Emberger classification, the southern part of the Tramuntana Range shows a Mediterranean warm sub-humid climate, while the central and eastern parts were

classified as Mediterranean humid and super-humid (Guijarro, 1986). Average annual rainfall ranges from 1,200 mm yr^{-1} to 700 mm yr^{-1} (Figure 2.1D) with a maximum rainfall in 24 hours for a return period of 25 years from 110mm in the western part to 250 mm in central areas.

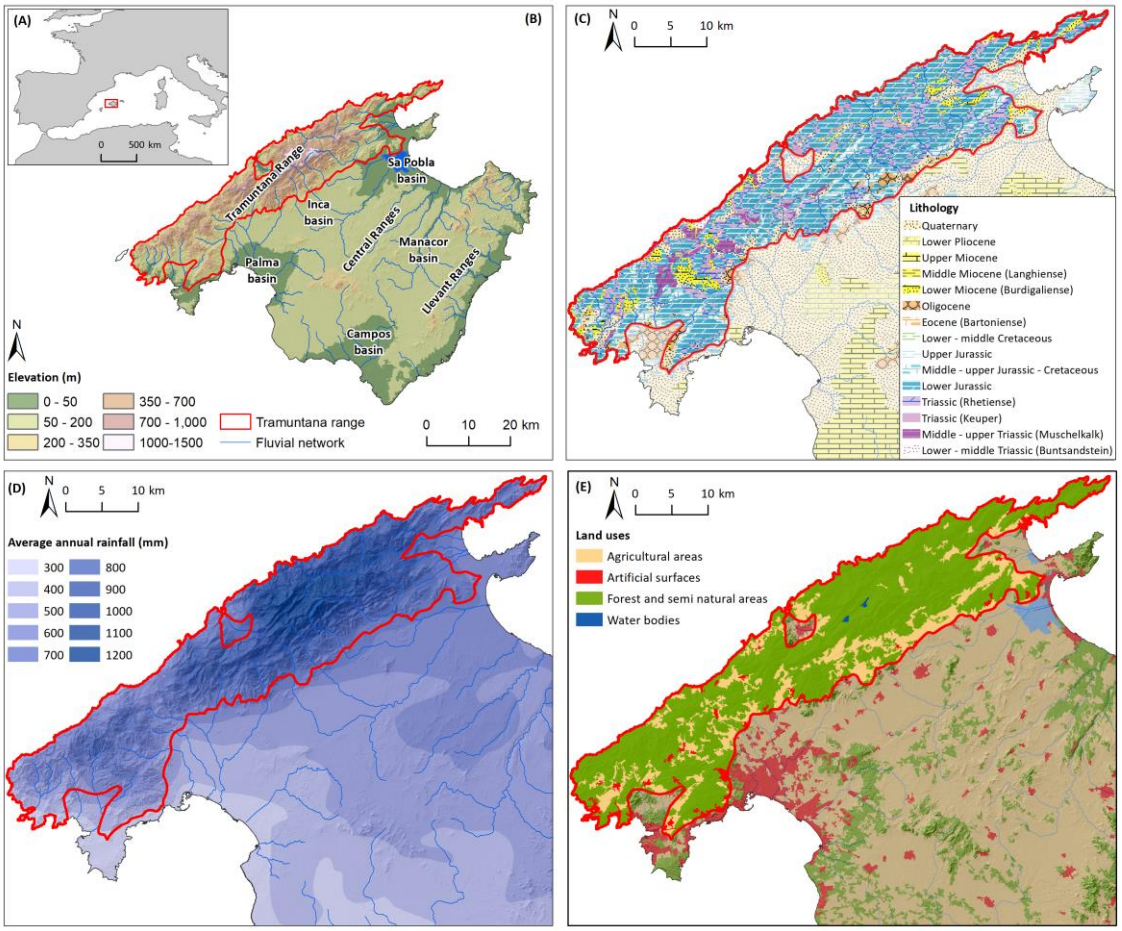

Figure 2.1. (A) Location of Mallorca Island in the Western Mediterranean Sea basin. (B) Physical characteristics of Mallorca Island and Tramuntana Range location (C) Tramnuntana Range lithology (D) rainfall distribution and (E) land use distribution.

The Tramuntana Range was occupied and exploited by humans during centuries. The landscape has been modified for agricultural use through the construction of dry stone agricultural terraces, check dam terraces and other human structures. However, the economic changes which occurred during the second half of the 20th century caused the depopulation of rural areas and a gradual abandonment of an agriculture-based economy. As a consequence, afforestation processes in former croplands caused an increase of the forest area estimated in Mallorca at 79% between 1971 and 2010 (MAGRAMA, 2012). Land use distribution according to Corine Land Cover 2018

(European Evironment Agency-EEA, 2018) were 72% forest and semi natural areas, 23.4% agricultural areas, 3.4% artificial surface and 0.6% water bodies (Figure 2.1E).

2.2. Sa Font de la Vila River catchment

The Sa Font de la Vila River is a Mediterranean catchment of 4.8 km^2 located in the Andratx municipality (western Mallorca, Spain; Figure 2.2A and 2.2B), which is affected by extensive afforestation of former agricultural land and recurrent wildfires. Catchment lithology in bottom valleys consists mainly of Upper Triassic (Keuper) clays and loams on gentle slopes (ca. < 10 degrees). Rhaetian dolomite and Lias limestone predominate in the upper parts with steeper slopes > 30% (Figure 2.2C). Soils are classified as *BK45-2bc*, corresponding to *Calcic Cambisols* (Jahn et al., 2006). The fluvial network consists of two main streams: (a) Sa Coma Freda (east, 2.3 km^2), which has a significant groundwater influence with several karstic springs; and (b) Can Cabrit (west, 2.08 km^2), which is not affected by this groundwater influence due to the reduced presence of impervious materials. In addition, a check-dam was built at Can Cabrit in 2007 (5 m high and 16 m long; Figure 2.2D).

The climate is classified as Mediterranean temperate sub-humid at headwaters and warm sub-humid at the outlet (Emberger climatic classification; Guijarro, 1986). The average temperature is 16.5°C. The mean annual rainfall is 518 mm yr^{-1}, with an inter-annual coefficient of variation of 29%. High-intensity rainstorms with a recurrence period of 10 years may reach 85 mm in 24 hours (1974-2010; data from the B118 S'Alqueria meteorological station of the Spanish State Meteorological Agency (AEMET); Figure 2.2B).

In recent decades, the Sa Font de la Vila catchment has been affected by major wildfires in 1994 and 2013 (Figure 2.2E). Before the 2013 wildfire, the catchment was mainly covered by natural vegetation (84%; Figure 2.2C): 51% forest and 33% scrubland. The rest of the catchment was covered by rain-fed tree crops (12%), rain-fed herbaceous crops (1%) and urban uses (3%). Traditional soil and water conservation structures (i.e., hillslope and valley-bottom terraces) cover 37% of the total surface area (Figure 2.2D).

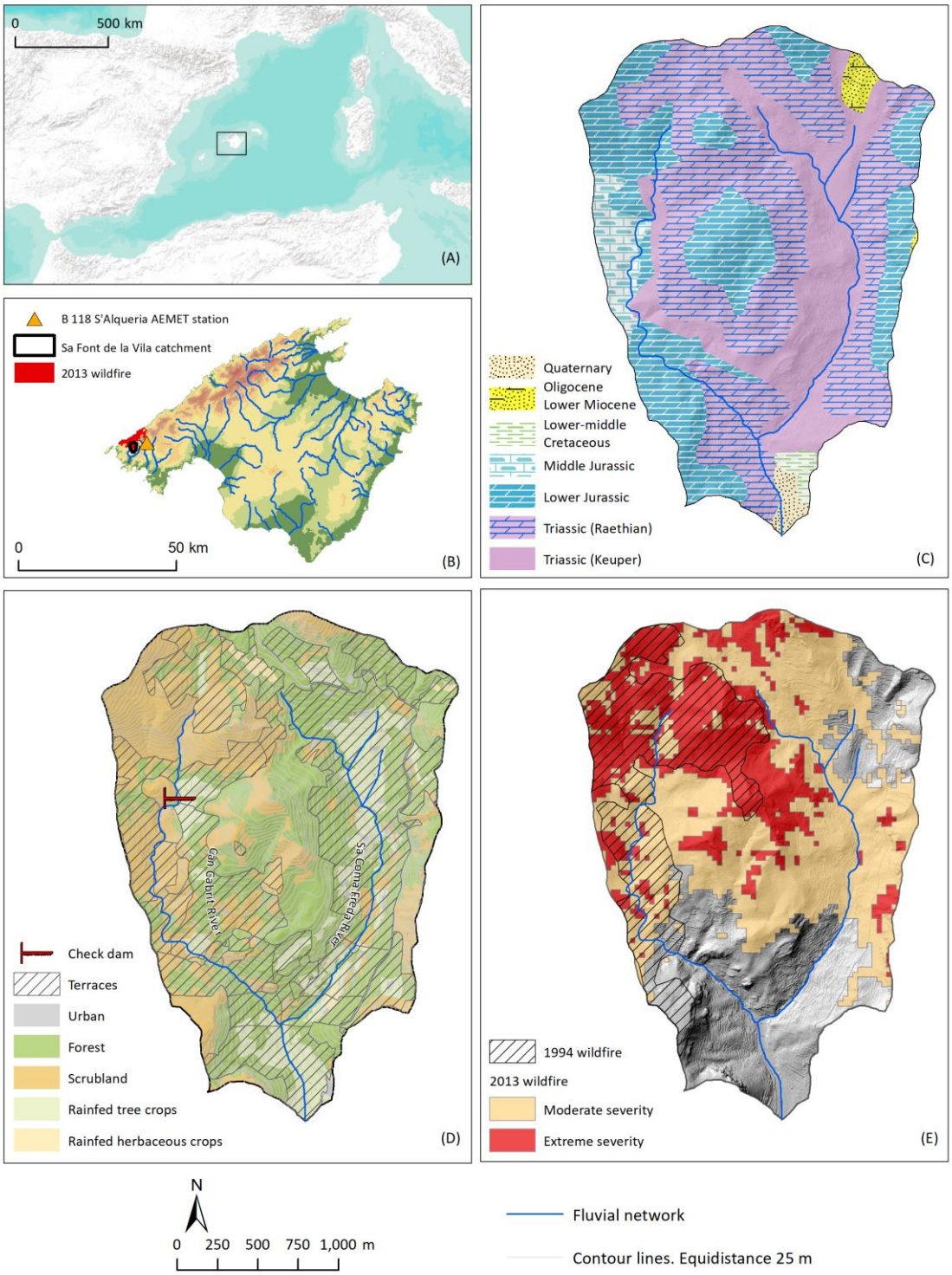

Figure 2.2. Location of the Mallorca Island within the Mediterranean Sea (A); location of the Sa Font de la Vila catchment, the area affected by the July 2013 wildfire, the B'12 S'Alqueria meteorological station and the village of Llucmajor (B); lithology (C) land uses and soil conservation practices (D) of the Sa Font de la Vila catchment (downstream site) and Sa Murtera sub-catchment (upstream site); and 1994 and 2013 wildfire affected areas as well as severity of the 2013 wildfire and 2016 sampling area (E). Channel bank and surface sampling points indicated as blue dots and orange squares, respectively

Its abandonment and degradation, involving the collapse of dry-stone walls, increased the sensitivity of the catchment (Calsamiglia et al., 2017). Collapses were higher on those abandoned terraces affected by recurrent fires due to soil degradation (Lucas-Borja et al., 2018).

The 1994 fire affected 45% of the catchment surface, whereas the 2013 one reached 71% (more than half of it had already been burned in 1994). A severity assessment with the Normalized Burn Ratio (Escuin et al., 2008) and Landsat 8 images for the 2013 wildfire assigned high and moderate severity to 24% and 47% of the catchment, respectively (Bauzà, 2014. Figure 2.2E). In addition, after the 2013 wildfire the Balearic Islands Department of the Environment (Conselleria de Medi Ambient, Agricultura i Pesca) implemented a series of post-fire strategies to prevent soil loss and degradation, which included mulching, tree planting and the creation of log barriers with dead biomass.

2.3. Es Fangar Creek catchment

Es Fangar catchment (3.4 km^2; Figure 2.3A and B) is located at the north-east side of the Tramuntana mountain range in Mallorca (Spain). Altitudes range between 404 m.a.s.l. and 72 m.a.s.l. with an average slope of 26%. The lithology is composed of massive calcareous and dolomite materials from lower Jurassic and dolomite and marls formations from the Triassic (Rhaetian) in the upper parts, being Jurassic and Cretaceous marl-limestone's in the valley bottoms (Figure 2.3C). As a consequence of its geologic structure, and the high water availability at field capacity of the valley soils, the catchment has had an intensive agricultural activity in the past. The stream network is natural at the upper parts, however, at the valley bottom the main channel was diverted and constricted by dry stone walls for better agricultural land exploitation. Check-dam and agricultural terraces were built to control torrential floods and avoid soil erosion (Figure 2.3C and D). In addition, subsurface tile drains were built in crop lands to promote drainage, avoiding soil saturation during the wet season. 16% of the catchment is occupied by soil and water conservation structures, which means 32.4 km of dry stone walls. Nowadays, land use occupation is forest (47%), rainfed herbaceous crops fields (36%) and scrubland (17%).

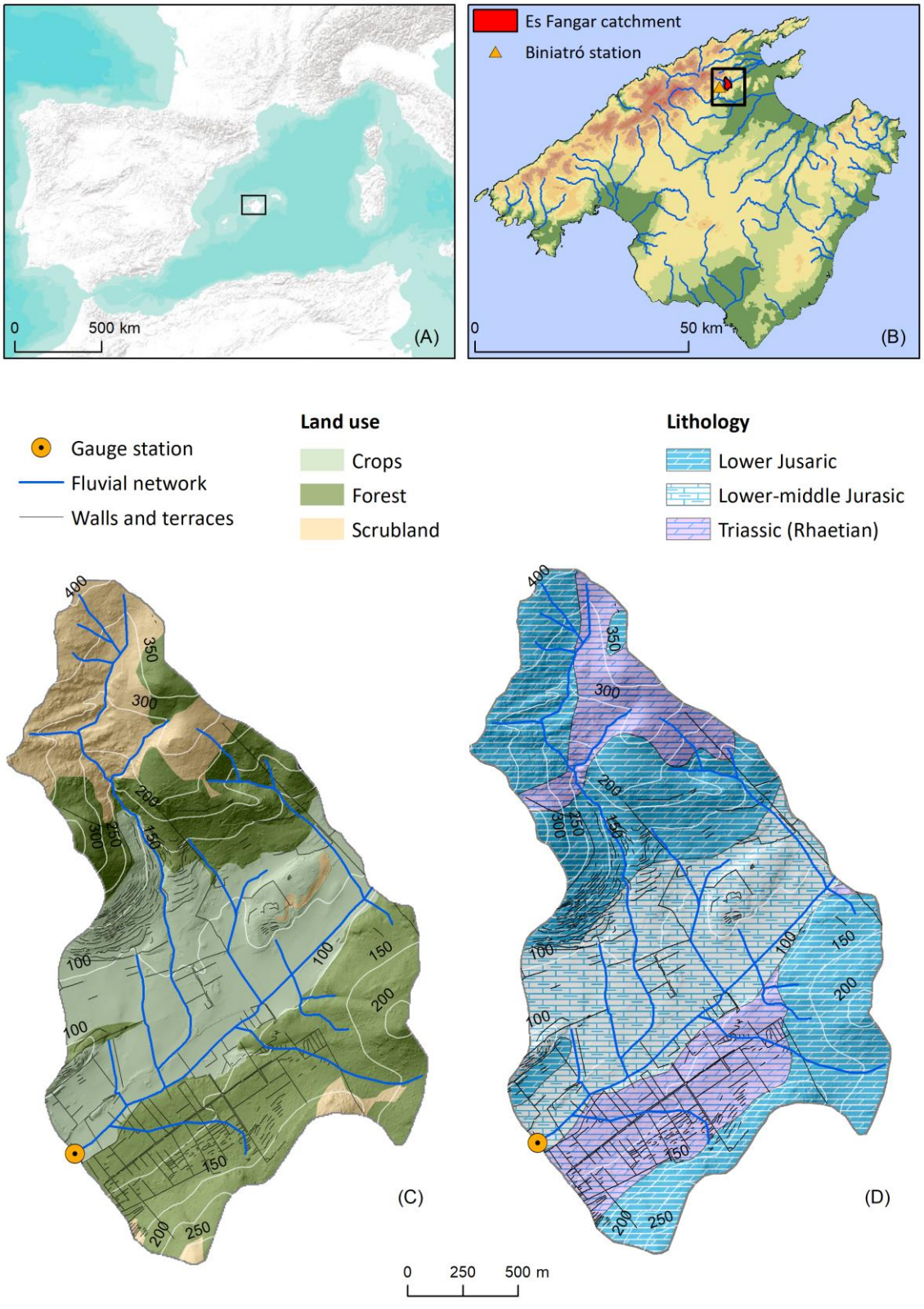

Figure 2.3. (A) Map showing the location of Mallorca in the Western Mediterranean. (B) Location of Es Fangar catchment within Mallorca island. Drainage network and terraced areas over (C) land use and (D) lithology maps.

Since the 1950s, as a consequence of an economic transition from the primary to the tertiary sector, the agricultural area was reduced by a ca. 17%. Afforestation processes have occurred in abandoned fields currently being covered by forests. According to the Emberger classification, the climate is Mediterranean temperate sub-humid (Guijarro, 1986). Mean annual rainfall is 926 mm yr^{-1} (1964-2017, Biniatró AEMET station, 1.1 km west from the study area) with a 23% coefficient of variation and the average annual temperature is 15.7 °C. Rainfall amount estimation of 180 mm in 24 hours in a recurrence period of 25 years. The hydrological regime is categorized as intermittent flashy (49% of zero days; Fortesa et al., 2020a). The annual runoff coefficient ranged from 2.9% to 14.2% (average of 10.4%) and quick flow contribution from 9.9% to 45% (average of 33%) illustrating a huge intra-annual variability of the rainfall-runoff relationship (Fortesa et al., 2020a). 80% of the sediment load is exported during autumn and winter, with an annual average sediment yield of 5.38 t km^{-2} y^{-1}.

2.4. References

Alvaro, M., Barnolas, A., Cabra, P., Comas-rengifo, M.J., Fernández-López, R., Goy, A., Del Olmo, P., Ramírez Del Pozo, J., Simo, A., Ureta, S., 1989. El Jurásico de Mallorca (Islas Baleares). Cuad. Geol. Ibéric 13, 67–120.

Bauzà, J., 2014. Els grans incendis forestals a les Illes Balears: una resposta des de la teledetecció. Bachelor Thesis. University of the Balearic Islands, Palma, Spain.

Escuin, S., Navarro, R., Fernández, P., 2008. Fire severity assessment by using NBR (Normalized Burn Ratio) and NDVI (Normalized Difference Vegetation Index) derived from LANDSAT TM/ETM images. Int. J. Remote Sens. 29, 1053–1073. https://doi.org/10.1080/01431160701281072

European Evironment Agency (EEA), 2018. Copernicus Land Monitoring Service. Eur. Union.

Fortesa, J., Latron, J., García-Comendador, J., Company, J., Estrany, J., 2020a. Runoff and soil moisture as driving factors in suspended sediment transport of a small mid-mountain Mediterranean catchment. Geomorphology 368, 107349. https://doi.org/10.1016/j.geomorph.2020.107349

Fortesa, J., Latron, J., García-Comendador, J., Tomàs-Burguera, M., Company, J., Calsamiglia, A., Estrany, J., 2020b. Multiple temporal scales assessment in the hydrological response of small mediterranean-climate catchments. Water 12, 299. https://doi.org/10.3390/w12010299

Guijarro, J.A., 1986. Contribucion a la bioclimatologia de Baleares. PhD Thesis. University of the Balearic Islands, Palma, Spain.

Jahn, R., Blume, H.P., Asio, V.B., Spaargaren, O., Schad, P., 2006. Guidelines for soil description, FAO. ed. Rome.

Ministerio de Agricultura, A. y M.A. (MAGRAMA), 2012. Cuarto Inventario Forestal Nacional. Madrid.

3. Methodology

3.1. Overview

In this chapter it is presented a summary of the main methods used in Chapters 4, 5, 6, 7 and 8. It is possible to divide in three different groups the principal methodologies used to reach the scientific objectives proposed (Figure 3.1). First group, continuous water and sediment monitoring (Figure 3.1A), encompass all methods related to hydro-sedimentary data acquisition and treatment, hysteretic loop analysis and detection of the main driving forces that control suspended sediment transport on the study areas (see section 3.2). Second and third groups are related with Sediment source fingerprinting. Within the second group are listed (Figure 3.1B) all steps followed to recognize main sediment sources in the study areas, including different source categories consideration, tracer's sets, tracer accuracy tests and statistical apportion models (see Chapter 3.3). Finally, the third group (Figure 3.1C) explain the methodology followed in Chapter 8 to perform the experiment on sediment properties conservative behaviour (see section 3.4).

3.2. Continuous water and sediment monitoring

Gauge stations were installed in the outlets of the two study areas (i.e. Sa Font de la Vila and Es Fangar catchments) to continuously monitor water and suspended sediment fluxes (Figure 3.2 and 3.3).

In Sa Font de la Vila catchment (Chapter 4, 5 and 6), a continuous water and sediment yield monitoring programme was implemented by instrumenting two nested gauging stations (Figure 3.2), Sa Murtera (an upstream sub-catchment; 1.1 km^2) and Sa Font de la Vila (closing 4.8 km^2). Sa Murtera gauging station is located in the northeast headwater area of the Sa Font de la Vila catchment (Figure 3.2A). The monitoring station was installed in a place where channel banks consist of dry-stone walls working as a control section for higher discharges and another smaller section built for measuring base flow.

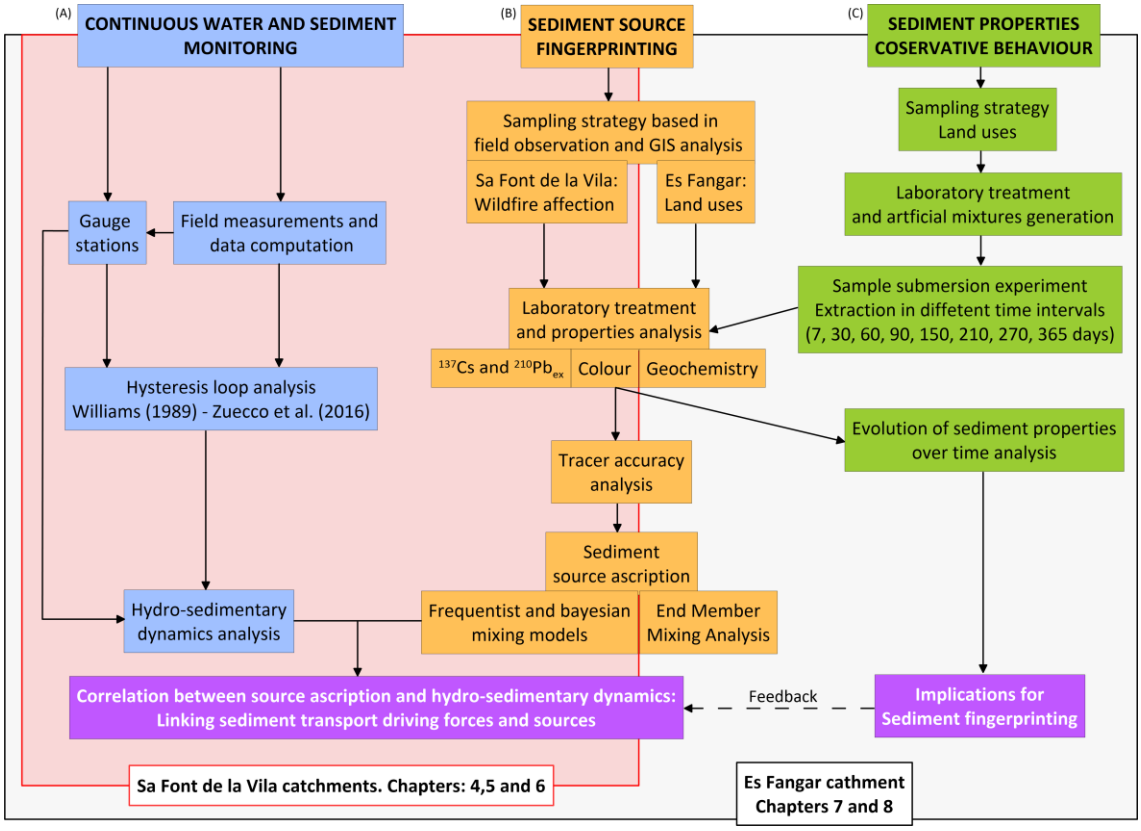

Figure 3.1. Methodological workflow encompassing main methodologies used for (A) continuous monitoring of water and sediment, (b) Sediment source Fingerprinting and (C) experiment on the conservative behaviour of sediment properties. Inside the red square are listed the methods applied in Sa Font the la Vila catchment and inside the black square the methods applied in Es Fangar catchment.

The gauging station was equipped with a Campbell Scientific CR200X data logger that stored the average values of water surface level and turbidity, based on 1-minute readings at 15-minute intervals collected by a Campbell Scientific CS451-L pressure probe and a OBS-3+ turbidimeter with a double measurement range of 0-1,000/1,000-4,000 NTU. Additionally, a rising-stage sampler modified from Schick (1967), with seven sampling bottles, was installed to provide more information on suspended sediment concentrations (SSCs). There is a 12 cm height gap between each bottle, totalling a 100 cm stage, with the first bottle located 21 cm above the riverbed. Additionally, a Casella tipping bucket rain gauge was installed.

The Sa Font de la Vila catchment gauging station was also installed in a place where channel banks consist of dry-stone walls working as a control section (Figure 3.2B). The instruments were the same as for the Sa Murtera gauging station. However, the rising-stage sampler was set up with twelve bottles, totalling a 200 cm stage.

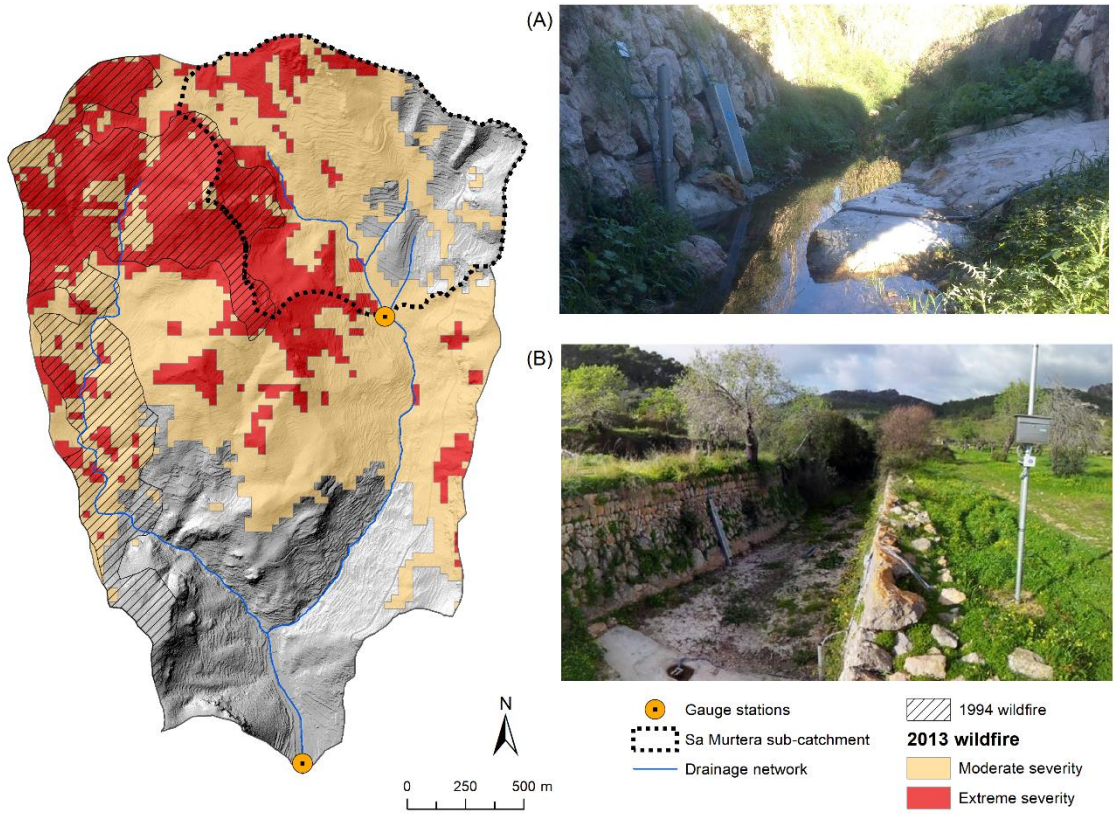

Figure 3.2. Left, Map of Sa Font the la Vila catchment with the area affected by the July 2013 wildfire, the delimitation of Sa Murtera sub-catchment and the gauge stations locations. (A) Upstream view of Sa Murtera cross section and gauge station. (B) Upstream view of Sa Font de la Vila cross section and gauge station.

In Es Fangar Creek catchment, a gauging station was installed in 2012 to continuously monitor water and suspended sediment fluxes (Figure 3.3). The station was equipped with a Campbell CS451 pressure probe and an OBS-3+ turbidimeter with a double measurement range of 0-1,000/1,000-4,000 NTU**.** Campbell CR200X logger stored 15-minutes average values of water stage and turbidity (based on 1-minute readings). In addition, in October 2014 a tipping bucket pluviometer was installed at 500 m.a.s.l. and located ca. 2.5 km away from the Es Fangar gauging station. The rain gauge was installed 1 m above the ground and connected to a HOBO Pendant G Data Logger - UA-004-64 recording rainfall at 0.2 mm resolution.

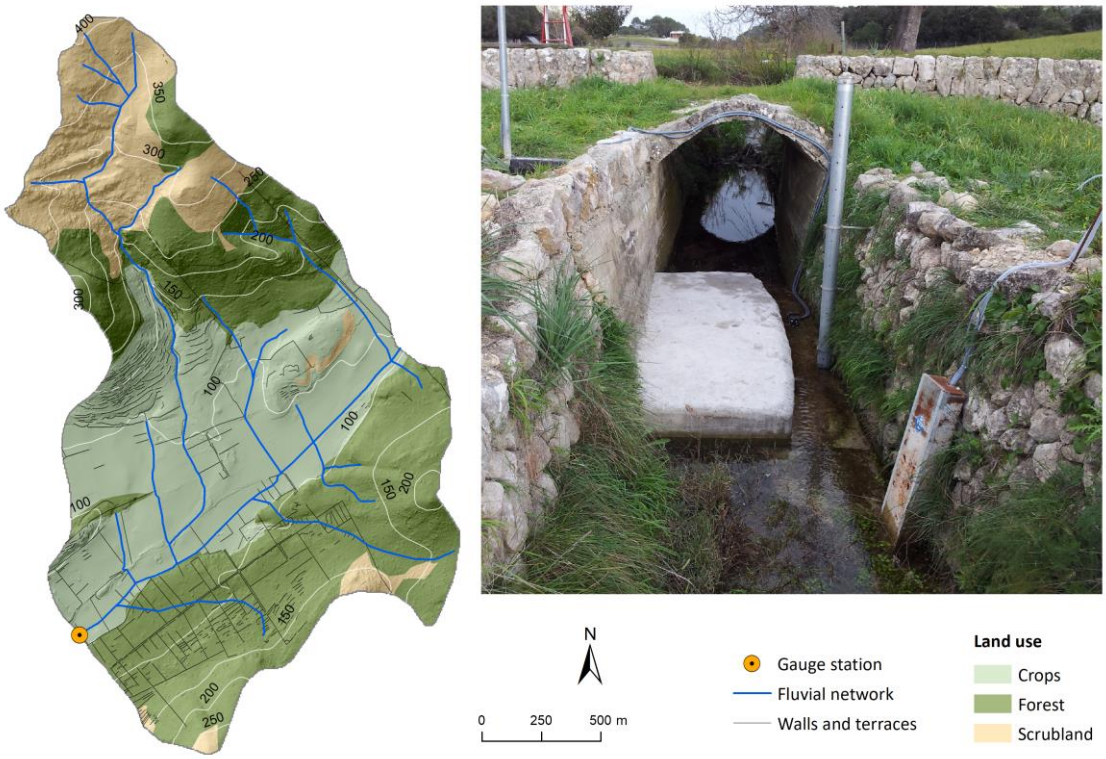

Figure 3.3. Left, Map of Es Fangar catchment with main land uses and the gauge stations location. Right, Upstream view Es Fangar cross section and gauge station.

3.2.1. Field measurements and data computation

In the three gauge stations, stream discharge was measured by an OTT MF pro inductive magnetic flow meter, with a measuring range of 0 to 6 m s^{-1} ± 2% accuracy, to develop and fit stage/discharge rating curves.

Manual depth-integrated suspended sediment samples were consistently collected (n= 55) during storm events and low flows. Samples were collected at the same sections on which turbidity probes and rising-stage samplers were installed. All the water samples were filtered by 0.45 µm cellulose esters; the filters were subsequently dried at room temperature and weighed on high-precision scales to determine the suspended sediment concentrations.

Turbidity probes were calibrated with commercial turbidity standards to check their long-term stability. The turbidity data were converted to a continuous record of SSCs by a site-specific concentration/turbidity calibration relationship. The SSCs used for calibration were measured in samples collected both manually and by rising-stage

samplers. Suspended sediment loads were calculated by combining the records of SSCs provided by the turbidity sensors with the continuous records of water discharge.

The kinetic rainfall energy was calculated by the equation described by Brown and Foster (1987):

$$e = 0.29[1 - 0.72\,exp(-0.05i)]$$

where *e* is the kinetic energy of 1 mm of rainfall expressed in Mj ha^{-1} mm, and i is the rainfall intensity expressed in mm hr^{-1}. The rainfall erosivity (R) was determined by multiplying the kinetic energy of each event and the maximum intensity attained in 30 minutes (I30). The results were expressed in MJ mm ha^{-1} h^{-1}.

$$eI_{30} = R$$

Finally, the spatio-temporal relationship between discharge and sediment transport at the event scale was analysed by means of hysteresis loops applying analysis applying the classification developed by Williams in Chapter 4 (Williams, 1989) and the *h* index developed by Zuecco et al. (2016) in Chapter 7.

3.3. Sediment source fingerprinting

3.3.1. Soil and sediment sampling

A stratified sampling strategy after field observation and GIS analysis was planned in the Sa Font de la Vila and Es Fangar catchments to collect soil samples from main sediment sources.

In Sa Font de la Vila source categories were burned surface soil surface (n= 31), unburned surface soil (n= 9) and channel banks (n= 20). However, in Es Fangar catchment main land uses were considered as main sources (i.e. forest (n= 5), crop (n= 6), scrubland soils (n=5) and channel banks (n= 16)). All samples were collected in areas with visual evidence of erosion. Surface soil samples were composed by four subsamples (0-2 cm depth) collected inside a ca. 3 m radius circular area in order to

include the spatial variability of the soil properties, whereas each channel bank sample was composed by three subsamples collected in a 10 m transect.

In addition, five bed sediment samples were collected along the main channel bed stem only in Sa Font de la Vila. The samples were collected a week after of high intensity storm occurred in 29th October 2013, considering the topographical characteristics of the main stem (see longitudinal profile of inlet in Figure 5.2, Chapter 5) and the wildfire's effects. During the bed sediment sampling campaign all main system channel was completely dry. Each sample consisted of two integrated subsamples, collected in the most superficial layer (ca. 5 mm) inside a heterogeneous circular area, depending on the surface of each pool.

Two parallel time integrated sediment trap samplers (Phillips et al., 2000) were installed over the channel bed in every gauge station (i.e. Sa Font de la Vila, Sa Murtera and Es Fangar) to collect time integrated suspended sediment samples, n= 4 in Sa Murtera, n= 5 in Sa Font de la Vila and n= 13 in Es Fangar.

3.3.2. Laboratory treatment and analysis

Soil and sediment samples were oven-dried at 40°C, disaggregated using a pestle and a mortar and sieved to <63 μm to minimize the differences in particle size composition between source/target samples (Walling et al., 1993). The particle size distribution and the specific surface area in source and sediment samples were determined using a Malvern Mastersizer 2000 (Chapters 5 and 6) and 3000 (Chapters 7 and 8). The Shapiro-Wilk ($p < 0.05$) normality test, Mann-Whitney *U* test and the Wilcoxon signed-rank test were applied to determine the particle size distribution similarity between each source group (soil samples) and target samples (bed and suspended sediment samples).

After the pre-treatment, each sample was closed tightly and left for more than 21 days before activity measurement, to ensure that secular equilibrium had been reached. The atmospherically-derived $^{210}Pb_{ex}$ concentration was determined by subtracting the ^{226}Ra-supported ^{210}Pb concentration from the total ^{210}Pb concentration, as $[^{210}Pb_{ex}] = [^{210}Pb] - 0.8\,[^{226}Ra]$, including a commonly used value for the reduction factor to take into account the radon emanation coefficient of soils. The ^{137}Cs, ^{226}Ra (via ^{214}Bi at 609.3 keV) and total ^{210}Pb

activity concentrations (Bq kg^{-1}) were measured by gamma spectrometry at the *Environmental Radioactivity Laboratory* of the University of the Balearic Islands using a high-purity coaxial intrinsic germanium (HPGe) detector, cooled by liquid nitrogen, shielded by 15 cm of low-background iron and equipped with high-voltage power supply, preamplifier, amplifier and multichannel analyser as an interface to a PC-type computer. The system was calibrated by a soil standard containing ^{210}Pb provided by Exeter University and a CG2-standard (^{241}Am, ^{109}Cd, ^{139}Ce, ^{57}Co, ^{60}Co, ^{137}Cs, ^{113}Sn, ^{85}Sr and ^{88}Y) prepared and certified by the *Centre for Energy, Environment and Technology Research* (CIEMAT, the Spanish National reference for nuclear physics magnitudes), thus achieving a useful energy range from 25 keV to 10 MeV with a resolution of 5 keV and a detection efficiency of 0.99% for ^{137}Cs, 1.10% for ^{226}Ra and 4.63% for ^{210}Pb. The minimum detectable activities have been of the order of 1 Bq kg^{-1} for ^{137}Cs, 2 Bq kg^{-1} for ^{226}Ra and 12 Bq kg^{-1} for ^{210}Pb, and the uncertainties of the measurements less than 10%. As the same geometry was used for the standards and samples (less than 100 g in a vessel wide enough to assume that there are no self-absorption effects), there was no need to apply any correction factor.

Total carbon (C) and nitrogen (N) were measured by high-temperature combustion using a TruSpec CHNS, LECO. Diffuse reflectance was measured in a dark room by a spectroradiometer (ASD FieldSpect-II) at 1 µm steps over the 400-2500 µm range. The spectrometer was located in a tripod perpendicular to a flat surface, at 10 cm from the reference standard panel of known reflectivity (Spectralon). The soil and sediment samples were placed in transparent P.V.C. round petri dishes (4.7 cm diameter; Pall Corporation) and carefully smoothed with a spatula to minimize micro shadow effects due to surface roughness. The samples and the Spectralon were illuminated at an angle of 30º by a 50-w quartz halogen lamp placed at ca. 30 cm of distance. Following the International Commission on Illumination (CIE, 1931), CIE xyY colour coefficients were computed (i.e. cie x, cie y and cie yy) from the spectra reflectance measurements and the RGB colour values (i.e. red, green and blue). Then, the ColoSol software, developed by Viscarra Rossel et al. (2006), was used to estimate the Munsell HVC (i.e. Munsell H, Munsell V and Munsell C), CIE XYZ (i.e. cie X, cie Y and cie Z), CIE LAB (cie L, cie a* and cie b*), CIELUB (i.e. cie L, cie u* and cie v*), CIELHC (i.e. cie L, cie H and cie C) and decorrelated RGB (i.e. HRGB, IRGB and SRGB) colour parameters, as well as the redness index (i.e. RI) and Helmholtz chromaticity coordinates (i.e. DW nm, Pe %).

In addition, samples were placed in transparent plastic bags (7 * 5 cm) and scanned with an office scanner (Konika Minolta bizhub C554e; e.g. Krein et al., 2003; Pulley and Rowntree, 2016). The instrument was not calibrated. Red, green and blue colour parameters (i.e. RGB model) were extracted from the scanned images using *GIMP 2* open-source image-editing software. Then, the procedure using ColoSol software described in the previous paragraph was applied to convert the red, green and blue into other colour parameters.

Samples were digested according to the microwave digestion USEPA 3051A method, as follows: Pulverized soil samples (0.5 g) were transferred into polytetrafluoroethylene tubes, where 9 ml of HNO_3 and 3 ml of HCl, of high analytical purity, were added. Samples were placed in a microwave oven (Multiwave GO, Anton Paar, Austria) for 5 minutes on the temperature ramp, the necessary time to reach 175 °C; then this temperature was maintained for an additional 10 minutes. After digestion, all extracts were transferred to 100 ml flasks, filling with ultrapure water (Millipore Direct-Q System) and were filtered through 0,45 µm nylon filters (Labbox Labware, S.L). High-purity acids were used in the analyses (PamReac ApplyChem, SLU). Glassware was cleaned and decontaminated in a 10% nitric acid solution for 24 hours and then rinsed with distilled water. Calibration curves for metals determination were prepared from standard 1,000 mg l^{-1} (Sharlau, Spain). The concentrations of metals in the extracts were determined by ICP-AES (DV Optima5300, Perkin Elmer®, Inc.) equipped with a GemCone pneumatic nebulizer for viscous solutions and solutions with high content of dissolved solids (Waltham, MA, USA).

3.3.3. Particle size correction

Particle size can affect tracer concentrations on soil and sediment samples (Laceby et al., 2017). For ^{137}Cs and $^{210}Pb_{ex}$, higher activity concentrations were observed in the fine particle size fractions (He and Walling, 1996) due to the increasing of the specific surface area (hereafter SSA, m^2 g^{-1}) in these fractions (Horowitz, 1991; Rawlins et al., 2010). In Chapter 5, to minimize the possible element concentration variations generated as a result of particle-size distribution between source and target sediment samples, size fractionation to 63 µm was combined with correction procedures.

Particle-size correction factor applied in Chapter 5 was:

$$C_c = \left(\frac{S_x}{S_s}\right) C$$

where C is the measured mean property concentration in source material, C_C the property concentration corrected for particle size using SSA, S_x the SSA of suspended or deposited sediment collected at each location x, and S_S is the mean SSA of the source to be corrected. Accordingly, the particle-size correction factor was applied to those source sample groups that showed significant statistical differences with each other and with the targeted bed sediments, to avoid errors in tracer concentrations caused by the differential tracer adsorption of the finest particles (Smith and Blake, 2014).

3.3.4. Tracers accuracy

Artificial mixtures were made from 2, 3 and 4 different source samples (Chapter 6 and 7). In addition, and to investigate ash influence on the colour parameters in Chapter 6, 18 artificial samples were created mixing suspended sediment and ash (black and grey) in different proportions. The ash proportion was gradually modified from 10% to 90% to observe the influence of ash on sediment colour variation.

The individual accuracy and linear additivity behaviour of some tracers were assessed by comparing measured values and predicted values by means of a mass balance approach in artificial mixtures (i.e. tracer values in the mixture are equal to the sum of contributions from each artificially mixed sample; Chapter 6 and 7).

Kruskal-Wallis H tests were performed to assess source discrimination potential of the selected tracer's. Discriminant Function Analysis (DFA) checked the discriminatory potential of each tracer group (taking selected tracers as independent variables) and calculated the percentage of correctly classified samples (leave-on-out cross-validation).

Range tests were used to exclude potentially non-conservative tracers in each individual suspended sediment sample. Therefore, the tracers in suspended sediment

and artificial mixtures that showed values outside minimum and maximum source range values were discarded.

3.3.5. Source apportionment of sediment sources

The relative contributions of the different sediment sources were determined by using different methodologies as shown in the different chapters.

In Chapter 5, it was used a frequentist multivariate mixing model proposed by Collins et al. (1997). The model solves a linear equations system, based in a conservative mass balance, multiplying different proportions of each of the sources and the sum between them. Results always reach a hypothetical sample that totals 100%. The procedure iterates a defined number of times until the options that are closest to the proportion of the target sample are determined.

Robustness of the solutions were assessed by a mean goodness of fit (*GOF*, modified from Motha et al. 2003):

$$GOF = 1 - \left\langle \frac{1}{n} \times \sum_{i=1}^{n} \left| b_i - \sum_{j=1}^{m} (a_{i,j} \cdot x_j) \right| / b_i \right\rangle$$

where b_i is the value of tracer property i (i = 1 to n) in the bed sediment sample, $a_{i,j}$ is the value of tracer property i in source type j (j = 1 to m), x_j is the unknown relative contribution of source type j to the bed sediment sample, m is the number of source types, and n is the number of tracer properties.

In Chapters 6 and 7 the MixSIAR Bayesian tracer mixing model framework (Stock et al., 2018), implemented by Stock and Semmens (2016) as an open-source R package, was used to estimate the relative contribution of each source to the suspended sediment samples and the artificial mixtures.

The fundamental mixing equation of a mixing model is:

$$b_i = \sum_{j=i}^{m} w_j \cdot a_{i,j}$$

where b_i is the tracer property i (i = 1 to n) measured in a suspended sediment sample, $a_{i,j}$ is the value of the tracer property i in each source sample j (j = 1 to m), w_j is the unknown relative contribution of each source j to the suspended sediment sample. MixSIAR accounts for variability in the source and mixture tracer data with the ability to incorporate covariance data to explain variability in the mixture proportions via fixed and random effects (Stock and Semmens, 2016; Stock et al., 2018). This is especially useful in this study because of the collinearity between colour parameters of the different chromaticity coordinates. Hence, a discriminant function was not used to select an optimum group of tracers, as weak tracers can only improve model representation. MixSIAR was formulated by using sediment type as a factor and an uninformative prior (Blake et al., 2018). The Markov Chain Monte Carlo parameters were set as very long: chain length = 1,000,000, burn = 700,000, thin = 300, chains = 3. Convergence of the models was evaluated by the Gelman-Rubin diagnosis.

Finally, the End Member Mixing Analysis (EMMA) approach (Christophersen and Hooper, 1992; Hooper, 2003) was applied in Chapter 7. Source categories were considered as end members with a fixed composition, conservative and distinguishable between them, while sediment samples were a mixture of these end members. We apply the diagnostic tools described by Hooper (2003). First, a bi-variable scatter plots were performed to identify if the tracers behave linearly conservative in the sediment samples. The tracers suggested linearly conservative mixing when had at least a linear trend of "$r^2 > 0.5$, p-value <0.01" with at least one of the other tracers used (James and Roulet, 2006). Then, a principal component analysis (PCA) was performed on the standardized values of the correlation matrix. The values were standardized by subtracting the average concentration of each tracer and dividing it by its standard deviation. Residuals were defined subtracting the original value from its orthogonal projection.

3.3.6. Experiment on conservative behaviour of sediment properties

In Chapter 8, twenty-seven representative samples of potential sediment sources were introduced within the channel of Es Fangar catchment during a whole year to investigate the conservative behaviour of sediment properties (i.e. total C, N, S, ^{137}Cs, $^{210}Pb_{ex}$, As, Ba, Cd, Co, Cr, Cu, Mn, Mo, Ni, Pb, Zn, Na, Fe, Ca, K and Mg and colour properties)

Samples were introduced in 5*7 cm white polyamide bag with a 25 µm diameter mesh and were sealed using cable ties. Sealed samples were placed inside a piece of the same mesh and were sealed again with cable ties. The double layer of polyamide mesh allowed water to flow avoiding an excessive material loss.

Samples were placed near the gauging station that close Es Fangar creek catchment (Figure 3.3). In this point the channel has a cross-section with a rectangular broad-crested weir for low water stages (see dimensions in Figure 8.2E and F, Chapter 8). Samples were located 70 cm downstream from the wide-crested weir concrete structure. Eight iron bars (70 cm each) were nailed in to the channel bed (ca. 30 cm) and samples were fixed to the metal bars using cable ties. In addition, four samples, were introduced inside a time-integrated sediment sampler (Phillips et al., 2000) fixed at 5 cm from the channel bed (Figure 8.2C, Chapter 8). After that, eight time intervals were stablished to collect the samples throughout the year (i.e. 7, 30, 60, 90, 150, 210, 270, 365 days). Sample properties and analysis were exposed in section 3.3.2. laboratory treatment and analysis.

Coefficients of variation expressed in % (i.e. dividing the sample standard deviation by the mean and multiplying it by 100) were calculated for all soil properties considered. Thus, the relative dispersion of every soil parameter data set can be determined and compared with data sets belonging to different soil parameters.

Coefficient of variation (CV) was calculated to measure samples time (samples introduced within the channel in different time intervals) and spatial variability. Time CV was also divided in four time intervals. The time intervals considered were the following: initial submersion (i.e. 0- days), the period with constant flow (wet period,

7-90 days), the period without flow (dry period, 150-270 days) and the whole year. To identify the spatial variability of the different soil parameters within the catchment, it has been used data from forest (n= 6), crop (n= 5) and scrubland (n= 5) source samples from Chapter 7. In addition, a Pearson and spearman correlation coefficients were performed to observe correlations between the different soil properties and grain size (expressed as SSA; m^2 kg^{-1}), and between soil properties and total C content in percentage, as an approximation to organic matter content.

3.4. References

Blake, W.H., Boeckx, P., Stock, B.C., Smith, H.G., Bodé, S., Upadhayay, H.R., Gaspar, L., Goddard, R., Lennard, A.T., Lizaga, I., Lobb, D.A., Owens, P.N., Petticrew, E.L., Kuzyk, Z.Z.A., Gari, B.D., Munishi, L., Mtei, K., Nebiyu, A., Mabit, L., Navas, A., Semmens, B.X., 2018. A deconvolutional Bayesian mixing model approach for river basin sediment source apportionment. Sci. Rep. 8, 1–12. https://doi.org/10.1038/s41598-018-30905-9

Brown, L.C., Foster, G.R., 1987. STORM EROSIVITY USING IDEALIZED INTENSITY DISTRIBUTIONS. Trans. Am. Soc. Agric. Eng. 30, 379–386. https://doi.org/10.13031/2013.31957

Christophersen, N., Hooper, R.P., 1992. Multivariate analysis of stream water chemical data: The use of principal components analysis for the end-member mixing problem. Water Resour. Res. 28, 99–107. https://doi.org/10.1029/91WR02518

Collins, A.L.L., Walling, D.E.E., Leeks, G.J.L.J.L., 1997. Source type ascription for fluvial suspended sediment based on a quantitative composite fingerprinting technique. Catena 29, 1–27. https://doi.org/10.1016/S0341-8162(96)00064-1

He, Q., Walling, D.E., 1996. Interpreting particle size effects in the adsorption of ^{137}Cs and unsupported ^{210}Pb by mineral soils and sediments. J. Environ. Radioact. 30, 117–137. https://doi.org/10.1016/0265-931X(96)89275-7

Hooper, R.P., 2003. Diagnostic tools for mixing models of stream water chemistry. Water Resour. Res. 39, 1055. https://doi.org/10.1029/2002WR001528

Horowitz, A.J., 1991. A Primer on Sediment-Trace Element Chemistry, 2nd. Edition, Open-File Report. https://doi.org/10.3133/OFR9176

James, A.L., Roulet, N.T., 2006. Investigating the applicability of end-member mixing analysis (EMMA) across scale: A study of eight small, nested catchments in a temperate forested watershed. Water Resour. Res. 42, W08434. https://doi.org/10.1029/2005WR004419

Krein, A., Petticrew, E., Udelhoven, T., 2003. The use of fine sediment fractal dimensions and colour to determine sediment sources in a small watershed. Catena 53, 165–179. https://doi.org/10.1016/S0341-8162(03)00021-3

Laceby, J.P., Evrard, O., Smith, H.G., Blake, W.H., Olley, J.M., Minella, J.P.G., Owens, P.N., 2017. The challenges and opportunities of addressing particle size effects in sediment source fingerprinting: A review, Earth-Science Reviews. Elsevier. https://doi.org/10.1016/j.earscirev.2017.04.009

Motha, J.A., Wallbrink, P.J., Hairsine, P.B., Grayson, R.B., 2003. Determining the sources of suspended sediment in a forested catchment in southeastern Australia. Water Resour. Res. 39, 1056. https://doi.org/10.1029/2001WR000794

Phillips, J.M., Russell, M.A., Walling, D.E., 2000. Time-integrated sampling of fluvial suspended sediment: A simple methodology for small catchments. Hydrol. Process. 14, 2589–2602. https://doi.org/10.1002/1099-1085(20001015)14:14<2589::AID-HYP94>3.0.CO;2-D

Pulley, S., Rowntree, K., 2016. The use of an ordinary colour scanner to fingerprint sediment sources in the South African Karoo. J. Environ. Manage. 165, 253–262. https://doi.org/10.1016/j.jenvman.2015.09.037

Rawlins, B.G., Turner, G., Mounteney, I., Wildman, G., 2010. Estimating specific surface area of

fine stream bed sediments from geochemistry. Appl. Geochemistry 25, 1291–1300. https://doi.org/10.1016/j.apgeochem.2010.05.009

Schick, P.A., 1967. Suspended sampler and bedload trap. F. methods study slope Fluv. Process. Rev. Geormorphologie Dyn. 17, 181–182.

Smith, H.G., Blake, W.H., 2014. Sediment fingerprinting in agricultural catchments: A critical re-examination of source discrimination and data corrections. Geomorphology 204, 177–191. https://doi.org/10.1016/j.geomorph.2013.08.003

Stock, B., Semmens, B., 2016. MixSIAR GUI User Manual v3.1. https://doi.org/10.5281/ZENODO.47719

Stock, B.C., Jackson, A.L., Ward, E.J., Parnell, A.C., Phillips, D.L., Semmens, B.X., 2018. Analyzing mixing systems using a new generation of Bayesian tracer mixing models. PeerJ 6, e5096. https://doi.org/10.7717/peerj.5096

Viscarra Rossel, R.A., Minasny, B., Roudier, P., McBratney, A.B., 2006. Colour space models for soil science. Geoderma 133, 320–337. https://doi.org/10.1016/J.GEODERMA.2005.07.017

Walling, D.W., Woodward, J.C., Nicholas, A.P., 1993. A multi-parameter approach to fingerprinting suspended-sediment sources. Tracers Hydrol. Proc. Int. Symp. Yokohama, 1993 329–338.

Williams, G.P., 1989. Sediment concentration versus water discharge during single hydrologic events in rivers. J. Hydrol. 111, 89–106. https://doi.org/10.1016/0022-1694(89)90254-0

Zuecco, G., Penna, D., Borga, M., van Meerveld, H.J., 2016. A versatile index to characterize hysteresis between hydrological variables at the runoff event timescale. Hydrol. Process. 30, 1449–1466. https://doi.org/10.1002/hyp.10681

4. Post-fire hydrological response and suspended sediment transport of a terraced Mediterranean catchment

Abstract

In July 2013, a wildfire severely affected the western part of the island of Mallorca (Spain). During the first three post-fire hydrological years, when the window of disturbance tends to be more open, the hydrological and sediment delivery processes and dynamics were assessed in a representative catchment intensively shaped by terracing that covered 37% of its surface area. A nested approach was applied with two gauging stations (covering 1.2 km^2 and 4.8 km^2) built in September 2013 that took continuous measurements of rainfall, water and sediment yield. Average Suspended Sediment Concentration (1,503 mg l^{-1}) and the maximum peak (33,618 mg l^{-1}) were two orders of magnitude higher than those obtained in non-burned terraced catchments of Mallorca. This factor may be related to changes in soils and the massive incorporation of ash into the Suspended Sediment flux during the most extreme post-fire event; 50 mm of rainfall in 15 minutes, reaching an erosivity of 2,886 MJ mm ha^{-1} h^{-1}. Moreover, hysteretic counter-clockwise loops were predominant (60%), probably related to the increased sensitivity of the landscape after wildfire perturbation. Though the study period was average in terms of total annual precipitation (even higher in intensities), minimal runoff (2%) and low sediment yield (6.3 t km^2 y^{-1}) illustrated how the intrinsic characteristics of the catchment, i.e. calcareous soils, terraces and the application of post-fire measures, limited the hydrosedimentary response despite the wildfire impact.

Keywords: Sediment delivery processes; wildfires; terraces; nested catchments; Mediterranean fluvial systems

Reference

García-Comendador, J., Fortesa, J., Calsamiglia, A., Calvo-Cases, A., and Estrany, J. 2017. Post-fire hydrological response and suspended sediment transport of a terraced Mediterranean catchment. Earth Surface Processes and Landforms, 42: 2254– 2265. doi: 10.1002/esp.4181.

4.1. Introduction

Wildfires seriously disturb the dynamics and processes of natural environments, causing severe changes in the hydrological and geomorphological cycles of fire-prone landscapes (Shakesby and Doerr, 2006). The modification or complete removal of the vegetation and litter cover, which reduces interception, infiltration, evapotranspiration and sediment trapping following a wildfire, and the alteration of important physicochemical soil properties, such as water repellence, structure stability, texture and particle size distribution (Boix-Fayos, 1997; Úbeda and Outeiro, 2009), can change the channel-slope connectivity scenario, the overland flow rates and the sediment yield during the window of disturbance, as originally described by Prosser and Williams (1998). Many studies have documented an increase in overland flow generation (Scott et al., 1998; Cerdà and Doerr, 2005) and the reduction of the rainfall-runoff response time (Candela et al., 2005), especially during the first post-fire year. This scenario increases the sediment yield on hillslopes, as well as sediment delivery to river channels and sediment fluxes within them, which can lead to irreversible soil degradation (Castillo et al., 1997).

The Mediterranean basin is a fire-prone environment. The climate, characterized by a warm, dry summer season, is the primary factor that controls the pyrogeography of its landscapes, in which the irregular rainfall regime with torrential events substantially increases the risk of post-fire erosion. Furthermore, human land use during the last millennium has led to extensive changes in Mediterranean landscapes (Hooke, 2006). Deforestation and terracing of marginal lands for agricultural purposes changed the natural fire regime for centuries, providing soil stability and substantially reducing slope-to-channel sediment connectivity. Since the second half of the 20th century, the abandonment of these traditional agricultural lands –resulting from rural depopulation and the outsourcing of the economy– has generated afforestation processes in those areas previously occupied by crops (Grimalt et al., 1992; Tomaz et al., 2013). The colonization of these areas by natural vegetation in combination with a lack of management makes them a potential source of sediments that can be abruptly released after wall collapse (Lesschen et al., 2008; Calsamiglia et al., 2017). In addition, few appropriate fire prevention measures are taken. These measures, together with

the effective fire suppression policies implemented in recent years, have promoted an increase of fuel loads in the Mediterranean forests. As an example, in the Balearic Islands (archipelago located in the Western Mediterranean), forest fuel loads increased by 19% between 1999 and 2010 (MAGRAMA 2012). This process intensifies the risk of Large Forest Fires (LFF; i.e. > 500 ha) that may result in several changes in hydrological and geomorphological processes in the affected catchments.

Water and sediment flux monitoring at the catchment scale can provide more knowledge of the spatial and temporal evolution of these burned areas. Their role in delivering sediment and associated chemicals (e.g., nutrients and contaminants) to downstream water bodies, with associated consequences for water resources and aquatic habitats, can be defined (Smith et al. 2011a; Owens et al. 2013). In a nested catchment approach, spatial variations in the sediment delivery processes can be assessed, leading to greater understanding of the relationship between the catchment area and the sediment yield (Ferreira et al., 2008; Lane et al., 2011 and 2012). Although wildfires tend to increase sediment delivery and sediment fluxes within river channels, recent studies have emphasized that there is considerable variation in hydrological and sediment transport processes at different temporal and spatial scales, even within the same catchment (Mayor et al., 2007; Owens et al., 2013; Vieira et al., 2015). Therefore, the nested catchment approach is a reliable method for evaluating runoff generation and sediment transport and their evolution over time at catchment scale in burned landscapes.

The aim of this paper is to assess the water and suspended sediment (SS) yields and their dynamics in a small catchment (i.e. < 5 km^2) during the first three hydrological years (2013-2016) after the largest wildfire in the Balearic Islands (2,450 ha in July-August 2013), using the nested catchment approach (i.e. 1 and 5 km^2) during the period in which the window of disturbance is precisely most open. The specific objectives were to (a) analyse the runoff and SS transport dynamics and their post-fire evolution and (b) determine the different hydrological and sediment dynamics along the main channel system in a representative catchment of terraced landscapes affected by afforestation and recurrent wildfires.

4.2. Study area

Sa Font de la Vila (Figure 4.1A and 4.1B) is a 4.8 km^2 catchment located in Pariatge County (Andratx, western part of Mallorca Island). It is characterized by the afforestation of former agricultural land and has been affected by recurrent wildfires. The lithology is mainly composed of Upper Triassic (Keuper) clays and loams in the valley bottoms with gentle gradient slopes (ca. <10%), which –together with the high water availability at field capacity of the soils– facilitate agricultural development. Raethian dolomites and Lias limestones predominate in the upper parts of the catchment (Figure 4.1E). The average gradient of the Sa Font de la Vila catchment is 38% (Figure 4.1F), although 50% of the surface area features gradients less than 15%. The soils are classified as BK45-2bc, corresponding to Calcic cambisols (FAO, 2006). The fluvial network consists of two main catchments: Sa Coma Freda (2.3 km^2) and Can Cabrit (2.08 km^2) rivers. The Sa Coma Freda fluvial regime is characterized by substantial groundwater influence, with several karstic springs. The Can Cabrit catchment is not affected by this groundwater influence, as there are fewer impervious materials that minimize groundwater upwelling. In addition, the Can Cabrit River is also constricted by a check dam, built in 2007. This is 5 m high and 16 m long (Figure 4.1C) and retains most of the fluxes before they reach the downstream part of the Sa Font de la Vila catchment. Sediment deposits of up to ≈ 40 cm on the bottom behind the dam were observed during fieldwork in January 2016.

The climate is classified on the Emberger climate scale (Guijarro, 1986) as Mediterranean temperate sub-humid at the catchment headwaters and warm sub-humid at the outlet. The average temperature is 16.5°C (1974-2010, data from AEMET –the Spanish Meteorological Agency). The mean annual rainfall is 531.7 mm y^{-1} (1974-2010, data from B118 s'Alqueria d'Andratx AEMET station, see location in Figure 4.1B), with an inter-annual coefficient of variation of 23%. High-intensity rainstorms with a recurrence period of 10 years may generate 85 mm of rainfall in 24 hours. Before the wildfire in 2013, the Sa Font de la Vila catchment was mainly covered by natural vegetation (71%; i.e. 52% forest and 19% scrubland, Figure 4.1C). The rest of the catchment was covered by rain-fed trees (23%) and herbaceous crops (6%). As a result of past intensive farming, agricultural terraces (i.e. terraced fields, step terraces and

check dam terraces) occupy 37% of the area (179 ha) with a total length of 147 km of dry-stone walls (Figure 4.1C), of which 75.1 ha are well-maintained and 103.7 ha abandoned, with an average collapse point density of 12 collapses km^{-1} and 55 collapses km^{-1}, respectively (Calsamiglia et al., 2017).

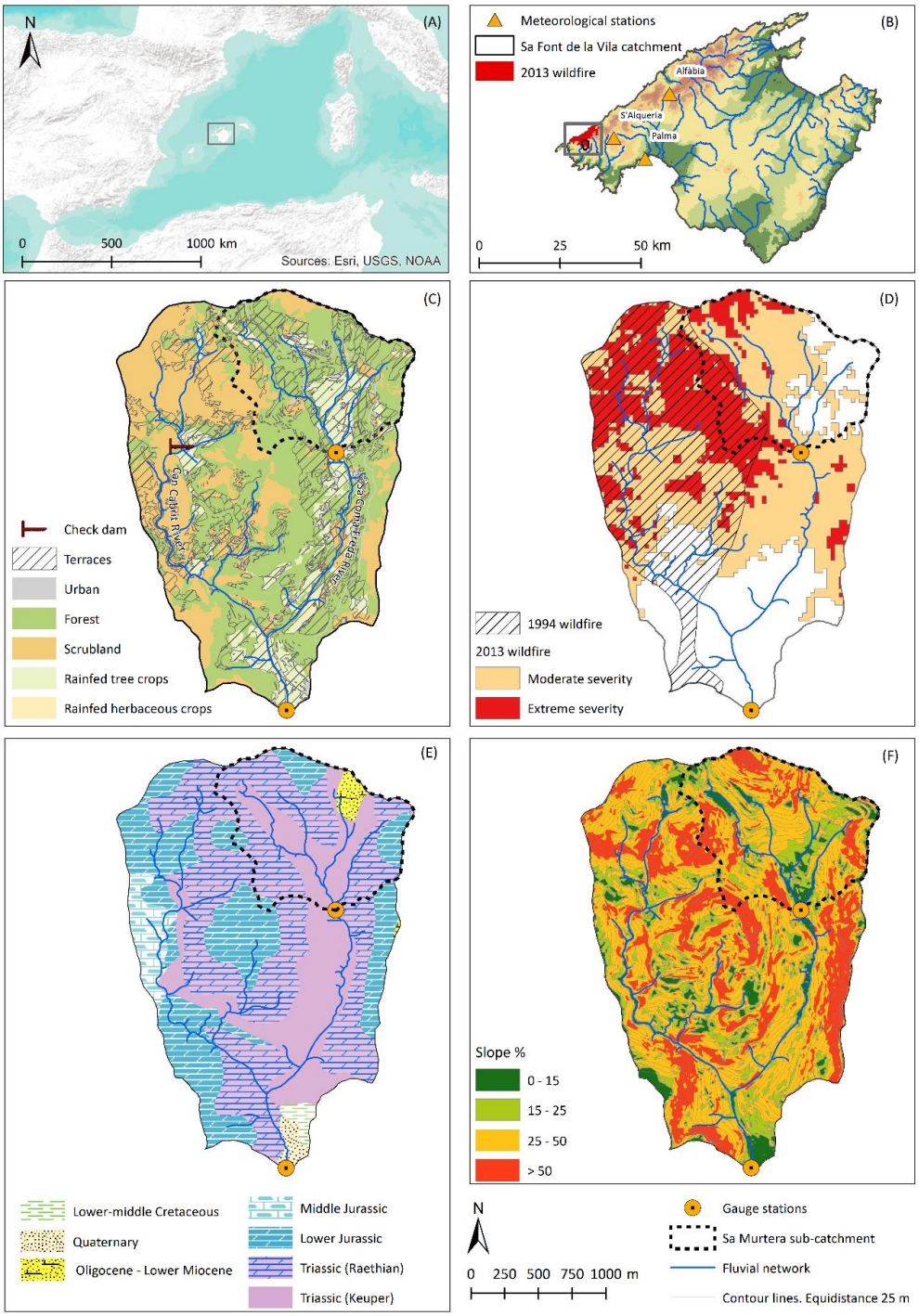

Figure 4.1. (a) Map of the location of Mallorca in the Mediterranean Sea; (b) location of the area affected by the July 2013 wildfire in Pariatge County; (c) land uses and soil conservation practices; (d) 1994 and 2013 wildfire-affected areas, as well as severity of 2013 wildfire; (e) lithology; and (f) gradient slope of the Sa Font de la Vila catchment.

The catchment has been affected by two major wildfires in the last twenty years, as depicted in Figure 4.1D. In 1994 25% of the catchment area was burned, while in 2013 the fire reached 71% of its surface, 30% of which had already burned in 1994. In the 2013 wildfire, the results of a burn severity assessment that followed the Normalized Burn Ratio approach (Escuín et al., 2008) and used Landsat 8 images indicated extreme fire severity for 24% of the catchment and moderate fire severity for 47% (Bauzà, 2014).

4.3. Material and Methods

4.3.1. Continuous monitoring network

In September 2013, one month after the wildfire, gauging stations were installed at the outlet of two nested catchments, i.e. Sa Murtera (the upstream site; hereafter the US, 1.1 km^2) and Sa Font de la Vila (the downstream site; hereafter the DS, 4.8 km^2), for use in a nested approach for the continuous measurement of water and sediment yields.

The US gauging station is located in the northeast headwater area of the Sa Font de la Vila catchment at an elevation of 185 m (Figure 4.1). It was installed in a place where channel banks consist of dry-stone walls working as a control section for higher discharges and another smaller section built for measuring baseflow. Its sub-catchment is characterized by an average gradient slope of 36% and the same lithology as the entire Sa Font de la Vila catchment. Land use previous to the 2013 wildfire was forest (66%), followed by scrubland (14%), rain-fed tree crops (14%), urban areas (4%) and rain-fed herbaceous crops (2%). Abandoned and active agricultural terraces cover 65% of its area. The 1994 wildfire event burned 17% of the area. In 2013, the wildfire burned 85% of the sub-catchment area, with 25% extreme burn severity and 60% moderate burn severity (Figure 4.1D). The gauging station was equipped with a Campbell Scientific *CR200X* data logger that stored the average values of water surface level and turbidity, based on 1 minute readings at 15 minute intervals collected by a Campbell Scientific *CS451-L* pressure probe and a *OBS-3+* turbidimeter with a double measurement range of 0-1.000/1.000-4.000 NTU. Where instantaneous turbidity peaks

were known to be spurious, manual manipulation and interpolation were used to correct the data (Wass and Leeks, 1999). Additionally, a rising-stage sampler modified from Schick (1967), with seven sampling bottles, was installed to provide more information on suspended sediment concentrations (SSCs). The bottles were 12 cm apart, totalling a 100 cm stage, with the first bottle located 21 cm above the riverbed.

The DS gauging station was also installed in a place where channel banks consist of dry-stone walls working as a control section. The instruments were the same as for the US. However, the rising-stage sampler was set up with twelve bottles, totalling a 200 cm stage.

A Casella tipping bucket rain gauge was also installed at US. This instrument was fixed 1 m above the ground and connected to a *HOBO UA-003-64* Pendant Temp/Event data logger that recorded precipitation in 0.2 mm increments.

4.3.2. Field measurements and data computation

Stream discharge (Q) was measured by an *OTT MF* pro inductive magnetic flow meter, with a measuring range of 0 to 6 m s^{-1} and ±2% accuracy, to develop and fit stage/discharge rating curves.

Manual depth-integrated SS samples were consistently collected during storm events and every week during low flows, at both the US and DS sites. They were collected at the same sections on which turbidity probes and rising-stage samplers were installed. Differences may exist between data collected at manual and rising-stage sampling points; previous studies in large rivers have reported differences between 10 and 20% (e.g., Batalla, 1993). However, direct observations indicate that water flows are notably turbulent through the sections of the channels at the US and the DS; any spatial difference of SS Concentrations (SSCs) within the sections is considered negligible. All the water samples were filtered by 0.45-µm cellulose esters; the filters were subsequently dried at room temperature and weighed on high-precision scales to determine the SSCs (Estrany, 2009).

Turbidity probes were calibrated with commercial turbidity standards to check their long-term stability. The turbidity data were converted to a continuous record of SSCs

by a site-specific concentration/turbidity calibration relationship. The SSCs used for calibration were measured in samples collected both manually and by rising-stage samplers. Suspended sediment loads were calculated by combining the records of SSCs provided by the turbidity sensors with the continuous records of water discharge.

The analysis of the relationship between rainfall intensity and kinetic energy and its variations in time and space are important for erosion prediction (van Dijk et al., 2002). The kinetic rainfall energy was calculated by the equation described by Brown and Foster (1987):

$$e = 0.29[1 - 0.72\,exp(-0.05i)]$$

where e is the kinetic energy of 1 mm of rainfall expressed in Mj ha^{-1} mm, and i is the rainfall intensity expressed in mm h^{-1}. The rainfall erosivity (R) was determined by multiplying the kinetic energy of each event and the maximum intensity attained in 30 minutes (I30). The results were expressed in MJ mm ha^{-1} h^{-1}.

$$eI_{30} = R$$

Finally, the spatio-temporal relationship between discharge and sediment transport at the event scale was analysed by means of the hysteresis loop classification developed by Williams (1989). Because of monitoring problems at the US, the results of the first post-fire year (2013-2014) were only available at the DS.

4.4. Results

4.4.1. Rainfall

Rainfall during the study period can be considered representative of the catchment. The long-term dynamics (period 1974-2010) were compared with records of 517 mm in 2013-2014, 578 mm in 2014-2015 and 309 mm in 2015-2016 (Figure 4.2) with a 20% coefficient of variation. Four rainfall events with runoff response were recorded in 2013-2014, five in 2014-2015, and one in 2015-2016. During the first two hydrological

years the rainiest season was autumn, with 359 mm in 2013-2014 and 227 mm in 2014-2015. In the third year, winter was the season with the highest rainfall value (125 mm).

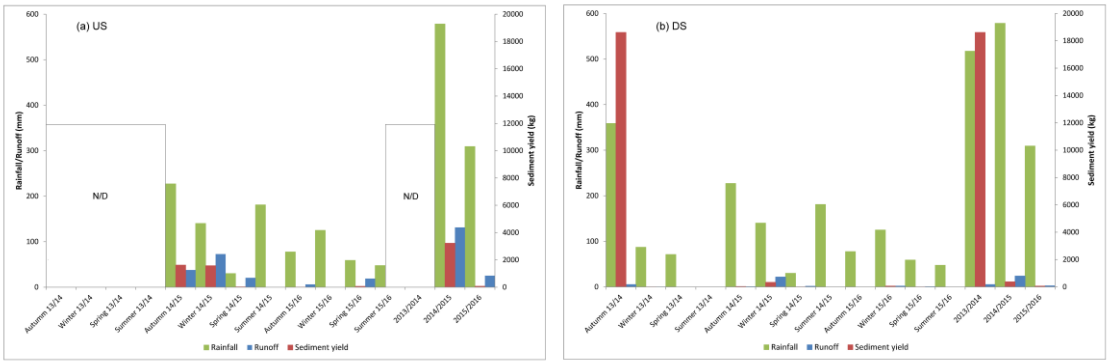

Figure 4.2. (A) Rainfall, runoff and suspended sediment yield for the US-Sa Murtera (2014-2016); and (B) rainfall, runoff and suspended sediment yield for the DS-Sa Font de la Vila station (2013-2016).

The maximum amounts of daily rainfall during the study period were 61 mm on 20th January 2015 (T = 2.7 years) and 57 mm on 29th October 2013 (T = 2.3 years). The 29th October 2013 storm was the first with runoff generation occurring after the 2013 wildfire. Most of the rain (50 of the 57 mm) fell in only 15 minutes, reaching an intensity (I30) of 100 mm h^{-1} and rainfall erosivity (R) of 2,886 MJ mm ha^{-1} h^{-1}. Hereafter, rainfall I30 intensities were lower during the entire study period, with no event exceeding 30 mm h^{-1}. Excluding this first event, the average rainfall I30 was 12 mm h^{-1}. I30 for the 2013-2014 storms was between 10 and 100 mm h^{-1}, with an R average of 861 MJ mm ha^{-1} h^{-1}. In 2014-2015, the storms' I30 was between 0.4 and 30 mm h^{-1}, with an R average of 158 MJ mm ha^{-1} h^{-1}. Finally, in 2015-2016, only one event was recorded, showing I30 of 11 mm h^{-1}, with R of 118 MJ mm ha^{-1} h^{-1}. For further details, see Supplementary table 4.1.

The long-term rainfall intensity data series recorded at the Palma (1964-2001) and Alfàbia (1994-2001) AEMET rain gauges (20 km and 32 km, respectively, from the Sa Font de la Vila catchment, see Figure 4.1B) confirmed that the maximum annual I30 for the entire study period of 2013-2016 was representative of the long-term record, except for the extreme event of October 2013. Thus, the average maximum annual I30 at these reference sites was 30.6 ±12.9 mm h^{-1} at Palma and 24.9 ± 9.2 mm h^{-1} at Alfàbia (YACU 2002), whereas the average for the study period was 47 mm h^{-1}.

However, if the October 2013 event was not included in the statistics, the average decreased to 19.6 mm h^{-1}.

Table 4.1. Suspended sediment yield comparison between burned catchments in different environments and unburned catchments in Mediterranean environments with the values reported in this study (adapted from Smith et al. 2011; Owens et al. 2013).

	Location	Catchment area (km^2)	Average rainfall (mm yr^{-1})	Average sediment yield (t km^{-2} yr^{-1})	Study reference
Mediterranean Burned	Xortà Range, Spain	0.02	658	65	Mayor et al. (2007)
	Mount Carmel, Israel	1.1	750	36	Inbar et al. (1998)
	Sa Murtera, Spain	1.1	444*	1.6*	This study (2017)
	Sa Font de la Vila, Spain	4.8	468	6.3	This study (2017)
Non Mediterranean Burned	Slippery Rock Creek, Australia	1.4	1,800	122	Lane et al. (2006)
	Springs Creek, Australia	2.4	1,800	61	Lane et al. (2006)
	Cerro Grande, USA	16.6	650	354	Reneau et al. (2007)
	Colorado Front Range, USA	46.9	440	5,000	Moody & Martin (2001, 2009)
	Fishtrap Creek, Canada	135.0	487	3	Owens et al. (2013)
	Little River, Australia	183.0	1,000	62	Wilkinson et al. (2009)
Mediterranean unburned	Valdivia, Chile	0.9	2,170	90	Iroumé (1990)
	Araguás, Spain	0.5	720	15,300	Nadal-Romero et al. (2008)
	Vernegà, Spain	2.4	646	8	Pacheco et al. (2011)
	Jasenica, Serbia	96.0	760	32	Djorovic (1992)
	Silaro, Italia	138.0	942	732	Pavanelli & Pagliarini (2002)
	Na Borges, Spain	319.0	572	0.3	Estrany et al. (2009)
	Tordera, Spain	785.0	1,000	50	Rovira & Batalla (2006)

(*) Only computed during 2014-2015 and 2015-2016 hydrological years

4.4.2. Streamflow

At US, 6 flood events were recorded during 2014-2015 and 1 in 2015-2016, while at DS there were 4 events during 2013-2014, 5 in 2014-2015 and 1 in 2015-2016 (Figure 4.3A and 4.3C).

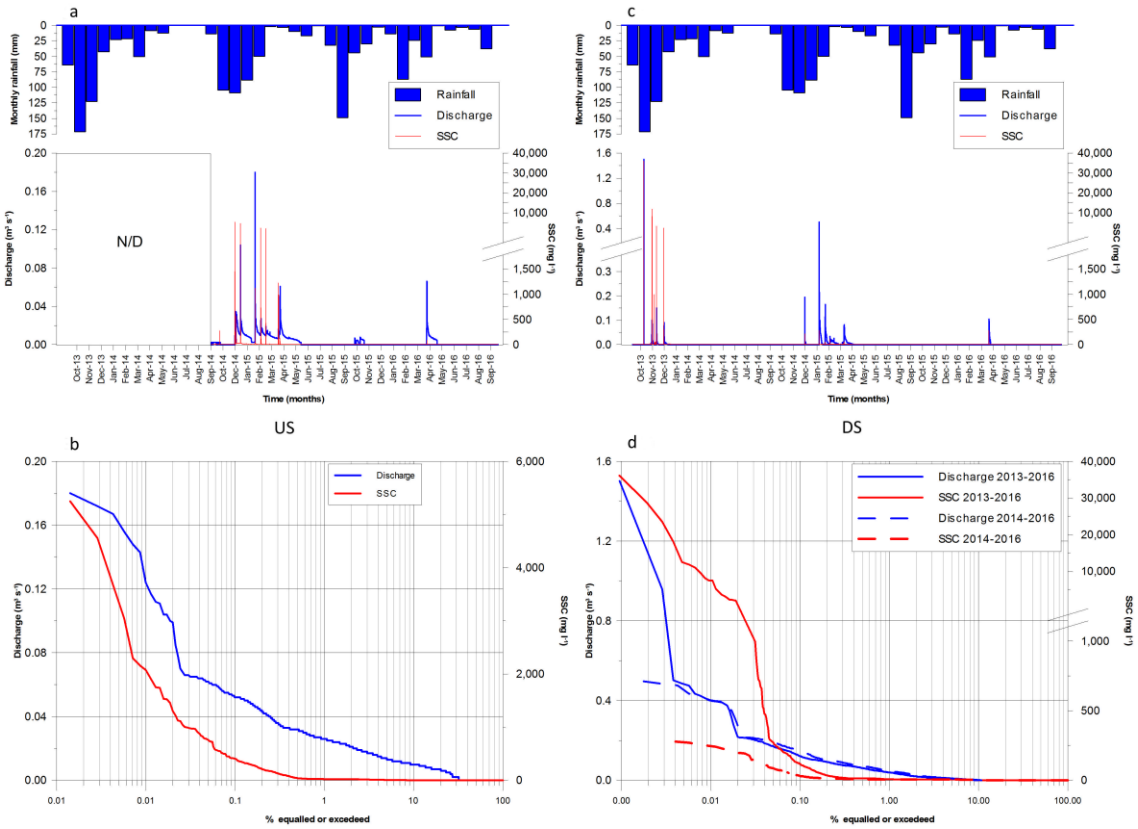

Figure 4.3. Hydrograph, sedigraph, hyetograph and SSC-Q frequency based on 15-minute recordings at the US-Sa Murtera (A-B) during the study period 2014-2016 and at the DS-Sa Font de la Vila (C-D) during the study periods 2013-2016 and 2014-2016 for better comparison.

At US (Figure 4.2A), 131 mm of runoff were measured in 2014-2015 and 25 mm in 2015-2016. In 2014-2015, a notable presence of baseflow was observed during the wet season, influenced by the karstic sources that maintained an influent regime in the upper catchment. Floods showed Q peaks ranging from 0.01 to 0.20 $m^3 s^{-1}$, an average discharge of 0.005 $m^3 s^{-1}$ and a specific contribution of 4.2 $m^3 s^{-1} km^{-2}$. The annual runoff coefficient was 23%. In 2015-2016, the very low precipitation recorded (309 mm) was not sufficient to maintain the baseflow. The only flood that occurred in 2015-2016 reached a Q peak of 0.07 $m^3 s^{-1}$, average of 0.03 $m^3 s^{-1}$ and a specific contribution of 0.8 $m^3 s^{-1} km^{-2}$. The annual runoff coefficient was 8%.

At the larger catchment (DS), 5 mm of runoff was recorded in the first post-fire year, 24 mm in the second and 3 mm in the third (Figure 4.2B). During 2013-2014, 4 events occurred, with Q peaks ranging from 0.09 to 1.5 $m^3 s^{-1}$. Under a shorter-term intermittent fluvial regime, the annual average discharge was 0.001 $m^3 s^{-1}$, while the specific contribution was 0.170 m3 $s^{-1} km^{-2}$. In 2014-2015 the Q peaks for the 5 floods

ranged between 0.07 and 0.50 $m^3 s^{-1}$. The average discharge was 0.004 $m^3 s^{-1}$, with a specific contribution of 0.727 $m^3 s^{-1} km^{-2}$. Finally, in 2015-2016 only one flood was recorded, with a Q peak of 0.10 $m^3 s^{-1}$ (average of 0.05 $m^3 s^{-1}$). The mean annual discharge was 0.001 $m^3 s^{-1}$, reaching a specific contribution of 0.810 $m^3 s^{-1} km^{-2}$. The annual runoff coefficient was 1% for the first post-fire year, 4% for the second and 0.8% for the third, resulting in an average of 2%.

4.4.3. Suspended sediment concentrations and yields

At US, in 2014-2015, the 6 flood events averaged an SSC of 309.5 mg l^{-1}, with maximum peaks ranging between 133.7 and 5,244.7 mg l^{-1}. The annual SS yield was 3.2 t km^2, with autumn the season with the highest SS yield (1.6 t), representing 50% of the total SS load exported. In 2015-2016 the only recorded flood reached an SSC peak of 91 mg l^{-1}, averaging 7.2 mg l^{-1}. The highest sediment load was recorded in spring, reaching 0.063 t. The annual SS yield was only 0.071 t km^{-2} (Figure 4.2A).

At DS, in 2013-14, the first flood after the wildfire (29th October 2013) reached an SSC peak of 33,618 mg l^{-1} (average of 17,000 mg l^{-1}). Ninety-two percent (92%) of the SS load during the three years was released from the catchment in this first flood. For the other three floods, the SSC peaks were substantially lower, ranging from 2,300 to 12,000 mg l^{-1} and averaging 160 mg l^{-1}. 99% of the SS load was released in autumn, which showed clearly both maximum soil erodibility after the fire and an exhaustion process. The SS yield for this first post-fire year was 19 t km^{-2} (Figure 4.2B). During 2014-2015, the SSC average for the five recorded floods was 22 mg l^{-1}, with maximum SSC peaks ranging between 62 and 285 mg l^{-1}. The maximum SS load (1,630 kg) was recorded in winter, representing 90% of the annual load and concentrated mainly in the 20th January 2015 event (1,099 kg). The SS yield was then reduced in this second post-fire year to ca. 0.5 t km^{-2} (Figure 4.2B). Finally, in the third post-fire year, the SS yield was the lowest recorded during the study period with 0.07 t km-2 (Figure 4.2B). The only flood occurring (March 29th) reached an SSC peak of 285 mg l^{-1} (average 22 mg l^{-1}). Winter was the season when 0.3 t of the SS load were released, which represented 99% of the annual SS load. The average SS yield for the whole study

period was 6.3 t yr^{-1} km^{-2}. For further details, Supplementary table 4.1 provides specific data on the event scale.

The dynamics show how 99% of the total SS transport occurred in only 1% of the time at DS during 2013-2016 (Figure 4.4). However, if only the period 2014-2016 is computed, at US 90% of the SS load was released in 10% of the time, whilst at DS the same relative value of load was released in 20% of the time.

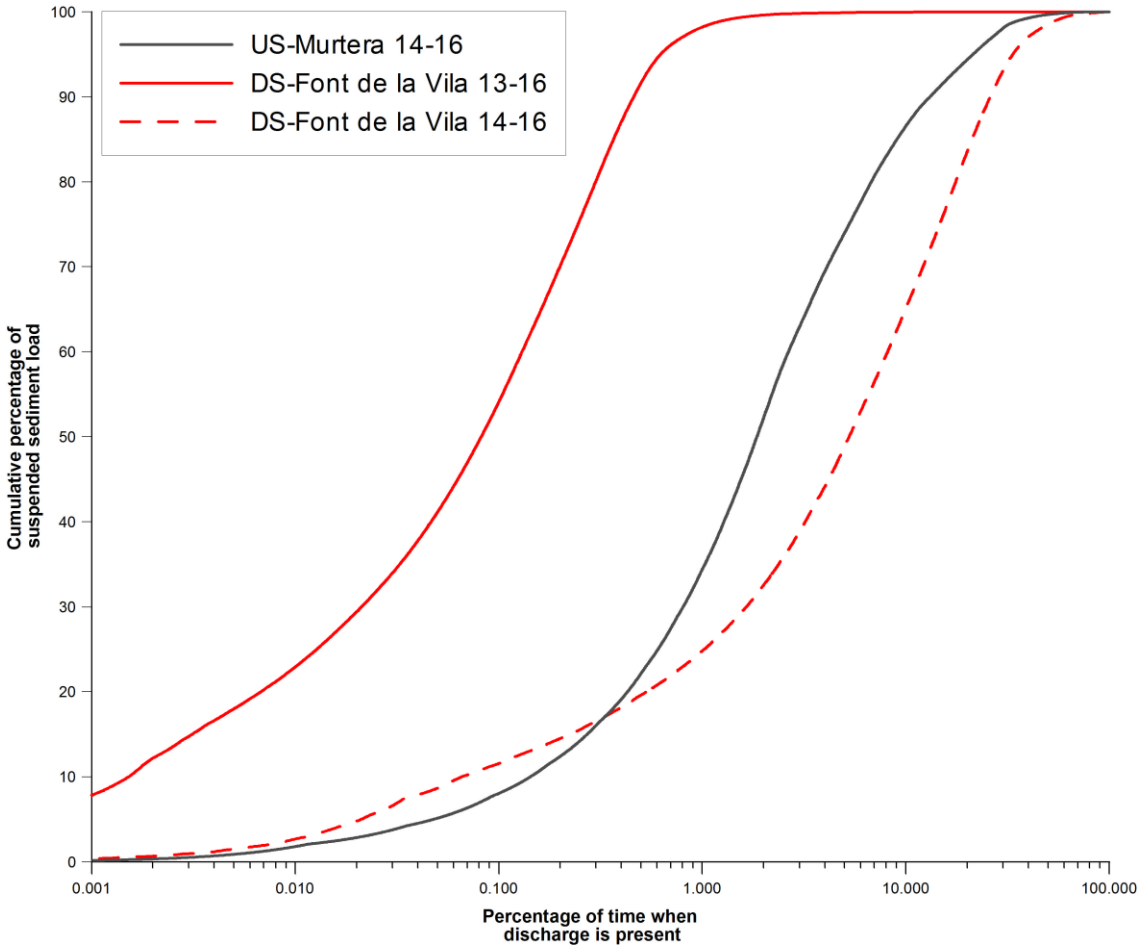

Figure 4.4. Total cumulative sediment load duration curve, 2013-2016, at DS-Font de la Vila and 2014-2016 at the US-Sa Murtera and DS-Sa Font de la Vila gauging stations.

4.4.4. Nestedness and wildfire effects on runoff and suspended sediment dynamics

Comparing the Q and SSC frequency curves for both stations during the two monitored years in common (2014-2015 and 2015-2016; Figure 4.3B and 4.3D) allows a first approach to the nestedness. At US, the Q was present 32% of the time, 19% longer than at DS (13%) due to karstic springs at headwaters and downstream transmission

losses along the main channel. The SSC values showed an extremely ephemeral transport during floods at both stations, exceeding 50 mg l^{-1} for only 0.46% of the time at US and 0.07% at DS (Figure 4.3B and 4.3D). For 2014-2015, a runoff and SS load downstream reduction between stations of 27% and 53%, respectively, was observed. For 2015-2016, runoff showed again a downstream reduction of 60%, but the SS load increased by 73%.

A hysteretic analysis was carried out for each individual flood event at both stations to characterize the hydrosedimentary post-fire dynamics (Figure 4.5). For the whole study period, the percentage distribution was 43% (US; two monitored years) and 40% (DS; three monitored years) for clockwise loops, against 57% (US) and 60% (DS) for counter-clockwise loops (Supplementary table 4.1). The high percentage of counter-clockwise loops and their irregular distribution within the wet season (Supplementary table 4.1) may indicate the influence of fire on these dynamics. On the annual scale, in US, the observed hysteresis in 2014-2015 (all occurring in the wet period; i.e. autumn and winter) were 3 clockwise and 3 counter-clockwise loops (Supplementary table 1). In 2015-2016, the sole event occurring drew a counter-clockwise loop. This was in spring after 50 mm of rain fell at low intensity (I30 11.2 mm h^{-1}) under dry preceding conditions and did not reach the DS station. At DS the 4 floods occurring in 2013-14 - only in the autumn- were all counter-clockwise loops (Supplementary table 4.1). The first flood after the wildfire (29th October 2013) was a flash flood generated by a 50 mm high-intensity rainfall (I30 of 100 mm h^{-1}) under dry preceding conditions, reaching Q and SSC peaks of 1.5 m^3 s^{-1} and 33,618 mg l^{-1}, respectively. The next two floods (17/11/2013 and 01/12/13) had wet preceding conditions, with 78 and 30 mm of precipitation, respectively, seven days before. The last event was provoked by a 69 mm low-intensity storm (I30 10 mm h^{-1}) under dry conditions. In 2014-2015, one event was in autumn and four in winter. Three of them had a clockwise hysteresis loop; and two, multi-peak counter-clockwise loops. The preceding conditions were dry in all cases. Only on 20th January, 2015 was there rainfall: 12 mm seven days before. Finally, in 2015-2016, one flood was generated in winter under dry preceding conditions by a 50 mm storm with a low I30 (11 mm h^{-1}), drawing a clockwise loop hysteresis.

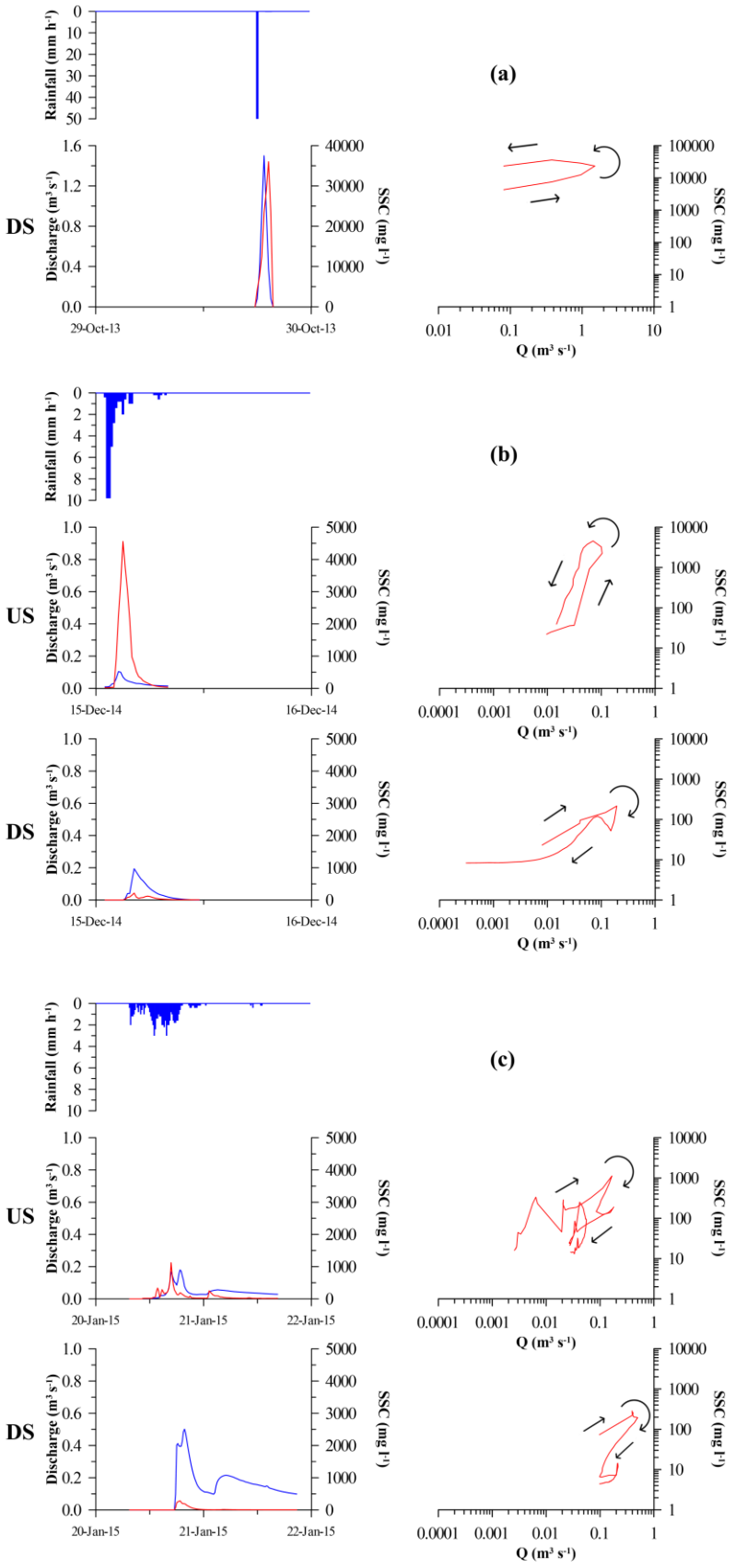

Figure 4.5. Hysteretic behaviour types for the first post-fire flood event at DS-Sa Font de la Vila gauging station (A- 29/10/2013) and for coinciding flood events (B- 15/12/14; C- 20/01/15) at the US-Sa Murtera and DS-Sa Font de la Vila gauging stations.

4.5. Discussion

4.5.1. Landscape response to wildfire

During the first few years after a wildfire, landscapes are prone to intensified soil erosion and sediment transport dynamics (e.g. Shakesby and Doerr, 2006). Therefore, higher SS yields should be interpreted as indicators of erosion processes in a catchment affected by a severe wildfire, especially in a highly energetic environment such as the Mediterranean (García-Ruiz et al., 2013). However, the very low results obtained in the Sa Font de la Vila catchment during the first three post-fire years indicate that other factors were involved in the hydrosedimentary response.

The landscape response to a fire disturbance is basically determined by the fire's severity when torrential rains occur after fires (De Luís et al., 2003). However, when rainfall intensity is not torrential, then the intrinsic characteristics of the rainfall event has more influence on the erosional soil response than the severity of the fire has (Gimeno-García et al., 2007). Accordingly, Moody and Martin (2009) and Smith et al. (2011b) suggested that magnitude, intensity and frequency of rainfall and derived flood events are the main drivers of erosion and sediment delivery in many burned catchments. They stress that rainfall patterns explain the large variation in post-fire SS yields in contrasted environments and catchment sizes. Therefore, the limited response in terms of SS fluxes in burned catchments can be ascribed to a lack of a driving force for such rainfall intensity (Owens et al., 2012). During the entire study period of 2013-2016, rainfall intensities in the Sa Font de la Vila catchment were representative of the long-term record, although the high-energy Mediterranean environment may lead to flash floods caused by high-intensity rainfall (Estrany and Grimalt, 2014). This process only occurred in October 2013 with the highest intensity and erosivity of the study period. It caused the transport of 92% of the total load.

Sa Font de la Vila is a highly modified catchment because of its traditional agricultural use in such marginal lands. The massive presence of terraces (Figure 4.1) involved a general decoupling effect and showed the anthropogenic control of resistance forces in reducing the water and sediment yields of river systems (e.g. Walling, 1999; Estrany et al., 2010). In addition, Arnáez et al. (2015) suggested that runoff coefficients for

abandoned terraces are, at the hillslope scale, between 20% and 40% in Mediterranean areas, depending on the percentage of plant cover or the grazing pressure. In turn, Calsamiglia et al. (2017), applying the morphometric Index of Connectivity (IC) in our studied catchment, observed important decoupling effects. Results of this study showed that 62% of the area covered by terraces had lower IC values than the average of the catchment. Similarly, the abandonment of agriculture during the 1960s promoted forest transition processes on these terraced fields. In addition to the buffer effect of these fields, vegetation growth may also lead to decline in runoff and SS transport rates (Morán-Tejeda et al., 2010; Buendia et al., 2015) at the catchment scale. Estrany et al. (2017) calculated –using the blue normalized difference vegetation index (BNDVI)– 11.5% recovery of vegetation cover in two representative micro-catchments of the Sa Font de la Vila catchment, 14 months after the wildfire (October 2014). In addition, an aerial image analysis showed that the recovery had increased to 26% by April 2015.

Moreover, the parent material may play a significant role in the hydrosedimentary response. Calvo-Cases et al. (2003 and 2005) obtained low erosion rates and high infiltration capacities in several study areas with calcareous soils after rainfall simulation experiments and in erosion plots. They concluded that this behaviour is related to the bedrock cracks, stoniness, thickness, soil organic matter content, bulk density and vegetation typical of these soils, generating patches of runoff and re-infiltration at hillslopes as modelled in Arnau-Rosalén et al. (2008). Our results indicate an average runoff coefficient ca. 2% for the entire catchment (1% in the first post-fire year, 4.2% in the second and 0.8% in the third), probably caused by the combination of terraces and calcareous lithology. This process is comparable to similar Mediterranean catchments, in which notable transmission losses are mainly caused by lithological variations in permeability (Tzoraki and Nikolaidis, 2007; Estrany et al., 2009). Finally, the post-fire management actions implemented during the first year after the fire (i.e. log barriers, mulching and tree removal) to control and reduce runoff and SS delivery from hillslopes to the fluvial channels can also be related to these very low SS transport rates (Robichaud et al., 2013).

Terraces disturb hydrological and sediment connectivity, imposing large rainfall thresholds for the generation of runoff and SS transport (Lasanta et al., 2001; Cammeraat, 2004). Nevertheless, if the magnitude of future rainfall intensities and derived flood events exceeds the threshold capacities of these structures, a general collapse can occur, which accelerates erosion processes and associated damage (Estrany and Grimalt, 2014; Tarolli et al., 2014). Moreover, wildfire may be an added factor directly affecting the dynamics of these terraced lands (Dunjó et al., 2003), as erosion of abandoned terraces is directly related to the amount of plant cover, soil characteristics, environmental conditions and the time terraces had been abandoned (Arnáez et al., 2015). Accordingly, land abandonment and wildfire recurrence illustrate abrupt changes along the sediment pathways caused by wall failures within those much-decoupled terraced areas (Calsamiglia et al., 2017). The general collapse of these structures has been measured in the Tramuntana Range since the 1960s. They occurred during rainy years and were caused by either soil expansion or the direct action of overflowing drainage ditches (Grimalt et al., 1992). Additionally, since these collapses were primarily produced without the impact of wildfires, it must be emphasized that shallow landslides and other mass movement events are often more frequent between 5 and 20 years after a wildfire due to the time required for the complete decay of the root systems of burned vegetation (Meyer et al., 2001). The recurrence of forest fires, even to the limited extent that occurs under traditional management systems, periodically enhances soil erosion and steadily reduces the potential for plant recolonization (Ruiz-Flaño et al., 1992), which results in the acceleration of the collapse processes for these structures.

Calsamiglia et al. (2015) developed an assessment of the erosional processes after the fire by using a drone for generate a High-Resolution DTM (5 cm px^{-1}) derived from automated digital photogrammetry (SfM; Structure from Motion algorithms) in a micro-catchment (3 ha) located in the upstream part of the Sa Font de la Vila catchment. Two flights in October 2014 and April 2015 were used for build both HR-DTM. Applying the DEM of Difference (DoD) technique, no significant erosion or deposition processes were detected in this micro-catchment because geomorphic change detection in any case exceeded the minimum level of detection (≈12 cm, p

95%). These results were also corroborated by field observations. Therefore, despite the lack of protection and the vulnerability of the soil after the wildfire, field observations did not show relevant erosive and depositional processes on hillslopes.

4.5.2. Post-fire suspended sediment yield at catchment scale

To the best of our knowledge, only two studies (Inbar et al., 1998; Mayor et al., 2007) have reported SS yield data (i.e. 36 and 65 t ha^{-1} yr^{-1}, respectively) from other burned Mediterranean environments at catchment scale during the window of disturbance period. In the case of Mayor et al. (2007), these higher SS yield values correlated directly with torrential storms during the first years after the fires, since 75% of the SS yield during the study period (7 years) was generated in only one storm with a peak of 98 mm h^{-1} during 15 minutes. Moreover, Inbar et al. (1998) indicate that the low rainfall intensity in the two post-fire years included in their study was the dominant factor for explaining the low sediment yield and erosion records. In addition, for a Californian fire-prone chaparral, Warrick et al. (2012) determined that low rainfall intensity results in the detachment of loose soil and dry gravel talus after a wildfire, whereas heavy rainfall generates overland flow at rates that cut rills and gullies into the soil and may generate debris flows.

It is therefore difficult to assess whether the minimal SS yield data reported in the literature are typical. It should also be remembered that most of the research was developed at the plot and hillslope scale, in which the derived results cannot be directly scaled to catchments (Shakesby, 2011). However, a comparison with other similar unburned Mediterranean catchments can be established. For comparison, the observed high variability between years at Sa Font de la Vila catchment indicated a SS yield of 19 t km^{-2} yr^{-1} in 2013-2014, but the SS decreased sharply to 0.5 t km^{-2} yr^{-1} in 2014-2015 and 0.07 t km^{-2} yr^{-1} in 2015-2016. As a result, the mean annual SS yield was 6.3 t yr^{-1} km^{-2}, a value that can be considered low for Mediterranean Europe (Vanmaercke et al., 2011). Conversely, this indicates that the SS yield for the entire study period is very similar to the values recorded in unburned Mediterranean catchments characterized by analogous driving factors (i.e. catchment area and climate; Table 4.1). The studies focusing on non-Mediterranean burned catchments,

developed in Australia and North America (Table 4.1), reported how intensity of rainfall is also the key driver (Smith et al., 2011b). Therefore, especially during the first post-fire year, the magnitude of SS yields (ranging from 8.6 to 2,524 t km^{-2} yr^{-1}) in these catchments fluctuates considerably because the sediment response also depends on the occurrence of torrential storms. Other factors such as lithology (the catchments studied rested mainly on igneous and metamorphic terrains) and land uses (i.e. mainly without terraces) do not reflect a different pattern from Mediterranean burned catchments (ranging from 1.6 to 456 t km^{-2} yr^{-1}). The few studies that have analysed the hydrological and geomorphological responses to wildfire at catchment scale require further research to provide more comprehensive insights into wildfire impact on magnitude, spatial variation and temporal patterns.

As Figure 4.4 shows, SS transport was extremely ephemeral in comparison with other Mediterranean unburned catchments (Gallart et al., 2013; Buendía et al. 2015; De Girolamo et al., 2015). These notably short-lived dynamics of the sediment transfer are, however, comparable with other studies conducted in catchments largely modified by terraces with underlying carbonate lithology in Mallorca (Estrany et al., 2009). It should be noted that the increase of two orders of magnitude of SSC reported in the first event (October 2013) –compared with the average values measured during the study period– was probably caused by changes in soil water repellence, hillslope surface roughness and the massive incorporation of ash in the SS flux during this first post-fire event (Smith et al., 2011b), combined with high-intensity rainfall. The ash deposits were incorporated into the soil through infiltration because between the wildfire and first flood 107 mm of rain under low-intensity conditions fell (data from B118 s'Alqueria d'Andratx AEMET station, Figure 4.1B). In addition, a post-fire sediment source ascription analysis carried out by García-Comendador et al. (2017) observed higher concentrations of ^{137}Cs and $^{210}Pb_{ex}$ in the hillslope source samples collected in those fire-affected areas, indicating the fire's impact on the soil (Smith et al. 2013).

The reported SS yield confirms that higher rainfall intensities are required in order to generate an effective slope-to-channel sediment delivery response. Accordingly, the intrinsic characteristics of the catchment –such as the stoniness and thickness of the

soils, the terraces and the application of post-fire measures– limited the sediment response to a certain rainfall threshold able to connect runoff along the hillslopes by means of sink saturation (see Calvo-Cases et al., 2003).

4.5.3. Nestedness effects on post-fire hydrosedimentary response

The nested catchment approach enabled the sediment conveyance losses along the main channel of the Sa Font de la Vila catchment to be identified, taking into account that the increased stormflow response to rainfall events that may occur after a wildfire also decreases with post-fire recovery, thereby potentially reducing the capacity of subsequent flows to remove stored sediment and increasing residence times (Moody and Martin 2001). The downstream reduction of 27% in runoff and 53% in SS load during 2014-2015 indicated that water percolation and sediment deposition were the primary processes that were active between the two nested catchments. As a result, the driving forces during the post-fire study period did not allow any effective downstream sediment release, which caused an accumulation along the main channel that required a major flood event to mobilize the stored sediment (Estrany et al., 2011). In 2015-2016, runoff showed again a reduction between US and DS of 60%. However, the SS load increased by 73%, but with negligible records (85 kg at US and 310 kg at DS).

For the hysteretic analysis, Sa Font de la Vila showed a predominance of counter-clockwise loops (60%) for the three post-fire years, indicating that the main sediment sources were located at a certain distance from the channel (Oeurng et al., 2010). This percentage of counter-clockwise loops is higher than in other studies of non-burned Mediterranean catchments (Seeger et al., 2004; Rovira & Batalla 2006; Oeurng et al., 2010; López-Tarazón and Estrany, 2017), which is probably related to the increased sensitivity of the landscape after wildfire perturbations. It should be noted that 67% of the counter-clockwise loops in DS occurred during the first post-fire year (2013-2014), when the highest annual sediment yield was recorded. During the following years, this percentage –as well as the sediment yield– decreased significantly, which may be

related to vegetation cover conditions on the burnt hillslopes (Lane et al. 2006; Smith et al. 2011b).

The same hysteresis behaviour only occurred in 40% of the floods that coincided between US and DS (Supplementary table 4.1). Counter-clockwise loops predominated in US and clockwise loops in DS, which was indicative of the mobilization of sediment deposited along the river channel and its adjacent areas (Klein 1984). These distinct patterns can be attributed to the sediment conveyance losses and storage along the channel between stations, the size characteristics and the buffering effect of the nested catchments.

4.6. Conclusions

The immediate installation of two nested monitoring stations after a severe wildfire in a terraced Mediterranean catchment facilitated the study of hydrological and sediment delivery dynamics during the three hydrological years following the wildfire, when the window of disturbance period is expected to be more active.

The low values of post-fire suspended sediment delivery –especially compared to those reported in other burned catchments for similar environments– can be explained by the calcareous soils and the massive presence of terraces. In addition, these same driving factors caused very low runoff coefficients (<5%) under average rainfall intensity consistent with long-term records. However, high-intensity rainfall proved essential to attaining effective slope-to-channel sediment connectivity. The storm that occurred on 29th October 2013 generated a SS yield of 17 t km^2 yr^{-1} in only 15 minutes at the catchment outlet, which was 92% of the sediment load measured during the study period.

Although the probable divergence between hillslope erosion and sediment delivery responses to wildfire may encompass detailed information on individual components of a suspended sediment budget, the nested approach has increased understanding of post-fire hydrological responses and sediment transport dynamics at the catchment scale. This approach is particularly effective in Mediterranean environments, where there are large areas of permeable lithology (i.e. limestone) that cause the interaction

of influent and effluent processes along the channel systems. In addition, the old and new terraces contribute to an increase in water storage on the hillslopes and an increase in runoff and sediment disconnectivity. Finally, if fire affects the ecosystem's resilience, a delayed response of the landscape must be hypothesized. Further analysis of the medium- and long-term impacts would explain better when and how fire disturbances act. Thus, the need for long-term monitoring programmes should be emphasized.

Acknowledgments

This research was supported by the Balearic Forest Service (Department of the Environment, Agriculture and Fisheries of the Balearic Autonomous Government) and the research project CGL2012-32446 "Assessing hydrological and sediment connectivity in contrasting Mediterranean catchments. Impacts of Global Change-MEDhyCON", funded by the Ministry of Economy and Competitiveness of the Spanish Government. Julián García-Comendador is in receipt of a pre-doctoral contract (FPU15/05239) funded by the Spanish Ministry of Education and Culture. Josep Fortesa has a contract funded by the European Commission - Directorate-General for European Civil Protection and Humanitarian Aid Operations. Aleix Calsamiglia acknowledges support from the Spanish Ministry of Economy and Competitiveness through a pre-doctoral contract EEBB-I-15-10280. Meteorological data were facilitated by the Spanish Meteorological Agency (AEMET). Thanks must also be expressed to Joan Bauzà Llinàs for his assistance during the construction of the gauging stations.

4.7. References

Arnáez J, Lana-Renault N, Lasanta T, Ruiz-Flaño P, Castroviejo J. 2015. Effects of farming terraces on hydrological and geomorphological processes. A review. Catena 128: 122–134.

Arnau-Rosalén, E., Calvo Cases, A., Boix-Fayos, C., Lavee, H., Sarah, P., 2008. Analysis of soil surface component patterns affecting runoff generation. An example of methods applied to Mediterranean hillslopes (Alicante, Spain). Geomorphology 101 (4), 595-606

Batalla RJ. 1993. Sand-bed transport contribution to the sediment budget of a granitic Mediterranean drainage basin. Unpublished PhD Thesis. University of Barcelona: Barcelona.

Bauzà J. 2014. Els grans incendis forestals a les Illes Balears: una resposta des de la teledetecció. (Bachelor thesis). Universitat de les Illes Balears, Spain. 37 pp.

Boix Fayos, C. 1997. The roles of texture and structure in the water retention capacity of burnt Mediterranean soils with varying rainfall. Catena 31: 219–236

Brown LC, Foster GR.1987. Storm erosivity using idealized intensity distributions. Transactions of the ASAE-American Society of Agricultural Engineers 30: 379–386.

Buendia C, Bussi G, Tuset J, Vericat D, Sabater S, Palau A, Batalla RJ. 2015. Effects of afforestation on runoff and sediment load in an upland Mediterranean catchment. Science of The Total Environment 540: 144-157.

Calsamiglia A, Gago J, García-Comendador J, Fortesa J, Medrano H, Estrany J. 2015. Effects of soil conservation structures and post-fire management practices in functional connectivity and erosion with a Mediterranean catchment. British Society for Geomorphology Annual Meeting.

Calsamiglia A, Fortesa J, Garcia-Comendador J, Calvo-Cases A, Estrany J. 2017. Spatial patterns of sediment connectivity in terraced lands: anthropogenic controls on catchment sensitivity. Land Degradation & Development. Under review.

Calvo-Cases A, Boix-Fayos C, Imeson AC. 2003. Runoff generation, sediment movement and soil water behaviour on calcareous (limestone) slopes of some Mediterranean environments in southeast Spain. Geomorphology 50: 269–291.

Calvo-Cases A, Boix-Fayos C, Arnau-Rosalen E. 2005. Patterns and thresholds of runoff and sediment transport on some Mediterranean hillslopes. In: Garcia, C. y Batalla, R. J (Eds.), Catchment Dynamics and River Processes: Mediterranean and Other Climate Regions. Elsevier, Amsterdam, 31 – 51.

Cammeraat EL. 2004. Scale dependent thresholds in hydrological and erosion response of a semi-arid catchment in southeast Spain. Agriculture, ecosystems & environment 104: 317-332.

Candela A, Aronica G, Santoro M. 2005. Effects of Forest Fires on Flood Frequency Curves in a Mediterranean Catchment. Hydrological Sciences Journal 50: 193-206.

Castillo VM, Martinez-Mena M, Albadalejo J. 1997. Runoff and soil loss response to vegetation removal in a semiarid environment. Soil Science Society of America Journal 61: 1116-1121.

Cavalli M, Trevisani S, Comiti F, Marchi L. 2013. Geomorphometric assessment of spatial sediment connectivity in small Alpine catchments. Geomorphology, 188: 31-41.

Cerdà A, Doerr SH. 2005. Long-term soil erosion changes under simulated rainfall for different vegetation types following a wildfire in eastern Spain. Journal of Wildland Fire 14: 423-437.

De Girolamo AM, Pappagallo G, Lo Porto A. 2015. Temporal variability of suspended sediment transport and rating curves in a Mediterranean river basin: The Celone (SE Italy). CATENA 128: 135-143.

Djorovic M. 1992. Ten-years of sediment discharge measurement in the Jasenica research drainage basin, Yugoslavia. Erosion, debris flows and environment in mountain regions (proceedings of the Chengdu Symposium, July 1992). 209: 37-40.

De Luís M, González-Hidalgo JC, Raventós J. 2003. Effects of fire and torrential rainfall on erosion in a Mediterranean gorse community. Land Degradation & Development 14: 203-213.

Dunjó G, Pardini G, Gispert M. 2003. Land use change effects on abandoned terraced soils in a Mediterranean catchment, NE Spain. CATENA 52: 23-37.

Escuín S, Navarro R, Fernandez P. 2008. Fire severity assessment by using NBR (Normalized Burn Ratio) and NDVI (Normalized Difference Vegetation Index) derived from LANDSAT TM/ETM images. International Journal of Remote Sensing 29: 1053-1073.

Estrany J, Garcia C, Batalla RJ. 2009. Groundwater control on the suspended sediment load in the Na Borges River, Mallorca, Spain. Geomorphology 106: 292-303.

Estrany J, 2009. Hydrology and sediment transport in the agricultural Na Borges River basin (Mallorca, Balearic Islands). A Mediterranean groundwater-dominated river under traditional soil conservation practices. Unpublished PhD thesis, Palma, Universitat de les Illes Balears.

Estrany J, Garcia C, Batalla RJ. 2010. Hydrological response of a small mediterranean agricultural catchment. Journal of Hydrology 380, 180-190.

Estrany J, Garcia C, Walling DE, Ferrer L. 2011. Fluxes and storage of fine-grained sediment and associated contaminants in the Na Borges River (Mallorca, Spain). CATENA 87:291-305. DOI: 10.1016/j.catena.2011.06.009

Estrany J, Grimalt M. 2014. Catchment controls and human disturbances on the geomorphology of small Mediterranean estuarine systems. Estuarine, Coastal and Shelf Science 150: 230-241.

Estrany J, López-Tarazón JA, Smith H. 2016. Wildfire effects on suspended sediment delivery quantified using fallout radionuclides tracers in a Mediterranean catchment. Land Degradation & Development 27:1501-1512. DOI: 10.1002/ldr.2462

Estrany J, Calsamiglia A, Ruiz M, Carriquí M, García-Comendador J, Nadal M, Fortesa J, Medrano H, Gago J. 2019. Sediment connectivity linked to vegetation using UAVs: high-resolution imagery for ecosystem management. Sci Total Environ. 671: 1192-1205. DOI: https://doi.org/10.1016/j.scitotenv.2019.03.399.

FAO .2006. Guidelines for soil description. 4th Ed. (revised). Soil Resources, Management and Conservation Service, Land and Water Development Division. FAO, Roma. 70 pp.

Ferreira AJD, Coelho COA, Ritsema CJ, Boulet AK, Keizer JJ. 2008. Soil and water degradation

processes in burned areas: Lessons learned from a nested approach. Catena 74: 273-285.

Gallart F, Pérez-Gallego N, Latron J, Catari G, Martínez-Carreras N, Nord G. 2013. Short- and long-term studies of sediment dynamics in a small humid mountain Mediterranean basin with badlands. Geomorphology 196: 242–251.

García-Comendador J, Fortesa J, Calsamiglia A, Garcias F, Estrany J. 2017. Source ascription in bed sediments of a Mediterranean temporary stream after the first post-fire flush. Journal of Soils and Sediments. Under review.

García-Ruiz JM, Nadal-Romero E, Lana-Renault N, Beguería S. 2013. Erosion in Mediterranean landscapes: Changes and future challenges. Geomorphology 198: 20-36.

Gimeno-García E, Andreu V, Rubio JL. 2007. Influence of vegetation recovery on water erosion at short and medium-term after experimental fires in a Mediterranean shrubland. Catena 69: 150-160.

Grimalt M, Blázquez M, Rodríguez R. 1992. Physical factors, distribution and present land-use of terraces in the Tramuntana Range. Pirineos 139: 15-25.

Guijarro JA. 1986. Contribución a la Bioclimatología de Baleares. (Doctoral Thesis resume summary), Universitat de les Illes Balears, 36 pp.

Hooke JM. 2006. Human impacts on fluvial systems in the Mediterranean region. Geomorphology 79: 311-335.

Iroumé A. 1990. Assessment of runoff and suspended sediment yield in a partially forested catchment in Southern Chile. Water Resources Research 26: 2637-2642.

Inbar M, Tamir M, Wittenberg L. 1998. Runoff and erosion processes after a forest fire in Mount Carmel, a Mediterranean area. Geomorphology 24: 17-33.

Klein M. 1984. Anti-clockwise hysteresis in suspended sediment concentration during individual storms: Holbeck Catchment; Yorkshire, England. Catena 11: 251-257.

Lane PN, Sheridan GJ, Noske PJ. 2006. Changes in sediment loads and discharge from small mountain catchments following wildfire in south eastern Australia. Journal of Hydrology 331: 495-510.

Lane PN, Noske PJ, Sheridan GJ .2011. Phosphorus enrichment from point to catchment scale following fire in eucalypt forests. Catena 87: 157-162.

Lane PN, Sheridan GJ, Noske PJ, Sherwin CB, Costenaro JL, Nyman P, Smith HG. 2012. Fire effects on forest hydrology: lessons from a multi-scale catchment experiment in SE Australia. 137-143. In: Webb AA, Bonell M, Bren L, Lane PN, McGuire D, Neary DG (eds.) Revisiting Experimental Catchment Studies in Forest Hydrology. IAHS Publ. 353, IAHS Press, Wallingford, pp. 137-143.

Lasanta T, Arnáez J, Oserín M, Ortigosa LM. 2001. Marginal lands and erosion in terraced fields in the Mediterranean mountains: a case study in the Camero Viejo (Northwestern Iberian System, Spain). Mountain Research and Development 21: 69-76.

Lesschen JP, Cammeraat LH, Nieman T, 2008. Erosion and terrace failure due to agricultural land abandonment in a semi-arid environment. Earth Surface Processes & Landforms 33: 1574–1584.

López-Tarazón JA, Estrany J. 2017. Exploring suspended sediment delivery dynamics of two Mediterranean nested catchments. Hydrological Processes 31(3): 698-715.

Ministerio de Agricultura, Alimentación y Medio Ambiente (MAGRAMA). 2012. Cuarto Inventario Forestal Nacional. 48 pp.

Mayor AG, Bautista S, Llovet J, Bellot J. 2007: Post-fire hydrological and erosional responses of a Mediterranean landscape: Seven years of catchment-scale dynamics. Catena 71: 68-75.

Meyer GA, Pierce JL, Wood SH, Jull AJT. 2001. Fire, storms, and erosional events in the Idaho batholith. Hydrological Processes 15: 3025-3038.

Moody JA, Martin DA. 2001. Initial hydrologic and geomorphic response following a wildfire in the Colorado Front Range. Earth Surface Processes and Landforms 26: 1049-1070.

Moody JA, Martin DA. 2009. Synthesis of sediment yields after wildland fire in different rainfall regimes in the western United States. International Journal of Wildland Fire 18: 96-115.

Morán-Tejeda E, Ceballos-Barbancho A, Llorente-Pinto JM. 2010. Hydrological response of Mediterranean headwaters to climate oscillations and land-cover changes: The mountains of Duero River basin (Central Spain). Global and Planetary Change 72: 39-49.

Nadal-Romero E, Latron J, Martí-Bono C, Regüés D. 2008. Temporal distribution of suspended sediment transport in a humid Mediterranean badland area: the Araguás catchment, Central Pyrenees. Geomorphology 97: 601-616.

Oeurng C, Sauvage S, Sánchez-Pérez JM. 2010. Dynamics of suspended sediment transport and yield in a large agricultural catchment, southwest France. Earth Surface Processes and Landforms 35, 1289-1301.

Owens PN, Blake WH, Giles TR, Williams ND. 2012. Determining the effects of wildfire on sediment sources using ^{137}Cs and unsupported ^{210}Pb: the role of landscape disturbances and driving forces. Journal of Soils and Sediments 12: 982-994.

Owens PN, Giles TR, Petticrew EL, Leggat MS, Moore RD, Eaton BC. 2013. Muted responses of streamflow and suspended sediment flux in a wildfire-affected watershed. Geomorphology 202: 128-139.

Pacheco E, Farguell J, Úbeda X, Outeiro L, Miguel A. 2011 Runoff and sediment production in a Mediterranean basin under two different land uses. Cuaternario & Geomorfología 25:103-114.

Pavanelli D, Pagliarani A. 2002. SW- Soil and Water: Monitoring Water Flow, Turbidity and Suspended Sediment Load, from an Apennine Catchment Basin, Italy. Biosystems Engineering 83: 463-468.

Prosser IP, Williams L. 1998. The effect of wildfire on runoff and erosion in native Eucalyptus forest. Hydrological Processes 12: 251-265.

Reneau SL, Katzman D, Kuyumjian GA, Lavine A, Malmon DV. 2007. Sediment delivery after a wildfire. Geology 35: 151-154.

Robichaud PR, Wagenbrenner JW, Lewis SA, Ashmun LE, Brown RE, Wohlgemuth PM. 2013. Post-fire mulching for runoff and erosion mitigation Part II: Effectiveness in reducing runoff and sediment yields from small catchments. Catena 105: 93–111.

Rovira A, Batalla RJ. 2006. Temporal distribution of suspended sediment transport in a Mediterranean basin: The Lower Tordera (NE SPAIN). Geomorphology 79: 58-71.

Schick PA. 1967. Suspended sampler and bedload trap. In Field methods for the study of slope and fluvial processes. Rev. Geomorphologie Dynamique 17: 181-182.

Scott DF, Versfeld DB, Lesch W. 1998. Erosion and sediment yield in relation to afforestation and fire in the mountains of the Western Cape Province, South Africa. South African Geographical Journal 80: 52-59.

Seeger M, Errea MP, Begueria S, Arnáez J, Martı C, Garcıa-Ruiz,JM. 2004. Catchment soil moisture and rainfall characteristics as determinant factors for discharge/suspended sediment hysteretic loops in a small headwater catchment in the Spanish Pyrenees. Journal of Hydrology 288: 299-311.

Shakesby RA, Doerr SH. 2006. Wildfire as a hydrological and geomorphological agent. Earth Science Reviews 74: 269-307.

Shakesby RA. 2011. Post-wildfire soil erosion in the Mediterranean: review and future research directions. Earth-Science Reviews 105: 71-100.

Smith HG, Sheridan GJ, Lane PN, Noske PJ, Heijnis H. 2011a. Changes to sediment sources following wildfire in a forested upland catchment, southeastern Australia. Hydrological Processes, 25: 2878-2889.

Smith HG, Sheridan GJ, Lane PN, Nyman P, Haydon S. 2011b. Wildfire effects on water quality in forest catchments: a review with implications for water supply. Journal of Hydrology 396: 170-192.

Smith HG, Blake WH, Owens PN. 2013. Discriminating fine sediment sources and the application of sediment tracers in burned catchments: a review. Hydrological Processes 27: 943-958.

Tarolli P, Preti F, Romano N. 2014. Terraced landscapes: From an old best practice to a potential hazard for soil degradation due to land abandonment. Anthropocene 6: 10-25.

Tomaz C, Alegria C, Monteiro JM, Teixeira MC. 2013. Land cover change and afforestation of marginal and abandoned agricultural land: A 10 year analysis in a Mediterranean region. Forest Ecology and Management 308: 40-49.

Tzoraki O, Nikolaidis NP. 2007. A generalized framework for modeling the hydrologic and biogeochemical response of a Mediterranean temporary river basin. Journal of Hydrology 346: 112-121.

Úbeda X, Outeiro L. 2009. Physical and chemical effects of fire on soil. In 'Fire Effects on Soils and Restoration Strategies'. (Eds A Cerdà, PR Robichaud) pp 105-132. (Science Publishers Endfield Nh: USA).

Van Dijk AIJM, Bruijnzeel LA, Rosewell CJ. 2002. Rainfall intensity–kinetic energy relationships: a critical literature appraisal. Journal of Hydrology 261: 1-23.

Vanmaercke M, Poesen J, Verstraeten G, de Vente J, Ocakoglu F. 2011. Sediment yield in Europe: spatial patterns and scale dependency. Geomorphology 130: 142-161.

Vieira DCS, Fernández C, Vega JA, Keizer JJ. 2015. Does soil burn severity affect the post-fire runoff and interrill erosion response? A review based on meta-analysis of field rainfall simulation data. Journal of Hydrology 523: 452-464.

Walling DE. 1999. Linking land use, erosion and sediment yields in river basins. Hydrobiologia 410, 223–240.

Warrick JA, Hatten JA, Pasternack GB, Gray AB, Goni MA, Wheatcroft RA. 2012. The effects of wildfire on the sediment yield of a coastal California watershed. Geological Society of America Bulletin 124: 1130-1146.

Wass PD, Leeks GJL. 1999. Suspended sediment fluxes in the Humber catchment, UK. Hydrological Processes 13: 935–953.

Wilkinson SN, Wallbrink PJ, Hancock GJ, Blake WH, Shakesby RA, Doerr SH. 2009. Fallout radionuclide tracers identify a switch in sediment sources and transport-limited sediment yield following wildfire in a eucalypt forest. Geomorphology 110: 140-151.

Williams GP. 1989. Sediment concentration versus water discharge during single hydrologic events in rivers. Journal of Hydrology 111: 89-106.

YACU. 2002. Estudio de caracterización del régimen extremo de precipitaciones en la isla de Mallorca. Memoria [translation to English: Characterization of the extreme rainfall regime on the island of Mallorca]. Secció d'Estudis i Projectes, Direcció General de Recursos Hídrics, Conselleria de Medi Ambient, Govern de les Illes Balears (Palma de Mallorca, SP).

4.8. Supplementary material

Supplementary table 4.1. Description of the rainfall-derived runoff and sediment transport-derived variables analysed for all the floods recorded at US-Sa Murtera and DS-Sa Font de la Vila gauging stations.

Flood	Ptot (mm)	Imax30 (mm h^{-1})	Erosivity (Mj*mm/ha*h)	P1d (mm)	P7d (mm)
29/10/2013	50.00	100.00	2,885.93	3.00	3.02
17/11/2013	65.80	18.00	310.71	17.00	77.80
01/12/2013	29.00	10.00	80.10	3.40	30.20
19/12/2013	69.00	10.00	167.78	0.20	1.00
01/12/2014	25.60	21.20	179.22	19.60	35.40
15/12/2014	29.60	29.60	430.26	0.00	0.20
20/01/2015	61.80	10.80	178.29	4.80	11.80
04/02/2015	8.20	0.40	0.55	1.00	4.00
17/02/2015	2.60	0.40	0.16	0.20	0.40
25/03/2015	N/D	N/D	N/D	N/D	N/D
29/03/2016	N/D	N/D	N/D	N/D	N/D
01/04/2016	49.60	11.2	118.15	0	0.2

Flood	Dur. (min)		Volume (m^3)		Q peak (m^3 s^{-1})	
	US	DS	US	DS	US	DS
29/10/2013	N/D	105.00	N/D	3,898.10	N/D	1.50
17/11/2013	N/D	3,915.00	N/D	3,819.14	N/D	0.10
01/12/2013	N/D	2,610.00	N/D	4,536.82	N/D	0.15
19/12/2013	N/D	3,210.00	N/D	5,725.80	N/D	0.09
01/12/2014	450.00	-	168.55	0.00	0.01	0.00
15/12/2014	435.00	510.00	856.00	1,443.38	0.10	0.19
20/01/2015	1,815.00	1,635.00	4,850.75	18,018.17	0.18	0.50
04/02/2015	1,800.00	1,845.00	1,760.20	6572.82	0.03	0.17
17/02/2015	2,970.00	4,425.00	2,324.95	4,478.51	0.02	0.07
25/03/2015	2,235.00	1,845.00	5,007.88	6,544.27	0.06	0.08
29/03/2016	-	2,595.00	0.00	8,516.54	0.00	0.10
01/04/2016	2,175.00	-	1,375.64	0.00	0.07	0.00

Flood	Q mean (m^3 s^{-1})		Qb (m^3 s^{-1})		Runoff ratio (mm)	
	US	DS	US	DS	US	DS
29/10/2013	N/D	0.61	N/D	0.00	N/D	0.81
17/11/2013	N/D	0.02	N/D	0.00	N/D	0.79
01/12/2013	N/D	0.03	N/D	0.00	N/D	0.94
19/12/2013	N/D	0.03	N/D	0.00	N/D	1.19
01/12/2014	0.01	0.00	0.00	0.00	0.14	0.00
15/12/2014	0.03	0.05	0.01	0.00	0.72	0.30
20/01/2015	0.05	0.18	0.00	0.00	4.07	3.75
04/02/2015	0.02	0.06	0.01	0.00	1.48	1.37
17/02/2015	0.01	0.02	0.00	0.00	1.95	0.93
25/03/2015	0.06	0.06	0.01	0.01	4.20	1.36

29/03/2016	0.00	0.05	0.00	0.00	0.00	1.77
01/04/2016	0.03	0.00	0.00	0.00	1.15	0.00

Flood	Runoff coefficient (%)		Sediment load (kg)		Sediment yield (t km^{-2})	
	US	DS	US	DS	US	DS
29/10/2013	N/D	1.62	N/D	84,098.74	N/D	17.44
17/11/2013	N/D	1.21	N/D	3,176.93	N/D	0.66
01/12/2013	N/D	3.25	N/D	1,803.48	N/D	0.38
19/12/2013	N/D	1.73	N/D	649.48	N/D	0.14
01/12/2014	0.55	0.00	131.38	0.00	131.38	0.00
15/12/2014	2.42	1.01	770.50	137.66	700.45	0.03
20/01/2015	6.58	6.07	745.76	1,099.95	677.96	0.23
04/02/2015	18.00	16.68	408.43	72.41	371.30	0.02
17/02/2015	74.97	35.84	256.36	37.62	233.05	0.01
25/03/2015	N/D	N/D	91.39	96.17	83.08	0.02
29/03/2016	N/D	N/D	0.00	295.40	0.00	0.06
01/04/2016	2.33	0.00	5.64	0.00	5.13	0.00

Flood	Average SSC (mg l^{-1})		SSC peak (mg l^{-1})		Hysteresis loop	
	US	DS	US	DS	US	DS
29/10/2013	N/D	17,417.25	N/D	33,617.98	N/D	Counterclokwise
17/11/2013	N/D	261.34	N/D	11,848.27	N/D	Counterclokwise*
01/12/2013	N/D	161.00	N/D	3,178.72	N/D	Counterclokwise*
19/12/2013	N/D	67.33	N/D	2,259.93	N/D	Counterclokwise*
01/12/2014	587.53	0.00	5,244.72	0.00	Clockwise*	-
15/12/2014	834.34	48.80	4,556.95	215.18	Counterclokwise	Clockwise
20/01/2015	87.90	32.30	1,124.69	285.13	Clockwise*	Clockwise
04/02/2015	223.51	8.40	2,299.74	56.48	Counterclokwise*	Counterclokwise*
17/02/2015	104.91	8.60	2,074.77	107.34	Counterclokwise*	Clockwise
25/03/2015	18.67	13.30	133.79	61.78	Clockwise*	Counterclokwise*
29/03/2016	0.00	21.64	0.00	285.13	-	Clockwise
01/04/2016	7.23	0.00	91.14	0.00	Counterclokwise*	-

* Multipeack floods

5. Source ascription in bed sediments of a Mediterranean temporary stream after the first post-fire flush

Abstract

Purpose: First flushes can be crucial to sediment transport in fluvial systems of drylands, as temporary streams are a characteristic feature of Mediterranean basins. After a wildfire, storm flows may enhance runoff delivery to channels, so increasing the first-flush effect. ^{137}Cs and $^{210}Pb_{ex}$ were used as tracers for recognizing the first post-fire flush effect on the source ascription of bed sediments temporarily stored in a Mediterranean temporary stream severely affected by a wildfire.

Materials and Methods: Thirty sediment source samples were collected along one of the tributaries of a catchment (4.8 km^2) located in Mallorca during a field campaign some weeks after the wildfire. The sample collection took into account effects of the wildfire and distinguished between soil surface and channel bank. To measure the source contribution temporarily stored with the bed sediment, five sediment samples –deposited during the first storm, occurring three months after the wildfire– were collected from the bed stream of the main channel. The ^{137}Cs and $^{210}Pb_{ex}$ concentrations were measured by gamma spectrometry. Then, a linear mixing model was used to establish the contribution of each source type to the bed sediments along the main stream.

Results and Discussion: Post-fire first-flush effect was generated by a torrential event with a suspended-sediment concentration peak of 33,618 mg L^{-1}, although transmission losses under a very low runoff coefficient (1%) promoted sediment deposition. Significant differences were observed in fallout radionuclide concentrations between burned surface soil and burned channel bank samples ($p < 0.05$), as well as between burned and unburned sources in the downstream part of the catchment ($p < 0.01$). The radioactivity concentrations in bed sediment samples were statistically similar ($p > 0.05$). Source ascription in bed sediments upstream shows that 67% was generated from burned hillslopes, reaching 75% in the downstream part because downstream propagation of the sediment derived from the burned area.

Conclusions: Bed sediments were mostly generated on burned surface soils because of the fire's effect on soil and sediment availability, high-intensity rainfall and the limited contribution of channel banks, because these are fixed by dry-stone walls. This hydro-sedimentary response indicates an association between these factors driving erosion and sediment delivery, generating effective slope-to-channel sediment connectivity. The integration of the short-response with the medium and long term analysis will allow the analysis of the catchment sediment sources evolution in future studies, determining if fire modifies the catchment sensitivity to that specific disturbance.

Keywords: First flush sediment sources, Wildfire disturbances, Fingerprinting technique, Fallout radionuclides, Mediterranean fluvial systems

Reference

García-Comendador, J., Fortesa, J., Calsamiglia, A., Garcias, F., and Estrany, J. 2017. Source ascription in bed sediments of a Mediterranean temporary stream after the first post-fire flush. J Soils Sediments 17, 2582–2595. doi: 10.1007/s11368-017-1806-1

5.1. Introduction

Processes not seen in perennial flow characterize the hydrological response of catchments in arid or semi-arid ecosystems. Rivers under perennial regimes are regularly fed by water from contiguous compartments. In contrast, water-flow pathways in semi-arid river catchments are disrupted for longer periods of months or even years. In this context, a significant amount of water is lost through the river bed or by evaporation, leading to the complete drying up of the river in many cases. First flushes are of great importance for particulate and dissolved transport in dryland fluvial systems in Mediterranean basins, where temporary streams are very common (Bull and Kirkby, 2002). The term “first flush effect” refers to rapid changes in water quality (concentration or load) within a distinct flood event (Obermann et al., 2009). These occur frequently after early-season rains with a previous accumulation of mass. Sediments and other accumulated organic particles on the riverbed are remobilized and can be flushed out into the streams. In-channel sediment storage is favoured in temporary rivers, because precipitation or other sources are insufficient to produce uninterrupted discharge into the entire length of the river. In humid temperate rivers characterised by relatively stable hydrological regimes, these temporarily stored sediments are often flushed annually (Walling et al., 1998). However, in Mediterranean temporary rivers, sediment may be accumulated steadily over several hydrological years until a major flood event evacuates the stored sediment (Estrany et al., 2011).

After a wildfire, many complex variables are involved in erosion processes in catchments. Vegetation status, slope, soil type, severity of effect, heavy rainfall, presence of soil and water conservation structures (i.e. hillslope and valley-bottom terraces) and post-fire management are some of the most important. All these cause divergent responses by varying erosion rates and sediment yields (Shakesby and Doerr, 2006; Moody et al., 2013). Nevertheless, the overall hydrological impact of wildfire at catchment scale is related to the increase of overland flow (Shakesby and Doerr, 2006), either by infiltration-excess or by saturation. Complete or partial removal of the vegetation and litter cover as well as the formation of surface ash deposits generally lead to higher percentages of rainfall available for overland flow (Bochet et al., 2002;

Candela et al., 2005). As a result, post-fire storm flows may enhance runoff delivery to channels, thus increasing the first-flush effect. Specifically, low-intensity rainfall may promote the integration of ash deposits into the soil through infiltration. However, under intense rainfall, the ash layer is removed and released to the fluvial network, with significant repercussions on calculation of hillslope surface source contributions to post-fire catchment sediment exports (Smith et al., 2011a). Shakesby (2011) highlighted the distinctive characteristics of wildfire impacts on hydrology, soil properties and soil erosion by water in Mediterranean landscapes due to intricate land-use patterns, abandoned terraces and tracks interrupting slopes. The integrated catchment perspective is then required to understand how wildfire perturbations affect the internal dynamics of catchment sediment cascades (Fryirs et al., 2013), i.e. the downstream sediment delivery to a basin outlet. In addition, fine sediment plays a significant role in the transfer and fate of nutrients (Horowitz et al., 2007), a process enhanced after wildfire (Smith et al. 2011a). However, hydrological responses to wildfire at the catchment scale have received much less attention than at smaller scales at both Mediterranean and world-wide locations, mainly because of the greater practical difficulties and expense involved when monitoring at this scale (Shakesby and Doerr, 2006).

Therefore, information on the nature and relative contributions of the different sources of sediment in fluvial systems may be a key factor in the design and implementation of specific strategies for post-fire erosion control. Sediment fingerprinting approaches continue to be used to determine sediment sources, providing spatiotemporal data on the main production areas and their quantitative contributions to the fluvial network at the catchment scale (Walling, 2013; Haddadchi et al., 2013; Owens et al., 2016). The implementation of this technique still involves several uncertainties (Pulley et al., 2015), due to variability of potential sources (Du and Walling, 2017), the possible alteration of sediment properties during transport (Poulenard et al., 2012) and the methods of sampling (Manjoro et al., 2017), analysis and statistics (Haddadchi et al. 2014; Palazón and Navas 2017). In addition, a wide variety of different tracers has been employed in the published literature, as Collins et al. (2017) recently reviewed. However, most of these focus on natural and burn-

related variability, in order to distinguish burned and unburned sources (Smith et al., 2013).

To date, fallout radionuclide tracers (hereafter FRN) provide the best available fine-sediment tracers for surface soil and channel source discrimination following a wildfire (Smith et al., 2011b; Owens et al., 2012; Zhang et al., 2016) and for evaluating the spatial provenance of sediment in terms of burned and unburned areas (Stone et al., 2014; Estrany et al., 2016). The activity concentrations of both radionuclides in burned landscapes tend to increase – especially for $^{210}Pb_{ex}$- due to soil mass reduction by organic matter combustion and radionuclide transfer and redistribution from burned vegetation to the soil (Johansen et al., 2003; Wilkinson et al., 2009). Consequently, these FRN provide quality information about distribution and discrimination of sediment sources in catchments affected by wildfires (Smith et al., 2013). However, to date their use has been limited to North America (Moody and Martin, 2001; Owens et al., 2012), Australia (Blake et al., 2009; Wilkinson et al., 2009; Smith et al., 2011b) and, to a lesser extent, the European Mediterranean region (Estrany et al., 2016), even though wildfire is a significant agent in shaping hydrological and geomorphological dynamics (Shakesby, 2011).

The aim of this study was to use ^{137}Cs and $^{210}Pb_{ex}$ radioisotopes as tracers to recognize the effect of fire on the catchment's sediment source response during the first post-fire flush along the main stem of a Mediterranean temporary stream three months after a severe wildfire that occurred in July 2013. Specific objectives focused on (i) quantifying the relative contributions of hillslopes and channel banks within the fine bed sediment temporarily stored on the riverbed surface during the first post-fire flush; and (ii) determining the contribution of burned and unburned material to sediment in the downstream part of the catchment.

5.2. Material and Methods

5.2.1. Study area

The Sa Font de la Vila is a Mediterranean catchment of 4.8 km^2, located in Pariatge County (Andratx, western part of Mallorca; Figure 5.1A and 5.1B), characterized by

afforestation of former agricultural land and the effects of recurrent wildfires. The catchment's morphology is complex, with height ranging between 63 and 517 m.a.s.l. and a mean gradient slope of 38% (Figure 5.1D); although 50% of the surface area has gradients lower than 15%. Currently, agricultural activities are restricted to the valley bottoms, where the slope is less pronounced (<10%). Lithology (Figure 5.1C) consists mainly of Upper Triassic (Keuper) clays and loams. In the upper parts, where Triassic (Rhaetian) dolomites and Lower Jurassic limestone predominate, the slope gradients are steeper than 30%. Under the Soil Taxonomy System, the soils can be classified as Entisols at the catchment headwaters and Alfisols in the lower parts. The fluvial network consists of two main sub-catchments: Sa Coma Freda (2.3 km^2) and Can Cabrit (2.1 km^2) rivers. The former is characterized by an intermittent regime maintained by several karstic springs, whilst the latter is ephemeral. Can Cabrit River is also constricted by a check dam built in 2007 (Figure 5.1E), which retained most of the post-fire fluxes before they reached the downstream part of the Sa Font de la Vila mainstream.

Under the Emberger climate classification, the climate is Mediterranean temperate sub-humid at headwaters and warm sub-humid at the outlet (Guijarro, 1986). The average temperature is 16.5 °C and the mean annual rainfall 517.8 mm yr^{-1} with an interannual coefficient of variation of 29%. High-intensity rainstorms with a recurrence period of 10 years may reach 85 mm in 24 hours following the statistics of the 1974-2010 period in the B118 S'Alqueria station (see location in Figure 5.1B) of the Spanish Meteorological Agency – AEMET. This meteorological station is located 4 km from the Sa Font de la Vila River catchment within the same daily rainfall affinity area in Mallorca (Sumner et al., 1993).

Before the 2013 wildfire, the Sa Font de la Vila catchment was mainly covered by natural vegetation (71%, with 52% forest and 19% scrubland; Figure 5.1E). The rest of the catchment was covered by tree crops (23%) and herbaceous (6%) rain-fed crops. There is also a massive presence of traditional soil and water conservation structures (i.e. hillslope and valley-bottom terraces), occupying 37% of the total surface area and a linear length of 147 km (Figure 5.1E), of which 75.1 ha are well-maintained and 103.7

ha abandoned, with an average collapse point density of 12 collapses km^{-1} and 55 collapses km^{-1}, respectively (Calsamiglia et al., 2017).

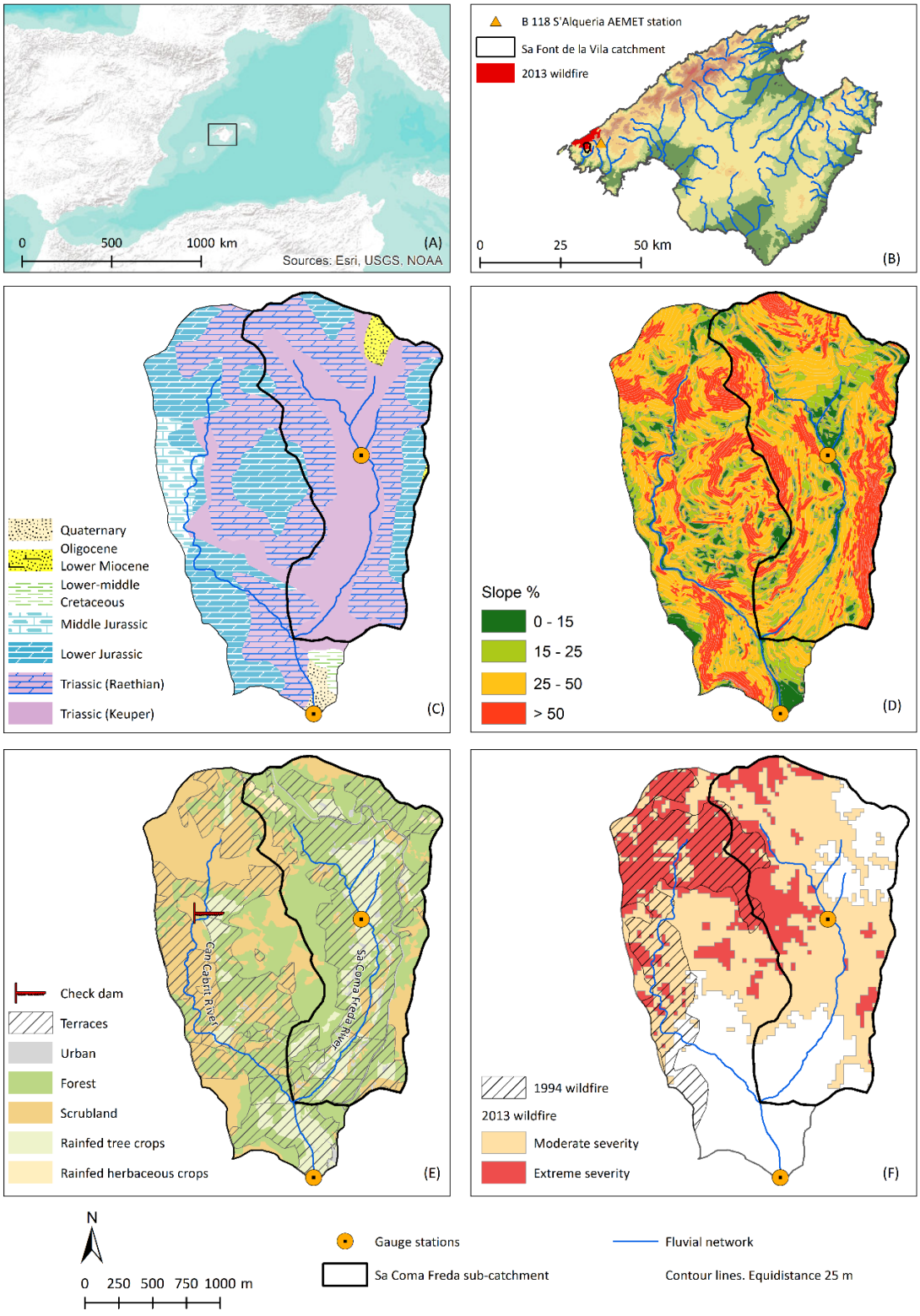

Figure 5.1. (A) Map showing the location of Mallorca in the Mediterranean Sea; (B) location of the Sa Font de la Vila catchment and the area affected by the July 2013 wildfire in Pariatge County; (C) lithology; (D) gradient slope; (E) land uses and soil conservation practices; and (F) 1994 and 2013 wildfire-affected areas and severity of 2013 wildfire.

The catchment has been affected by two major wildfires in the last twenty years. The first, occurring in 1994, affected 25% of the catchment area. In the second one, occurring in July 2013, 71% of its surface area was burned. 30% of this affected area had already burned in 1994 (Figure 5.1F). Using *Landsat 8* images, the burn severity assessment of the most recent wildfire –applying the Normalized Burn Ratio pre-/post-fire difference values (*dNBR*; Escuín et al., 2008)– depicted extreme severity in 24% of the catchment and moderate severity in 47% (Bauzà, 2014).

5.2.2. Monitoring hydro-sedimentary dynamics after the 2013 wildfire

In September 2013 a programme of continuous water and sediment yield measurements was implemented by instruments at two nested gauging stations (Figure 5.1), Sa Murtera (the upstream site, hereafter US; 1.1 km^2) and Sa Font de la Vila (the downstream site, hereafter DS; 4.8 km^2). *Campbell CR200* loggers stored the average values of water stage and turbidity, based on 1-minute readings at 15-minute intervals collected by a *Campbell Scientific CS451-L* pressure probe and an *OBS-3+* turbidimeter with a double measurement range of 0-1,000/1,000-4,000 NTU. Additionally, a *Casella* tipping bucket rain gauge was installed at US for analysing the rainfall dynamics within the catchment. For deeper comprehension, García-Comendador et al. (2017) provide a detailed analysis of the instruments as well as the hydro-sedimentary response of the catchment during the 2013-2016 period, in which calcareous soils, terraces and the application of post-fire measures limited this response despite the wildfire's impact.

The analysis of bed sediment temporarily stored in the channel is based on the first erosive storm after the wildfire (Supplementary figure 5.1), which only affected the Sa Coma Freda River.

5.2.3. Field sampling

Although a wider sediment source monitoring programme was developed in the whole Sa Font de la Vila catchment, this study only used those sediment source samples (30)

collected along the Sa Coma Freda River (Figure 5.2) because the first flush only affected this sub-catchment, as explained in section 5.2.2. The field campaign was carried out in September 2013, only a few weeks after the wildfire. There was low-intensity precipitation of 107 mm between the wildfire and the campaign without runoff generation (data from B118 S'Alqueria AEMET station, see location in Figure 5.1B), which caused the incorporation of part of the ash deposits into the soil through infiltration. The contribution of ash to the change in FRN concentrations in burned surface soils allows the differentiation of surface and sub-surface (e.g. channel bank) sources of sediment due to differences in activity concentrations at soil depths and to estimates of burned vs. unburned source contributions (Smith et al., 2013). Accordingly, sample collection was designed (Supplementary figure 5.2) to take into account the effects of the wildfire and to distinguish between surface soil (from hillslopes) and channel bank, with the number of samples approximately proportional to the area occupied by each source (Figure 5.2). Samples were collected from surface soils (0-2 cm depth) on hillslopes with active slope-to-channel connectivity and from actively eroding channel banks (most of them constrained by dry-stone walls), ranging in height from ca. 0.3 to 2.0 m with vertical faces. Each sample consisted of three integrated subsamples, collected inside a circular area with a radius of ca. 10 m, in order to include the spatial variability of the sediment's properties. At sites with an intense presence of ash, the surface ash layer was carefully removed so as not to modify the intrinsic sediment properties. In the case of surface soil samples collected from the area affected by the wildfire, material was collected from the upper soil layers likely to have been modified by the fire (i.e. exposed, charred soil material in areas devoid of vegetation).

To estimate the relative source contribution to the bed sediment temporarily stored within the Sa Coma Freda River, five samples of the sediment deposited during the first storm after the wildfire were collected along the main channel bed stem. The samples were collected a week after the storm, with the topographical characteristics of the main stem (see longitudinal profile of inlet in Figure 5.2) and the wildfire's effects taken into account.

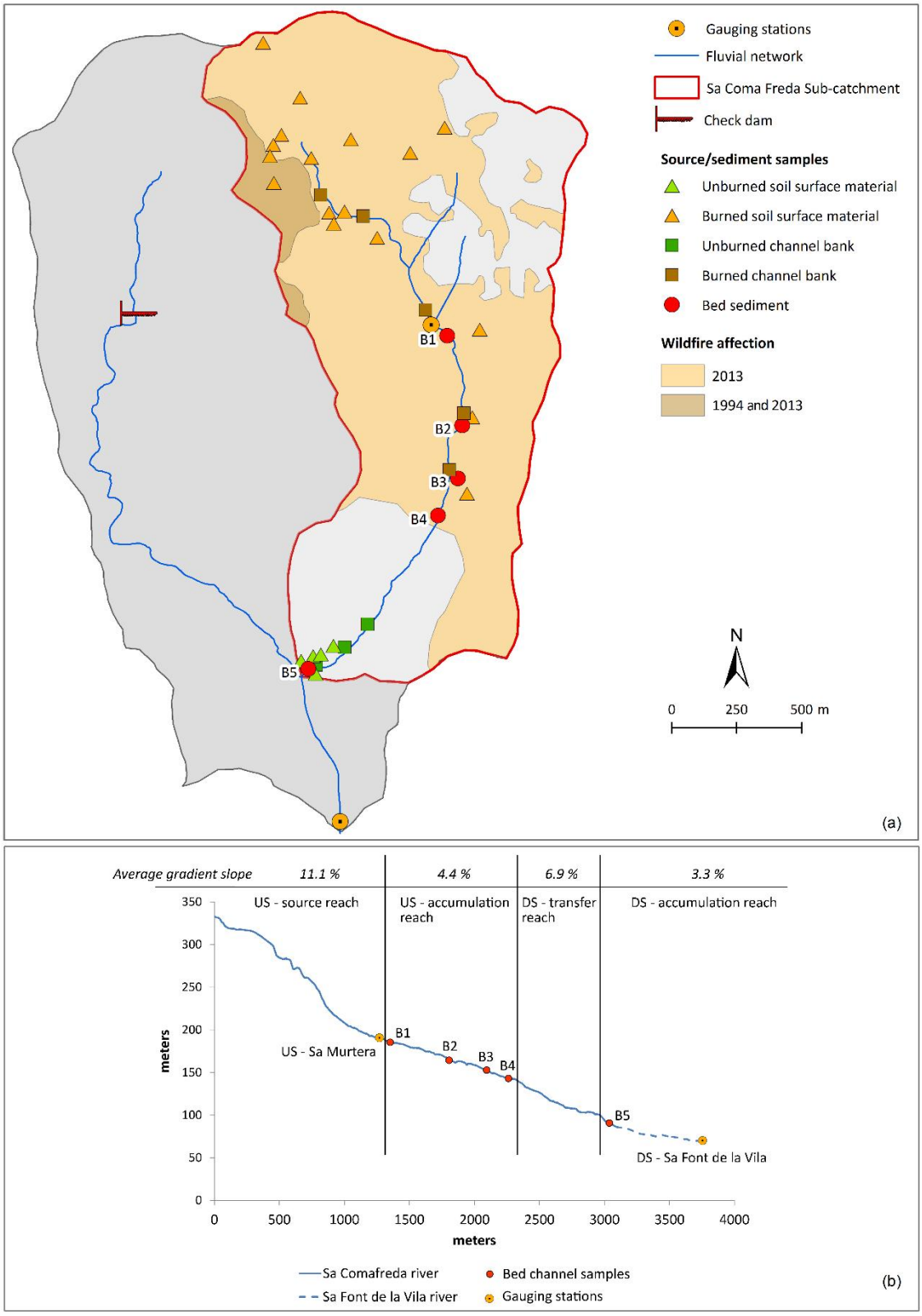

Figure 5.2. Map of the Sa Font de la Vila catchment showing the monitoring network and sediment source sampling points. The wildfire recurrence effect is also shown, together with the post-fire treatment carried out after the 2013 wildfire.

The type and spatial sequence of source, transfer and accumulation zones in any given catchment constitute a complex process mostly dependent on the potential of flows for activating the functions of different zones within a catchment (Thompson et al., 2015). In this way, topography is both a resisting and disturbing force (Brunsden, 2001). The longitudinal section was divided into four topographical sections shown in the inlet longitudinal profile in Figure 5.2. Therefore, five samples were collected in the accumulation pools of both the upstream and downstream parts of the main channel. All the main system channel –also the pools– was completely dry with high transmission losses under effluent dynamics. Each sample consisted of two integrated subsamples, collected in the most superficial layer (ca. 5 mm) inside a heterogeneous circular area, depending on the surface of each pool. Specifically, four samples were collected on the US-accumulation reach. However, only one sample was collected on the DS-accumulation reach of the Sa Coma Freda River because it is only 200 m long.

Since the most upstream part of the catchment (US-source reach in Figure 5.2B) was severely affected by the wildfire (Figure 5.1F), sediment source discrimination focused on 17 soil surface and 5 channel bank samples, involving 4 targeted bed sediment channels (B1 to B4) collected in the US-accumulation reach (Figure 5.2B). In the DS-accumulation reach, the analysis encompassed the 17 soil surface and 5 channel bank samples previously described, as well as 5 soil surface and 3 channel bank samples collected in the unburned DS part of the Sa Coma Freda sub-catchment, totalling 30 potential source samples for 1 targeted bed sediment channel (B5). Thus, at DS it was possible to distinguish between soil surface and channel bank as sediment source, as well as the effect of fire in terms of unburned or burned materials.

5.2.4. Laboratory work

Source and targeted sediment samples were oven-dried at 40°C, carefully disaggregated using a pestle and a mortar and sieved to < 63 µm to ensure direct comparison. The absolute grain size and the specific surface area were determined by using a *Malvern Mastersizer 2000* at the *Institute of Environmental Assessment and Water Research* (IDAEA-CSIC). The samples were previously treated with chemical/ultrasonic dispersion and hydrogen peroxide (H_2O_2) to remove the organic

fraction. After the pre-treatment, each sample was closed tightly and left for more than 21 days before activity measurement, to ensure that secular equilibrium had been reached. The atmospherically-derived $^{210}Pb_{ex}$ concentration was determined by subtracting the ^{226}Ra-supported ^{210}Pb concentration from the total ^{210}Pb concentration, as $[^{210}Pb_{ex}] = [^{210}Pb] - 0.8\ [^{226}Ra]$, including a commonly used value for the reduction factor to take into account the radon emanation coefficient of soils. The ^{137}Cs, ^{226}Ra (via ^{214}Bi at 609.3 keV) and total ^{210}Pb activity concentrations (Bq kg^{-1}) were measured by gamma spectrometry at the *Environmental Radioactivity Laboratory* of the University of the Balearic Islands using a high-purity coaxial intrinsic germanium (HPGe) detector, cooled by liquid nitrogen, shielded by 15 cm of low-background iron and equipped with high-voltage power supply, preamplifier, amplifier and multichannel analyser as an interface to a PC-type computer. The system was calibrated by a soil standard containing ^{210}Pb provided by Exeter University and a CG2-standard (^{241}Am, ^{109}Cd, ^{139}Ce, ^{57}Co, ^{60}Co, ^{137}Cs, ^{113}Sn, ^{85}Sr and ^{88}Y) prepared and certified by the *Centre for Energy, Environment and Technology Research* (CIEMAT, the Spanish National reference for nuclear physics magnitudes), thus achieving a useful energy range from 25 keV to 10 MeV with a resolution of 5 keV and a detection efficiency of 0.99% for ^{137}Cs, 1.10% for ^{226}Ra and 4.63% for ^{210}Pb. The minimum detectable activities have been of the order of 1 Bq kg^{-1} for ^{137}Cs, 2 Bq kg^{-1} for ^{226}Ra and 12 Bq kg^{-1} for ^{210}Pb, and the uncertainties of the measurements less than 10%. As the same geometry was used for the standards and samples (less than 100 g in a vessel wide enough to assume that there are no self-absorption effects), there was no need to apply any correction factor.

5.2.5. Particle size correction

The particle size can affect the concentration values of the tracers selected to the source sediment adscription (Laceby et al., 2017). For ^{137}Cs and $^{210}Pb_{ex}$, higher activity concentrations were observed in the fine particle size fractions (He and Walling, 1996) due to the increasing of the specific surface area (hereafter SSA, $m^2\ g^{-1}$) in these fractions (Horowitz, 1991; Rawlins et al., 2010). Accordingly, to minimize the possible element concentration variations generated as a result of particle-size distribution

between source and target sediment samples, in this research was combined the size fractionation of the samples and the use of correction procedures.

As explained in section 5.2.4 Laboratory work all the material was sieved to < 63 µm -. This fraction was selected for their representativeness of the suspended material transported preferentially by riverine systems (Laceby et al., 2017). In addition, the SSA was used as a metric to specify the existence of significant differences between sample groups. These sample groups were established in terms of spatial provenance (burned vs. unburned) and source type (soil surface vs. channel bank) at accumulation reaches in the upstream and downstream stems of the Sa Coma Freda River. To determine the presence of significant differences, the SSA values for sediment and source samples were compared with the Kruskal-Wallis test. Particle-size correction was applied when statistical differences (*p-value* < 0.05) were observed between sample groups (He and Walling, 1996):

$$C_c = \left(\frac{S_x}{S_s}\right) C$$

where C is the measured mean property concentration in source material, C_C the property concentration corrected for particle size using SSA, S_x the SSA of suspended or deposited sediment collected at each location x, and S_S is the mean SSA of the source to be corrected. Accordingly, the particle-size correction factor was applied to those source sample groups that showed significant statistical differences with each other and with the targeted bed sediments, to avoid errors in tracer concentrations caused by the differential tracer adsorption of the finest particles (Smith and Blake, 2014).

5.2.6. Source apportionment of suspended sediment sources

The relative contributions of the different sediment sources were determined for the bed sediment samples located in the accumulation reaches of the Sa Coma Freda main stem. First, the Mann-Whitney U test was used to define whether the FRN as tracers were suitable to distinguish the sources (using SPSS computer software package).

Then, a linear mixing model was used to establish the relative contribution of each source to the individual bed sediment samples. The model minimizes the sum of squares of the relative errors between FRN-measured mean activity concentrations in source and bed sediment samples (Walden et al., 1997; Collins et al., 1997). The Monte Carlo simulation technique was used with 1,000 iterations to calculate the model uncertainties associated with the tracer's spatial variability values (Martinez-Carreras et al. 2008) for each bed sediment sample and to compute mean (50th percentile) source contributions and uncertainty ranges (10th and 90th percentiles). Negative tracer values were discarded and mixing diagrams included bed sediment values in each run. These linear mixing models with uncertainty evaluations used Matlab software. This uncertainty reflects equifinality in the mixing model solution. Therefore, the robustness of the source ascription solutions was assessed by a mean goodness of fit (*GOF*, modified from Motha et al., 2003):

$$GOF = 1 - \left\langle \frac{1}{n} \times \sum_{i=1}^{n} \left| b_i - \sum_{j=1}^{m} (a_{i,j} \cdot x_j) \right| / b_i \right\rangle$$

where b_i is the value of tracer property i (i = 1 to n) in the bed sediment sample, $a_{i,j}$ is the value of tracer property i in source type j (j = 1 to m), x_j is the unknown relative contribution of source type j to the bed sediment sample, m is the number of source types, and n is the number of tracer properties.

Source contribution uncertainty depends not only on the spatial variability of the tracers associated with an individual source, but also on the tracer property values for the bed sediment, since the location of the tracer values therein will also constrain the output uncertainty (Martínez-Carreras et al., 2008). The most certain source ascriptions (lower uncertainty ranges) were obtained, not when the contributions of the individual potential sources were similar, but rather when the bed sediment tracer values were close to the values for the source that has lower tracer variabilities and when that source dominates (Joerin et al., 2002). Note that the centroid of the likelihood-weighted confidence intervals was used as a measurement of modal behaviour (Beven and Binley, 1992).

5.3. Results

The 29 October 2013 convective storm was the first with runoff generation occurring after the 2013 wildfire, in which 50 mm accumulated in only 15 minutes with an intensity of 200 mm h^{-1}. Following the method and the classification developed by Brown and Foster (1987), the rainfall erosivity of this event was 2,886 MJ mm ha^{-1} h^{-1}, rated as medium. As a result, this storm generated a flow response with a peak discharge of 1.5 m^3 s^{-1} and a maximum suspended sediment concentration (SSC) of 33,618 mg l^{-1}, recorded at the Sa Font de la Vila gauging station. The suspended sediment load was ca. 110 t and yielded 23 t km^{-2}. This value represented 99% of the sediment exported during the first post-fire hydrological year (2013-2014). Although wildfire reduces the catchment's erosion threshold by enhancing the erosional response to high-intensity rainfall (Moody and Martin, 2001) –such as occurred in the Sa Font de la Vila catchment–, flow was not sufficient to completely transfer the sediment released into the main stem, which caused sediment deposition on the riverbed surface. Pervious materials and dry preceding conditions in the main stem during summer –intensified by wildfire– resulted in a very low runoff coefficient (i.e. 1 %) and deposition dynamics during this first post-fire flush. Romero et al. (2014) provide an observational characterization of this storm in the Balearic Islands based on surface reports, remote sensing products, radio soundings and synoptic information.

The variations of SSA in river fine sediment could be largely ascribed to differences between sources, meaning that particle-size differences between sample groups must be carefully assessed (Smith and Blake, 2014). This assessment resulted in significant differences (*p-value* < 0.05; Table 5.1) in particle size between source and bed sediment samples in the US-accumulation reach as well as between bed sediment and both burned and unburned sources in the DS-accumulation reach. Accordingly, particle-size corrections were only applied on these sources. The use of these corrections caused a reduction of FRN concentration values for all the source samples located in both the US- and DS-accumulation reaches (Table 5.2).

Table 5.1. Basic statistics and p-values derived from the discrimination analysis of the specific surface area ($m^2\ g^{-1}$) between source materials and bed sediment samples.

Site	Type	N	Minimum	Maximum	Average	St. Dev.	p-value
US-accumulation reach	1. Sources	22	0.71	2.02	1.48	0.36	**0.040**
	2. Bed sediment	4	0.77	1.21	1.00	0.22	
DS-accumulation reach	1. Sources	30	0.71	2.41	1.58	0.38	0.154
	2. Bed sediment	1	0.91	0.91	0.91	-	
US-accumulation reach	1. Burned soil surface	17 *	0.71	2.02	1.45	0.37	0.095
	2. Burned channel bank	5*	1.36	1.99	1.64	0.32	
	3. Bed sediment	4	0.77	1.21	1.00	0.22	
DS-accumulation reach	1. Burned sources	22 *	0.71	2.02	1.48	0.36	**0.039**
	2. Unburned sources	8	1.50	2.41	1.83	0.32	
	3. Bed sediment	1	0.91	0.91	0.91	-	
DS-accumulation reach	1. Unburned soil surface	5	1.50	2.41	1.81	0.36	0.145
	2. Unburned channel bank	3	1.66	2.19	1.84	0.30	
	3. Burned soil surface	17 *	0.71	2.02	1.45	0.37	
	4. Burned channel bank	5*	1.36	1.99	1.64	0.32	
	5. Bed sediment	1	0.91	0.91	0.91	-	

p-values in bold are significant ** Burned source samples are the same at US and DS*

Table 5.2. Effects of the particle-size correction factor on the ^{137}Cs and $^{210}Pb_{ex}$ activity concentrations of source and sediment materials.

			^{137}Cs (Bq kg^{-1})				**$^{210}Pb_{ex}$ (Bq kg^{-1})**			
			Uncorrected		***Corrected***		***Uncorrected***		***Corrected***	
Site	Type	N	Average	St. Dev.	Average	St. Dev.	Average	St. Dev.	Average	St. Dev.
US-accumulation reach	1. Sources	22	28.8	21.0	20.2	14.8	218.1	110.7	153.1	77.9
	2. Bed sediment	4	17.1	10.6	-	-	202.9	107.7	-	-
DS-accumulation reach	1. Burned sources	22	28.8	21.0	16.8	13.6	218.1	110.7	127.4	75.9
	2. Unburned sources	8	7.8	6.1	4.6	3.4	70.4	54.3	42.4	29.6
	3. Bed sediment	1	25.6	-	-	-	218.6	-	-	-

Table 5.3. ^{137}Cs and $^{210}Pb_{ex}$ activity concentrations of source and bed sediment materials.

			^{137}Cs (Bq kg^{-1})				$^{210}Pb_{ex}$ (Bq kg^{-1})			
Site	Type	n	Min.	Max.	Avg.	St. Dev.	Min.	Max.	Avg.	St. Dev.
US-accumulation reach	1. Burned soil surface	17*	13.5	90.1	32.8	20.2	129.5	518.1	240.6	102.7
	2. Burned channel bank	5*	2.7	12.7	6.3	5.5	44.8	157.7	91.0	59.2
	3. Bed sediment	4	1.4	25.1	17.1	10.6	48.9	282.1	202.9	107.7
	P-value			< 0.01				< 0.05		
DS-accumulation reach	1. Burned sources	22*	2.7	90.1	28.8	21.0	44.8	518.1	218.1	110.7
	2. Unburned sources	8	3.8	21.4	7.8	6.1	24.9	194.3	70.4	54.3
	3. Bed sediment	1	25.6	25.6	25.6	-	218.6	218.6	218.6	-
	P-value			< 0.01				< 0.01		
DS-accumulation reach	1. Unburned soil surface	5	3.9	21.4	8.5	7.3	47.1	194.3	87.7	63.3
	2. Unburned channel bank	3	3.8	11.9	6.7	4.5	24.9	59.3	41.6	17.3
	3. Burned soil surface	17*	13.5	90.1	32.8	20.2	129.5	518.1	240.6	102.7
	4. Burned channel bank	5*	2.7	12.7	6.3	5.5	44.8	157.7	91.0	59.2
	5. Bed sediment	1	25.6	25.6	25.6	-	218.6	218.6	218.6	-
	P-value			> 0.05				> 0.05		

** Burned source samples at US and DS are the same*

Significant differences were observed in ^{137}Cs activity concentrations ($p < 0.01$) between burned surface soil and burned channel bank samples collected upstream of the bed sediments of the US-accumulation reach. Concentrations were higher in burned soil surface material, with an average of 32.8 Bq kg^{-1} against 6.3 Bq kg^{-1} in burned channel banks (Table 5.3 and Figure 5.3A). For $^{210}Pb_{ex}$, differences in activity concentrations between sources ($p < 0.05$) were also higher in burned soil surface material, with a mean value of 240.6 Bq kg^{-1} vs. 91.0 Bq kg^{-1} in burned channel banks.

FRN concentration patterns between burned and unburned sources at DS-accumulation reach (Table 5.3 and Figure 5.3B) were very different ($p < 0.01$) both in ^{137}Cs and $^{210}Pb_{ex}$, being significantly higher in the fire-affected samples (mean values of 28.8 Bq kg^{-1} for ^{137}Cs and 218.0 Bq kg^{-1} for $^{210}Pb_{ex}$) than in unburned samples (mean values of 7.8 Bq kg^{-1} for ^{137}Cs and 70.4 Bq kg^{-1} for $^{210}Pb_{ex}$). However, when the source

grouping is a combination of spatial (i.e. burned vs unburned) and source types (i.e. surface soil vs. channel bank), FRNs could not significantly discriminate sources at DS-accumulation reach due to concentrations being similar (p > 0.05) for both radioisotopes (8.5 Bq kg^{-1} of ^{137}Cs and 87.7 Bq kg^{-1} of ^{210}Pb$_{ex}$ for unburned surface soils, 6.7 Bq kg^{-1} of ^{137}Cs and 41.6 Bq kg^{-1} of ^{210}Pb$_{ex}$ for unburned channel bank samples, 32.8 Bq kg^{-1} of ^{137}Cs and 240.6 Bq kg^{-1} of ^{210}Pb$_{ex}$ burned surface soil samples, and 6.3 Bq kg^{-1} of ^{137}Cs and 91 Bq kg^{-1} of ^{210}Pb$_{ex}$ for burned channel bank material).

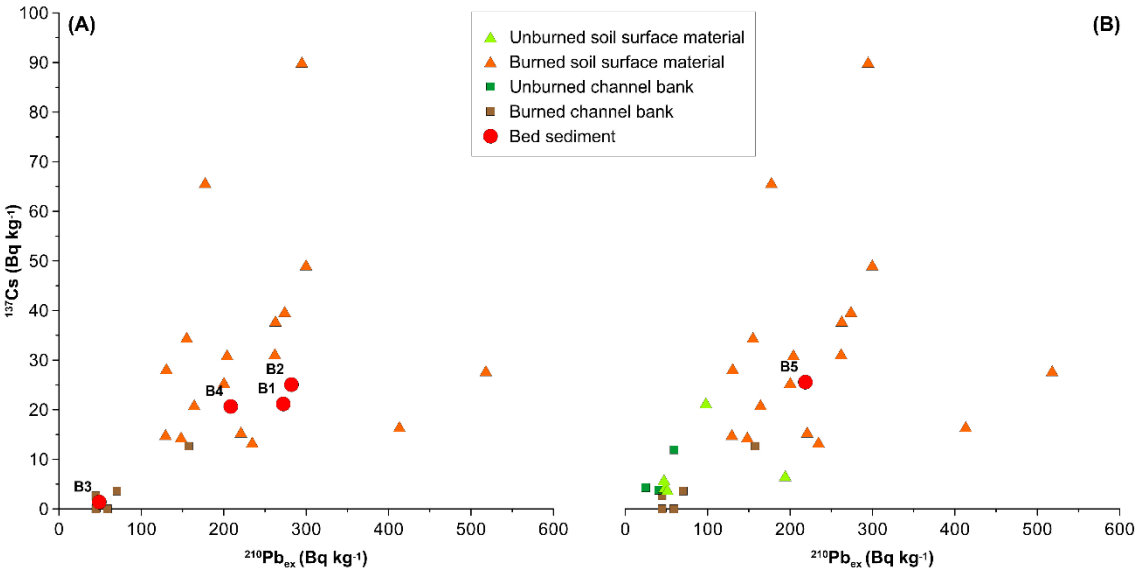

Figure 5.3. ^{137}Cs and ^{210}Pb$_{ex}$ activity concentrations (Bq kg^{-1}) of source and bed sediment samples for (A) MS-middle stream source samples defined in terms of burned soil surface and burned channel bank material and (B) DS-downstream source samples defined in terms of burned and unburned soil surface and burned and unburned channel bank.

FRN concentrations in bed sediments for the accumulation reaches in US and DS samples were statistically similar (p > 0.05), with mean ^{137}Cs concentrations of 17.1 and 25.6 Bq kg^{-1}, whilst the ^{210}Pb$_{ex}$ figures were 202.9 and 218.6 Bq kg^{-1}, respectively (Table 5.3).

Figure 5.4 illustrates the predicted relative contribution in bed sediment samples of each source in both sections of the Sa Coma Freda River. For the US-accumulation reach, sediment sources were distinguished in terms of burned surface soils and burned channel bank material, as the flush was generated in the upstream catchment area highly affected by the 2013 wildfire. Surface soils were the main origin within the bed sediments along the US-accumulation reach. At the B1, B2 and B4 sites, the soil surface contributions were 86%, 91% and 84%, respectively (average of 87 %).

However, at the B3 site, the channel bank contribution was clearly predominant (ca. 96%; Figure 5.4A). In the DS-accumulation reach sample (B5), the post-fire sediment source contributions within the bed sediment were distinguished through both source type (i.e. surface soil and channel banks) and burned or unburned material (Figure 5.4B).

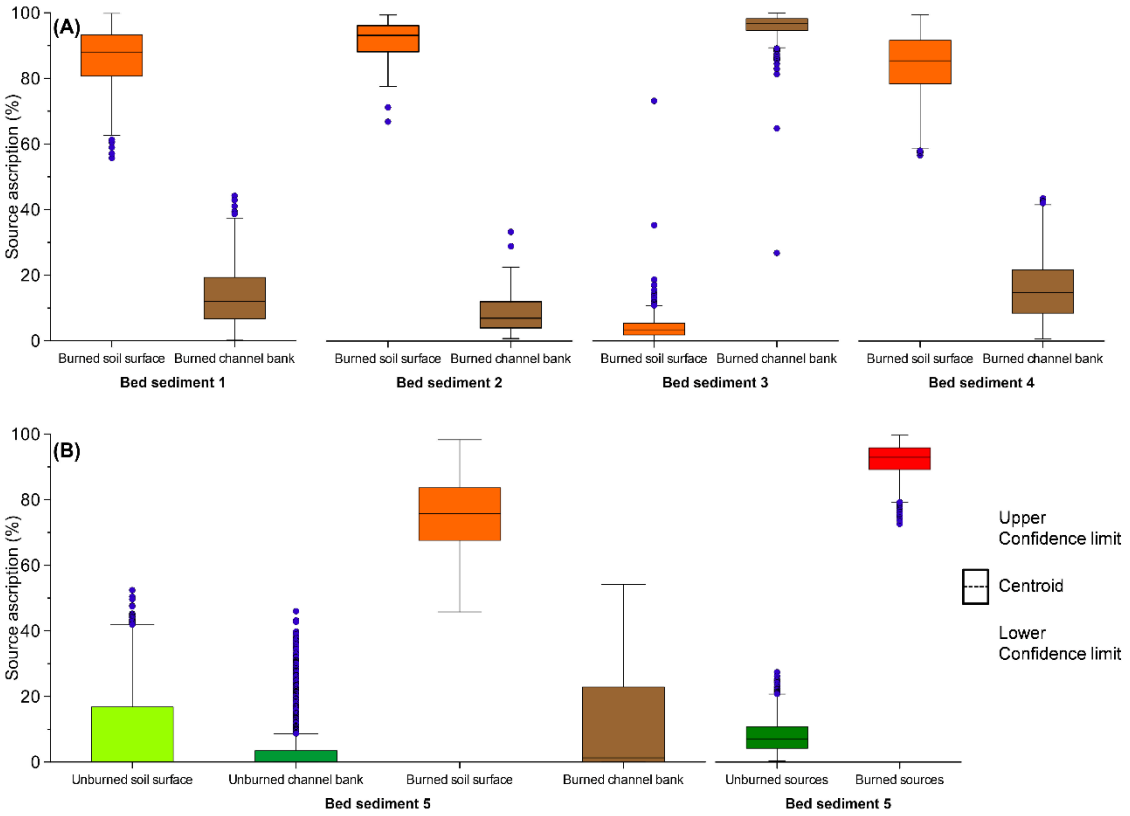

Figure 5.4. Source relative contribution to the bed sediments of (A) MS-middle stream sites and (B) DS-downstream site. Potential outliers are plotted as points.

This design allows the assessment of the sediment transfer along the fluvial network downstream from the burned area in terms of source type, despite the low level of significance discriminating sources. The contribution from the burned area were 75% for soil surface material and 13% for channel banks. From the unburned areas 7 % of the contribution was soil surface material and 5% channel banks. To provide robustness to the source ascription, sources and targeted bed sediments were compared only by distinguishing unburned vs. burned materials. The result was that burned sources predominated, with an average contribution of 92% (Figure 5.4B). The sediment source dynamics observed in the DS-accumulation reach were then similar to

those observed in the US-accumulation reach, confirming a downstream propagation of sediment derived from the burned area.

5.4. Discussion

Fallout radionuclides (^{137}Cs and $^{210}Pb_{ex}$) were used as tracers to determine the relative contributions of sediment sources in terms of spatial provenance (burned vs. unburned) and source type (soil surface vs. channel bank) in bed sediments temporarily stored along the main stem of a Mediterranean catchment severely affected by a wildfire. Pervious materials and dry preceding conditions –with an absence of baseflow– promoted the deposition of sediments on the riverbed surface along the main stem due to transmission losses. The differences between source sample groups at both accumulation reaches (i.e. burned soil surface vs. burned channel bank materials at US and burned vs. unburned sources at DS; Table 5.3) were detected by increased FRN concentrations in areas affected by fire (Wilkinson et al., 2009), due to fire causing the loss of surface soil organic mass (Smith et al., 2013). The similar values obtained in the targeted bed sediment samples (i.e. US and DS), as well as the high SSC and suspended sediment load recorded at the Sa Font de la Vila gauging station, indicate that the energy of the storm was uniformly distributed along the main stem to release sediment, whereas the influent conditions within the stream promoted bed deposition by transmission losses.

Despite the solutions from the mixing model obtained high GOF, these findings may be involved by some uncertainties associated with measurement error, the particle-size correction factor and the mixing model application. Haddadchi et al. (2013, 2014) compared several mixing models and optimization methods at two catchment datasets by using artificial mixtures of sediments from different sources observing important differences depending on the used mixing model. Nevertheless, to achieve a complete understanding of the sediment sources in the burned Sa Font de la Vila River, the measurement of artificial mixtures composed by representative source material will be applied in future studies to reduce uncertainties related to mixing model selection (Laceby and Olley, 2015; Palazón et al., 2015). Despite this, the results indicate clearly that the wildfire affected sediment redistribution along the main stem of the

catchment, with a high contribution from hillslope burned areas. Therefore, bed sediments deposited during the first flush after the wildfire were mostly generated on hillslopes due to vegetation loss and the increased sediment availability caused by the fire alterations. In addition, channel bank contributions are limited by soil conservation practices, i.e. dry-stone walls to prevent erosion. This is a common practice in the bottom valleys, where the natural stream is systematically diverted to a margin of the floodplain, which provides further fertile agricultural land and avoids erosion because slope and channel are not connected. However, this action involves increased flow velocity, promoted by stream banks being fixed by dry-stone walls, which also avoids erosion (Estrany and Grimalt, 2014). Thus, the channel bank contribution was only predominant (ca. 96%) at one bed sampling site (B3), which was probably caused by a local collapse of these dry-stone walls releasing sediment from the river channel bank.

The significant hillslope contribution may be caused by a reduction in evapotranspiration, infiltration, interception and sediment trapping –promoted by the modification of vegetation and litter cover– and the alteration of physicochemical soil properties such as structure stability, texture and particle-size distribution and water repellence (Úbeda and Outeiro, 2009). Furthermore, the predominance of soil surface origin in the sediments temporarily stored in the riverbed along the main stem indicates a significant first-flush effect generated by a short-duration rainfall event (i.e. 15 mins.). In fact, the most damaging events are related to short high-intensity rainfall events, because of the changes in the rainfall-runoff processes caused by burning (Shakesby and Doerr, 2006; Moody and Martin 2009). These changes are mainly characterized by the increase in overland flow and soil erosion during the most active period of the window of disturbance after a wildfire (Prosser and Williams, 1998; Scott et al., 1998; Cerdà and Doerr, 2005), especially during the first post-fire year (Candela et al., 2005). Accordingly, the first heavy rainfall after the dry season was a high-energy torrential storm that generated a great slope-to-channel sediment delivery favoured by the landscape's post-fire conditions.

The first flush, occurring three months after the wildfire (October 29th), involved a significant increase in the concentration of suspended matter from the first runoff event after the summer under post-fire conditions. The SSC peak recorded (i.e. 33,618

mg l^{-1}) demonstrated the post-fire first-flush effect. Since delivery processes are limited by the historical contingency of geomorphic responses and by low runoff coefficients of Mediterranean areas (Estrany, 2009), the SSC peak measured was three orders of magnitude higher than the SSC peaks recorded in the 2013-2014 hydrological year in similar Mallorcan catchments (Calsamiglia et al., 2016). Likewise, other worldwide studies of post-fire hydrosedimentary dynamics at the catchment scale have documented increases of between one and three orders of magnitude in SSC values (Smith et al., 2011a). Moreover, 99% of the suspended sediment load of the 2013-2014 hydrological year was exported during this event. Nevertheless, the absence of baseflow promoted sediment deposition along the main stem due to transmission losses with a very low runoff coefficient (1%) of this event. In this way, deposition of sediment in the channels was more important than transport, until a major flood event (return period ≈ 5 years) evacuates the stored sediment in Mediterranean temporary rivers (Estrany et al., 2011).

A catchment's sediment source response to wildfire –in terms of source type; i.e. soil surface vs. channel bank– is highly dependent on its biogeoclimatic setting (Smith et al., 2013). Post-fire sediment sourcing studies have mainly focused on North America and Australia, illustrating different responses. In the forested highlands of south-eastern Australia, hillslope sediment contribution was predominant in both small (Smith et al., 2011b) and medium-size catchments (Wilkinson et al., 2009) despite differences in geology, topography soils and forest type. However, studies from western North America reported channel source dominance in conifer forest environments (Moody and Martin, 2001; Owens et al., 2012), probably caused by a loss of root strength (Eaton et al., 2010). As far as the authors are aware, only Estrany et al. (2016) have developed comparable research of catchment sediment sources by using FRN concentrations (^{137}Cs and $^{210}Pb_{ex}$) as tracers in a Mediterranean temporary stream partially affected by wildfire. In this study, the post-fire dynamics were characterized by a small contribution, only 12% on average, from the burned area to the bed sediments, after a single low flood event (i.e. return period <1 year). The smaller burned area and the subsequent lower availability of burned sediment combined with the absence of heavy rainfall, limited the activation of the sediment

cascade. As pointed out previously, Smith et al. (2011b) determined that the hillslope contribution declined with gradual post-fire landscape recuperation in a burned Australian catchment during the first 4 post-fire years. These landscape dynamics seem to match the results obtained in the Sa Coma Freda catchment, where most of the sediment of the first flush was generated on burned hillslopes under heavy rainfall conditions. García-Comendador et al. (2017) analysed the spatio-temporal relationship between discharge and sediment transport at the event scale during the first three post-fire years at the Sa Font de la Vila gauging station by means of hysteresis loop classification. The results showed how 67% of the counter-clockwise loops occurred during the first post-fire year (2013-2014), which indicated that the main sediment sources were located at a certain distance from the channel. During the following years, this percentage –as well as the sediment yield– decreased significantly, which may be related to vegetation cover conditions on the burnt hillslopes (Lane et al., 2006; Smith et al., 2011a). Nevertheless, the adjustment in the catchment sediment source response requires long-term monitoring because differences in the distribution of land uses and land cover may determine how much different sediment sources contribute (Palazón et al., 2015; Estrany et al., 2016).

5.5. Conclusions

The findings of this study provide valuable insight into the short-term response of catchment sediment sources in a Mediterranean temporary river during the first post-fire flush. Despite the uncertainties related with the application of the sediment source fingerprinting technique, the contributions from different sediment sources to bed sediments lead to the following conclusions: (i) the main contribution to the bed sediments (both US-upper stream and DS-downstream accumulation reaches) was delivered from burned hillslopes due to the fire's physicochemical alterations promoting bare soils and sediment availability; and (ii) high-intensity rainfall (high-energy storm) is clarified as the main factor driving effective slope-to-channel sediment connectivity. In the Sa Font de la Vila catchment, this short-term response indicates a direct association between these post-fire runoff and sediment generation factors and sediment cascade activation at catchment scale. However, the distinctive

characteristics of wildfire impact on Mediterranean ecosystems involve uncertainties on the most effective period of the disturbance window, as the resilience capacity of these highly modified ecosystems may alter their response. There is clearly a need for extending over time the programme monitoring catchment sediment sources, in order to determine how Sa Coma Freda will respond to the severe wildfire of summer 2013 in the medium and long terms.

Acknowledgements

This research was supported by the Spanish Ministry of Economy and Competitiveness (CGL2012-32446). Specifically, the study was supported by the Balearic Forest Service (Department of Environment, Agriculture and Fishery of the Balearic Autonomous Government) and by the "la Caixa" Foundation. Julián García-Comendador is in receipt of a postgraduate contract (FPU15/05239) funded by the Spanish Ministry of Education and Culture. Josep Fortesa has a contract funded by the European Commission - Directorate-General for European Civil Protection and Humanitarian Aid Operations. Aleix Calsamiglia acknowledges the support from the Spanish Ministry of Economy and Competitiveness through a postgraduate contract EEBB-I-15-10280. Meteorological data were provided by the Spanish Meteorological Agency (AEMET). The authors are grateful to the Environmental Radioactivity Laboratory at the University of the Balearic Islands for determining fallout radionuclide concentrations and Prof. Francesc Gallart at the Institute of Environmental Assessment and Water Research (IDAEA-CSIC) for determining particle size. Thanks must also be expressed to Joan Bauzà Llinàs for his assistance during the fieldwork.

5.6. References

Bauzà J. 2014. Els grans incendis forestals a les Illes Balears: una resposta des de la teledetecció. (Bachelor thesis). Universitat de les Illes Balears, Spain. 37 pp

Beven KJ, Binley AM. 1992. The future of distributed models: calibration and predictive uncertainty. Hydrol Process 6:279–298.

Blake WH, Wallbrink PJ, Wilkinson SN, Humphreys GS, Doerr SH, Shakesby RA, Tomkins KM. 2009 Deriving hillslope sediment budgets in wildfire–affected forests using fallout radionuclide tracers. Geomorphology 104:105-116. doi: 10.1016/j.geomorph.2008.08.004

Bochet E, Poesen J, Rubio JL. 2002. Influence of plant morphology on splash erosion in a Mediterranean matorral. Z Geomorphol 46:223-243

Brown LC, Foster GR. 1987 Storm erosivity using idealized intensity distributions. T ASAE 30:379-386. doi: 10.13031/2013.31957

Brunsden D. 2001 A critical assessment of the sensitivity concept in geomorphology. Catena 42(2):99-123. doi: 10.1016/S0341-8162(00)00134-X

Bull LJ, Kirkby MJ. 2002. Dryland Rivers: Hydrology and Geomorphology of Semi-arid Channels. John Wiley and Sons, New York.

Calsamiglia A, Fortesa J, García-Comendador J, Estrany J. 2016. Respuesta hidro-sedimentaria en dos cuencas mediterráneas representativas afectadas por el cambio global. Cuaternario & Geomorfología 30(1-2): 87-103. doi: 10.17735/cyg.v30i1-2.45900

Calsamiglia A, Fortesa J, Garcia-Comendador J, Calvo-Cases A, Estrany J. 2017. Spatial patterns of sediment connectivity in terraced lands: anthropogenic controls on catchment sensitivity. Under review.

Candela A, Aronica G, Santoro M. 2005. Effects of Forest Fires on Flood Frequency Curves in a Mediterranean Catchment. Hydrolog Sci J 50:193-206. doi: 10.1623/hysj.50.2.193.61795

Cerdà A, Doerr SH. 2005. Long-term soil erosion changes under simulated rainfall for different vegetation types following a wildfire in eastern Spain. Int J Wildland Fire 14:423-437. doi: 10.1071/WF05044

Collins AL, Walling DE, Leeks GJL. 1997. Sediment sources in the Upper Severn catchment: a fingerprinting approach. Hydrol Earth Syst Sci 1:509–522. doi:10.5194/hess-1-509-1997

Collins AL, Pulley S, Foster IDL, Gellis A, Porto P, Horowitz AJ. 2017. Sediment source fingerprinting as an aid to catchment management: A review of the current state of knowledge and a methodological decision-tree for end-users. J Environ Manage 194:86-108. doi: 10.1016/j.jenvman.2016.09.075

Diaz-Palmer A, Garcia C, Servera J, Úbeda X. 2006. Spatial variability of total nitrogen, total carbon and organic carbon content in the top-soil of the Na Borges basin, Mallorca, Spain. Z Geomorphol Supp 143:83–94

Du P, Walling DE. 2017. Fingerprinting surficial sediment sources: Exploring some potential problems associated with the spatial variability of source material properties. J Environ Manage 194:4-15. doi: 10.1016/j.jenvman.2016.05.066

Eaton BC, Moore RD, Giles TR. 2010. Forest fire, bank strength and channel instability: the 'unusual' response of Fishtrap Creek, British Columbia. Earth Surf Proc Land 35(10):1167-1183. doi: 10.1002/esp.1946

Escuín S, Navarro R, Fernández P. 2008. Fire severity assessment by using NBR (Normalized Burn Ratio) and NDVI (Normalized Difference Vegetation Index) derived from LANDSAT TM/ETM images. Int J Remote Sens 29:1053-1073. doi: 10.1080/01431160701281072

Estrany J. 2009. Hydrology and sediment transport in the agricultural Na Borges River basin (Mallorca, Balearic Islands). A Mediterranean groundwater-dominated river under traditional soil conservation practices. PhD thesis unpublished, Universitat de les Illes Balears, Spain

Estrany J, Garcia C, Walling DE, Ferrer L. 2011. Fluxes and storage of fine-grained sediment and associated contaminants in the Na Borges River (Mallorca, Spain). Catena 87:291-305. doi: 10.1016/j.catena.2011.06.009

Estrany J, Grimalt M. 2014. Catchment controls and human disturbances on the geomorphology of small Mediterranean estuarine systems. Estuar Coast Shelf S 150:230-241. doi: 10.1016/j.ecss.2014.03.021

Estrany J, López-Tarazón JA, Smith HG. 2016. Wildfire effects on suspended sediment delivery quantified using fallout radionuclide tracers in a Mediterranean catchment. Land Degrad Dev 27:1501-1512. doi: 10.1002/ldr.2462

Fryirs K. 2013. (Dis)Connectivity in catchment sediment cascades: a fresh look at the sediment delivery problem. Earth Surf Proc Land 38(1):30-46. doi: 10.1002/esp.3242

García-Comendador J, Fortesa J, Calsamiglia A, Calvo-Cases A, Estrany J. 2017. Post-fire hydrological response and suspended sediment transport of a terraced Mediterranean catchment. Earth Surf Proc Land, doi: 10.1002/esp.4181

Guijarro JA. 1986. Contribución a la Bioclimatología de Baleares. (PhD thesis summary), Universitat de les Illes Balears, Spain. 36 pp.

Haddadchi A, Ryder DS, Evrard O, Olley J. 2013. Sediment fingerprinting in fluvial systems: review of tracers, sediment sources and mixing models. Int J Sediment Res 28:560-578. doi: 10.1016/S1001-6279(14)60013-5

Haddadchi A, Olley J, Laceby P. 2014. Accuracy of mixing models in predicting sediment source contributions. Sci Total Environ 497:139-152. doi: 10.1016/j.scitotenv.2014.07.105

He Q, Walling DE. 1996. Interpreting particle size effects in the adsorption of ^{137}Cs and unsupported ^{210}Pb by mineral soils and sediments. J Environ Radioactiv 30:117–137. doi:10.1016/0265-931X

Horowitz A, Elrick KA, Smith JJ. 2007. Measuring the fluxes of suspended sediment, trace elements and nutrients for the city of Atlanta, USA: insights on the global water quality impacts of increasing urbanization. In: Webb BW, De Boer D (eds.) Water Quality and Sediment Behaviour of the Future: Predictions for the 21st Century. IAHS Publ. 314, IAHS Press, Wallingford, pp 57-70

Joerin C, Beven KJ, Iorgulescu I, Musy A. 2002 Uncertainty in hydrograph separation based on geochemical mixing models. J Hydrol 255:90-106

Johansen MP, Hakonson TE, Whicker FW, Breshears DD. 2003. Pulsed redistribution of a contaminant following forest fire. J Environ Qual 32(6):2150-2157. doi:

10.2134/jeq2003.2150

Laceby JP, Olley J. 2015. An examination of geochemical modelling approaches to tracing sediment sources incorporating distribution mixing and elemental correlations. Hydrol Process 29(6): 1669-1685.

Laceby JP, Evrard O, Smith HG, Blake WH, Olley J, M., Minella JP, Owens PN. 2017. The challenges and opportunities of addressing particle size effects in sediment source fingerprinting: A review. Earth-Sci Rev 169: 85-103.

Lane PN, Sheridan GJ, Noske PJ. 2006. Changes in sediment loads and discharge from small mountain catchments following wildfire in south-eastern Australia. J Hydrol 331:495-510.

Manjoro M, Rowntree K, Kakembo V, Foster I, Collins AL. 2017. Use of sediment source fingerprinting to assess the role of subsurface erosion in the supply of fine sediment in a degraded catchment in the Eastern Cape, South Africa. J Environ Manage 194:27-41. doi: 10.1016/j.jenvman.2016.07.019

Martínez-Carreras N, Gallart F, Iffly JF, Pfister L, Walling DE, Krein A. 200. Uncertainty assessment in suspended sediment fingerprinting based on tracer mixing models: a case study from Luxembourg. Proceedings of a symposium on 'sediment dynamics in changing environments'. Christchurch, New Zealand. IAHS Publ. 325, IAHS Press, Wallingford, pp 94–105

Martínez-Carreras N, Krein A, Udelhoven T, Gallart F, Iffly J, Hoffmann L, Pfister L, Walling D. 2010. A rapid spectral-reflectance-based fingerprinting approach for documenting suspended sediment sources during storm runoff events. J Soil Sediment 10(3):400–413. doi:10.1007/s11368-009-0162-1

Moody JA, Martin DA. 2001. Initial hydrologic and geomorphic response following a wildfire in the Colorado Front Range. Earth Surf Proc Land 26:1049-1070

Moody JA, Martin DA. 2009. Forest fire effects on geomorphic processes. In: Cerdà A, Robichaud PR (eds) Fire effects on soils and restoration strategies. Science Publishers, New Hampshire, pp 41-79

Moody JA, Shakesby RA, Robichaud PR, Cannon SH, Martin DA. 2013. Current research issues related to post-wildfire runoff and erosion processes. Earth-Sci Rev 122:10-37. doi: 10.1016/j.earscirev.2013.03.004

Motha JA, Wallbrink PJ, Hairsine PB, Grayson RB. 2003. Determining the sources of suspended sediment in a forested catchment in southeastern Australia. Water Resour Res 39(3):1056. doi: 10.1029/2001wr000794

Obermann M, Rosenwinkel KH, Tournoud MG. 2009. Investigation of first flushes in a medium-sized Mediterranean catchment. J Hydrol 373:405-415. doi: 10.1016/j.jhydrol.2009.04.038

Owens PN, Blake WH, Giles TR, Williams ND. 2012. Determining the effects of wildfire on sediment sources using ^{137}Cs and unsupported ^{210}Pb: the role of landscape disturbances and driving forces. J Soil Sediment 12:982-994. doi: 10.1007/s11368-012-0497-x

Owens PN, Blake WH, Gaspar L, Gateuille D, Koiter AJ, Lobb DA, Perricrew EL, Reiffarth DG, Smith HG, Woodward JC. 2016. Fingerprinting and tracing the sources of soils and sediments: Earth and ocean science, geoarchaeological, forensic, and human health applications. Earth-Sci Rev 162:1-23. doi: 10.1016/j.earscirev.2016.08.012

Palazón L, Gaspar L, Latorre B, Blake WH, Navas A. 2015. Identifying sediment sources by applying a fingerprinting mixing model in a Pyrenean drainage catchment. J Soil Sediment 15:2067-2085. doi: 10.1007/s11368-015-1175-6

Palazón L, Latorre B, Gaspar L, Blake WH, Smith HG, Navas A. 2015. Comparing catchment sediment fingerprinting procedures using an auto-evaluation approach with virtual sample mixtures. Sci Total Environ 532: 456-466.

Palazón L, Navas A. 2017. Variability in source sediment contributions by applying different statistic test for a Pyrenean catchment. J Environ Manage 194:42-53. doi:10.1016/j.jenvman.2016.07.058

Poulenard J, Legout C, Némery J, Bramorski J, Navratil O, Douchin A, Fanget B, Perrette Y, Evard O, Esteves M. 2012. Tracing sediment sources during floods using Diffuse Reflectance Infrared Fourier Transform Spectrometry (DRIFTS): A case study in a highly erosive mountainous catchment (Southern French Alps). J Hydrol 414-415:452-462. doi: 10.1016/j.jhydrol.2011.11.022

Prosser IP, Williams L. 1998. The effect of wildfire on runoff and erosion in native Eucalyptus forest. Hydrol Process 12:251-265. doi: 10.1002/(SICI)1099-1085(199802)12:2<251::AID-HYP574>3.0.CO;2-4

Pulley S, Foster I, Antunes P. 2015. The application of sediment fingerprinting to floodplain and lake sediment cores: assumptions and uncertainties evaluated through case studies in the Nene Basin, UK. J Soil Sediment 15:2132-2154. doi: 10.1007/s11368-015-1136-0

Rawlins BG, Turner G, Mounteney I, Wildman G. 2010. Estimating specific surface area of fine stream bed sediments from geochemistry. Appl Geochem 25(9), 1291-1300.

Romero R, Ramis C, Homar V. 2014. On the severe convective storm of 29th October 2013 in the Balearic Islands: observational and numerical study. Q J Roy Meteor Soc. 141:1208-1222. doi: 10.1002/qj.2429

Scott DF, Versfeld DB, Lesch W. 1998. Erosion and sediment yield in relation to afforestation and fire in the mountains of the Western Cape Province, South Africa. S Afr Geogr J 80:52-59. doi: 10.1080/03736245.1998.9713644

Shakesby RA, Doerr SH. 2006. Wildfire as a hydrological and geomorphological agent. Earth-Sci Rev 74:269-307. doi: 10.1016/j.earscirev.2005.10.006.

Shakesby RA. 2011. Post-wildfire soil erosion in the Mediterranean: review and future research directions. Earth-Sci Rev 105:71-100. doi: 10.1016/j.earscirev.2011.01.001

Smith HG, Sheridan GJ, Lane PN, Nyman P, Haydon S. 2011a. Wildfire effects on water quality in forest catchments: a review with implications for water supply. J Hydrol 396:170-192. doi: 10.1016/j.jhydrol.2010.10.043

Smith HG, Sheridan GJ, Lane PNJ, Noske PJ, Heijnis H. 2011b Changes to sediment sources following wildfire in a forested upland catchment, southeastern Australia. Hydrol Process 25(18):2878-2889. doi: 10.1002/hyp.8050

Smith HG, Blake WH, Owens PN. 2013. Discriminating fine sediment sources and the application of sediment tracers in burned catchments: a review. Hydrol Process 27:943-958. doi: 10.1002/hyp.9537

Smith HG, Blake WH. 2014. Sediment fingerprinting in agricultural catchments: a critical re-examination of source discrimination and data corrections. Geomorphology 204:177-191.

doi: 10.1016/j.geomorph.2013.08.003

Stone M, Collins AL, Silins U, Emelko MB, Zhang YS. 2014. The use of composite fingerprints to quantify sediment sources in a wildfire impacted landscape, Alberta, Canada. Sci Total Environ 473–474:642–650. doi:10.1016/j.scitotenv.2013.12.052

Sumner G, Ramis C, Guijarro JA. 1993. The spatial organization of daily rainfall over Mallorca, Spain. Int J Climatol 13(1): 89-109. http://dx.doi.org/10.1002/joc.3370130107

Thompson CJ, Fryirs K, Croke J. 2015. The Disconnected Sediment Conveyor Belt: Patterns of Longitudinal and Lateral Erosion and Deposition During a Catastrophic Flood in the Lockyer Valley, South East Queensland, Australia. River Res Appl 32:540-551. doi:10.1002/rra.2897

Úbeda X, Outeiroo L. 2009. Physical and chemical effects of fire on soil. In: Cerdà A, Robichaud PR (eds) Fire effects on soils and restoration strategies. Science Publishers, New Hampshire, pp 105-132

Walden J, Slattery MC, Burt TP. 1997. Use of mineral magnetic measurements to fingerprint suspended sediment sources: approaches and techniques for data analysis. J Hydrol 202:353–372. doi: 10.1016/S0022-1694(97)00078-4

Walling DE, Owens PN, Leeks GJL. 1998. The role of channel and floodplain storage in the suspended sediment budget of the River Ouse, Yorkshire, UK. Geomorphology 22:225-242. doi: 10.1016/S0169-555X(97)00086-X

Walling DE. 2013. The evolution of sediment source fingerprinting investigations in fluvial systems. J Soil Sediment 13:1658-1675. doi: 10.1007/s11368-013-0767-2

Wilkinson SN, Wallbrink PJ, Hancock GJ, Blake WH, Shakesby RA, Doerr SH. 2009. Fallout radionuclide tracers identify a switch in sediment sources and transport-limited sediment yield following wildfire in a eucalypt forest. Geomorphology 110:140-151. doi: 10.1016/j.geomorph.2009.04.001

Zhang XJ, Zhang GH, Liu BL, Liu B. 2016. Using cesium-137 to quantify sediment source contribution and uncertainty in a small watershed. Catena 140:116-124. doi: 10.1016/j.catena.2016.01.021

5.7. Supplementary material

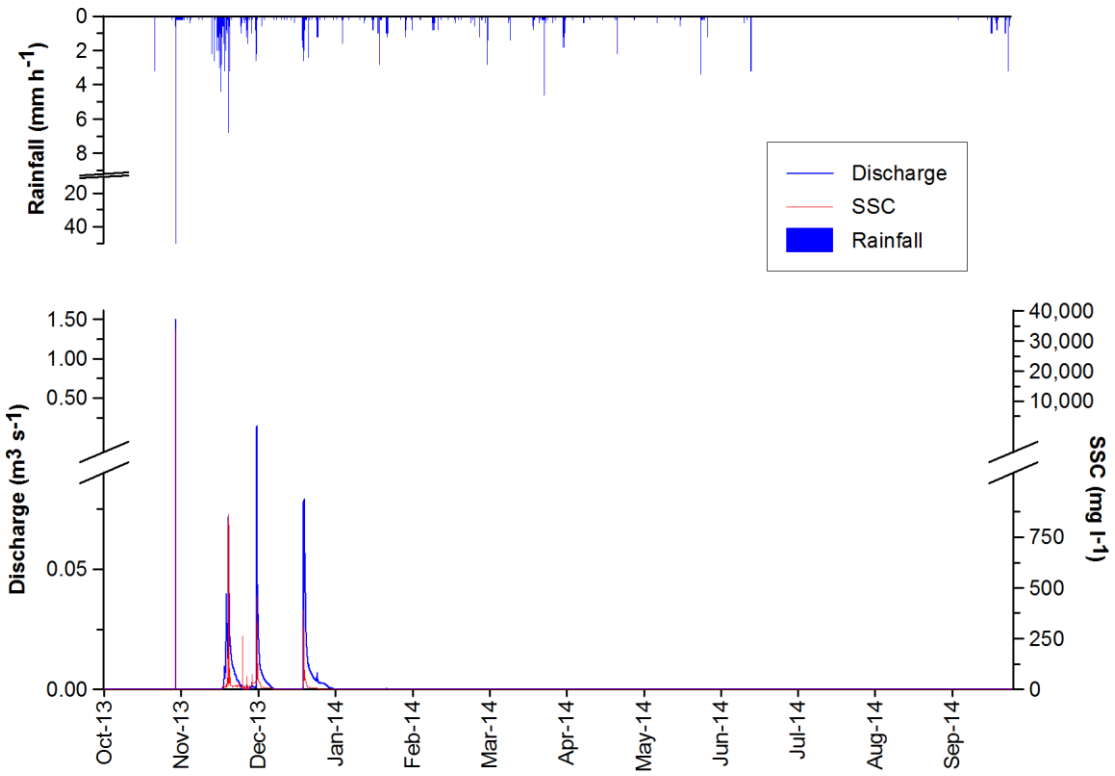

Supplementary figure 5.1. Hydrograph, sedigraph and hyetograph for the hydrological year 2013-2014 at the Sa Font de la Vila gauging station.

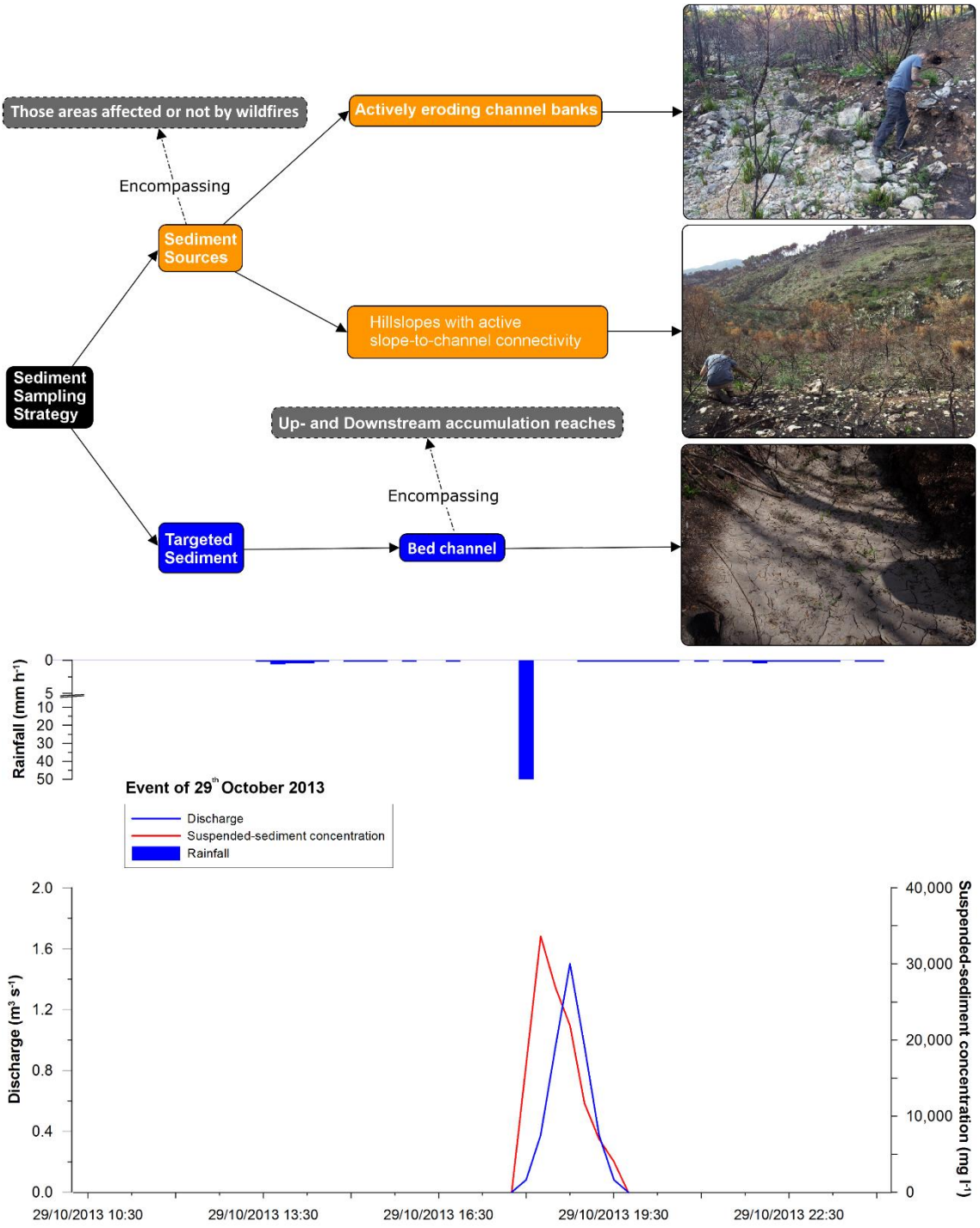

Supplementary figure 5.2. Experimental design, including the hydrograph, sedigraph and hyetograph for 29th October 2013 at the Sa Font de la Vila gauging station.

6. Analysis of post-fire suspended sediment sources by using colour parameters

Abstract

After a wildfire, total or partial removal of vegetal biomass and changes in physicochemical soil properties lead to an increase in overland flow and sediment yield. Eventual damage must be counteracted urgently by identifying erosion hotspots and by implementing post-fire management programmes and sampling campaigns. In this context, the sediment source fingerprinting technique is widely used to determine the origin of suspended sediments in catchments and to evaluate the effectiveness of sediment management programmes. It traditionally relies on the use of physical, biochemical and geochemical properties as tracers. However, measuring these tracers in the laboratory is often expensive and time-consuming. Colour tracers have been shown to greatly reduce time and cost, especially if a normal office scanner is used for measurements. Here we explored whether colour parameters can be used to investigate suspended sediment origin in burned catchments. To this end, sediment and ash were mixed artificially to verify colour linear additivity and ash influence on colour parameters. Colour parameters were then used for source ascription of suspended sediment samples (n=9) collected during two years after a fire in a small Mediterranean catchment (Mallorca, Spain). In addition, reflectance-derived colour parameters were compared with those obtained using a normal office scanner. The close correlation between most chromatic indexes (obtained using both methods; $p < 0.01$) suggested that scanning is a good alternative for measuring soil and sediment colour. A Bayesian tracer mixing model (MixSIAR) determined the relative contribution of each source. The type of mixing model enables appropriate representation of natural and sampling uncertainty in tracer data. During the first events, suspended sediment originated mainly in burned surfaces, whereas the contribution of these decreased throughout the study period. Tracing results obtained using colour parameters were compared with calculations using ^{137}Cs and $^{210}Pb_{ex}$, as recognized tracers to discriminate between surface and subsurface sediment sources after wildfires. Estimated source ascriptions with both methods (i.e. reflectance-derived colour parameters and radionuclides) coincided in predicting the dominant source in 7 of the 9 samples measured. Colour tracers proved useful in discriminating between burned and unburned sources, making them suitable for suspended sediment source ascription and monitoring as part of post-fire management strategies.

Keywords: Sediment fingerprinting, colour, fallout radionuclides, wildfire, ash, suspended sediment sources

Graphical abstract:

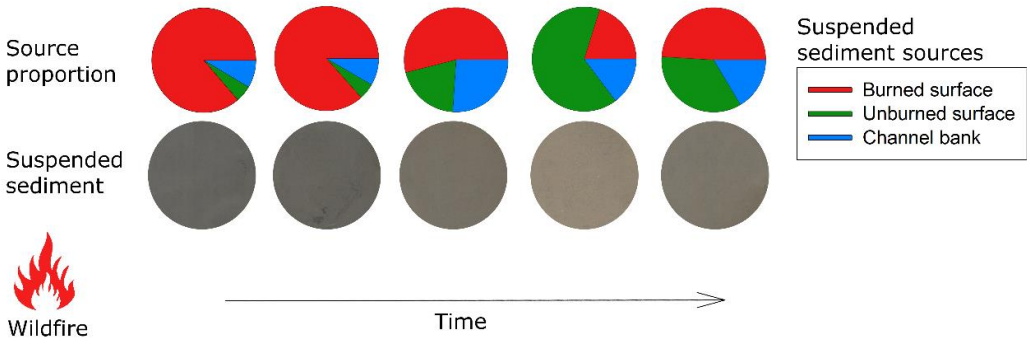

Reference

García-Comendador, J., Martínez-Carreras, N., Fortesa, J., Borràs, A., Calsamiglia, A., & Estrany, J. 2020. Analysis of post-fire suspended sediment sources by using colour parameters. Geoderma, 379, 114638. doi: 10.1016/j.geoderma.2020.114638

6.1. Introduction

Wildfires greatly change the hydrological response and sediment dynamics of river systems (Moody et al., 2013; Shakesby, 2011; Shakesby and Doerr, 2006). The reduction or elimination of vegetation cover (Candela et al., 2005) and the alteration of physicochemical soil characteristics (Úbeda and Outeiro, 2009) normally increase overland flow and sediment yield from hillslopes and reduce the rainfall-runoff response time, especially during the first post-fire year (Candela et al., 2005; Scott et al., 1998). Other variables that affect the increase in erosion and sediment yield after a fire are the fire's severity (Keeley, 2009), post-fire rainfall patterns (Warrick et al., 2012), lithology and the presence of agricultural terraces (García-Comendador et al., 2017a), and post-fire management (Spanos et al., 2005). In addition, the increase in slope-to-channel sediment connectivity may generate downstream impacts related to fine sediment transport and its associated pollutants (Collins et al., 2017), such as dam siltation (Navas et al., 2004), decreased water quality (Horowitz et al., 2007; Smith et al., 2011a) and the contamination of aquatic ecosystems (Newcombe and Macdonald, 1991; Verkaik et al., 2013).

Fire transforms biomass, necromass and soil organic matter into ash, consisting of mineral materials and charred organic components (Bodí et al., 2014). A non-homogenous ash layer covers the soil surface immediately after a wildfire creating a two-layer system (Nyman et al., 2014), influencing soil wettability (Balfour and Woods, 2013; Bodí et al., 2014; Cerdà and Doerr, 2008) and altering its hydrological behaviour (Brook et al., 2018). Nevertheless, ash does not remain on the soil surface for very long, but is redistributed or removed in days or weeks after a fire (Cerdà and Doerr, 2008; Pereira et al., 2015), is transported in the river in combination with fine sediment (Reneau et al., 2007) and/or migrates downward into the soil (Pereira et al., 2015). However, little is known about how ash reaches the stream network after a fire and its progressive wash-out as suspended sediment, as this process is highly dependent on ash properties, terrain features and meteorological conditions (Bodí et al., 2014). Accurate identification of the suspended sediment sources contributing to sediment load after a wildfire and of routine monitoring programmes are needed to

correctly design and evaluate post-fire management strategies, which are crucial in fire-prone, human-modified environments.

In river catchments, fingerprinting and unmixing techniques are often used to calculate the different pre-defined sources in a downstream suspended sediment mixture (Davis and Fox, 2009; Walling et al., 1993). Traditionally, physical, biochemical and geochemical sediment properties are used as tracers (Walling, 2013). Sediment fingerprinting assumes that tracer properties are measurable, conservative and representative, which needs to be carefully scrutinized (Collins et al., 2017; Smith and Blake, 2014). In addition, the tracers must behave in a linearly additive way during the mixing process (Lees, 1997). Previous studies have shown that the use of some of these tracers is not appropriate in burned catchments. For example, susceptibility to the variation of soil geochemical properties after a fire hinders the distinction between burned and unburned areas (Smith et al., 2013). On the contrary, the fallout radionuclides (FRNs), caesium-137 (^{137}Cs) and excess lead-210 ($^{210}Pb_{ex}$), normally increase their activity in soils after a wildfire due to soil mass reduction by organic matter combustion and to radionuclide transfer and redistribution from burned vegetation to the soil (Wilkinson et al., 2009), which discriminates between burned and unburned areas (Estrany et al., 2016; García-Comendador et al., 2017b). In addition, their exposure to atmospheric precipitation discriminates between surface and subsurface sources (Owens et al., 2012; Wilkinson et al., 2009), which has led to their extensive use in burned catchments. However, catchment vulnerability to erosion processes during the first post-fire year highlights the need to define and apply cost-effective and fast post-fire management strategies, whereas FRN counting times in samples with relatively low activity are rather long.

Soil and sediment colour can also be used for tracing, the main advantage being that this can be measured by fast, cheap and non-destructive methods. Colour coefficients use as tracers for source ascription has increased in the last decade (Evrard et al., 2019; Martínez-Carreras et al., 2010b; Pulley et al., 2018; Tiecher et al., 2015), as the results obtained were found to be comparable to those obtained with classical tracers (i.e. radionuclides, geochemistry and organic compounds) in small catchments (Martínez-Carreras et al., 2010a, 2010c). Pulley et al. (2018) found high consistency

between estimates based on mineral magnetic tracers and ones based on colour coefficients in clarifying the sediment sources of historically deposited sediments. However, special attention should be paid to how changes in organic matter content, particle size distribution and moisture alter colour properties (Pulley and Rowntree, 2016). These parameters may affect the probabilistic distributions calculated by mixing models, which may in turn lead to wrong conclusions. Nonetheless, the elimination of organic matter or the use of particle size correction factors may not be suitable in all cases and may even reduce the discriminative potential of colour tracers (Pulley et al., 2018; Pulley and Rowntree, 2016).

Previous studies used ash colour (Úbeda et al., 2009) and changes in soil colour (D'Haen et al., 2013; Ketterings and Bigham, 2000; Pérez-Bejarano and Guerrero, 2018) to determine the temperature reached during a fire. Normally, black ashes appear at low temperatures (ca. 250 °C) because of the residual carbon content derived from the incomplete combustion of the organic matter; and grey ashes, at temperatures above ca. 450ºC due to the mineral residue after complete combustion (Lentile et al., 2006; Smith et al., 2005; Úbeda et al., 2009). The presence of black ash after fire tends to decrease visible and near-infrared reflectance. In contrast, the silica mineral present in grey ash tends to increase it greatly (Lentile et al., 2006). Furthermore, soil tends to become redder when temperature reaches a range between 200-500°C. This is due to the transformation of iron oxides hydrated first into maghemite and then hematite (Terefe et al., 2008). These features help to distinguish sediment origin when using colour tracers after a fire.

This paper puts forward the proposition that suspended sediment colour shows the relative contributions of burned and unburned surfaces in river catchments. Artificial mixtures of sediment and ash were created to verify linear additivity and ash influence on colour parameters. Suspended sediment tracing results obtained by colour parameters calculated from reflectance diffuse spectrometry were compared, in order to investigate the sediment's consistency, with those obtained (i) using an ordinary office scanner and (ii) fallout radionuclides.

6.2. Study area

The Sa Font de la Vila River is a Mediterranean catchment of 4.8 km^2 located in the Andratx municipality (western Mallorca, Spain; Figure 6.1A and 6.1B), which is affected by extensive afforestation of former agricultural land and recurrent wildfires. The lithology of the catchment's bottom valleys consists mainly of Upper Triassic (Keuper) clays and loams on gentle slopes (ca. < 10 degrees). Rhaetian dolomite and Lias limestone predominate in the upper parts of the catchment with steeper slopes > 30% (Figure 6.1C). Soils are classified as *BK45-2bc*, corresponding to *Calcic Cambisols* (Jahn et al., 2006). The fluvial network consists of two main streams: (a) Sa Coma Freda (east, 2.3 km^2), which has a significant groundwater influence with several karstic springs; and (b) Can Cabrit (west, 2.08 km^2), not affected by this groundwater influence due to the reduced presence of impervious materials. In addition, a check-dam was built at Can Cabrit in 2007 (5 m high and 16 m long; Figure 6.1D).

The climate is Mediterranean temperate sub-humid at headwaters and warm sub-humid at the outlet (Emberger climatic classification; Guijarro, 1986). The average temperature is 16.5 °C. The mean annual rainfall is 518 mm yr^{-1}, with an inter-annual coefficient of variation of 29%. High-intensity rainstorms with a recurrence period of 10 years may reach 85 mm in 24 hours (1974-2010; data from the B118 S'Alqueria meteorological station of the Spanish State Meteorological Agency (AEMET); Figure 6.1B).

In the last twenty years, the Sa Font de la Vila catchment has been affected by major wildfires in 1994 and 2013 (Figure 6.1E). Before the 2013 wildfire, the catchment was mainly covered by natural vegetation (84%; Figure 6.1C): 51% forest and 33% scrubland. The rest of the catchment was covered by rain-fed tree crops (12%), rain-fed herbaceous crops (1%) and urban uses (3%). Traditional soil and water conservation structures (i.e., hillslope and valley-bottom terraces) cover 37% of the total surface area (Figure 6.1D). Their abandonment and degradation, involving the collapse of dry-stone walls, increased the sensitivity of the catchment (Calsamiglia et al., 2017). Collapses were higher on those abandoned terraces affected by recurrent fires due to soil degradation (Lucas-Borja et al., 2018).

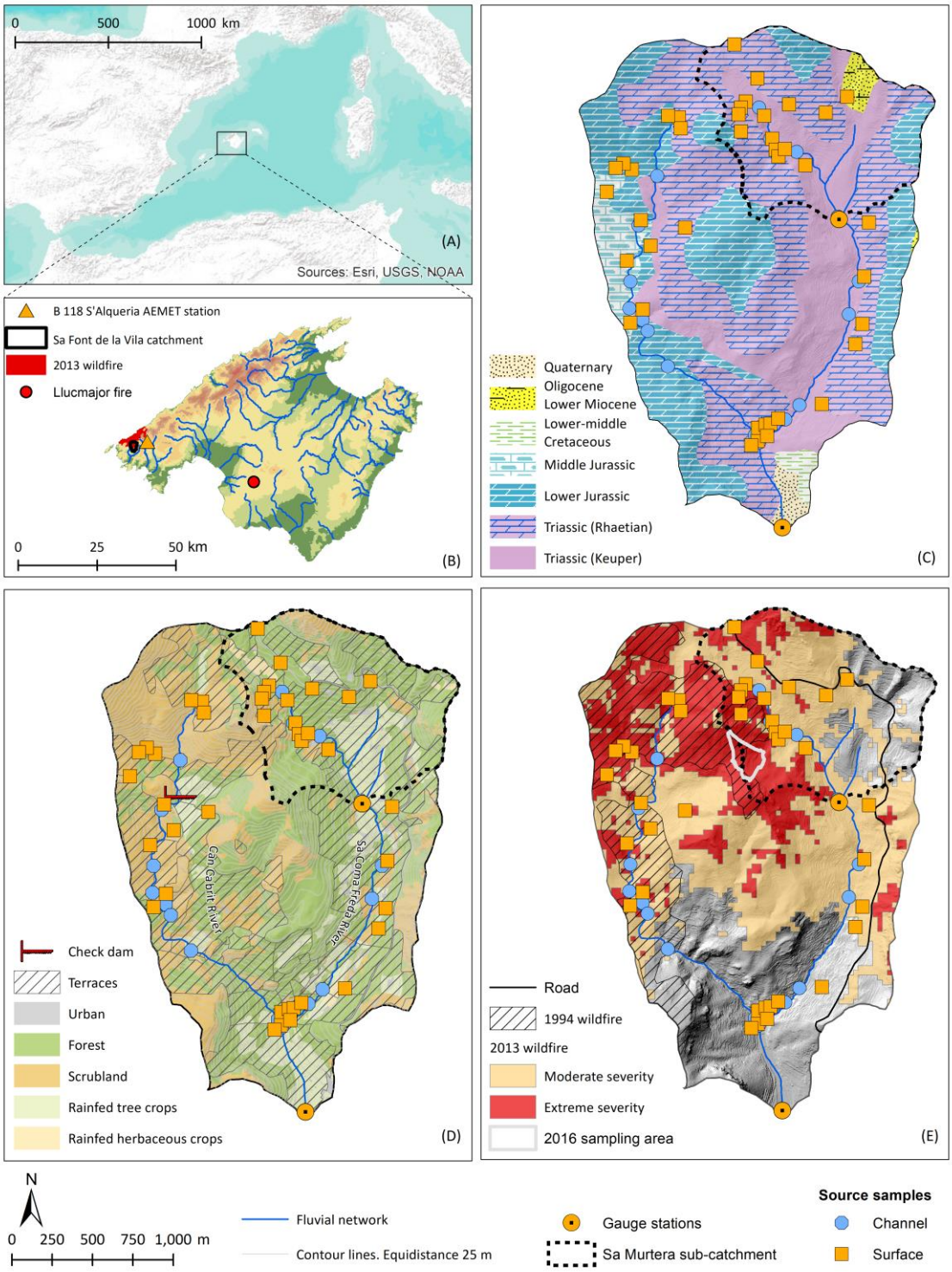

Figure 6.1. Location of the Mallorca Island within the Mediterranean Sea (A); location of the Sa Font de la Vila catchment, the area affected by the July 2013 wildfire, the B'12 S'Alqueria meteorological station and the village of Llucmajor (B); lithology (C) land uses and soil conservation practices (D) of the Sa Font de la Vila catchment (downstream site) and Sa Murtera sub-catchment (upstream site); and 1994 and 2013 wildfire affected areas as well as severity of the 2013 wildfire and 2016 sampling area (E). Channel bank and surface sampling points indicated as blue dots and orange squares, respectively.

The 1994 fire affected 45% of the catchment surface, whereas the 2013 one reached 71% (more than half of it had already been burned in 1994). A severity assessment with the Normalized Burn Ratio (Escuin et al., 2008) and Landsat 8 images for the 2013

wildfire assigned high and moderate severity to 24% and 47% of the catchment, respectively (Bauzà, 2014. Figure 6.1E). In addition, after the 2013 wildfire the Balearic Islands Department of the Environment (Conselleria de Medi Ambient, Agricultura i Pesca) implemented a series of post-fire strategies to prevent soil loss and degradation, which included mulching, tree planting and the creation of log barriers with dead biomass.

6.3. Materials and methods

6.3.1. Water and sediment monitoring programme

Two nested gauging stations were installed in Sa Font de la Vila catchment to record continuous water and suspended sediment fluxes, one at the Sa Murtera sub-catchment (1.1 km^2; *upstream site*) and one at the outlet of the catchment (4.8 km^2; *downstream site*; Figure 6.1). As the *upstream site* gauging station was not set up till September 2014, hydrological data are not available for the first post-fire year. Both stations were equipped with *Campbell Scientific CS451-L* pressure probes and *OBS-3+* turbidimeters with a double measurement range of 0-1,000 and 1,000-4,000 NTU**.** *Campbell CR200* loggers recorded 15-min average values of water stage and turbidity (based on 1-minute readings). In addition, a *Casella* tipping bucket rain gauge was installed at the *upstream site*.

6.3.2. Soil, ash and sediment sampling

After careful examination of the site, samples of potential sediment sources were collected immediately after the last wildfire (September 2013; Figure 6.1) on soil hillslopes with an apparently active sediment slope-to-channel connectivity (0-2 cm depth; n = 40) and potential erodible channel banks (n = 20). To encompass the spatial variability of the soil properties, each surface soil sample consisted of three integrated subsamples collected inside a ca. 10 m-radius circular area; and each channel bank sample, of three subsamples collected along a 10 m transect. The fire impact was taken into account when designing the surface sample collection strategy. Thirty-one surface samples were collected from burned areas (burned surface samples) and 9

from unburned areas (unburned surface samples; Figure 6.1E). For the *upstream site* only 4 channel bank samples and 15 burned surface samples were collected. The unburned surface category was not included as a potential suspended sediment source in the *upstream site* because of its small area (i.e. 19% of total catchment area) and its very limited hydrological connectivity with the stream network. This latter factor is due to the presence of well-maintained agricultural terraces (cf. Calsamiglia et al., 2017) and a road that isolates most of the unburned area (Figure 6.1E), acting as an artificial longitudinal buffer against the fire and directing most runoff outside the catchment.

The catchment's hydrological dynamics between the wildfire and the sampling campaign resulted in the accumulation of 107 mm of low-intensity precipitation, which did not generate surface runoff at the catchment outlet (precipitation data from B118 S'Alqueria AEMET station, Figure 6.1B). Visual evidence during the sampling campaign suggested incorporation of part of the ash deposits in the soil profile through infiltration (see ash cover in photos taken during the sampling campaign; Supplementary figure 6.1). For a few samples, the remaining ash cover was carefully removed to collect representative samples of the soil surface and minimise alteration of intrinsic soil properties.

Suspended sediment samples (n=9) were collected during the hydrological years between 2013 and 2015 at both sampling sites (i.e. *upstream site* and *downstream site*), using time-integrated samplers (Phillips et al., 2000; two samplers per site). Ash was not collected at the study site. However, ash samples were collected from a fire-affected area in August 2018 in the municipality of Llucmajor (southwest Mallorca; Figure 6.1B). This burned site had similar soil types, climate and vegetation patterns. Representative ashes with a wide spectrum of colours (white, grey and black) were collected, avoiding the inclusion of the underlying soil layer (Bodí et al., 2014). In a simplified procedure, the samples were combined in two groups representing the overall gradient of ash colours, namely the black ashes (n=10), i.e. the darker samples, and the grey ashes (n=9), the lighter samples. Although the ash sampling area and the study area encompass similar characteristics, collecting ash samples in the study area just after the 2013 wildfire have been preferable. Thereby, even incorporating ashes

with a large range of colours in the analysis, eventual difference between ashes from both sites remain unknown

6.3.3. Laboratory treatment and analysis

The source and target sediment samples were oven-dried at 40 °C, disaggregated using a pestle and a mortar and sieved to <63 μm to minimize the differences in particle size composition between source/target samples (Walling et al., 1993). The particle size distribution (PSD) and the specific surface area (SSA) of all source samples and 3 suspended sediment samples were determined after sieving by using a Malvern Mastersizer 2000 at the Institute of Environmental Assessment and Water Research (IDAEA-CSIC, Spain). The Shapiro-Wilk ($p < 0.05$) normality test and the Mann-Whitney *U* test checked the similarity in the PSD of each source group and target sample. ^{137}Cs and $^{210}Pb_{ex}$ activity concentrations ($Bq \cdot kg^{-1}$) were measured by gamma spectrometry at the *Environmental Radioactivity Laboratory* of the University of the Balearic Islands (Mallorca, Spain), using a high-purity coaxial intrinsic germanium (HPGe) detector. Total C and N were measured by high-temperature combustion using a TruSpec CHNS, LECO at the Luxembourg Institute of Science and Technology (LIST, Luxembourg).

Diffuse reflectance was measured in a dark room by a spectroradiometer (ASD FieldSpect-II) at 1 μm steps over the 400-2500 μm range. The spectrometer was located in a tripod perpendicular to a flat surface, at 10 cm from the reference standard panel of known reflectivity (Spectralon). The soil and sediment samples were placed in transparent P.V.C. round petri dishes (4.7 cm diameter; Pall Corporation) and carefully smoothed with a spatula to minimize micro shadow effects due to surface roughness. The samples and the Spectralon were illuminated at an angle of 30° by a 50-w quartz halogen lamp placed at ca. 30 cm of distance. Following the International Commission on Illumination (CIE, 1931), CIE xyY colour coefficients were computed (i.e. cie x, cie y and cie yy) from the spectra reflectance measurements and the RGB colour values (i.e. red, green and blue). Then, the ColoSol software, developed by Viscarra Rossel et al. (2006), was used to estimate the Munsell HVC (i.e. Munsell H, Munsell V and Munsell C), CIE XYZ (i.e. cie X, cie Y and cie Z), CIE LAB (cie L, cie a* and cie b*), CIELUB (i.e. cie L, cie u* and cie v*), CIELHC (i.e. cie L, cie H and cie C) and

decorrelated RGB (i.e. HRGB, IRGB and SRGB) colour parameters, as well as the redness index (i.e. RI) and Helmoltz chromaticity coordinates (i.e. DW nm, Pe %).

All the samples were placed in transparent plastic bags (7 * 5 cm) and scanned with an office scanner (Konika Minolta bizhub C554e; e.g. Krein et al., 2003; Pulley and Rowntree, 2016). The instrument was not calibrated. Red, green and blue colour parameters (i.e. RGB model) were extracted from the scanned images by the GIMP 2 open-source image-editing software. Then, the procedure described in the previous paragraph was applied to convert the red, green and blue colour parameters into the other colour parameters. This allowed us to determine whether colour parameters calculated from diffuse reflectance (hereafter referred to as spectrometer-based colour parameters) and with an ordinary office scanner (hereafter referred to as scanner-based colour parameters) were consistent.

Ash exhaustion and soil recovery over time could alter source colour values, resulting in larger source ascription uncertainties in the medium to long term after the fire. However, sources were only sampled once (1 month after the fire). To partially mitigate this limitation, we made use of 24 soil samples collected in 2016 (29 months after the fire) from a headwater field on the study site (Figure 6.1E). Samples were collected following the same methodology as in 2013 and scanned to measure their colour parameters. The samples were originally collected to analyse soil quality parameters after a wildfire (Calsamiglia et al., 2017 and Lucas-Borja et al., 2018).

6.3.4. Artificial laboratory mixtures

Thirty artificial mixtures of 2, 3 and 4 different source samples, ash and suspended sediment were created (Table 6.1 and Supplementary table 6.1). Mixtures of different sample types and a reduced number of mixtures with two or three samples of the same source were created. In the latter case, as all samples were considered as different sources, they permitted the uncertainty assessment when source tracer signatures were less distant. In addition, and to investigate ash influence on the colour parameters, 18 artificial samples mixing suspended sediment (collected at the *upstream site* in 2015) and ash (black and grey) in different proportions were created (Table 6.1 and Supplementary table 6.2). The ash proportion was gradually modified

from 10% to 90% to observe the influence of ash on sediment colour variation. Colour parameters of all the artificial mixtures were measured with the spectrometer and the scanner following the methodology described in Section 6.3.3.

6.3.5. Accuracy of colour tracers

The individual accuracy and linear additivity behaviour of colour tracers were assessed by comparing measured values (i.e. spectrometer- and colour-based ones) and predicted values by means of a mass balance approach (i.e. tracer values in the mixture are equal to the sum of contributions from each artificially mixed sample). To compare colour tracers with different scales, the normalized root mean square error (nRMSE) was calculated by dividing the RMSE by the mean of the measured data. The nRMSE was expressed as a percentage. The tracers with a nRMSE >15% were discarded.

A Kruskal-Wallis H test was performed to find how well the colour tracers discriminated between source groups. Then, a Discriminant Function Analysis (DFA) checked the discriminatory potential of each tracer group (taking selected tracers as independent variables) and calculated the percentage of correctly classified samples (leave-on-out cross-validation).

6.3.6. Suspended sediment fingerprinting and unmixing of artificial mixtures

A range test was used to exclude potentially non-conservative tracers in each individual suspended sediment sample. Therefore, the tracers in suspended sediment and artificial mixtures that showed values outside minimum and maximum source range values were discarded.

The MixSIAR Bayesian tracer mixing model framework (Stock et al., 2018), implemented by Stock and Semmens (2016) as an open-source R package, was used to estimate the relative contribution of each source to the suspended sediment samples and the artificial mixtures. Previous studies using Bayesian mixing models to unmix sediment sources include Abban et al., 2016; Blake et al., 2018; Massoudieh et al., 2013; and Nosrati et al., 2014.

The fundamental mixing equation of a mixing model is:

$$b_i = \sum_{j=i}^{m} w_j \cdot a_{i,j}$$

where b_i is the tracer property i (i = 1 to n) measured in a suspended sediment sample, $a_{i,j}$ is the value of the tracer property i in each source sample j (j = 1 to m), w_j is the unknown relative contribution of each source j to the suspended sediment sample. MixSIAR accounts for variability in the source and mixture tracer data with the ability to incorporate covariance data to explain variability in the mixture proportions via fixed and random effects (Stock and Semmens, 2016; Stock et al., 2018). This is especially useful in this study because of the collinearity between colour parameters of the different chromaticity coordinates. Hence, a discriminant function was not used to select an optimum group of tracers, as weak tracers can only improve model representation. In this study, MixSIAR was formulated by using sediment type as a factor and an uninformative prior (Blake et al., 2018). The Markov Chain Monte Carlo parameters were set as very long: chain length = 1,000,000, burn = 700,000, thin = 300, chains = 3. Convergence of the models was evaluated by the Gelman-Rubin diagnosis.

MixSIAR was used to unmix the artificial mixtures (see Section 6.3.4) and ultimately to evaluate and compare the performance of the two different colour tracer groups and FRNs. A constant residual error of 5% in the mixed samples was taken as creating the artificial mixtures to account for potential variability (e.g. measurement error). It should be noted that tracers that showed no individual discriminatory accuracy were excluded from the model (see Section 6.3.5). Accuracy in predicting the source contribution of each tracer group was evaluated by computing absolute errors (i.e. absolute value of the difference between the real proportions in the mixture and the estimated contributions; AE).

6.4. Results

6.4.1. Artificial laboratory mixtures and ash influence

Colour parameters showed individual contrasting performance to predict the colour of artificial mixtures (Figure 6.2; Table 6.1). Chromatic coordinates *cie x* and *cie y* showed a maximum nRMSE between estimated and predicted values of 2% and 5% for the spectrometer-based (Figures 6.2A and 6.2C) and scanner-based (Figures 6.2B and 6.2D) parameters, respectively. Regardless of the measurement technique, *cie x* and *cie y* had lower nRMSE than red, green and blue colour parameters. In contrast, *cie yy* (brightness) had larger errors. The spectrometer-based *cie yy* parameter showed a minimum of 21% nRMSE (Figure 6.2A); and the *cie yy* scanner-based one, a minimum of 15% (Figure 6.2B). Thus, as *Cie yy* performance was low, it was not considered a linearly additive tracer. Figures 6.2A and 6.2B also show that the divergence between estimated and measured *cie yy*, red, green and blue (i.e. nRMSE values) decreased when discarding one artificial mixture with black ash (n=9; Figure 6.2A and 6.2B). For instance, the average spectrometer- and scanner-based *cie yy*, red, green and blue nRMSEs decreased to 13%, 6%, 4% and 5%, respectively. Linear additivity tests were performed for all other spectrometer- and scanner-based colour parameters to discard non-linearly additive tracers. The remaining colour parameters were used to predict suspended sediment sources (Table 6.2).

The average nRMSE between estimated and predicted values was slightly higher for the 3-sample mixtures than for the 2-sample ones, for both the spectrometer- (4.2% higher) and the scanner-based (1.1% higher) colour parameters (Figure 6.2). The 4-sample mixtures' average nRMSE was lower than the 2-sample mixtures' average nRMSE for both the spectrometer-based (1.3% lower) and the scanner-based (2.4% lower) colour parameters.

Accuracy of spectrometer- and scanner-based colour parameters was similar. Accordingly, colour parameters calculated using the two independent techniques correlated closely (n = 24; confidence limit 99%; P < 0.01) (see Supplementary figure 6.2). Despite this, the relationship between colour parameters calculated with the two techniques does not always follow the identity line.

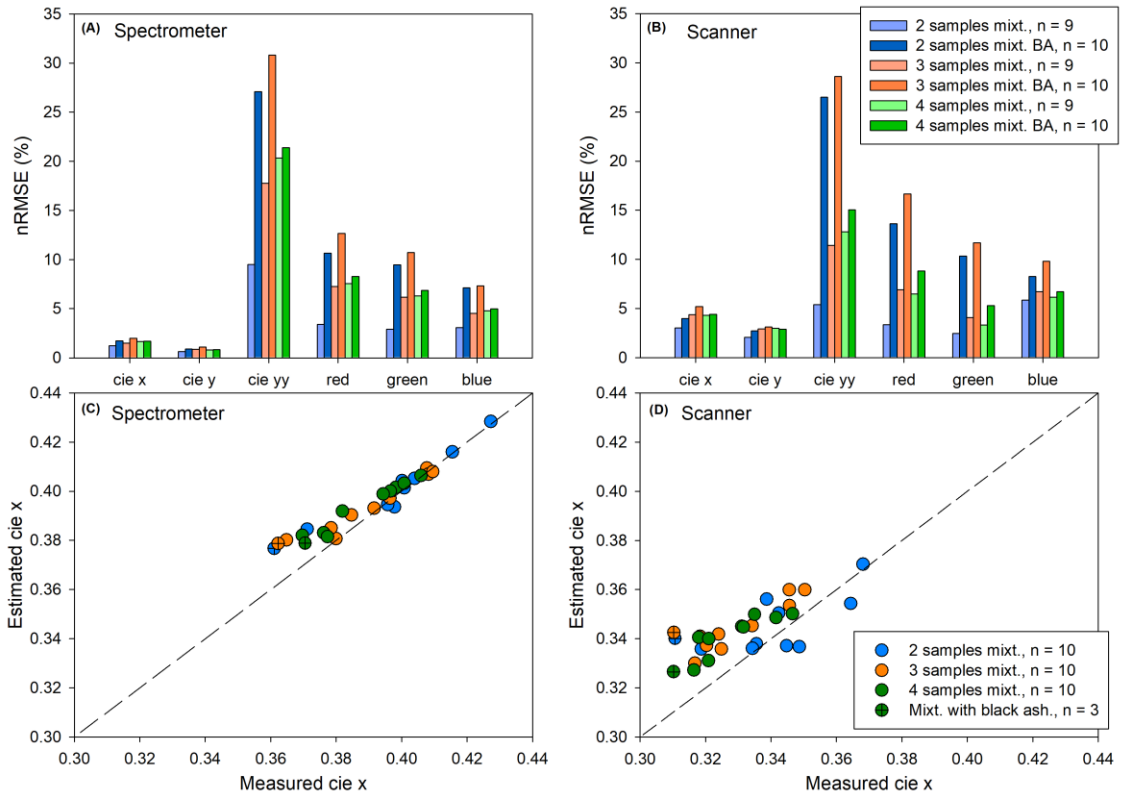

Figure 6.2. Normalized root mean square error (nRMSE) between estimated and measured spectrometer-based (A) and scanner-based colour parameters (B). Note that nRMSE results are shown when including samples containing black ashes (BA; i.e. '2 samples mixt. BA', '3 samples mixt. BA' and '4 samples mixt. BA') and excluding them from the mixtures (i.e., '2 samples mixt.', '3 samples mixt.' and '4 samples mixt.'). Note that accuracy increase in the latest case. Scatter plot showing estimated versus measured cie x spectrometer-based parameter (C) and cie x scanner-based parameter (D) when mixing 2, 3 and 4 samples.

Figure 6.3 shows the estimated *vs* measured spectrometer-based colour parameters of the artificial sediment-ash mixtures (*cie x*, *cie y* and *cie yy*; Figures 6.3A-C) and the nRMSE (*cie x*, *cie y*, *cie yy*, red, green and blue; Figure 6.3D). Colour parameters changed clearly when regular proportions of ash were added to a suspended sediment sample (i.e., from 10 to 90%). For all colour parameters except green, the real measurements are over-estimated when a mass-balance approach is used (data not shown). *Cie x* and *cie y* parameters' nRMSE values were relatively low (i.e. < 3%) for both grey and black ash mixtures. However, *cie yy* showed a larger nRMSE (i.e. 10% for grey ash mixtures and 74% for black ash mixtures), confirming that it did not behave as a linearly additive tracer.

The nRMSE values were higher on the RGB chromatic scale than on *cie x* and *cie y*. Mixtures with black ash showed larger errors than grey ash mixtures. Grey ash mixtures' nRMSEs for red, green and blue were < 10% (Figure 6.3D). On the contrary, nRMSEs for black ash mixtures were > 10%. Errors were lower with a large contribution

of one of the samples to the mixture (i.e. less deviation from the identity line in Figures 6.3A-C), whereas errors increased if the proportion of both samples mixed was similar. In addition, and for comparison, analysis of the redness index evolution in black and grey artificial mixtures showed close positive correlation with $R^2 > 0.9$ in both cases (Figure 6.3F and 6.3G).

Table 6.1. Summary table of the type and number of artificial mixtures created in the laboratory. Average absolute error between real and estimated proportions using spectrometer-based colour parameter in MixSIAR. Real and estimated proportions of samples mixed are listed in Supplementary table 6.3, Table 6.4, Table 6.5.

Samples	Number of samples mixed (n-sources)	Number of mixtures (n)	Average absolute error (%)	Type of samples mixed
2-samples mixtures	2	10	12.3	Channel bank, surface unburned, surface burned, grey ash, black ash
3-samples mixtures	3	10	12.3	Channel bank, surface unburned, surface burned, grey ash, black ash
4-samples mixtures	4	10	10.1	Channel bank, surface unburned, surface burned, grey ash, black ash
Black ash mixtures	2	9	-	Ash and suspended sediment
Grey ash mixtures	2	9	-	Ash and suspended sediment

Table 6.2. Tracers with a linear additivity behaviour.

	Spectrometer-based parameters	Scanner-based parameters
Linear additivity test:		
Colour parameters with nRMSE < 15%	cie x, cie y, red, green, blue, HRGB, IRGB, cie L, cie H, Munsell H, Munsell V, DW nm, Pe %	cie x, cie y, green, blue, IRGB, cie L, Munsell V, DW nm

In addition, increases in total C and total N were observed when the proportion of ash in the mixtures increased (Figures 6.3H and 6.3I). On average, total C content increased by 0.6% and 6.4% for each 10% increase in grey and black ash content, respectively. Total N average increase was 0.01% and 0.04% for grey and black ash mixtures, respectively.

The MixSIAR Bayesian tracer mixing model framework was used to calculate the contribution of each sample to the artificial laboratory mixtures and to evaluate the overall unmixing performance of the colour tracers (using parameters showing a nRMSE < 15% on passing a range test for each mixture; unmixing results shown in

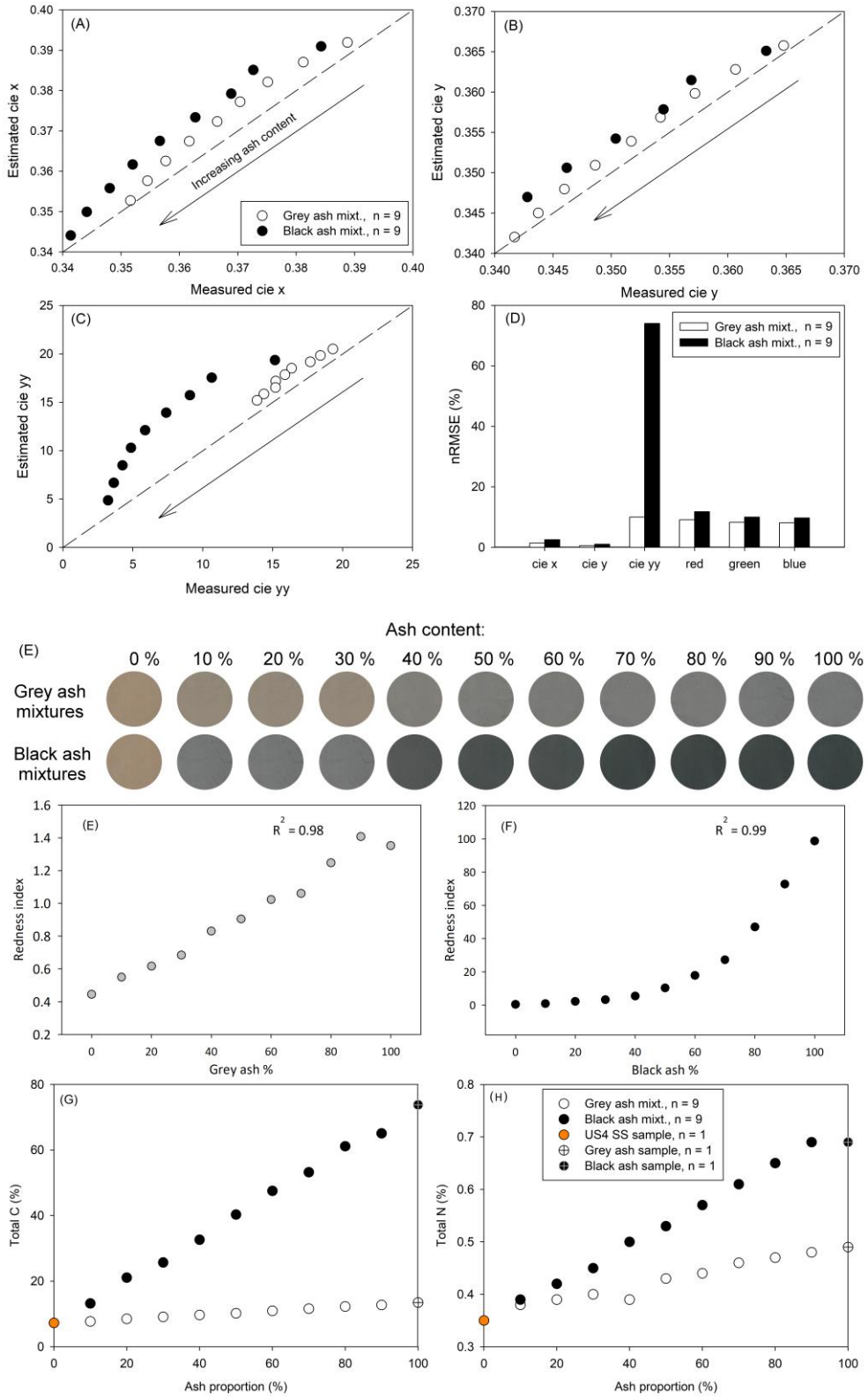

Figure 6.3. Scatter plots showing estimated versus measured cie x (A), cie y (B) and cie yy (C) spectrometer-based colour parameter when adding increasing proportions of ash (black and grey ash; 0–100%) to a suspended sediment sample. (D) Normalized root mean square error (nRMSE) between estimated and measured spectrometer-based cie x, cie y, cie yy, red, green and blue colour parameters of the artificial sediment-ash mixtures. (E) Scanned images of the sediment-ash artificial mixtures when increasing the ash proportion (grey and black ash mixtures). (F) correlation between grey and (G) black ash % and redness index measured in the artificial mixtures. (H) scatter plot between total C and cie x and (I) between total N and cie x of the sediment-ash artificial mixtures, the US4 suspended sediment sample (US4 SS), and black and grey ash.

Supplementary tables 6.3, 6.4 and 6.5 for 2, 3 and 4 samples mixed, respectively). MixSIAR predictions were compared with the real proportions mixed. The average absolute error when mixing 2, 3 and 4 samples ranged between 10.1 and 12.3% (Table 6.1). When unmixing 2 samples and one of the samples contributed more than 60% to the mixture, MixSIAR was able to identify the dominant sample in 4 of 6 cases. For 3-sample mixtures, MixSIAR was able to identify the dominant source in the 2 artificial samples when one of the samples contributed more than 60% to the mixture. Finally, when unmixing 4-sample mixtures, MixSIAR correctly identified the sample with a contribution > 40% to the mixture in 4 of 6 samples. In addition, some samples showed widespread distribution in the solutions of the model (e.g. mix2-m7), though the distribution did not include the real mixed sample proportion (e.g. mix2-m2).

6.4.2. Colour, particle size, organic matter content and FRN activity of sources, ash and suspended sediment samples

Samples collected at the downstream site from distinct sources had distinct colour values (Figure 6.4; $p < 0.05$, K-Wallis test at 95% confidence interval; Supplementary table 6.6). The unburned surface samples showed the highest values of all measured colour parameters, followed by the channel bank and the burned surface samples. Suspended sediment colour measurements fall within the limits of the sources, with no evidence of missed sources seen. The values of suspended sediments were usually medium-low and similar to the values measured in the burned surface and channel bank samples. Black ash samples showed the lowest colour values. However, grey ash samples showed very low values for *cie x* and *cie y*, but notably higher values for *cie yy*.

At the downstream site, burned surface samples showed the highest redness index values, followed by channel banks and unburned surfaces (Figure 6.5A). Accordingly, suspended sediment samples showed a higher redness index during the first event, which decreased over time at both sampling sites (Figure 6.5B).

The discriminant function analysis showed that the selected spectrometer- and scanner-based parameters (Table 6.2) correctly classified 80% and 78.3% of the source samples, respectively, and that the selected tracers were able to distinguish sediment sources (Figure 6.6).

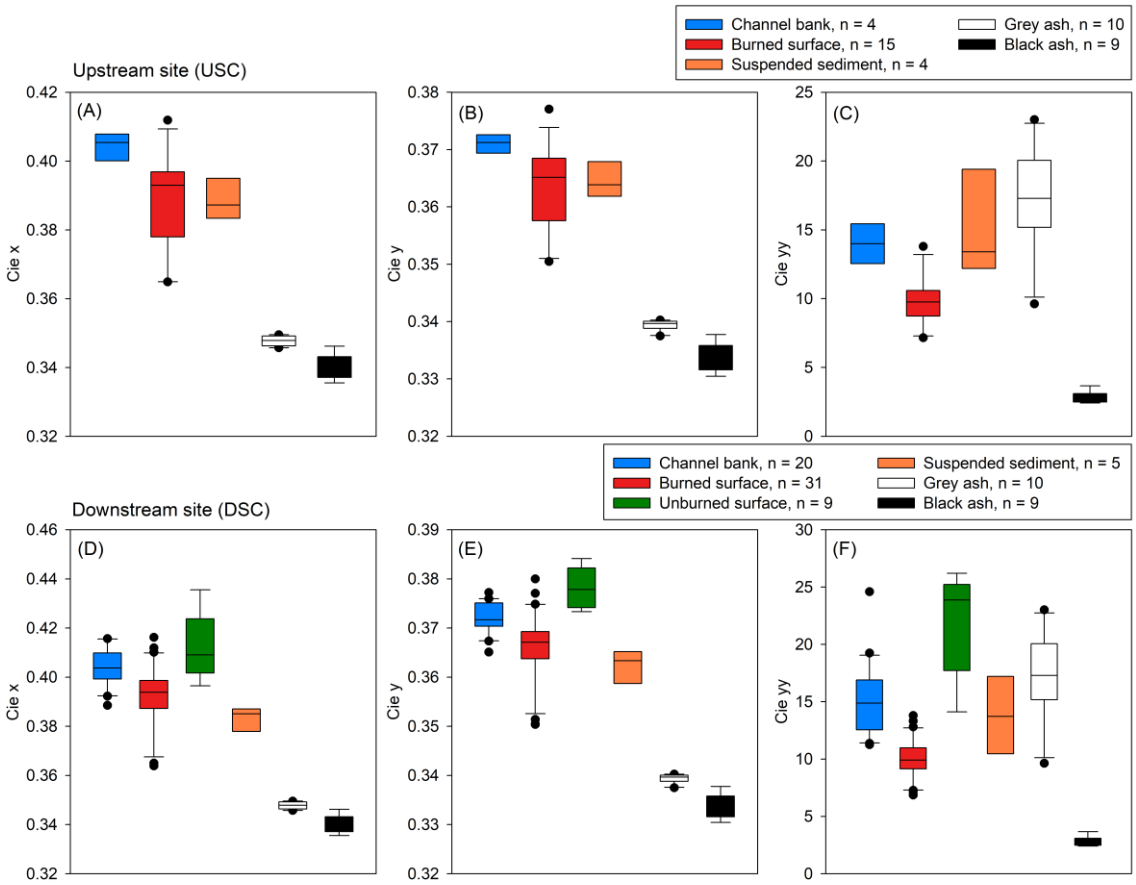

Figure 6.4. Box plots of cie x, cie y and cie yy reflectance-based colour parameters measured in source and suspended sediment samples at the Sa Murtera sub-catchment (upstream site; A, B and C) and at the Font de la Vila catchment (downstream site; D, E and F). Values measured on grey and black ashes are plotted for comparison.

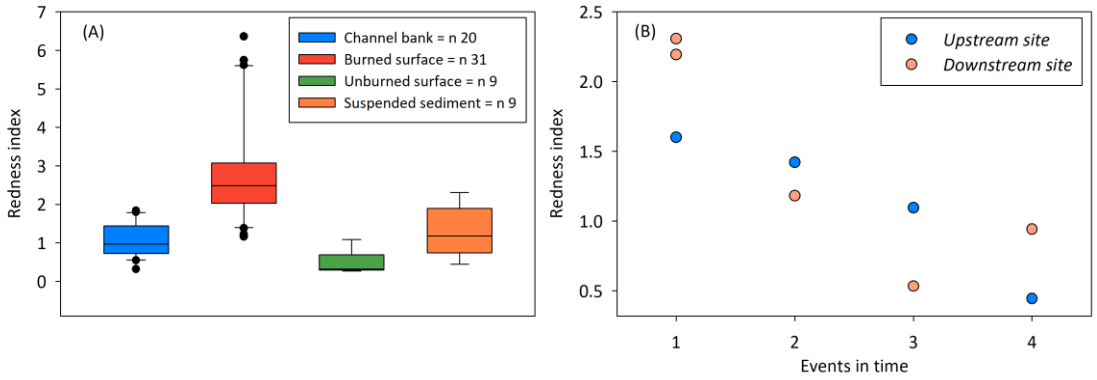

Figure 6.5. (A) Boxplots showing the spectrometer-based redness index distribution values measured in sediment sources and suspended sediment samples from the downstream site; (B) evolution of the redness index values in suspended sediment samples trough time (x axis represents the chronological order of the events; see Table 6.3).

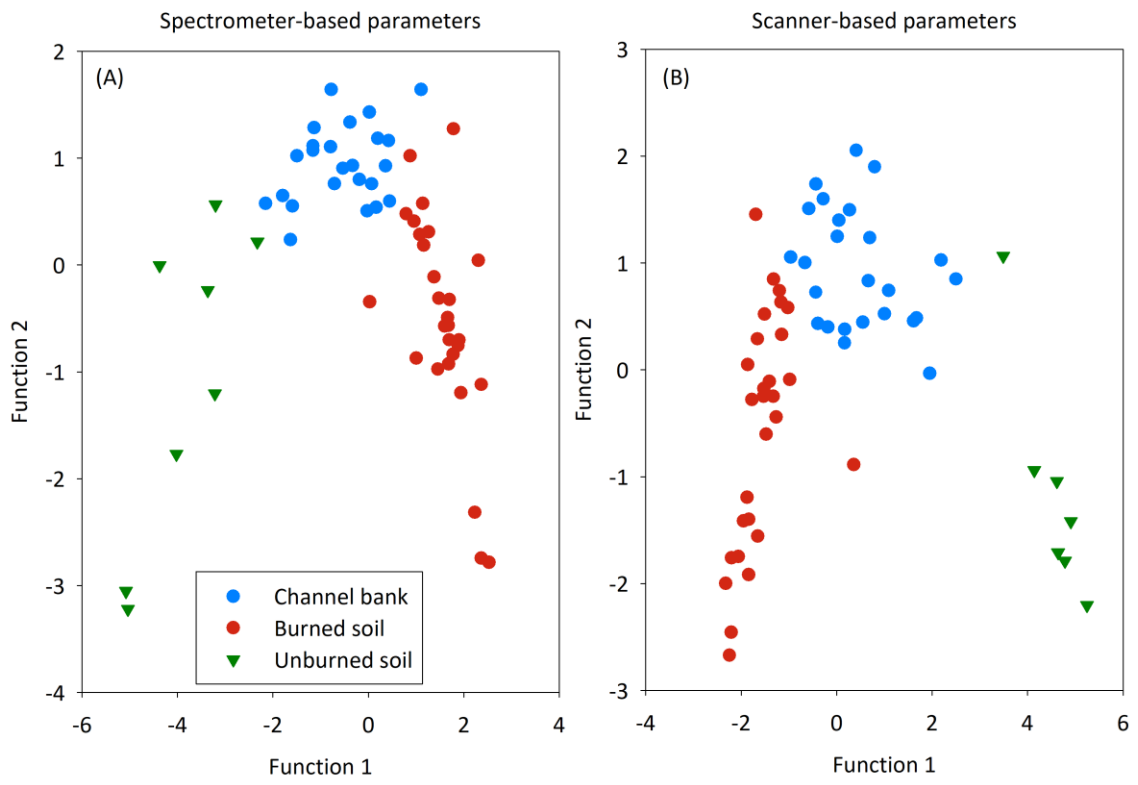

Figure 6.6. Bi-plot showing the first and second discriminant functions for the spectrometer- (A) and scanner-based colour parameters (B) measured on the different source types of Sa Font de la Vila catchment (downstream site). Tracers used are listed in Table 6.2.

Particle size distribution between source groups and suspended sediment samples was not normal (Shapiro-Wilk, p <0.05). When applying the Mann-Whitney U test, all source sample groups showed statistical similarity with the suspended sediment samples (channel bank: U = 2281, p=0.894; burned surface: U = 2280, p = 0.890; unburned surface: U = 2267, p = 0.846; Figure 6.7).

Total C and N measured in source, suspended sediment and ash samples are shown in Figure 6.8. Total C and N measured in suspended sediment and source samples showed significant inverse correlation with spectrometer-based *cie x* (R = 0.71 for both total C and N, n = 67, p < 0.05; Figure 6.8) and *cie y* colour parameters (R = 0.72 and 0.77, for total C and N, respectively, n = 67, p < 0.05; data not shown).

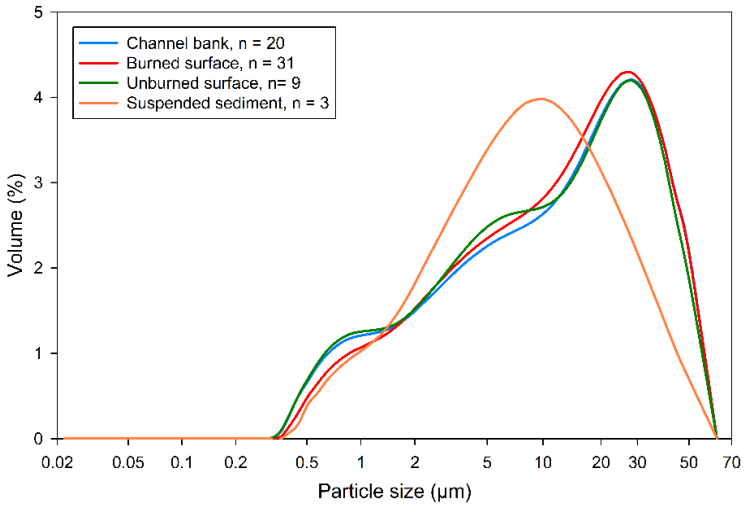

Figure 6.7. Average particle size distributions of the different source types of Sa Font de la Vila catchment (downstream site) and suspended sediment samples.

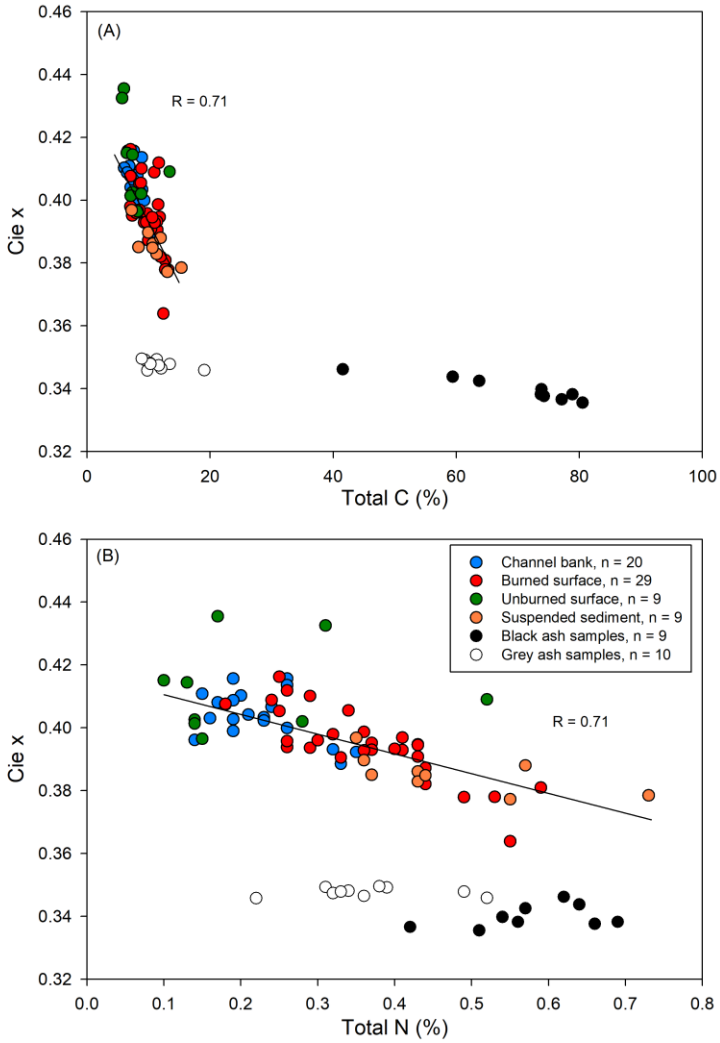

Figure 6.8. Scatter plots between suspended sediment, source samples, black ash and grey ash chromatic coordinate cie x and Total C (A), and Total N (B). R2 linear correlation coefficients for the source and sediment samples.

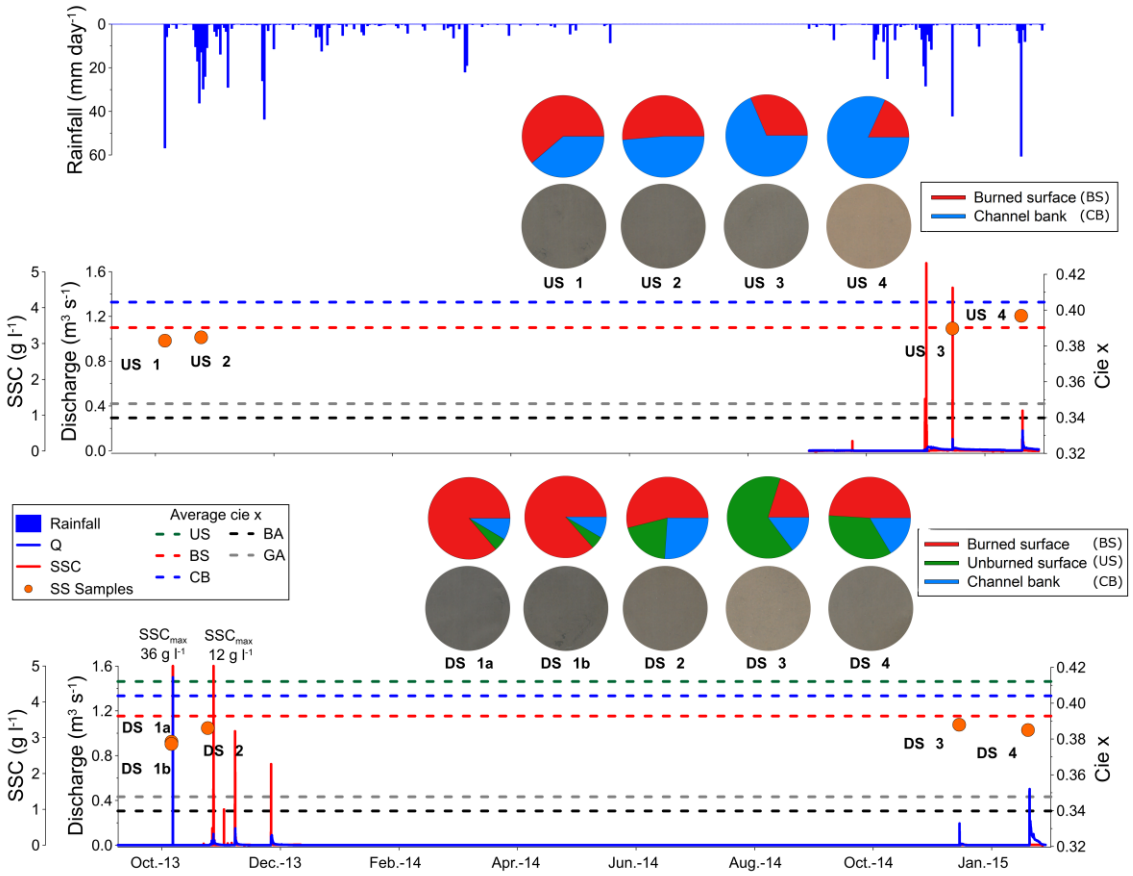

Figure 6.9. Hydrograph, suspended sediment concentration (SSC) and hyetograph at the Sa Murtera sub-catchment (middle plot; upstream site) and the Sa Font de la Vila catchment (lower plot; downstream site) during the study period. Average cie x colour parameter values for each potential suspended sediment sources type (unburned surface (US), burned surface (BS) and channel bank (CB), grey and black ashes (GA and BA, respectively) represented as dotted lines. Cie x colour parameter values measured on the suspended sediment (SS) samples represented as orange dots. Pie charts show suspended sediment average source ascription at both sampling sites together with a picture of the suspended sediment collected with the time-integrated sampler during each event.

Suspended sediment samples from the *upstream* and *downstream sites* were collected for (i) two events occurring in the first post-fire hydrological year and (ii) two events in the second post-fire hydrological year (Figure 6.9). Table 6.3 summarizes the hydrological and sediment transport dynamics of the events. It is of note that during the 29/10/2013 event, when precipitation intensity was ca. 5 times higher than the average of the rest of events, discharge and suspended sediment concentration peaks were an order of magnitude higher. At both sites, suspended sediment collected during the first event had the lowest colour values for *cie x*, *cie y* and *cie yy*, whereas values tended to increase in consecutive events (Table 6.3). However, it is the last event that shows the highest values at the *upstream site*. At the *downstream site*, the highest values were measured during the 15/12/2014 event, followed by the last event.

Burned surface samples showed the highest average activity values for ^{137}Cs and $^{210}Pb_{ex}$ (Table 4). Channel bank and unburned surface samples had very similar average FRN activities. These samples did not pass the K-Wallis distribution test ($p > 0.05$) and were grouped into a single source (i.e. referred to as unburned-channel).

Table 6.3. List of events sampled in the upstream site (Sa Murtera) and downstream site (Sa Font de la Vila). Total rainfall (P.tot.); maximum rainfall intensity in 30 min (IPmax-30); total sediment load (Load); maximum sediment concentration (SS peak), and the cie x, cie y and cie yy spectrometer-based colour parameters measured in the suspended sediment samples. DS1a and DS1b were sampled simultaneously in the same event.

Site	SS Samples	Date	P.tot.	IPmax-30	Q peak	Load	SS peak	Colour parameters		
			(mm)	($mm \cdot h^{-1}$)	($m^3 \cdot s^{-1}$)	(t)	($mg \cdot l^{-1}$)	Cie x	Cie y	Cie yy
Upstream site	US1	29/10/2013	51	100	-	-	-	0.3829	0.3617	12.0399
	US2	17/11/2013	66	18	-	-	-	0.3848	0.3624	12.6789
	US3	15/12/2014	30	29.6	0.1	0.8	4.557	0.3897	0.3654	14.1313
	US4	20/01/2015	62	10.8	0.2	0.7	11.245	0.3968	0.3687	21.1625
Downstream site	DS1a*	29/10/2013	51	100	1.5	84	36.030	0.3785	0.3592	10.5616
	DS1b*	29/10/2013	51	100	1.5	84	36.030	0.3772	0.3582	10.3677
	DS2	17/11/2013	66	18	0.1	3	11.848	0.3861	0.3633	13.7114
	DS3	15/12/2014	30	29.6	0.2	0.1	215	0.388	0.3665	19.3448
	DS4	20/01/2015	62	10.8	0.5	1.1	285	0.3851	0.3639	15.0774

** Samples DS1a and DS1b were collected during the same event using two time-integrated suspended sediment samplers.*

Similar FRNs activities in unburned surface and channel bank samples can be explained as a consequence of a patchy fire effect within some streams. Flame turbulent processes can patchily influence the combustion in channel banks of intermittent streams, particularly considering those constrained by dry stone walls. However, some samples collected in unburned areas also showed high ^{137}Cs and $^{210}Pb_{ex}$ activities (Supplementary figure 6.3A). The low energy conditions at the lower Sa Font de la Vila River (i.e. low gradient of the main channel) together with the dry conditions promoted sediment deposition in the mainstream. As most of the channel banks in this lowest reach were completely constrained by dry-stone walls, the samples were collected in the most bottom part of the channel banks. The sediment released from burned areas just after the first effective event (29th October 2013) were deposited within the channel bed and also affecting the bottom part of channel banks, thus promoting the increase of FRNs concentrations (Supplementary figure 6.3B).

Both FRNs passed the K-Wallis test when two sources instead of three were considered: burned surface and unburned-channel. Suspended sediment samples' FRN values fell within the range of activities measured on the sources.

Table 6.4. Average Fallout radionuclide (FRNs) activity (Bq kg^{-1}) in the different source and sediment sample groups.

Tracers	Sample groups	Mean (Bq kg^{-1})	Sta.Dev.
$^{210}Pb_{ex}$	Channel bank	46.377	40.814
	Burned surface	204.138	98.312
	Unburned surface	42.045	52.376
	Suspended sediment	177.835	102.389
^{137}Cs	Channel bank	6.260	3.803
	Burned surface	28.665	16.076
	Unburned surface	5.811	6.118
	Suspended sediment	20.800	8.754

6.4.3. Suspended sediment fingerprinting

All colour tracers that surpassed the linear additive test also passed the range test (spectrometer- and scanner-based colour parameters, Table 6.2) for the first two suspended sediment samples collected at the *upstream site* (i.e. US1 and US2). However, some colour parameters did not pass the test for the US3 samples (i.e. blue with scanner-based colour parameters) and US4 (green, blue, *cie L*, Munsell V with scanner and red, green, blue, IRGB, *cie L*, Munsell V with spectrometer-based colour parameters). For the suspended sediment samples collected at the *downstream site*, all tracers passing the linear additive test also passed the range test (spectrometer- and scanner-based colour parameters). Both ^{137}Cs and $^{210}Pb_{ex}$ passed the range test.

When using spectrometer-based colour parameters at the *upstream site*, mixing models predicted that burned soil contributed to the largest extent to the suspended sediment samples US1 and US2 (Table 6.5); whereas predictions for the US3 and US4 suspended sediment samples determined channel bank as the dominant source. At the *downstream site*, predicted suspended sediment sources changed over time. DS1a and DS1b were collected in parallel during the same event and predicted similar contributions (the first post-fire flush 29/10/2013). The mixing models predicted a dominant contribution of burned soil over the other sources (Table 6.5). The predominant source was still burned soil for the next sample collected (DS2), but the

predicted predominant source changed towards unburned soil for the DS3 sample. Finally, for the DS4 sample, the mixing models predicted that the main suspended sediment source was again burned soil, followed by unburned soil.

Table 6.5. MixSIAR source apportionment using spectrometer-based colour parameters, scanner-based colour parameters and fallout radionuclides activity (FRNs) for the suspended sediment samples collected at the upstream and downstream sites. It should be note that unburned surface and channel bank sources were joined for FRNs at the downstream site.

		Spectrometer		Scanner		FRNs	
SS sample	Sources	Average (%)	Quantile distribution 2.5% - 97.5%	Average (%)	Quantile distribution 2.5% - 97.5%	Average (%)	Quantile distribution 2.5% - 97.5%
				Upstream site			
US1	Burned surface	**61.3 ± 10.3**	43.5 - 83.9	39 ± 10.4	21.3 - 66.2	**83.3 ± 12.3**	52.2 -99.3
	Channel bank	38.7 ± 10.3	16.1 - 56.5	**61 ± 10.4**	37.8 - 78.7	16.7 ± 12.3	0.7 - 44.8
US2	Burned surface	**51.4 ± 9.1**	36.1 - 71.9	31.6 ± 12.3	8.3 - 58.4	**55.1 ± 20.3**	20.4 - 96.1
	Channel bank	48.6 ± 9.1	28.1 - 63.9	**68.4 ± 12.3**	41.6 - 91.7	44.9 ± 20.3	3.9 - 79.6
US3	Burned surface	31.4 ± 9.4	11.7 - 50.1	8 ± 8.7	0.2 - 29.2	27.9 ± 19.5	2.5 - 80.3
	Channel bank	**68.6 ± 9.4**	49.9 - 88.3	**92 ± 8.7**	70.8 - 99.8	**72.1 ± 19.5**	19.7 - 97.5
US4	Burned surface	18.1 ± 11.2	1.2 - 43.7	21.2 ± 2.2	0.6 - 85.8	21.3 ± 18.8	0.9 - 75.5
	Channel bank	**81.9 ± 11.2**	56.3 - 98.8	**78.8 ± 2.2**	14.2 - 99.4	**78.7 ± 18.8**	24.5 - 99.1
				Downstream site			
DS1a	Burned surface	**84.6 ± 6.4**	70.9 - 96	**88.4 ± 5.7**	75.2 - 97.5	**85.8 ± 10.3**	62.4 - 99.5
	Unburned surface	5.7 ± 4.2	0.3 -15.9	4.4 ± 3.4	0.2 - 12.8	14.2 ± 10.3	0.5 - 37.6
	Channel bank	9.7 ± 6.8	0.4 - 25.5	7.2 ± 5.8	0.2- 21.8		
DS1b	Burned surface	**86.2 ± 6.1**	73.3 - 96.7	**81.3 ± 7.5**	65.3 - 94.8	**70.3 ± 16**	40 - 97.8
	Unburned surface	5.1 ± 3.9	0.2 - 14.6	6.5 ± 4.7	0.3 - 17.2	29.7 ± 16	2.2 - 60
	Channel bank	8.7 ± 6.2	0.4 - 23	12.2 ± 8.4	0.5 - 30.4		
DS2	Burned surface	**53.8 ± 8.7**	36.8 - 70.3	**53 ± 10.2**	31.7 - 70.9	**72.7 ± 15.3**	43.5 - 98.1
	Unburned surface	19.8 ± 10	1.6 - 38	19 ± 10	1.4 - 38.1	27.3 ± 15.3	1.9 - 56.5
	Channel bank	26.4 ± 15.7	1.9 - 58.3	27.9 ± 17.2	1.4 - 63.1		
DS3	Burned surface	20.3 ± 9.5	2.1 - 38.2	8.6 ± 7.1	0.2 - 26	-	-
	Unburned surface	**65 ± 10.5**	45 - 84.2	**65.9 ± 17.4**	21.2 - 91.3	-	-
	Channel bank	14.7 ± 12.9	0.5 - 44.9	25.4 ± 20	1 - 75.1		
DS4	Burned surface	**49 ± 7.9**	32.7 - 63.3	28.4 ± 15.4	3 - 56.5	38.4 ± 19.8	7.9 - 86.4
	Unburned surface	34.4 ± 9.7	9.8 - 50.4	19.6 ± 162	0.5 - 52	**61.6 ± 19.8**	13.6 - 92.1
	Channel bank	16.6 ± 13.8	0.6 - 52.9	**52.1 ± 29.1**	1.6 - 91.8		

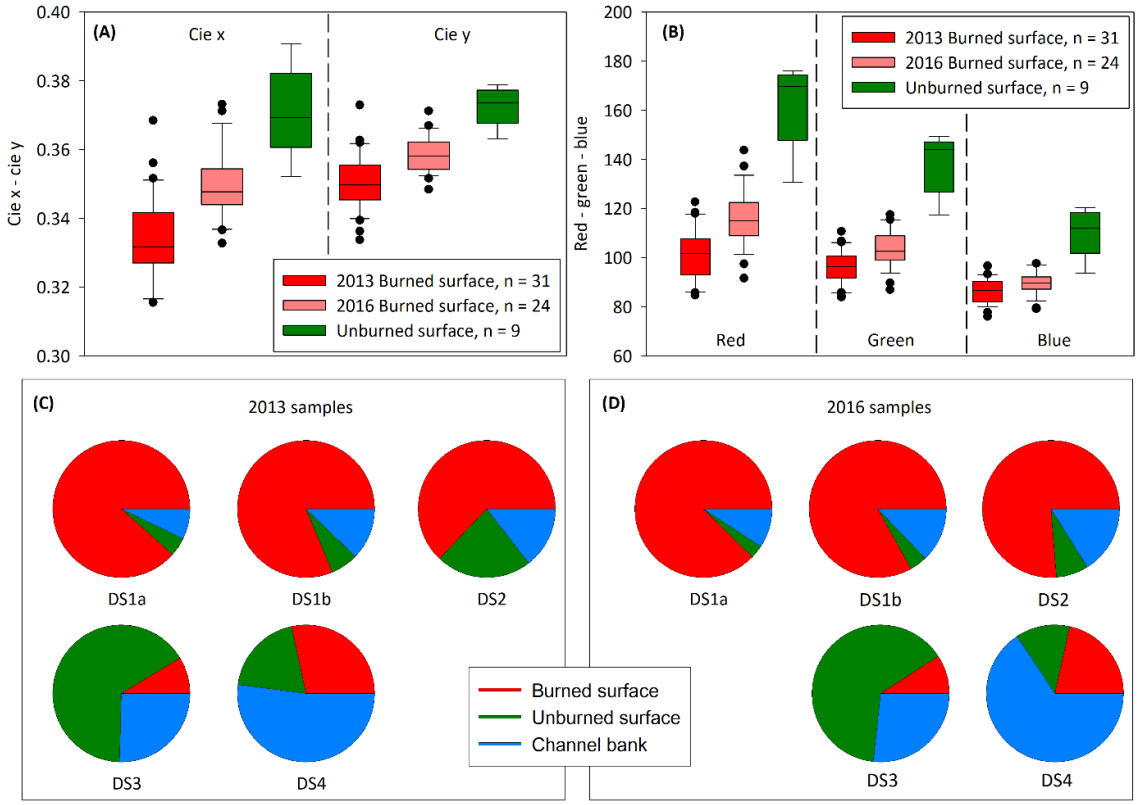

Figure 6.10. (A) Box plots of cie x and cie y scanner-based colour parameters measured in 2013 burned source samples, 2016 burned source samples and 2013 unburned source samples; (B) Box plots of red, green, blue scanner-based colour parameters measured in 2013 burned source samples, 2016 burned source samples and 2013 unburned source samples; (C) Average MixSIAR source apportionment results using 2013 burned surface scanner-based colour parameters; (D) Average MixSIAR source apportionment results using 2016 burned surface scanner-based colour parameters.

When comparing the MixSIAR predictions obtained using different groups of tracers (i.e. spectrometer- and scanner-based colour parameters and FRNs), the three tracer groups predicted the same dominant source in all samples except three (US1, US2 and DS4; Table 6.5). When only comparing the spectrometer colour-based parameters and the FRN results, the two groups always identified the same dominant source (Table 6.5) except for the DS4 sample.

The source samples collected in 2016 showed scanner-based colour values that range between the burned soil and the unburned soil samples (Figure 6.10A and 6.10B). To verify eventual ash exhaustion impact on our results, we determined suspended sediment sources by using MixSIAR and the colour parameters measured in the 2016 soil samples as burned sources (i.e. instead of the samples collected in 2013). The results did not substantially change, with an average absolute error of 5.7 ± 6.6% (Figure 6.10B and 6.10C).

6.5. Discussion

6.5.1. On the use of colour to trace suspended sediment sources in burned Mediterranean catchments

The presence of ash after a wildfire tends to change the soil's visible reflectance (Lentile et al., 2006) and its carbon content (Bodí et al., 2014) and, in consequence, the colour of the upper soil layer. Results illustrated how colour parameters estimated from diffuse reflectance laboratory measurements discriminate between burned surface soil, unburned surface soil and channel bank sources. Artificial mixtures showed that most colour parameters were linear additive and, individually, were able to predict the colour of the mixtures by using a mass balance approach. The highest errors were observed for the *cie yy*, SRGB, *cie X*, *cie Z*, *cie a**, *cie b**, *cie u**, *cie v**, *cie C*, Munsell C and redness index parameters (nRMSE>15%). Therefore, they were discarded as reliable sediment tracers. Once the non-conservative tracers were discarded, the average nRMSE was equal to 5.1% ± 2.9. Errors were comparable with values reported in the literature. Martínez-Carreras et al. (2010c) reported errors <5% for 75% of their artificial mixtures using *cie x*, *cie y* and *cie yy* colour parameters, whilst the nRMSE ranged between 0.2 and 6.3% when 15 colour coefficients were used by Uber et al. (Uber et al., 2019) and between 0.4 and 5.6% by Gaspar et al. (2019) with geochemical tracers.

Furthermore, the presence of black ash in the artificial mixtures resulted in increased nRMSEs for some colour coefficients (e.g. *cie yy*; Figure 6.2), suggesting that (i) these tracers should be discarded and (ii) colour tracers should be evaluated locally and carefully when source and sediment tracers contain black ashes. The differences in cie yy nRMSE obtained in artificial samples containing grey and black ashes may be due to different optical absorption. Black ashes had a lower reflectance with an average brightness (i.e. *cie yy*) of 2.8 ± 0.4, while grey ashes showed an average of 17.3 ± 3.8 (spectrometer-based colour data). However, other parameters (e.g. *cie x* and *cie y*) were not significantly affected when black ash was added to the artificial mixtures (nRMSE always < 4%). These were the most reliable colour tracers.

Cie x and *cie y* values decreased when the ash proportion in the artificial mixtures increased (Figure 6.3), whereas total C and N content increased. The average increase in the sediment total C content caused for each increase of 10% in the proportion of black ash is 10 times higher than for each increase of grey ash. Suspended sediment samples collected at the *upstream* and *downstream sites* and the grey ash sediment mixtures have similar proportions of C (i.e. ranging from 7.2 to 15.3%). However, even with similar total C content, the suspended sediment samples had higher *cie x* and *cie y* colour values than the grey ash artificial mixtures did (Figure 6.11). This, together with the results of the mixing experiments, suggests that most of the suspended sediment samples contained < 20% of black ash (92.5% of the samples showed values higher than those of the samples containing 20% of black ash; Figure 6.11) or < 30% of grey ash (Figure 6.11). Thus, colour parameters can be used to calculate the ash content of soil and sediment samples. For instance, a gradual increase in the *cie x* and *cie y* colour values was observed in the suspended sediment samples collected at the *upstream* and *downstream sites* during subsequent events (Figure 6.9), suggesting a decrease in their ash content. Likewise, Reneau et al. (2007) used ^{137}C activity to demonstrate that the proportion of ash in suspended sediment steadily decreased through the first rainy post-fire season and was lower in the second one.

The apparent decrease in ash content in suspended sediment samples over time (Figure 6.11) could be associated, not only with a variation in the main source of sediment (i.e. burned surface), but also with ash exhaustion on the hillslopes. The latter is informed by the redness index, which correlates closely with the percentage of grey and black ash in the artificial mixtures (Figure 6.3F and G). Hence, the ash experiments showed that the amount of ash also alters the redness index regardless of the temperature reached during the fire. Therefore, even if the redness index steadily decreases over time at both the *upstream* and *downstream sites* (Figure 6.5B), it alone cannot confirm that there were contributions from sources affected by fire, irrespective of the ash content in sediment.

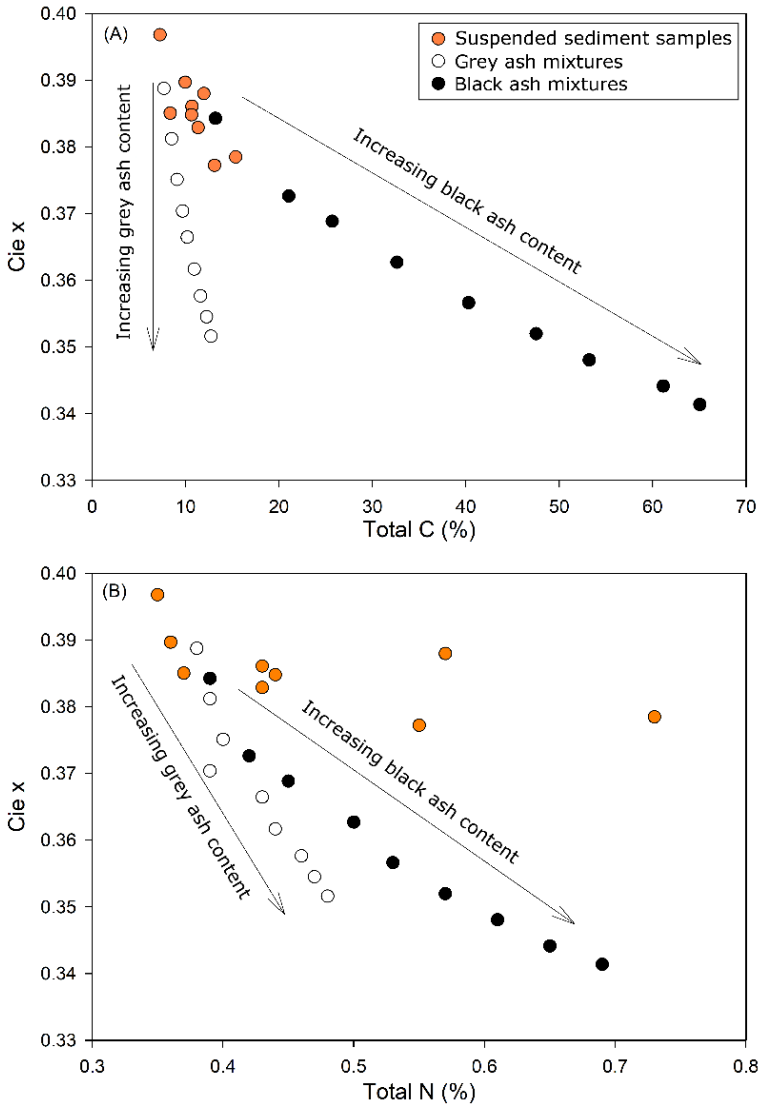

Figure 6.11. Scatter plots showing suspended sediment samples, grey ash and sediment artificial mixtures and black ash and sediment artificial mixtures relationship of cie x values and Total C (A), and Total N (B). Arrows indicate ash content increase in the artificial mixtures.

Some studies report changes in the clay-sized material in sediments after a fire by the fusion of the finest particles, generating coarser aggregates (Blake et al., 2007; Dyrness and Youngberg, 1957; Ternan and Neller, 1999). However, García-Corona et al. (2004) found no significant changes in aggregate size distribution in burned soils during a laboratory experiment. In this study, even if there were differences in particle size distribution between suspended sediment and source samples (Figure 6.5), they were not statistically significant. Nevertheless, samples were not sieved at different fractions and the influence of PSD on colour parameters was not addressed and should be further explored. Pulley and Rowntree (2016) found that the intensity of red, green and blue light reflected from the < 32 µm fraction of the sediment was significantly

higher than that of coarser particles (i.e. 63-32 µm and 125-63 µm fractions). When these authors, working in the Karoo region of the Eastern Cape of South Africa, separated the < 32 µm fraction of the sources and sediments from the > 32 µm fraction, there was less tracing uncertainty. Even though the Karoo region covers a much larger area (> 150 km^2) where in-stream transformations are more likely to occur than at our study site (< 5 km^2), the extent of suspended sediment colour changes as a function of suspended sediment PSD and catchment size remains unknown and site-dependent.

Organic matter content also modifies the effectiveness of colour tracers to discriminate sediment sources if suspended sediment content increases during transport due to in-stream transformation. In non-burned catchments, Ankers et al. (2003) found C concentrations ranging from 4.5 to 12.2% in suspended sediment collected at 60 different catchments. In burned catchments, soil C content substantially increases when organic-rich ashes are incorporated into the soils at low combustion completeness (typically T < 450°C), with organic C content as the main component (Bodí et al., 2014). However, lower C content is expected in burned soils at high combustion completeness (typically T > 450°C), as most organic carbon is volatized. At our study site, the average total C content of burned soils was 2.3% higher than that of unburned soils, and 2.1% higher than in channel banks, which suggests the incorporation of low-combustion ashes. We argue that changes in total C content associated with ash incorporation and/or soil transformation after a wildfire, when low-combustion ashes are incorporated, are much larger than eventual changes due to in-stream transformation in small catchments. In this study, on average, total C increased by 0.6% ± 0.2 and 6.4% ± 2.5, respectively, when the proportion of grey and black ash in the artificial mixtures increased by 10% (Figure 6.11). Pulley and Rowntree (2016) used H_2O_2 to remove organic matter in their South Africa samples to evaluate the uncertainties associated with organic matter when using colour to trace suspended sediment sources. Their results showed that H_2O_2 treatment reduced source variability, homogenizing tracer values for each source and improving the discrimination capacity of colour tracers over untreated samples. However, the capacity of these tracers to discriminate between surface and subsurface sources was

reduced. The authors also artificially added organic matter to some mixtures and observed that it had very little impact on the precision of colour tracers when it was < 30% of the sample mass. In later research, Pulley et al. (2018) detected that differences of 44% resulted when treating or not with H_2O_2 sediment and soil samples. When comparing these results with those provided by mineral magnetic tracers, the authors concluded that the errors were lower in the untreated samples, which means that the elimination of organic matter using H_2O_2 added more uncertainties to the unmixing process.

The capacity of colour tracers to unmix artificial laboratory mixtures was evaluated by the MixSIAR software. The results of our study illustrated average absolute errors of 12.3% ± 9.1, 12.3% ± 4.2 and 10.1% ± 4.2 for 2-, 3- and 4-source mixtures, respectively. These errors were of the same order of magnitude as errors obtained by other authors using other tracers. Haddadchi et al. (2014) applied four different models using geochemical tracers to 20 artificial mixtures and obtained mean absolute errors ranging from 10.8% to 28.7%. Lower errors were found by Brosinski et al. (2014), who used VNIR-SWIR spectral features to unmix 33 artificial samples and found errors < 10% in practically all cases. Gaspar et al. (2019) also obtained similar results with RMSEs ranging between 0.4% and 5.9% when they unmixed 12 artificial mixtures (10 replicas each) from 3 sets of different geochemical tracers. Nevertheless, Uber et al. (2019) demonstrated, using three different mixing models (i.e. NNLS, SIMMR and PLSR), that the choice of tracers generates a greater impact on the model results than the type of model used. However, other authors found that different results might also be associated with the mixing models used (Haddadchi et al., 2014). In addition, if colour signatures are relatively similar (e.g. mix4-m4, mix4-m5, Supplementary table 6.5), colour tracer measurements are not precise enough to quantify source contributions accurately.

Chromatic parameters calculated from the spectrometer in the laboratory and scanner-based colour parameters correlate closely (p < 0.01), which confirms that colour parameters provided by an office scanner are as reliable as colour tracers from a spectrophotometer. The differences in the absolute values obtained with the two techniques are related to (i) different measurement environments (i.e. dark room vs.

office) and (ii) a lack of scanner calibration. Pulley et al. (2016) demonstrated the reliability of an ordinary scanner in sediment fingerprinting research. They compared colour signatures with mineral magnetic signatures to trace bed and suspended sediment in the South African Karoo. The discriminatory efficiency of colour signatures ranged between 92.2% and 96.7% and were comparable to the results obtained using mineral magnetic signatures (i.e. 94%).

6.5.2. Suspended sediment origin after a wildfire in a Mediterranean catchment

The use of colour parameters to determine suspended sediment sources in the Sa Murtera (*upstream site*) and Sa Font de la Vila (*downstream site*) catchments, both affected by a wildfire in 2013, was assessed. Since errors associated with the unmixing of artificial samples might be high (see Section 6.5.1), the results using reflectance-based and scanner-based colour parameters were compared with those obtained using radioisotopes (i.e. ^{137}Cs and $^{210}Pb_{ex}$). It had been shown previously that the FRNs were able to recognize sediment sources in burned catchments (Wilkinson et al., 2009). The use of multi-fingerprint techniques is crucial to detect and quantify potential biases between different tracer sets and obtain reliable and robust estimates (e.g. Uber et al., 2019). In general, results showed that the three tracer groups predicted the same dominant source (Table 6.5). Nevertheless, at the *upstream site*, tracing results for the first two samples (i.e. US1 and US2) obtained with the scanner-based colour parameters indicated a different dominant source from the spectrometer-based colour parameters and the FRNs (Table 6.5). When looking at the tracer values' distribution measured for both samples and sources (Supplementary figure 6.4), we can see that both the spectrometer- and scanner-based colour parameters show *cie x* and *cie y* values similar to the values measured on burned surfaces. However, green and blue tracer values are similar to the values measured in channel banks. We argue that these differences are the main cause of divergence in the source ascription results. Furthermore, the small number of channel bank samples (n = 4) could misrepresent the real colour tracer variability of this source and confuse the un-mixing results. The results obtained with FRNs help us to determine the main suspended sediment source for the US1 sample (burned soil with an average

contribution of 83.3 ± 12.3, Table 6.5). However, FRNs showed poor discrimination for US2, which does not allow clear determination of the main suspended sediment source contributing to this sample. Nevertheless, the main predicted source for the 4 *upstream site* suspended sediment samples always coincides in both the spectrometer-based colour parameters and the radionuclides. However, the results for US2 (Table 6.5) are not very reliable because of the similar proportions of the two sources considered. At the *downstream site*, the main contributing source was the same for the three groups of tracers in all cases except for the 4th sample, in which scanner-based parameters and FRNs indicated dominance of the channel bank and unburned surface areas. The low suspended sediment concentration peak and the delivered load during the 4th event (Table 6.3) may indicate not only a low slope-to-channel sediment mobilization, but also the activation of small or very specific sediment sources not well represented in the sampling. Limitations in the technique to identify sediment sources at low suspended sediment concentrations could be involved during these low magnitude events. Nevertheless, at both sites, results indicate that sediment contribution from burned surface sources dominated the first hydrological year, whereas unburned surface and channel banks dominated the second hydrological year.

The samples collected in 2016 were used to validate the hypothesis that some ash remained in the burned soils two years after the fire. Thus, source samples collected after the fire were representative of the entire sediment sampling period. The *cie x*, *cie y* and RGB scanner-based colour value distribution (Figure 6.10A and 6.10B) suggested that, although there were colour changes after the fire, most probably due to ash wash, there was still ash influence in the soil colour parameters. Furthermore, sediment ascription results in both 2013 and 2016 burned surface samples (Figure 6.10B and C) were similar. Even if the changes in soil colour properties caused by the fire still prevail today in some areas, the samples collected in 2016 are not representative of the entire catchment (see Section 6.3.2 for details). Catchment-wide representative sampling would have been needed to improve the robustness of the source ascription results for the 2014 and 2015 suspended sediment samples.

In this study, it is assumed that sediment and ash were transported in association on their way from the hillslopes to the stream and remained in association during eventual deposition. However, this was not investigated. Direct observations indicated that water flows are notably turbulent at the study sites, generating a relatively homogeneous mixture of suspended sediment within the water column. Nevertheless, the sediment originating at unburned areas could be influenced by the ash during in-stream transport, generating erroneous source ascription results. Many authors have documented increased erosion rates, runoff coefficients and sediment delivery in burned areas (e.g. Shakesby and Doerr, 2006; Vieira et al., 2015). In addition, the incorporation of ash to runoff tends to increase its density, resulting in greater erosivity potential and enhancing its sediment transport capacity (Gabet and Sternberg, 2008). Even so, the transport mechanisms of ash and mineral particles should be further explored to determine whether they are transported together and what influence they have on colour parameters. This would improve the robustness of the technique.

The main sediment sources in a burned catchment may vary according to catchment characteristics and the magnitude of post-fire rainfall events. Other studies of burned catchments also found temporal variations of the main sources of sediment. Distinguishing only between surface vs. subsurface sources and using radionuclides, Wilkinson et al. (2009) and Smith et al. (2011b) observed predominance of surface soil in two burned forested catchments in Australia, despite differences in fire severity patterns, size and geology characteristics. In addition, Smith et al. (2011b) found a gradual decrease of surface soil contributions during the first 4 years after the wildfire. However, Owens et al. (2012) found a predominance of subsurface/channel bank contributions in a semi-arid forested burned catchment in Canada, due to the low-intensity rainfall that constrained sediment delivery from hillslopes. Estrany et al. (2016) used radionuclides to trace suspended sediment sources after a wildfire in a small Mediterranean catchment in Spain. The authors also quantified a small contribution from burned areas (12% on average) to bed-sediment samples during a flood event characterised by 69 mm of total rainfall in 24 hours.

Studies show divergences in landscape response after a wildfire. Predominant factors influencing erosive processes in burned catchments, besides fire, are the magnitude, frequency and intensity of post-fire rainfall and any associated floods (Moody and Martin, 2009; Smith et al., 2011b). The Mediterranean is a highly energetic environment with large inter-annual variability of rainfall, resulting in different sediment yields and sediment origin depending on seasonality, preceding wetness conditions and intrinsic characteristics of each event. In addition, the important presence of agricultural terraces in the Sa Font de la Vila catchment (Figure 6.1D) plays an important role in sediment connectivity, by decreasing water and sediment yield (Calsamiglia et al., 2018). García-Comendador et al. (2017a) analysed the hydrological dynamics and suspended sediment transport in the catchment during the first three post-fire years (2013-2016). The hysteresis analysis during this period concluded that 67% of the counter-clockwise hysteresis (i.e. associated with distant sediment sources, potentially burned areas in this case) occurred during the first year after the fire, decreasing significantly in subsequent years together with sediment yield. During these three years, 92% of the sediment was exported during the first event (October 2013; samples US1, DS1a and DS1b). These results corroborate the tracing results obtained with the spectrometer-based colour tracers, showing a decrease over time in the contribution from distant areas (i.e. fire-affected hillslopes) and variations in the main sediment sources over time (Table 6.5). The decrease in the sediment contribution from burned hillslopes is related not only to partial vegetation recovery, but also to that rainfall events occurring during the second year after the fire did not exceed the intensity thresholds needed to generate effective slope-to-channel connectivity (Calvo-Cases et al., 2003), resulting in disconnected burned hillslopes.

6.6. Conclusions

Colour tracers measured with a spectrometer and a scanner discriminate usefully between burned and unburned sediment sources. This is a result of the soil colour changes associated with the transformation of biomass, necromass and soil organic matter into ash during a fire. Colour parameters can be used in unmixing approaches to tracing suspended sediment sources after wildfires in small Mediterranean

catchments, as our results are consistent - for most of the samples - with tracing results obtained with well-established radionuclides. The main advantage of colour parameters is that they can be measured quickly and are cheap and non-destructive. Hence, they enable post-fire management strategies to be decided quickly and their success to be followed up easily.

Nevertheless, results obtained using colour parameters must be carefully considered and cross-checked by use of other tracers. This might be even more important in burned catchments, where ash exhaustion and soil recovery during the disturbance period may affect colour parameters. Accordingly, variations in organic matter content and differences in particle size distribution need to be addressed.

In the Sa Font de la Vila catchment, the contribution of burned hillslopes to suspended sediment gradually decreased. We hypothesise that this might be related to partial vegetation recovery. However, it appears that the relatively low rainfall intensities measured during the second year after the fire might not have reached the thresholds for generating effective slope-to-channel connectivity. Further research is necessary to evaluate the recovery of the catchment, a highly variable and changing ecosystem.

Finally, the lack of standardized protocols for sampling sediment sources in burned catchments should not be forgotten. The values of not only soil colour parameters, but also other tracers, change on the incorporation of ashes. Therefore, the sampling protocol (e.g. incorporating the layer of ash partially or completely removing it to reach the soil surface) and the sampling time (e.g. immediately after the fire or a few days later) require further research. The use of a standardized sampling method will allow better comparison between studies of different sites, as it would take into account not only the fire and the characteristics of the study area, but also post-fire hydro-meteorological conditions.

ACKNOWLEDGMENTS

This research was supported by the Spanish Ministry of Science, Innovation and Universities, the Spanish Agency of Research (AEI) and the European Regional Development Funds (ERDF) through the project CGL2017-88200-R "Functional hydrological and sediment connectivity at Mediterranean catchments: global change scenarios –MEDhyCON2". Julián García-Comendador is in receipt of a pre-doctoral contract (FPU15/05239) funded by the Spanish Ministry of Education and Culture. Núria Martínez-Carreras acknowledges funding for this study from the Luxembourg National Research Fund (PAINLESS project, C17/SR/11699372). Josep Fortesa has a contract funded by the Vice-presidency and Ministry of Innovation, Research and Tourism of the Autonomous Government of the Balearic Islands (FPI/2048/2017). The contribution of Aleix Calsamiglia was supported by the Spanish Ministry of Science, Innovation and Universities through the pre-doctoral contract BES-2013-062887. Meteorological data were provided by the Spanish Meteorological Agency (AEMET). We would like to acknowledge support by François Barnich and Franz Kai Ronellenfitsch for the carbon and nitrogen measurements, and set-up of the spectroradiometer, respectively. We would like to also acknowledge the fundamental contribution of the reviewers in improving our manuscript.

6.7. References

Abban, B., Thanos Papanicolaou, A.N., Cowles, M.K., Wilson, C.G., Abaci, O., Wacha, K., Schilling, K., Schnoebelen, D., 2016. An enhanced Bayesian fingerprinting framework for studying sediment source dynamics in intensively managed landscapes. Water Resour. Res. 52, 4646–4673. https://doi.org/10.1002/2015WR018030

Ankers, C., Walling, D.E., Smith, R.P., 2003. The influence of catchment characteristics on suspended sediment properties. Hydrobiologia 494, 159–167. https://doi.org/10.1023/A:1025458114068

Balfour, V.N., Woods, S.W., 2013. The hydrological properties and the effects of hydration on vegetative ash from the Northern Rockies, USA. Catena 111, 9–24. https://doi.org/10.1016/j.catena.2013.06.014

Bauzà, J., 2014. Els grans incendis forestals a les Illes Balears: una resposta des de la teledetecció. Bachelor Thesis. University of the Balearic Islands, Palma, Spain.

Blake, W.H., Boeckx, P., Stock, B.C., Smith, H.G., Bodé, S., Upadhayay, H.R., Gaspar, L., Goddard, R., Lennard, A.T., Lizaga, I., Lobb, D.A., Owens, P.N., Petticrew, E.L., Kuzyk, Z.Z.A., Gari, B.D., Munishi, L., Mtei, K., Nebiyu, A., Mabit, L., Navas, A., Semmens, B.X., 2018. A deconvolutional Bayesian mixing model approach for river basin sediment source apportionment. Sci. Rep. 8, 1–12. https://doi.org/10.1038/s41598-018-30905-9

Blake, W.H., Droppo, I.G., Humphreys, G.S., Doerr, S.H., Shakesby, R.A., Wallbrink, P.J., 2007. Structural characteristics and behavior of fire-modified soil aggregates. J. Geophys. Res. Earth Surf. 112, F02020. https://doi.org/10.1029/2006JF000660

Bodí, M.B., Martin, D.A., Balfour, V.N., Santín, C., Doerr, S.H., Pereira, P., Cerdà, A., Mataix-Solera, J., 2014. Wildland fire ash: Production, composition and eco-hydro-geomorphic effects. Earth-Science Rev. 130, 103–127. https://doi.org/10.1016/j.earscirev.2013.12.007

Brook, A., Wittenberg, L., Kopel, D., Polinova, M., Roberts, D., Ichoku, C., Shtober-Zisu, N., 2018. Structural heterogeneity of vegetation fire ash. L. Degrad. Dev. 29, 2208–2221. https://doi.org/10.1002/ldr.2922

Brosinsky, A., Foerster, S., Segl, K., Kaufmann, H., 2014. Spectral fingerprinting: sediment source discrimination and contribution modelling of artificial mixtures based on VNIR-SWIR spectral properties. J. Soils Sediments 14, 1949–1964. https://doi.org/10.1007/s11368-014-0925-1

Calsamiglia, A., Fortesa, J., García-Comendador, J., Lucas-Borja, M.E., Calvo-Cases, A., Estrany, J., 2018. Spatial patterns of sediment connectivity in terraced lands: Anthropogenic controls of catchment sensitivity. L. Degrad. Dev. 29, 1198–1210. https://doi.org/10.1002/ldr.2840

Calsamiglia, A., Lucas-Borja, M.E., Fortesa, J., García-Comendador, J., Estrany, J., Calsamiglia, A., Lucas-Borja, M.E., Fortesa, J., García-Comendador, J., Estrany, J., 2017. Changes in Soil Quality and Hydrological Connectivity Caused by the Abandonment of Terraces in a Mediterranean Burned Catchment. Forests 8, 333. https://doi.org/10.3390/f8090333

Calvo-Cases, A., Boix-Fayos, C., Imeson, A.. C., 2003. Runoff generation, sediment movement and soil water behaviour on calcareous (limestone) slopes of some Mediterranean

environments in southeast Spain. Geomorphology 50, 269–291. https://doi.org/10.1016/S0169-555X(02)00218-0

Candela, A., Aronica, G., Santoro, M., 2005. Effects of Forest Fires on Flood Frequency Curves in a Mediterranean Catchment/Effets d'incendies de forêt sur les courbes de fréquence de crue dans un bassin versant Méditerranéen. Hydrol. Sci. J. 50, 206. https://doi.org/10.1623/hysj.50.2.193.61795

Cerdà, A., Doerr, S.H., 2008. The effect of ash and needle cover on surface runoff and erosion in the immediate post-fire period. Catena 74, 256–263. https://doi.org/10.1016/J.CATENA.2008.03.010

Collins, A.L.L., Pulley, S., Foster, I.D.L.D.L., Gellis, A., Porto, P., Horowitz, A.J.J., 2017. Sediment source fingerprinting as an aid to catchment management: A review of the current state of knowledge and a methodological decision-tree for end-users. J. Environ. Manage. 194, 86–108. https://doi.org/10.1016/j.jenvman.2016.09.075

D'Haen, K., Dusar, B., Verstraeten, G., Degryse, P., De Brue, H., 2013. A sediment fingerprinting approach to understand the geomorphic coupling in an eastern Mediterranean mountainous river catchment. Geomorphology 197, 64–75. https://doi.org/10.1016/j.geomorph.2013.04.038

Davis, C.M., Fox, J.F., 2009. Sediment Fingerprinting: Review of the Method and Future Improvements for Allocating Nonpoint Source Pollution. J. Environ. Eng. 135, 490–504. https://doi.org/10.1061/(ASCE)0733-9372(2009)135:7(490)

Dyrness, C.T., Youngberg, C.T., 1957. The Effect of Logging and Slash-Burning on Soil Structure. Soil Sci. Soc. Am. J. 21, 444–447. https://doi.org/10.2136/sssaj1957.03615995002100040022x

Escuin, S., Navarro, R., Fernández, P., 2008. Fire severity assessment by using NBR (Normalized Burn Ratio) and NDVI (Normalized Difference Vegetation Index) derived from LANDSAT TM/ETM images. Int. J. Remote Sens. 29, 1053–1073. https://doi.org/10.1080/01431160701281072

Estrany, J., López-Tarazón, J.A., Smith, H.G., 2016. Wildfire Effects on Suspended Sediment Delivery Quantified Using Fallout Radionuclide Tracers in a Mediterranean Catchment. L. Degrad. Dev. 27, 1501–1512. https://doi.org/10.1002/ldr.2462

Evrard, O., Durand, R., Foucher, A., Tiecher, T., Sellier, V., Onda, Y., Lefèvre, I., Cerdan, O., Laceby, J.P., 2019. Using spectrocolourimetry to trace sediment source dynamics in coastal catchments draining the main Fukushima radioactive pollution plume (2011–2017). J. Soils Sediments 19, 3290–3301. https://doi.org/10.1007/s11368-019-02302-w

Gabet, E.J., Sternberg, P., 2008. The effects of vegetative ash on infiltration capacity, sediment transport, and the generation of progressively bulked debris flows. Geomorphology 101, 666–673. https://doi.org/10.1016/j.geomorph.2008.03.005

García-Comendador, J., Fortesa, J., Calsamiglia, A., Calvo-Cases, A., Estrany, J., 2017a. Post-fire hydrological response and suspended sediment transport of a terraced Mediterranean catchment. Earth Surf. Process. Landforms 42, 2254–2265. https://doi.org/10.1002/esp.4181

García-Comendador, J., Fortesa, J., Calsamiglia, A., Garcias, F., Estrany, J., 2017b. Source ascription in bed sediments of a Mediterranean temporary stream after the first post-fire flush. J. Soils Sediments 17, 2582–2595. https://doi.org/10.1007/s11368-017-1806-1

García-Corona, R., Benito, E., De Blas, E., Varela, M.E., 2004. Effects of heating on some soil physical properties related to its hydrological behaviour in two north-western Spanish soils. Int. J. Wildl. Fire 13, 195–199. https://doi.org/10.1071/WF03068

Gaspar, L., Blake, W.H., Smith, H.G., Lizaga, I., Navas, A., 2019. Testing the sensitivity of a multivariate mixing model using geochemical fingerprints with artificial mixtures. Geoderma 337, 498–510. https://doi.org/10.1016/j.geoderma.2018.10.005

Guijarro, J.A., 1986. Contribucion a la bioclimatologia de Baleares. PhD Thesis. University of the Balearic Islands, Palma, Spain.

Haddadchi, A., Olley, J., Laceby, P., 2014. Accuracy of mixing models in predicting sediment source contributions. Sci. Total Environ. 497–498, 139–152. https://doi.org/10.1016/j.scitotenv.2014.07.105

Horowitz, A.J., Elrick, K.A., Smith, J.J., 2007. Measuring the fluxes of suspended sediment, trace elements and nutrients for the city of atlanta, USA: Insights on the global water quality impacts of increasing urbanization. IAHS-AISH Publ. 314, 57–70.

Jahn, R., Blume, H.P., Asio, V.B., Spaargaren, O., Schad, P., 2006. Guidelines for soil description, FAO. ed. Rome.

Keeley, J.E., 2009. Fire intensity, fire severity and burn severity: A brief review and suggested usage. Int. J. Wildl. Fire 18, 116–126. https://doi.org/10.1071/WF07049

Ketterings, Q.M., Bigham, J.M., 2000. Soil Color as an Indicator of Slash-and-Burn Fire Severity and Soil Fertility in Sumatra, Indonesia. Soil Sci. Soc. Am. J. 64, 1826–1833. https://doi.org/10.2136/sssaj2000.6451826x

Krein, A., Petticrew, E., Udelhoven, T., 2003. The use of fine sediment fractal dimensions and colour to determine sediment sources in a small watershed. Catena 53, 165–179. https://doi.org/10.1016/S0341-8162(03)00021-3

Lees, J.A., 1997. Mineral magnetic properties of mixtures of environmental and synthetic materials: Linear additivity and interaction effects. Geophys. J. Int. 131, 335–346. https://doi.org/10.1111/j.1365-246X.1997.tb01226.x

Lentile, L.B., Holden, Z.A., Smith, A.M.S., Falkowski, M.J., Hudak, A.T., Morgan, P., Lewis, S.A., Gessler, P.E., Benson, N.C., 2006. Remote sensing techniques to assess active fire characteristics and post-fire effects. Int. J. Wildl. Fire 15, 319–345. https://doi.org/10.1071/WF05097

Lucas-Borja, M.E., Calsamiglia, A., Fortesa, J., García-Comendador, J., Lozano Guardiola, E., García-Orenes, F., Gago, J., Estrany, J., 2018. The role of wildfire on soil quality in abandoned terraces of three Mediterranean micro-catchments. Catena 170, 246–256. https://doi.org/10.1016/j.catena.2018.06.014

Martínez-Carreras, N., Krein, A., Gallart, F., Iffly, J.F., Pfister, L., Hoffmann, L., Owens, P.N., 2010a. Assessment of different colour parameters for discriminating potential suspended sediment sources and provenance: A multi-scale study in Luxembourg. Geomorphology 118, 118–129. https://doi.org/10.1016/j.geomorph.2009.12.013

Martínez-Carreras, N., Krein, A., Udelhoven, T., Gallart, F., Iffly, J.F., Hoffmann, L., Pfister, L., Walling, D.E., 2010b. A rapid spectral-reflectance-based fingerprinting approach for documenting suspended sediment sources during storm runoff events. J. Soils Sediments 10, 400–413. https://doi.org/10.1007/s11368-009-0162-1

Martínez-Carreras, N., Udelhoven, T., Krein, A., Gallart, F., Iffly, J.F., Ziebel, J., Hoffmann, L., Pfister, L., Walling, D.E., 2010c. The use of sediment colour measured by diffuse reflectance spectrometry to determine sediment sources: Application to the Attert River catchment (Luxembourg). J. Hydrol. 382, 49–63. https://doi.org/10.1016/j.jhydrol.2009.12.017

Massoudieh, A., Gellis, A., Banks, W.S., Wieczorek, M.E., 2013. Suspended sediment source apportionment in Chesapeake Bay watershed using Bayesian chemical mass balance receptor modeling. Hydrol. Process. 27, 3363–3374. https://doi.org/10.1002/hyp.9429

Moody, J.A., Martin, D.A., 2009. Synthesis of sediment yields after wildland fire in different rainfall regimes in the western United States. Int. J. Wildl. Fire 18, 96–115. https://doi.org/10.1071/WF07162

Moody, J.A., Shakesby, R.A., Robichaud, P.R., Cannon, S.H., Martin, D. a., 2013. Current research issues related to post-wildfire runoff and erosion processes. Earth-Science Rev. 122, 10–37. https://doi.org/10.1016/j.earscirev.2013.03.004

Navas, A., Garcés, B.V., Machín, J., 2004. An approach to integrated assessement of reservoir siltation : the Joaquín Costa reservoir as a case study. Hydrol. Easrt Syst. Sci. 8, 1193–1199. https://doi.org/10.5194/hess-8-1193-2004

Newcombe, C.P., Macdonald, D.D., 1991. Effects of Suspended Sediments on Aquatic Ecosystems. North Am. J. Fish. Manag. 11, 72–82. https://doi.org/10.1577/1548-8675(1991)011<0072:EOSSOA>2.3.CO;2

Nosrati, K., Govers, G., Semmens, B.X., Ward, E.J., 2014. A mixing model to incorporate uncertainty in sediment fingerprinting. Geoderma 217–218, 173–180. https://doi.org/10.1016/j.geoderma.2013.12.002

Nyman, P., Sheridan, G.J., Smith, H.G., Lane, P.N.J., 2014. Modeling the effects of surface storage, macropore flow and water repellency on infiltration after wildfire. J. Hydrol. 513, 301–313. https://doi.org/10.1016/J.JHYDROL.2014.02.044

Owens, P.N., Blake, W.H., Giles, T.R., Williams, N.D., 2012. Determining the effects of wildfire on sediment sources using ^{137}Cs and unsupported ^{210}Pb: The role of landscape disturbances and driving forces. J. Soils Sediments 12, 982–994. https://doi.org/10.1007/s11368-012-0497-x

Pereira, P., Cerdà, A., Úbeda, X., Mataix-Solera, J., Arcenegui, V., Zavala, L.M., 2015. Modelling the Impacts of Wildfire on Ash Thickness in a Short-Term Period. L. Degrad. Dev. 26, 180–192. https://doi.org/10.1002/ldr.2195

Pérez-Bejarano, A., Guerrero, C., 2018. Near infrared spectroscopy to quantify the temperature reached in burned soils: Importance of calibration set variability. Geoderma 326, 133–143. https://doi.org/10.1016/j.geoderma.2018.03.038

Phillips, J.M., Russell, M.A., Walling, D.E., 2000. Time-integrated sampling of fluvial suspended sediment: A simple methodology for small catchments. Hydrol. Process. 14, 2589–2602. https://doi.org/10.1002/1099-1085(20001015)14:14<2589::AID-HYP94>3.0.CO;2-D

Pulley, S., Rowntree, K., 2016. The use of an ordinary colour scanner to fingerprint sediment sources in the South African Karoo. J. Environ. Manage. 165, 253–262. https://doi.org/10.1016/j.jenvman.2015.09.037

Pulley, S., Van der Waal, B., Rowntree, K., Collins, A.L., 2018. Colour as reliable tracer to identify the sources of historically deposited flood bench sediment in the Transkei, South

Africa: A comparison with mineral magnetic tracers before and after hydrogen peroxide pre-treatment. Catena 160, 242–251. https://doi.org/10.1016/j.catena.2017.09.018

Reneau, S.L., Katzman, D., Kuyumjian, G.A., Lavine, A., Malmon, D. V., 2007. Sediment delivery after a wildfire. Geology 35, 151–154. https://doi.org/10.1130/G23288A.1

Scott, D., Versfeld, D.B., Lesch, W., 1998. Erosion and sediment yield in relation to afforestation and fire in the mountains of the western cape province, south africa. South African Geogr. J. 80, 52–59. https://doi.org/10.1080/03736245.1998.9713644

Shakesby, R.A. a., 2011. Post-wildfire soil erosion in the Mediterranean: Review and future research directions. Earth-Science Rev. 105, 71–100. https://doi.org/10.1016/j.earscirev.2011.01.001

Shakesby, R.A. a., Doerr, S.H.H., 2006. Wildfire as a hydrological and geomorphological agent. Earth-Science Rev. 74, 269–307. https://doi.org/10.1016/j.earscirev.2005.10.006

Smith, A.M.S., Wooster, M.J., Drake, N.A., Dipotso, F.M., Falkowski, M.J., Hudak, A.T., 2005. Testing the potential of multi-spectral remote sensing for retrospectively estimating fire severity in African Savannahs. Remote Sens. Environ. 97, 92–115. https://doi.org/10.1016/j.rse.2005.04.014

Smith, H.G., Blake, W.H., 2014. Sediment fingerprinting in agricultural catchments: A critical re-examination of source discrimination and data corrections. Geomorphology 204, 177–191. https://doi.org/10.1016/j.geomorph.2013.08.003

Smith, H.G., Blake, W.H., Owens, P.N., 2013. Discriminating fine sediment sources and the application of sediment tracers in burned catchments: A review. Hydrol. Process. 27, 943–958. https://doi.org/10.1002/hyp.9537

Smith, H.G., Sheridan, G.J., Lane, P.N.J., Nyman, P., Haydon, S., 2011a. Wildfire effects on water quality in forest catchments: A review with implications for water supply. J. Hydrol. 396, 170–192. https://doi.org/10.1016/j.jhydrol.2010.10.043

Smith, H.G., Sheridan, G.J., Lane, P.N.J.J., Noske, P.J., Heijnis, H., 2011b. Changes to sediment sources following wildfire in a forested upland catchment, southeastern Australia. Hydrol. Process. 25, 2878–2889. https://doi.org/10.1002/hyp.8050

Spanos, I., Raftoyannis, Y., Goudelis, G., Xanthopoulou, E., Samara, T., Tsiontsis, A., 2005. Effects of postfire logging on soil and vegetation recovery in a Pinus halepensis Mill. Forest of Greece, in: Plant and Soil. Kluwer Academic Publishers, pp. 171–179. https://doi.org/10.1007/s11104-005-0807-9

Stock, B., Semmens, B., 2016. MixSIAR GUI User Manual v3.1. https://doi.org/10.5281/ZENODO.47719

Stock, B.C., Jackson, A.L., Ward, E.J., Parnell, A.C., Phillips, D.L., Semmens, B.X., 2018. Analyzing mixing systems using a new generation of Bayesian tracer mixing models. PeerJ 6, e5096. https://doi.org/10.7717/peerj.5096

Terefe, T., Mariscal-Sancho, I., Peregrina, F., Espejo, R., 2008. Influence of heating on various properties of six Mediterranean soils. A laboratory study. Geoderma 143, 273–280. https://doi.org/10.1016/j.geoderma.2007.11.018

Ternan, J.L., Neller, R., 1999. The erodibility of soils beneath wildfire prone grasslands in the humid tropics, Hong Kong. Catena 36, 49–64. https://doi.org/10.1016/S0341-8162(99)00011-9

Tiecher, T., Caner, L., Minella, J.P.G., Santos, D.R. dos, 2015. Combining visible-based-color parameters and geochemical tracers to improve sediment source discrimination and apportionment. Sci. Total Environ. 527–528, 135–149. https://doi.org/10.1016/j.scitotenv.2015.04.103

Úbeda, X., Outeiro, L., 2009. Physical and chemical effects of fire on soil, in: Cerdà, A., Robichaud, P. (Eds.), Fire Effects on Soils and Restoration Strategies. Science Publishers, New Hampshire, pp. 105–132.

Úbeda, X., Pereira, P., Outeiro, L., Martin, D.A., 2009. Effects of fire temperature on the physical and chemical characteristics of the ash from two plots of Cork oak (Quercus Suber). L. Degrad. Dev. 20, 589–608. https://doi.org/10.1002/ldr.930

Uber, M., Legout, C., Nord, G., Crouzet, C., Demory, F., Poulenard, J., 2019. Comparing alternative tracing measurements and mixing models to fingerprint suspended sediment sources in a mesoscale Mediterranean catchment. J. Soils Sediments 19, 3255–3273. https://doi.org/10.1007/s11368-019-02270-1

Verkaik, I., Vila-Escalé, M., Rieradevall, M., Prat, N., 2013. Seasonal drought plays a stronger role than wildfire in shaping macroinvertebrate communities of Mediterranean streams. Int. Rev. Hydrobiol. 98, 271–283. https://doi.org/10.1002/iroh.201201618

Vieira, D.C.S., Fernández, C., Vega, J. a., Keizer, J.J., 2015. Does soil burn severity affect the post-fire runoff and interrill erosion response? A review based on meta-analysis of field rainfall simulation data. J. Hydrol. 523, 452–464. https://doi.org/10.1016/j.jhydrol.2015.01.071

Viscarra Rossel, R.A., Minasny, B., Roudier, P., McBratney, A.B., 2006. Colour space models for soil science. Geoderma 133, 320–337. https://doi.org/10.1016/J.GEODERMA.2005.07.017

Walling, D.E., 2013. The evolution of sediment source fingerprinting investigations in fluvial systems. J. Soils Sediments 13, 1658–1675. https://doi.org/10.1007/s11368-013-0767-2

Walling, D.W., Woodward, J.C., Nicholas, A.P., 1993. A multi-parameter approach to fingerprinting suspended-sediment sources. Tracers Hydrol. Proc. Int. Symp. Yokohama, 1993 329–338.

Warrick, J.A., Hatten, J.A., Pasternack, G.B., Gray, A.B., Goni, M.A., Wheatcroft, R.A., 2012. The effects of wildfire on the sediment yield of a coastal California watershed. Bull. Geol. Soc. Am. 124, 1130–1146. https://doi.org/10.1130/B30451.1

Wilkinson, S.N.N., Wallbrink, P.J.J., Hancock, G.J.J., Blake, W.H.H., Shakesby, R.A.A., Doerr, S.H.H., 2009. Fallout radionuclide tracers identify a switch in sediment sources and transport-limited sediment yield following wildfire in a eucalypt forest. Geomorphology 110, 140–151. https://doi.org/10.1016/J.GEOMORPH.2009.04.001

6.8. Supplementary material

Supplementary figure 6.1. Study area status in during the source sampling campaign

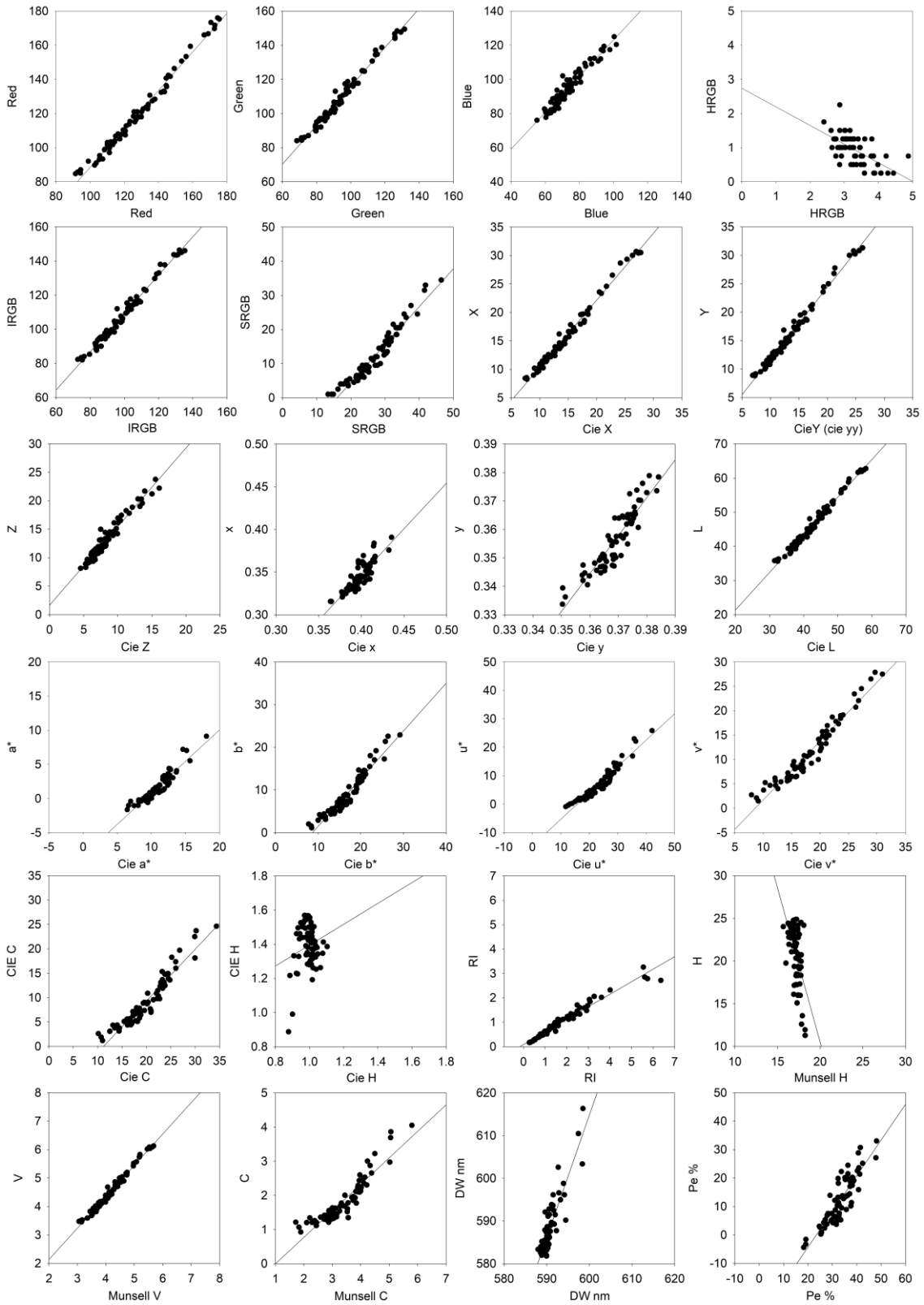

Supplementary figure 6.2. Correlations between measured reflectance-based colour parameters (y axis) and measured scanner colour parameters (x axis).

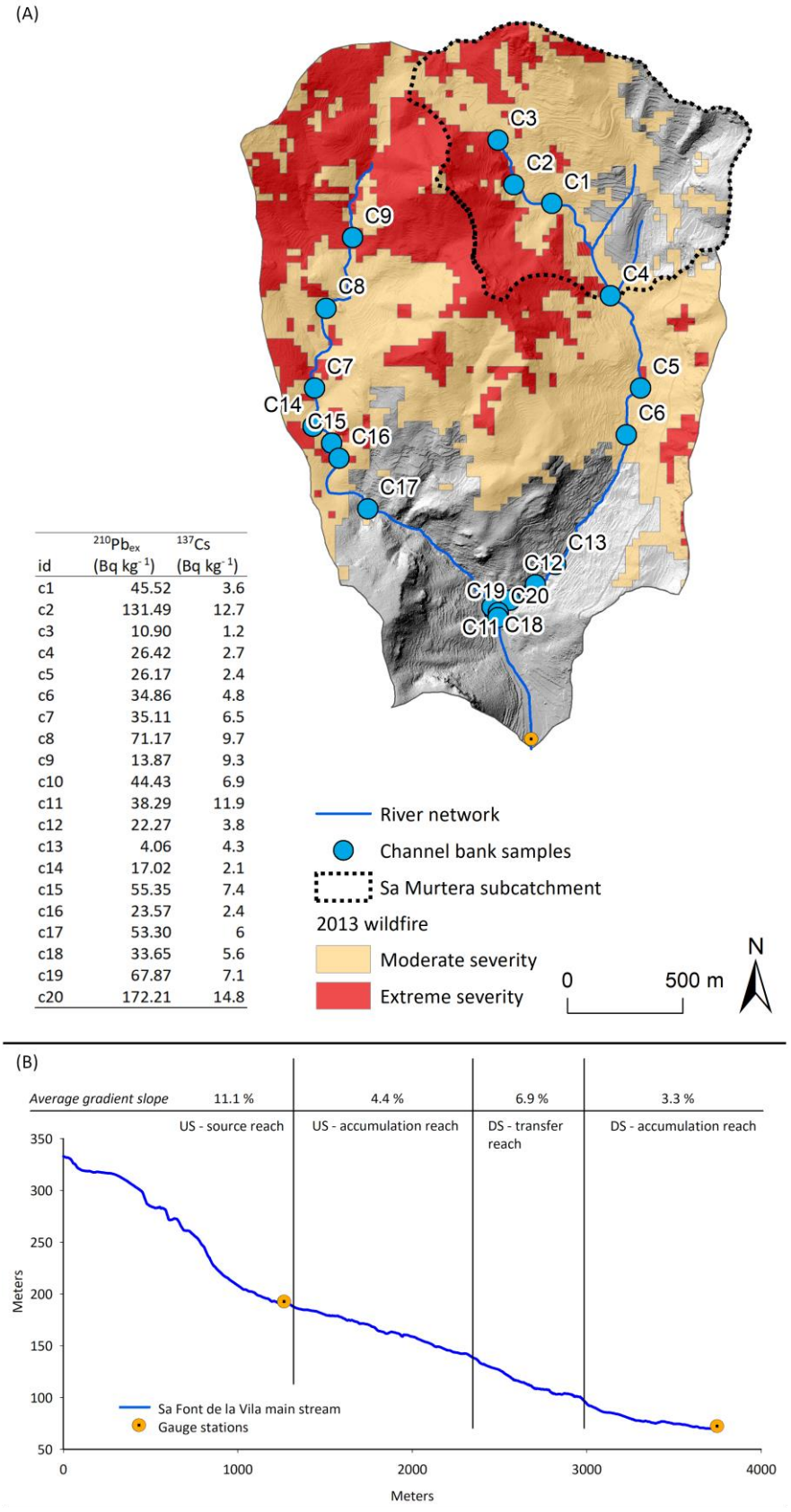

id	$^{210}Pb_{ex}$ (Bq kg^{-1})	^{137}Cs (Bq kg^{-1})
c1	45.52	3.6
c2	131.49	12.7
c3	10.90	1.2
c4	26.42	2.7
c5	26.17	2.4
c6	34.86	4.8
c7	35.11	6.5
c8	71.17	9.7
c9	13.87	9.3
c10	44.43	6.9
c11	38.29	11.9
c12	22.27	3.8
c13	4.06	4.3
c14	17.02	2.1
c15	55.35	7.4
c16	23.57	2.4
c17	53.30	6
c18	33.65	5.6
c19	67.87	7.1
c20	172.21	14.8

Supplementary figure 6.3. (A) Map of channel bank samples location within the Sa Font de la Vila River catchment. Inset table shows $^{210}Pb_{ex}$ and ^{137}Cs activities within the channel bank samples; (B) Longitudinal profile of the Sa Font de la Vila main stem (adapted from García-Comendador et al., 2017b). The intersection between DS- transfer reach and DS accumulation reach was approximately the C11 (before the B5 red point) and C20 (after B5 red point) sampling area.

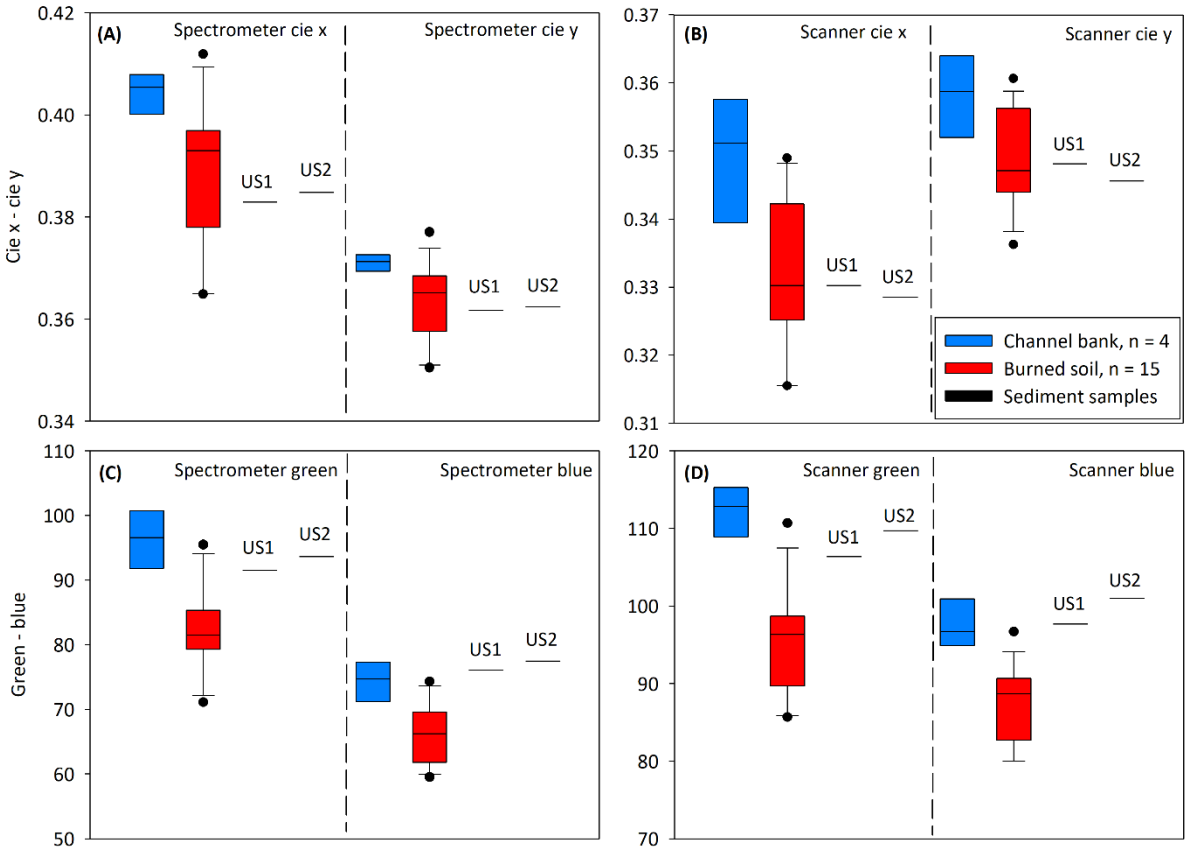

Supplementary figure 6.4. Box plots showing (A) spectrometer-based cie x and cie y parameters of channel bank, burned surface and suspended sediment samples US1 and US2 (see Table 5); (B) scanner-based cie x and cie y parameters of channel bank, burned surface, US1 and US2; (C) spectrometer-based green and blue parameters of channel bank, burned surface, US1 and US2; (C) scanner-based green and blue parameters of channel bank, burned surface, US1 and US2.

Supplementary table 6.1. Proportion of mixed sources for each sediment artificial mixture created in the laboratory.

Artificial mixtures		Source contribution %					
Mixtures	n sources	Channel Bank	Surface Unburned	Surface Burned	White Ash	Black Ash	SS
2 samples mixtures							
mix2-M1	2	100	0	0	0	0	0
mix2-M2	2	100	0	0	0	0	0
mix2-M3	2	0	80	20	0	0	0
mix2-M4	2	0	20	80	0	0	0
mix2-M5	2	0	50	50	0	0	0
mix2-M6	2	50	0	50	0	0	0
mix2-M7	2	50	0	50	0	0	0
mix2-M8	2	0	50	50	0	0	0
mix2-M9	2	0	60	0	40	0	0
mix2-M10	2	0	60	0	0	40	0
3 samples mixtures							
mix3-M1	3	40	0	60	0	0	0
mix3-M2	3	30	40	30	0	0	0
mix3-M3	3	0	20	80	0	0	0
mix3-M4	3	40	30	30	0	0	0
mix3-M5	3	100	0	0	0	0	0
mix3-M6	3	100	0	0	0	0	0
mix3-M7	3	20	0	80	0	0	0
mix3-M8	3	100	0	0	0	0	0
mix3-M9	3	0	60	0	40	0	0
mix3-M10	3	0	60	0	0	40	0
4 samples mixtures							
mix4-M1	4	50	25	25	0	0	0
mix4-M2	4	60	20	20	0	0	0
mix4-M3	4	40	20	40	0	0	0
mix4-M4	4	0	45	55	0	0	0
mix4-M5	4	70	0	30	0	0	0
mix4-M6	4	60	0	40	0	0	0
mix4-M7	4	33	0	67	0	0	0
mix4-M8	4	40	0	60	0	0	0
mix4-M9	4	0	30	40	30	0	0
mix4-M10	4	30	0	40	0	30	0

Supplementary table 6.2. Proportion of mixed sources for each ash-sediment artificial mixture created in the laboratory (GAmixt: mixtures made of grey ash and SS; BAmixt: mixtures made of black ash and SS).

Artificial mixtures		Source contribution %					
Mixtures	n sources	Channel Bank	Surface Unburned	Surface Burned	White Ash	Black Ash	SS
Grey ash - sediment samples							
GAmixt-M1	2	0	0	0	10	0	90
GAmixt-M2	2	0	0	0	20	0	80
GAmixt-M3	2	0	0	0	30	0	70
GAmixt-M4	2	0	0	0	40	0	60
GAmixt-M5	2	0	0	0	50	0	50
GAmixt-M6	2	0	0	0	60	0	40
GAmixt-M7	2	0	0	0	70	0	30
GAmixt-M8	2	0	0	0	80	0	20
GAmixt-M9	2	0	0	0	90	0	10
Black ash - sediment samples							
BAmixt-m1	2	0	0	0	0	10	90
BAmixt -m2	2	0	0	0	0	20	80
BAmixt -m3	2	0	0	0	0	30	70
BAmixt -m4	2	0	0	0	0	40	60
BAmixt -m5	2	0	0	0	0	50	50
BAmixt -m6	2	0	0	0	0	60	40
BAmixt -m7	2	0	0	0	0	70	30
BAmixt -m8	2	0	0	0	0	80	20
BAmixt -m9	2	0	0	0	0	90	10

Supplementary table 6.3. MixSIAR source apportionment, absolute error in comparison with real proportions and quantile 2.5% – 97.5% results distribution of the two sources artificial mixtures (CB: channel bank samples; BS: burned surface samples; US: unburned surface samples, GA: grey ash samples, BA: black ash samples).

Samples		Sources	Real proportions (%)	Estimated proportions and st. deviations(%)	Quantile distributión 2.5 % - 97.5 %	Error (%)	Average absolute error (%)
2 samples mixtures	mix2-M1	CB (C1)	80	83.1 ± 0	61.2 - 93	3.4	3.4
		CB (C10)	20	16.9 ± 0	7 - 38.8	3.4	
	mix2-M2	CB (C1)	20	43.2 ± 5.7	31.9 - 53.8	23.2	23.2
		CB (C10)	80	56.8 ± 5.7	46.2 - 68.1	23.2	
	mix2-M3	US (S36)	80	67.7 ± 6.3	56.1 - 80.6	12.3	12.3
		BS (S23)	20	32.3 ± 6.3	19.4 - 43.9	12.3	
	mix2-M4	US (S36)	20	20 ± 5.6	8.1 - 30.5	0.0	0.0
		BS (S23)	80	80 ± 5.6	69.5 - 91.9	0.0	
	mix2-M5	US (S33)	50	41.1 ± 3.1	34.9 - 47.1	8.9	8.9
		BS (S23)	50	58.9 ± 3.1	52.9 - 65.1	8.9	
	mix2-M6	CB (C20)	50	45.1 ± 10.2	24.5 - 65.5	4.9	4.9
		BS (S24)	50	54.9 ± 10.2	34.5 - 75.5	4.9	
	mix2-M7	CB (C19)	50	34.4 ± 7.4	19.9 - 48.6	15.6	15.6
		BS (S25)	50	65.6 ± 7.4	51.4 - 80.1	15.6	
	mix2-M8	US (S36)	50	41.4 ± 3.7	34.1 - 48.7	8.6	8.6
		BS (S26)	50	58.6 ± 3.7	51.3 - 65.9	8.6	
	mix2-M9	US (S37)	60	42.7 ± 2.6	37.9 - 48	17.3	17.3
		GA (A)	40	57.3 ± 2.6	52 - 62.1	17.3	
	mix2-M10	US (S38)	60	31.1 ± 13	28.6 - 33.7	28.9	28.9
		BA (A)	40	68.9 ± 13	66.3 - 71.4	28.9	

Supplementary table 6.4. MixSIAR source apportionment, absolute error in comparison with real proportions and quantile 2.5% – 97.5% results distribution of the three sources artificial mixtures (CB: channel bank samples; BS: burned surface samples; US: unburned surface samples, GA: grey ash samples, BA: black ash samples).

Samples		Sources	Real proportions (%)	Estimated proportions and st. deviations (%)	Quantile distributión 2.5 % - 97.5 %	Error (%)	Eaverage absolute error (%)
3 samples mixtures	mix3-M1	CB (C10)	20	9.4 ± 6.1	0.6 - 23.2	10.6	7.1
		CB (C14)	20	23.6 ± 5.4	12.2 - 32.8	3.6	
		BS (S1)	60	67 ± 3.1	61.1 - 73	7.0	
	mix3-M2	CB (C11)	30	24.2 ± 13.9	1.6 - 52.1	5.8	13.2
		BS (S2)	30	49.9 ± 3.3	43.1 - 55.9	19.9	
		US (S40)	40	26 ± 11.8	2.6 - 45.7	14.0	
	mix3-M3	BS (S3)	40	53.7 ± 4.8	44.3 - 63.2	13.7	11.2
		US (S39)	40	23.2 ± 2.4	18.4 - 27.9	16.8	
		BS (S31)	20	223.1 ± 4.3	14.7 - 31.3	3.1	
	mix3-M4	BS (S29)	30	44.7 ± 6.5	31.5 - 57.1	14.7	10.5
		US (S32)	32	23.2 ± 5.6	12.1 - 34.2	8.8	
		CB (C3)	40	32 ± 10.9	11.1 - 54	8.0	
	mix3-M5	CB (C20)	40	46.1 ± 9.7	26.9 - 65.3	6.1	5.1
		CB (C19)	30	22.4 ± 9	5.3 - 39.9	7.6	
		CB (C17)	30	31.6 ± 7.6	16.7 - 46.8	1.6	
	mix3-M6	CB (C4)	20	39.5 ± 14.6	10 - 68.3	19.5	13.0
		CB (C5)	40	37.6 ± 14.6	10.2 - 67.9	2.4	
		CB (C12)	40	22.8 ± 9.5	4.4 - 42	17.2	
	mix3-M7	BS (S5)	40	64 ± 0.5	62.4 - 65.4	24.0	16.0
		BS (S7)	40	31.3 ± 0.4	30.5 - 31.9	8.7	
		CB (C5)	20	4.7 ± 0.5	3.8 - 5.5	15.3	
	mix3-M8	CB (C10)	20	10.9 ± 6.7	0.7 - 25	9.1	12.2
		CB (C11)	20	10.9 ± 7	0.5 - 25.9	9.1	
		CB (C9)	60	78.3 ± 5.6	67.6 - 89.3	18.3	
	mix3-M9	US (S40)	30	16 ± 10.1	0.9 - 35.9	14.0	15.1
		US (S39)	30	21.3 ± 9.2	2 - 35.9	8.7	
		GA (A)	40	62.7 ± 2.3	58 - 66.8	22.7	
	mix3-M10	US (S32)	30	19.7 ± 7.4	1 - 30.1	10.3	19.9
		US (S33)	30	10.5 ± 7.7	0.4 - 30.2	19.5	
		BA (A)	40	69.8 ± 1.1	67.5 - 71.9	29.8	

Supplementary table 6.5. MixSIAR source apportionment, absolute error in comparison with real proportions and quantile 2.5% – 97.5% results distribution of the four sources artificial mixtures. (CB: channel bank samples; BS: burned surface samples; US: unburned surface samples, GA: grey ash samples, BA: black ash samples).

Samples		Sources	Real proportions (%)	Estimated proportions and st. deviations (%)	Quantile distributión 2.5 % - 97.5 %	Error (%)	Eaverage absolute error (%)
4 samples mixtures	mix4-M1	CB (C7)	25	0.3 ± 0.2	0.1 - 30.9	24.7	12.4
		CB (C11)	25	26.3 ± 2.5	21.3 - 30.9	1.3	
		BS (S31)	25	47.1 ± 0.8	45.6 - 48.6	22.1	
		US (S39)	25	26.4 ± 1.7	23.2 - 29.7	1.4	
	mix4-M2	CB (C7)	40	20.2 ± 0.4	19.4 - 20.9	19.8	11.8
		CB (C11)	20	16.3 ± 1.1	14.2 - 18.4	3.7	
		BS (S31)	20	40.7 ± 0.4	39.9 - 41.6	20.7	
		US (S39)	20	22.8 ± 0.8	21.2 - 24.4	2.8	
	mix4-M3	CB (C7)	20	12 ± 7.9	0.8 - 30.1	8.0	5.6
		CB (C11)	20	17.4 ± 8.8	2 - 35.4	2.6	
		BS (S31)	40	51.1 ± 4	42.8 - 58.8	11.1	
		US (S39)	20	19.5 ± 5.5	8.4 - 30.1	0.5	
	mix4-M4	BS (S2)	60	72.8 ± 2.6	67.5 - 76.8	12.8	10.1
		US (S32)	20	9.3 ± 5.7	0.5 - 19.2	10.7	
		US (S33)	20	5.6 ± 4.3	0.2 - 14.1	14.4	
		US (S40)	10	12.3 ± 7.4	0.8 - 25.1	2.3	
	mix4-M5	BS (S2)	30	46.4 ± 4.7	37 - 54.1	16.4	9.3
		CB (C17)	20	11.5 ± 7.2	0.6 - 24.2	8.5	
		CB (C9)	20	10 ± 6.2	0.5 - 20.9	10.0	
		CB (C20)	30	32.1 ± 9	14.2 - 47.2	2.1	
	mix4-M6	CB (C5)	20	8.1 ± 5.3	0.5 - 20.2	11.9	7.9
		CB (C9)	40	36.7 ± 9.2	18.4 - 54.7	3.3	
		BS (S5)	20	19.4 ± 7.9	3.3 - 34.9	0.6	
		BS (S31)	20	35.8 ± 6.1	24.1 - 48.2	15.8	
	mix4-M7	BS (S3)	60	42.2 ± 7.4	26.5 - 56.4	17.8	16.7
		BS (S7)	20	43.4 ± 9	25.6 - 61.5	23.4	
		CB (C3)	20	8 ± 4.8	0.5 - 17.8	12.0	
		CB (C4)	20	6.5 ± 4.1	0.3 - 15.2	13.5	
	mix4-M8	BS (S1)	20	30.6 ± 4.8	20.6 - 39.5	10.6	5.3
		BS (S29)	40	38.4 ± 7.1	24.2 - 52.4	1.6	
		CB (C12)	20	13.7 ± 6.5	1.7 - 25.8	6.3	
		CB (C14)	20	17.3 ± 8.7	1.6 - 34.1	2.7	
	mix4-M9	BS (S2)	20	13 ± 7.5	0.9 - 27.7	7.0	5.7
		BS (S26)	20	20.5 ± 10.9	10.9 - 40.3	0.5	
		US (S37)	30	25.6 ± 4.6	25.6 - 34.3	4.4	
		GA (A)	30	41 ± 3	35.2 - 47	11.0	
	mix4-M10	BS (S20)	30	2.5 ± 2.1	0.1 - 7.7	27.5	16.7
		BS (S23)	10	4.1 ± 5.8	0.1 - 13.8	5.9	
		BS (S24)	30	50.3 ± 7.2	38.2 - 58.9	20.3	
		BA (A)	30	43.1 ± 2.4	38.3 - 47.6	13.1	

Supplementary table 6.6. Summary statistics for all the spectrometer-based colour parameters measured for the three different source groups, channel bank (CB), burned surface (SB), unburned surface (SU) and K-wallis test results (95% confidence interval).

Summary statistics for each tracer and source type							Kwallis-Htest	
Tracers	Sources	Min.	Median	Mean	Max.	Sta.Dev.	p-value	chi-square
Cie x	CB	0.389	0.404	0.404	0.416	0.008	2.00E-05	24.50
	BS	0.364	0.394	0.393	0.416	0.013		
	US	0.397	0.409	0.412	0.436	0.014		
Cie y	CB	0.365	0.372	0.372	0.377	0.003	7.20E-07	31.30
	BS	0.350	0.367	0.366	0.380	0.007		
	US	0.373	0.378	0.378	0.384	0.004		
Cie Y	CB	11.250	14.880	15.190	24.600	3.149	1.91E-09	43.50
	BS	6.866	9.915	10.056	13.799	1.754		
	US	14.110	23.870	21.790	26.190	4.482		
Red	CB	119.900	137.200	137.600	169.100	12.074	1.82E-09	43.60
	BS	91.430	111.310	111.630	133.740	10.871		
	US	135.000	170.800	163.400	175.700	14.567		
Green	CB	86.010	99.870	100.010	127.160	9.729	1.95E-09	43.50
	BS	68.430	82.510	82.740	95.460	6.747		
	US	96.650	125.760	118.150	131.520	13.069		
Blue	CB	63.110	75.000	76.900	100.440	8.436	2.50E-07	33.50
	BS	55.120	66.120	66.200	75.840	4.799		
	US	66.820	91.010	87.060	101.660	11.891		
HRGB	CB	3.023	3.574	3.611	4.276	0.317	1.77E-04	19.90
	BS	2.613	3.013	3.091	4.443	0.406		
	US	2.401	3.497	3.545	7.877	0.741		
IRGB	CB	90.800	104.600	104.800	132.200	9.891	3.80E-09	2.10
	BS	72.660	86.410	86.860	100.780	6.912		
	US	101.400	129.000	122.900	135.300	12.634		
SRGB	CB	23.150	30.640	30.330	34.890	2.984	6.77E-09	40.90
	BS	13.310	23.070	22.720	31.030	4.633		
	US	31.100	37.610	38.180	46.470	1.695		
cie X	CB	12.310	16.090	16.480	26.320	3.339	4.07E-09	42.00
	BS	15.420	25.350	23.690	27.770	1.962		
	US	10.920	14.570	14.610	20.480	4.617		
cie Z	CB	6.235	8.738	9.163	9.986	2.081	1.29E-07	34.90
	BS	4.563	6.520	6.587	8.276	0.925		
	US	7.322	13.254	12.173	16.076	2.197		
cie L	CB	40.000	45.470	45.630	56.680	4.064	3.68E-09	42.20
	BS	31.500	37.690	37.760	43.940	3.157		
	US	44.390	55.950	53.480	58.220	5.123		
cie a*	CB	9.434	12.332	12.050	13.706	1.061	2.67E-07	33.40
	BS	4.471	9.568	9.634	12.625	1.567		

	US	11.710	12.700	13.850	18.080	2.164		
cie b*	CB	14.470	19.400	19.030	22.130	1.851	1.21E-08	39.70
	BS	7.788	14.814	14.335	20.613	3.245		
	US	19.750	23.610	24.080	29.200	2.435		
cie u*	CB	19.980	26.860	26.610	30.800	2.732	9.04E-09	40.30
	BS	11.690	19.890	19.760	27.130	4.011		
	US	27.300	31.470	32.920	42.030	4.730		
cie v*	CB	15.550	20.720	20.520	24.030	2.162	8.40E-09	40.50
	BS	7.926	15.393	14.863	21.259	3.451		
	US	20.990	26.760	26.720	30.950	3.060		
cie C	CB	17.270	23.040	22.520	26.030	2.107	1.49E-08	39.30
	BS	10.130	17.590	17.290	23.790	3.521		
	US	23.320	26.810	27.790	34.340	3.536		
cie H	CB	0.980	1.005	1.006	1.044	0.015	5.56E-05	22.30
	BS	0.878	0.979	0.972	1.048	0.046		
	US	1.010	1.039	1.050	1.104	0.033		
RI	CB	0.317	0.968	1.052	1.839	0.425	4.70E-09	41.70
	BS	1.163	2.485	2.811	6.361	1.362		
	US	0.269	0.324	0.488	1.086	0.299		
Munsell H	CB	16.240	16.860	16.840	17.480	0.308	1.75E-03	15.10
	BS	15.670	17.400	17.320	18.240	0.536		
	US	15.990	17.070	17.040	18.080	0.676		
Munsell V	CB	3.891	4.429	4.445	5.530	0.399	3.68E-09	42.20
	BS	3.057	3.664	3.672	4.279	0.310		
	US	4.323	5.459	5.216	5.681	0.503		
Munsell C	CB	2.917	3.882	3.803	4.382	0.356	1.39E-08	39.50
	BS	1.716	2.945	2.907	3.947	0.582		
	US	3.924	4.500	4.673	5.801	0.600		
DW nm	CB	558.900	589.800	589.700	590.500	0.376	3.41E-04	18.50
	BS	588.600	590.600	591.500	598.500	2.680		
	US	587.900	589.200	589.100	590.000	0.635		
Pe %	CB	29.710	36.010	36.000	41.260	3.264	4.77E-04	17.80
	BS	18.230	32.300	31.600	42.430	5.876		
	US	33.690	38.190	39.810	48.150	5.264		

p<0.05, significant

7. Combining sediment fingerprinting and hydro-sedimentary monitoring to assess the suspended sediment provenance in a mid-mountainous Mediterranean catchment

ABSTRACT

Soil erosion and sediment transport are controlled by complex factors promoting variable responses in catchment's erosion rates and sediment yields. To mitigate eventual negative effects derived from altered fluxes, integrated catchment management plans should assess the sediment cascade from upstream erosive processes, sediment mobilization through hillslopes and within the channel, up to downstream sediment yields. This study links hydro-sedimentary dynamics with sediment fingerprinting source ascription in a mid-mountainous Mediterranean catchment during five hydrological years (2013-2018). Soil colour parameters and fallout radionuclides were used as tracers within an integrated approach with (i) a Bayesian mixing model and (ii) an End Member Mixing Analysis in order to predict dominant suspended sediment sources. MixSIAR suggested that crops were the dominant sources. EMMA showed similar results, clustering all except one sediment samples close to the crop and channel bank signatures. In addition, a quantitative hysteresis index was calculated and floods were clustered in function of their hydro-sedimentary characteristics. Despite different patterns were associated to each of the four identified clusters (e.g. different sediment loads and maximum suspended sediment concentrations), correlation between sediment origin and hydro-sedimentary variables was not significant due to the little seasonal variation in the source contributions. Lithology, land uses (i.e. crop fields, scrubland and forest) and farm terraces might partially explain such low variability. Contrarily, monitored events showed variable hydro-sedimentary patterns, being a common feature in Mediterranean catchments.

Keywords: Sediment fingerprinting, End Member Mixing Analysis, hysteresis, hydro-sedimentary dynamics, sediment sources, Mediterranean catchments.

Reference

García-Comendador, J., Martínez-Carreras, N., Fortesa, J., Company, J. Borràs, A., & Estrany, J. 2021. Combining sediment fingerprinting and hydro-sedimentary monitoring to assess suspended sediment provenance in a mid-mountainous Mediterranean catchment. Journal of Environmental Management. **Under review**.

7.1. Introduction

Soil erosion and sediment transport are relevant natural processes affecting terrestrial geochemical cycles (López-Bermúdez, 1990; Ludwig and Probst, 1996). They are driven by complex factors (e.g. climate, vegetation status, topography, soil type and human disturbances; de Vente et al., 2011), which may promote divergent responses in erosion rates and sediment yields over time and space (Haddadchi et al., 2013) in catchment systems. Soil erosion and sediment transport downstream can also result in soil degradation and off-site effects such as the reduction of soil productivity or desertification processes in vulnerable areas (Bu et al., 2008; Estrany et al., 2010b; Walling, 2006), dam siltation (Navas et al., 2004), decrease in water quality (Horowitz et al., 2007) and contamination of aquatic ecosystems (Newcombe and Macdonald, 1991). Integrated catchment management plans to assess the sediment cascade between upstream erosive processes, sediment mobilization through hillslopes and within the channel, and downstream sediment yields are thus needed to mitigate as far as possible these negative effects. However, a widespread adoption of standard methodologies to evaluate sediment transport dynamics and identify major sediment production areas is still missing (Du and Walling, 2017; McCarney-Castle et al., 2017; Walling and Collins, 2008).

The sediment source fingerprinting technique has been widely used in the last decades for determining the provenance of fine sediment at catchment scale (Collins et al., 2020; Davis and Fox, 2009; Guzmán et al., 2013). It is applied at different temporal scales: from the flood event (García-Comendador et al., 2017) up to determining the origin of historically deposited sediments (e.g. over the last ca. 100 years; Pulley et al., 2018). Physical, biochemical and geochemical properties of soils and sediments are normally used as tracers (Walling, 2013), although other parameters as colour have increased its relevance in recent years (Martínez-Carreras et al., 2010a; Pulley et al., 2018; Tiecher et al., 2015). Their main advantage is the fast, cheap and non-destructive measurement methods (Barthod et al., 2015). Conversely, independently of the tracers used, fine sediment source ascription using the sediment fingerprinting technique is susceptible to several sources of uncertainties associated to sampling methodologies (Manjoro et al., 2017), spatial variability of source material properties (Du and Walling,

2017), alteration of the soil properties during conveyance within the river system (Poulenard et al., 2012) and sample analysis and un-mixing model statistics (Haddadchi et al., 2014; Nosrati et al., 2014; Palazón and Navas, 2017). Under this context, Bayesian mixing models have proven their worth in recent years (Abban et al., 2016; Stock et al., 2018). These models transform uncertainties into parameter probability distributions within a hierarchical framework (Cooper and Krueger, 2017), allowing a better representation of the natural variability in sources and sediment data due to their flexible likelihood-based structure (Blake et al., 2018; Cooper et al., 2015; Stock and Semmens, 2016). However, different tracer groups might result in ambiguous results due to its different discrimination potential (Collins et al., 2017). As a result, multi-tracer/multi-model ensemble predictions are needed as different mixing models and tracer groups respond differently to inherent sources of error (Uber et al., 2019).

Another widespread tool to assess sediment source variations in river catchments is the analysis of hysteretic patterns in the relationship between discharge (Q) and suspended sediment concentrations (SSC). These patterns are often non-linear at event scale and can inform about the distance of sediment sources according to the rotation direction, the shape of the loop and its area (Williams, 1989). Hysteretic counter-clockwise loops are associated to sediment mobilization from remote sites within a catchment, whilst clockwise are related to a closer provenance (Giménez et al., 2012; López-Tarazón and Estrany, 2017; Rovira and Batalla, 2006). More recently, several quantitative indexes have been developed to improve hysteretic classification (Aich et al., 2014; Langlois et al., 2005; Lawler et al., 2006; Lloyd et al., 2016). Particularly, Zuecco et al. (2016) developed a quantitative index based on the normalization of input data and the computation of definite integrals at fixed intervals of the independent variable. The index classifies the hysteretic loops, allowing a precise comparison at different spatio-temporal scales, detection of changes in patterns, as well as the possibility to correlate it with other hydro-meteorological variables such as rainfall, discharge or suspended sediment concentration. Despite this recent progress, the evaluation of hysteretic behaviour between Q and SSC has been scarcely integrated in catchment management strategies due to the difficult interpretation of sediment origin when hysteretic loop patterns are complex (Sherriff

et al., 2016) and the differential relationship between sediment and runoff depending on the scale of study (de Boer and Campbell, 1989).

The combination of sediment source fingerprinting and the analysis of river hydro-sedimentary dynamics (i.e. hysteretic patterns) has been proven useful to assess the factors controlling suspended sediment transport as a surrogate of erosion problems in river catchments, but both techniques have been rarely used together. Previous research includes the works of Evrard et al. (2011) –using bed sediment samples- and Navratil et al. (2012) –using suspended sediment samples- in the Southern French Alps and Vercruysse and Grabowski (2019) in the River Aire in UK. Their results showed the difficulty to elucidate clear patterns linking sediment fingerprinting and hydro-sedimentary behaviour in some catchments (Navratil et al., 2012). However, source variations in function of predominant hydro-meteorological drivers were found in others (Vercruysse and Grabowski, 2019). In the present study, the combined approach was applied in a mid-mountainous Mediterranean cathment. These environments are characterized by strong climate seasonality and are subject to high human pressure (García-Ruiz et al., 2013), resulting in complex and large spatiotemporal variations in sediment origin and hydro-sedimentary processes (Fortesa et al., 2020a; Merheb et al., 2016).

We advance the proposition that a better understanding of the links between hydro-sedimentary processes and sediment sources might shed some light on sediment transfer processes in Mediterranean catchments. For this purpose, we used a multi-tracer/multi-model approach (Uber et al., 2019). Several tracer groups (colour parameters and radionuclides) and two different sediment fingerprinting approaches were tested: (i) a Bayesian mixing model (MIxSIAR, Stock et al., 2018; Stock and Semmens, 2016) and (ii) an End Member Mixing Analysis (EMMA; Christophersen and Hooper, 1992). The latest method has been extensively used in hydrograph separation studies, but its use to assess the ability of potential suspended sediment sources to describe the composite signal of the sediment collected at the catchment outlet has been limited to the works of Munkundan et al. (2010) and Rose et al. (2018). EMMA is based on performing a principal component analysis (PCA) with the tracer data measured on the sediment samples collected at the outlet. The source data is then projected into the PCA distribution area to determine relations between sediment and

sources. Since EMMA does not solve a mass-balance approach but rather informs about dominant sources, results might eventually provide valuable information to validate the predictions of the Bayesian mixing model. Furthermore, the quantitative hysteresis index proposed by Zuecco et al. (2016) was calculated and floods were clustered in function of their hydro-sedimentary characteristics as to identify patterns.

To sum up, the main objectives of this study are to (i) analyse and link sediment sources contributions with the hydro-sedimentary response of the catchment, (ii) determine the main factors regulating sediment source contributions, and (iii) evaluate the potential of hydro-sedimentary monitoring combined with sediment fingerprinting as a sediment management tool in Mediterranean catchments.

7.2. Study area

The Es Fangar catchment (3.4 km^2; Figures 7.1A and B) is located at the north-east side of the Tramuntana mountain range in Mallorca (Spain). Altitudes range between 72 and 404 m.a.s.l., with an average slope of 26%. The lithology is composed by massive calcareous and dolomite materials from the lower Jurassic, and by dolomite and marls formations from the Triassic (Rhaetian) in the upper parts. Jurassic and Cretaceous marl-limestone's fill the valley bottoms (Figure 7.1C). The catchment was intensively affected by agricultural activities in the past. Only at the upper parts, the stream network is natural, whilst in the valley bottom the main channel was diverted and constricted by dry stone walls for a better agricultural land exploitation. Check-dams and farm terraces were built to control torrential floods and avoid soil erosion (Figure 7.1C and D). In addition, subsurface tile drains were built in crop lands to promote drainage, avoiding soil saturation during the wet season. The 16% of the catchment is occupied by soil and water conservation structures, resulting in 32.4 km of dry stone walls. Nowadays, land use occupation is forest (47%), rainfed herbaceous crops (36%) and scrubland (17%). Since the 1950s, as a consequence of the economic transition from the primary to the tertiary sector, the agricultural area has been reduced in a ca.

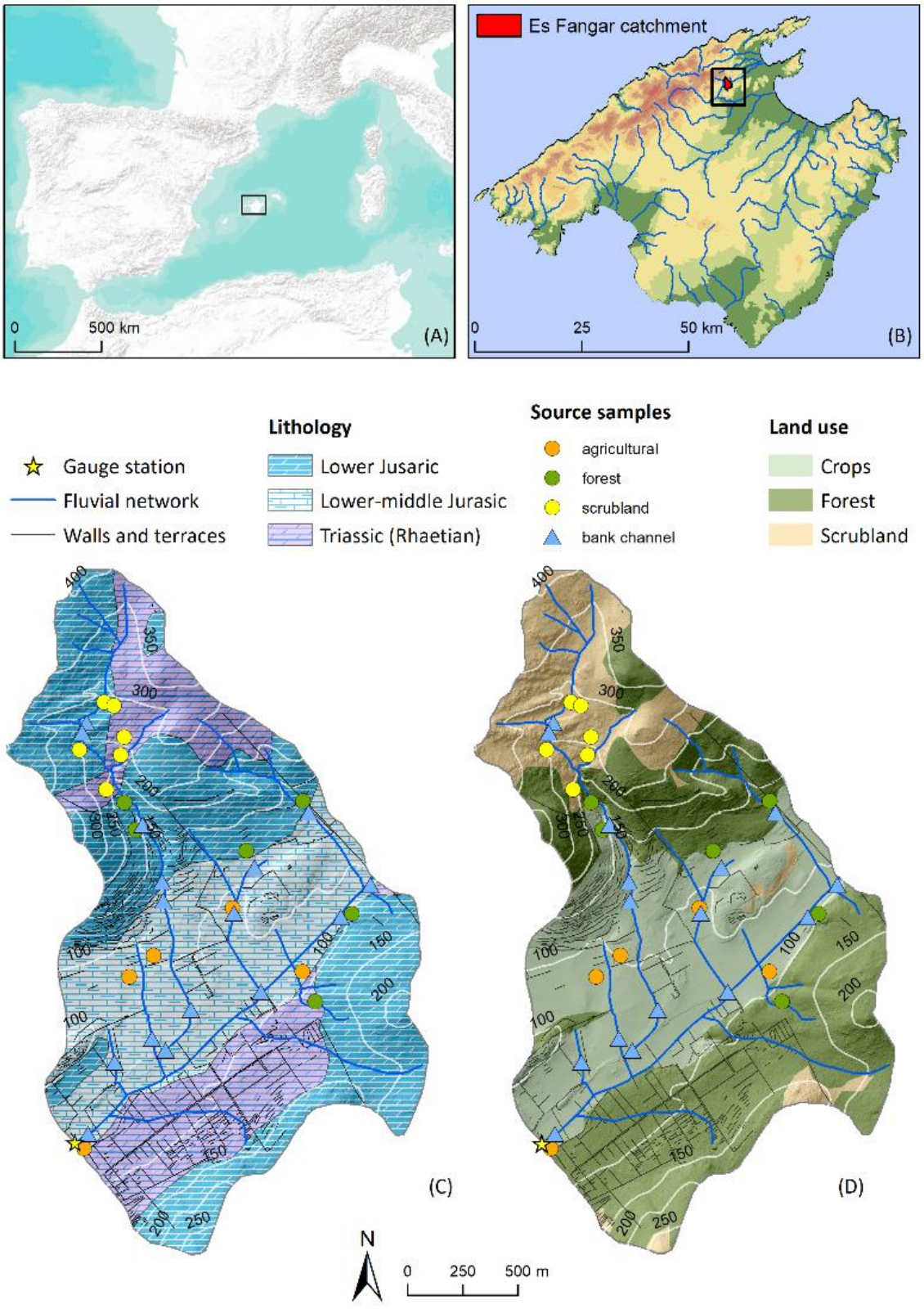

Figure 7.1. (A) Map showing the location of Mallorca in the Western Mediterranean Sea. (B) Location of the Es Fangar catchment within the island of Mallorca. Drainage network, terraced areas, soil and sediment sampling points over (C) lithology and (D) land use maps.

17%. Afforestation processes have occurred in abandoned agricultural fields being currently covered by forests, mostly located in the middle part of the catchment.

According to the Emberger classification, the climate is Mediterranean temperate sub-humid (Guijarro, 1986). The mean annual rainfall is 926 mm yr^{-1} (1964-2017, Biniatró AEMET station, 1.1 km west from the study area), with a 23% coefficient of variation. The average annual temperature is 15.7°C. The hydrological regime is categorized as intermittent flashy (49% of days with no flow; Fortesa et al., 2020a). The annual runoff coefficient ranged from 2.9% to 14.2% (average of 10.4%), whereas the quickflow contribution ranged from 9.9% to 45% (average of 33%), illustrating a huge inter-annual variability in the rainfall-runoff relationship (Fortesa et al., 2020b). During 2012-2017, the 80% of the sediment load was exported during autumn and winter, with an annual average sediment yield of 5.38 t km^{-2} y^{-1} (Fortesa et al., 2020a).

7.3. Material and methods

7.3.1. Source and sediment sampling

In August 2015, a stratified sampling was carried out in the Es Fangar catchment. Three surface sources groups (i.e. forest, crop and scrubland soils) and a subsurface source (channel banks) were identified (Figure 7.1C and D) after GIS analysis and field observations. Thirty-two source samples were collected: 16 in channel banks, 6 in crop fields, 5 in forests and 5 in scrubland. All samples were collected in areas with visual evidence of erosion. Surface soil samples (0-2 cm depth) were composed by four subsamples collected inside a ca. 3 m radius circular area, whereas each channel bank sample was composed by three subsamples collected in a 10 m transect. Thirteen integrated suspended sediment samples (Figure 7.2) were collected between 2013 and 2018 at the catchment outlet using two parallel time integrated sediment traps (Phillips et al., 2000) installed within the channel bed at the Es Fangar hydrometric station (see figure. 7.1C-D and further details on sub-section 7.3.5).

7.3.2. Laboratory analysis

The soil and sediment samples were oven dried at 40°C, disaggregated using a pestle and a mortar, and sieved to < 63 µm to reduce the differences in particle size distribution between sediment and source samples (Walling, 2013). The specific surface area (SSA) and the particle size distribution (PSD) were measured in all samples using a Malvern Mastersizer 3000 (Malvern instruments, Ltd.) at the Luxembourg Institute of Science and Technology (LIST, Luxembourg). The Shapiro-Wilk ($p < 0.05$) normality test and the Wilkoxon signed-rank test were applied to determine the PSDs similarity between each source (soil samples) and target samples (suspended sediment samples). ^{137}Cs and $^{210}Pb_{ex}$ (FRNs) activity (Bq kg^{-1}) were measured by gamma spectrometry using a high-purity coaxial intrinsic germanium (HPGe) detector at the Environmental Radioactivity Laboratory of the University of the Balearic Islands (Spain).

Total C and total N were measured by high-temperature combustion (TruSpec CHNS, LECO) at LIST. Biochemical processes can alter sediment colour within channel by organic matter addition, increasing the errors in source discrimination. Despite this, organic matter removal may not be suitable in some cases because it can reduce the discriminative potential of colour tracers (e.g. Pulley et al., 2018). Accordingly, it was decided avoiding the organic matter removal in this study.

Finally, diffuse reflectance measurements were taken with an ASD FieldSpect-II spectroradiometer in a dark room at 1 nm steps over the 400-2500 nm range. The soil and sediment samples were placed in transparent PVC round petri dishes (4.7 cm diameter; Pall Corporation) and smoothed with a spatula to homogenize the surface roughness and minimize micro shadow effects. The spectrometer optical lens was mounted in a tripod perpendicularly over a flat surface, at 10 cm of the reference standard panel of known reflectivity (spectralon). The samples and the spectralon were illuminated in an angle of 30º using a 50-w quartz halogen lamp placed at c.a. 30 cm of distance. Following the International Commission on Illumination (CIE, 1931), the CIE xyY colour coefficients (i.e. cie x, cie y and cie yy) were computed from the spectra reflectance measurements as well as the RGB colour values (i.e. Red, Green and Blue).

7.3.3. Tracer accuracy

The linear additivity of the tracers is an essential requirement to validate their use in sediment origin analysis (Lees, 1997). In order to assess it, we created 30 artificial mixtures of 2, 3, and 4 samples of different sources (i.e. forest, crop, scrubland soil and channel banks). Mixtures were made mixing different sample proportions (Supplementary table 7.1) using a precision balance and a PVC spatula. Mixtures were introduced in sterile tubes and mixed during 10 minutes before measurements. Due to economic and time constrains, the ^{137}Cs and $^{210}Pb_{ex}$ measurements were not performed on the artificial mixtures. A mass balance approach was used to predict the tracer values measured on the mixtures (i.e. tracer values in the mixtures are equal to the sum of the tracer values measured on the samples artificially mixed multiplied by their known contribution to the mixture). Predicted values were compared with those measured to determine the individual accuracy and linear additivity behaviour of each colour tracer. In order to compare colour values measured with different scales, we calculated the normalized root mean square error (nRMSE) by dividing the RMSE by the mean of the measured data. We expressed the nRMSE as a percentage. The Kruskal-Wallis H test (95% confidence interval) was used to check the capability of the tracers to differentiate the different sediment sources. A Principal Component Analysis (PCA) with a varimax rotation to simplify the factor structure was performed with SPSS (IBM Corp., Armonk, N.Y., USA) for analysing the tracer set variance. Furthermore, a Discriminant Function Analysis (DFA) was performed using SPSS with a leave-one-out cross-validation (considering selected tracers as independent variables) to determine the discriminating potential of each tracer group. Finally, we performed a range test for each individual sediment sample to exclude potential non-conservative tracers.

7.3.4. Suspended sediment fingerprinting

Two different approaches were used to estimate suspended sediment sources: (i) the Bayesian mixing model MixSIAR (Stock et al., 2018, Stock and Semmens, 2016) implemented as an R package (hereafter referred to as MixSIAR); and (ii) the End Member Mixing Analysis (EMMA; Christophersen and Hooper, 1992; Hooper, 2003). A result comparison on source predictions was carried out. For the un-mixing of artificial

mixtures, we used only colour tracers, the MixSIAR model, and every sample that composed the mixture was considered as a source.

The fundamental mixing equation of the MixSIAR mixing model is:

$$b_i = \sum_{j=i}^{m} w_j \cdot a_{i,j}$$

where *bi* is the tracer property *i* (*i* = 1 to n) measured in a suspended sediment sample, $a_{i,j}$ is the value of the tracer property *i* in each source sample *j* (*j* = 1 to m), w_j is the unknown relative contribution of each source *j* to the suspended sediment sample.

MixSIAR accounts for variability in the source and mixture tracer data and has the ability to incorporate covariance data to explain variability in the mixture proportions via fixed and random effects (Stock et al., 2018; Stock and Semmens, 2016). In this study, MixSIAR was formulated by using sediment type as a factor and an uninformative prior. The Markov Chain Monte Carlo parameters were set as very long: chain length = 1,000,000, burn = 500,000, thin = 500, chains = 3. Convergence of the models was evaluated using the Gelman-Rubin diagnostic.

In EMMA, the different source categories were considered as end members with a fixed composition, conservative and distinguishable between them, while sediment samples were a mixture of these end members. We apply the diagnostic tools described by Hooper (2003). First, a bi-variable scatter plots were performed to identify if the tracers behave linearly conservative in the sediment samples. The tracers suggested linearly conservative mixing when had at least a linear trend of "r^2> 0.5, p-value <0.01" with at least one of the other tracers used (James and Roulet, 2006). Then, a PCA was performed on the standardized values of the correlation matrix. The values were standardized by subtracting the average concentration of each tracer and dividing it by its standard deviation. Residuals were defined subtracting the original value from its orthogonal projection.

7.3.5. Catchment hydro-sedimentary response, hysteresis loops analysis and cluster classification of selected floods

A gauging station was installed in 2012 in Es Fangar Creek to continuously monitor water and suspended sediment fluxes (Figure 7.1C-D). The station was equipped with a *Campbell CS451* pressure probe and an *OBS-3+* turbidimeter with a double measurement range of 0-1,000/1,000-4,000 NTU**.** *Campbell CR200X* logger stored 15-minutes average values of water stage and turbidity (based on 1-minute readings). In addition, in October 2014 a tipping bucket pluviometer was installed at 500 m.a.s.l. and located ca. 2.5 km away from the Es Fangar gauging station. The rain gauge was installed 1 m above the ground and connected to a HOBO Pendant G Data Logger - UA-004-64 recording rainfall at 0.2 mm resolution.

The following variables were estimated for each of the 34 events occurred between 2013 and 2018: total rainfall (Rtot), rainfall maximum intensity in 30 minutes (Imax-30), total water volume (Wvol), maximum discharge peak (Qmax), average discharge (Qmean), total suspended sediment load (SSload), maximum suspended sediment concentration (SSCmax), mean suspended sediment concentration (SSCmean), one-day (AR_{1d}), three days (AR_{3d}) and seven days (AR_{7d}) antecedent rainfall. The seasonal distribution of the flood events (i.e. percentage of events per season) was as follows: winter 58.8% (n = 20), spring 8.8% (n = 3), summer 5.9% (n = 2) and autumn 26.5% (n = 9). The hydro-sedimentary response showed large variability (Figure 7.2).

Discharge (Q; $m^3\ s^{-1}$) and suspended sediment concentration (SSC; mg l^{-1}) hysteretic analysis was performed using the *h* index developed by Zuecco et al. (2016). It provides information on the direction and magnitude of hysteresis loops. The *h* index computes definitive integrals on the rising and falling curve of the independent variable (Q) defining eight hysteresis classes.

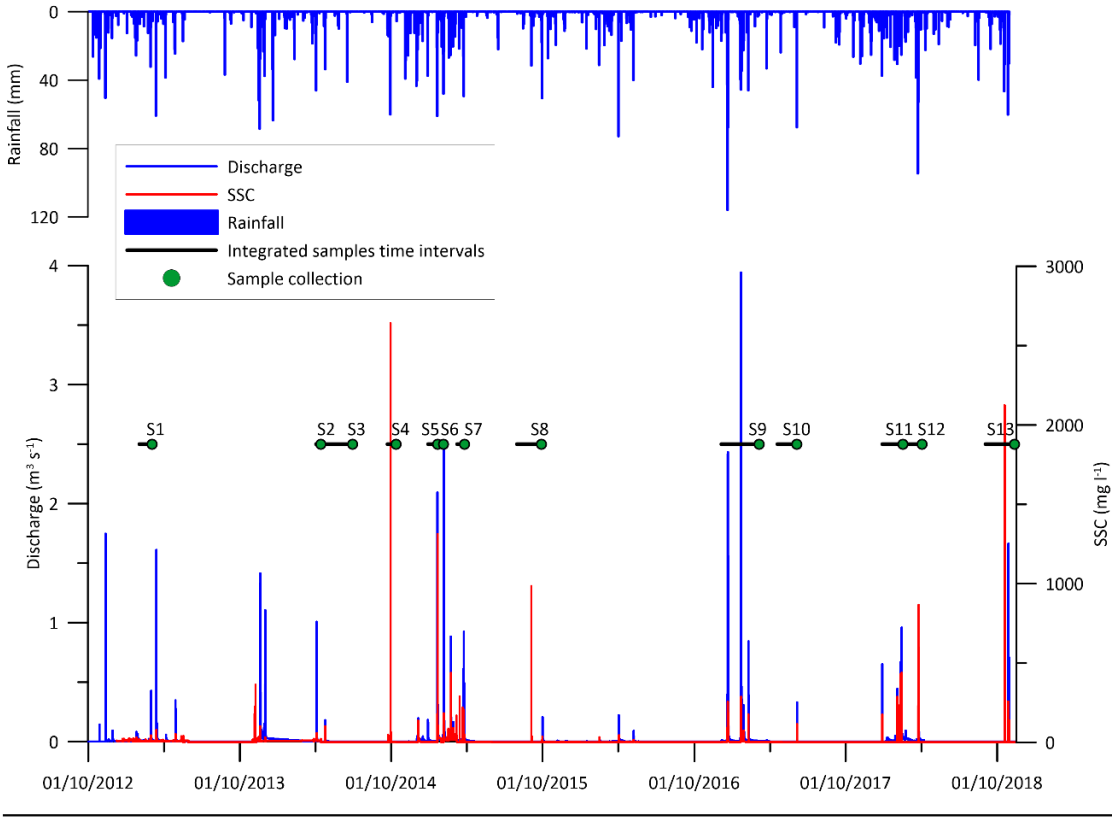

Integrated samples	Floods	Flood date	Season	Rtot (mm)	Imax-30 (mm h^{-1})	Wvol (m^3)	Qmax (m^3 s^{-1})	Qmean (m^3 s^{-1})	SSload (t)	SSCmax (mg l^{-1})	SSCmean (mg l^{-1})	AR$_{1d}$ (mm)	AR$_{3d}$ (mm)	AR$_{7d}$ (mm)	h index
S1	Flood 1	28/02/2013	winter	32.12	16.40	15051.78	0.43	0.11	0.26	44.26	16.48	4.60	11.00	34.90	0.13
S2	Flood 2	04/04/2014	spring	49.84	6.57	26057.61	1.01	0.16	0.71	58.99	30.20	3.76	8.00	47.60	-0.25
S3	Flood 3	25/04/2014	spring	28.59	14.38	2805.85	0.18	0.05	0.11	102.08	21.44	5.00	13.40	13.60	-0.12
S4	Flood 4	29/09/2014	summer	48.60	56.40	14144.94	2.36	0.28	11.56	2641.32	163.95	11.80	13.90	52.10	0.16
S5	Flood 5	20/01/2015	winter	81.00	12.40	58026.13	2.09	0.32	19.66	1312.74	118.84	9.00	9.00	9.00	-0.34
S6	Flood 6	04/02/2015	winter	73.60	5.20	131272.66	2.45	0.56	8.14	182.90	36.70	22.60	35.80	62.60	0.58
S7	Flood 7	14/03/2015	winter	21.60	10.40	5844.96	0.35	0.10	0.60	288.30	53.05	0.00	0.00	0.00	0.48
	Flood 8	22/03/2015	winter	6.20	11.20	1101.97	0.06	0.03	0.04	218.64	58.19	1.40	11.60	13.40	-0.28
	Flood 9	24/03/2015	winter	75.60	7.20	46567.79	0.92	0.30	2.18	80.20	205.10	0.00	7.60	19.20	0.32
S8	Flood 10	04/09/2015	summer	32.40	19.60	2270.14	0.78	0.28	0.96	984.00	416.60	0.60	2.60	2.60	0.21
S9	Flood 11	19/12/2016	autumn	46.40	7.60	14717.87	0.39	0.15	0.49	94.40	30.31	2.00	16.60	16.80	-0.17
	Flood 12	20/12/2016	autumn	115.80	21.60	78771.22	2.43	1.31	9.77	255.34	103.94	24.40	49.20	64.00	-0.04
	Flood 13	21/12/2016	autumn	61.40	9.60	58829.91	1.57	0.44	4.29	190.02	82.45	116.00	164.60	179.80	0.16
	Flood 14	20/01/2017	winter	14.60	7.60	19674.63	1.69	0.49	1.92	262.26	48.82	28.40	37.20	43.60	0.19
	Flood 15	21/01/2017	winter	44.20	7.60	96839.56	3.94	1.38	12.27	286.37	115.84	35.40	50.60	58.40	0.14
	Flood 16	22/01/2017	winter	5.20	4.00	14084.15	1.47	0.65	0.82	170.67	44.76	35.40	50.60	58.40	0.19
	Flood 17	22/01/2017	winter	12.20	4.00	9720.88	0.46	0.29	0.19	25.98	18.47	44.40	96.20	105.00	-0.08
	Flood 18	23/01/2017	winter	29.00	4.80	16057.95	0.36	0.17	0.32	30.06	28.20	20.20	87.20	128.00	0.09
	Flood 19	25/01/2017	winter	5.40	4.80	980.45	0.23	0.09	0.11	41.39	15.97	0.00	51.60	149.60	-0.40
	Flood 20	27/01/2017	winter	23.00	11.60	18911.66	0.31	0.10	0.26	74.54	17.98	0.00	5.60	120.80	0.21
S10	Flood 21	05/06/2017	spring	67.60	21.60	1502.98	0.33	0.07	0.07	114.50	46.07	2.60	2.60	11.60	0.27
S11	Flood 22	02/02/2018	winter	53.20	6.80	19984.62	0.44	0.20	2.63	286.69	107.79	22.60	22.60	51.60	0.41
	Flood 23	06/02/2018	winter	20.00	2.20	6892.34	0.23	0.15	0.95	232.24	123.26	13.40	17.20	70.40	0.27
	Flood 24	09/02/2018	winter	18.40	2.40	6334.20	0.18	0.11	0.62	203.48	75.67	17.60	38.20	53.20	0.28
	Flood 25	10/02/2018	winter	10.60	2.60	17347.30	0.67	0.23	3.02	430.33	105.05	13.80	26.00	51.00	0.23
	Flood 26	12/02/2018	winter	25.00	3.00	19417.08	0.96	0.38	4.48	438.03	196.77	7.20	20.20	63.60	0.34
S12	Flood 27	24/03/2018	winter	98.60	9.00	3232.63	0.39	0.26	1.78	817.32	486.81	84.00	84.00	133.00	0.46
	Flood 28	25/03/2018	winter	142.60	9.00	8678.38	0.63	0.42	5.81	865.69	653.89	129.60	133.00	182.00	-0.15
S13	Flood 29	18/10/2018	autumn	30.80	13.40	14839.81	1.95	0.75	15.74	2124.75	547.52	30.80	88.80	99.00	-0.01
	Flood 30	19/10/2018	autumn	30.80	13.40	33044.38	2.08	0.94	9.20	523.22	172.74	4.40	88.60	99.00	-0.41
	Flood 31	27/10/2018	autumn	17.20	2.80	17256.68	1.62	1.07	2.92	257.20	159.11	23.00	73.20	73.40	-0.16
	Flood 32	28/10/2018	autumn	39.90	3.60	19845.00	1.66	0.79	2.81	243.38	103.34	17.60	79.80	80.00	0.06
	Flood 33	28/10/2018	autumn	41.50	3.60	3609.47	0.59	0.33	0.29	149.35	60.95	33.40	103.20	103.40	0.39
	Flood 34	29/10/2018	autumn	45.10	3.60	14366.41	0.71	0.33	0.54	140.31	19.90	13.40	106.80	107.00	-0.03

Figure 7.2. Hydrograph, suspended sediment concentration (SSC) and hyetograph at the Es Fangar creek during the study period. Time intervals encompassed by every integrated suspended sediment samples (S1 to S13) were represented as black lines and sample collection data as green dots plotted in relation with the x axis (time). The inset table contains the main hydro-sedimentary variables for the 34 flood events: total rainfall (Rtot), rainfall maximum intensity in 30 minutes (Imax-30), total water volume (Wvol), maximum peak discharge (Qmax), mean discharge (Qmean), total suspended sediment load (SSload), maximum suspended sediment concentration peak (SSCmax), mean suspended sediment concentration (SSC mean) one-day (AR1d), three days (AR3d) and seven days (AR3d) antecedent rainfall and Zuecco et al. (2016) h index values (h index).

Classes I and V encompass clockwise hysteresis; IV and VIII, anticlockwise; II and VI, eight shaped or more complex when the main direction is clockwise; whilst III and VII anticlockwise complex hysteresis. It was computed using a MATLAB script (MathWorks, Inc., Natick, MA, USA; Zuecco et al. 2016).

In addition to the *h* class, information on the sum of integrals (*h*) was showed in the data. The *h* index value also gives information about the hysteresis size indicating a higher curve amplitude the farther it is from 0. Clockwise loops have an $h>0$ value, $h<0$ for anticlockwise and $h\approx0$ for symmetrical complex loops or no hysteresis. The dominant direction for the eight shaped and complex loops were defined by the relative size of the loops. To link main sediment sources and hysteretic loops in suspended sediment samples that encompass more than one flood, those that have contributed more to de sediment load will prevail.

A clustering of the 34 selected flood events was carried out based on their main hydro-sedimentary variables and the *h* index value. For this purpose, a hierarchical cluster analysis was performed with SPSS (IBM Corp., Armonk, N.Y., USA) using the Ward's method, based on the Euclidean squared distance (Murtagh and Legendre, 2014; Ward, 1963). Data was standardized using Z scores. A one-way ANOVA analysis was used to validate the significant difference between groups. To avoid inconsistent grouping, a Pearson correlation analysis was previously performed. Only the variables that showed significant $p<0.01$ correlations with another variable of different type, understanding rainfall (Rtot, Imax-30, AR_{1d}, AR_{3d}, AR_{3d}), water (Wvol, Qmax, Qmean, *h* index), and sediment (SSload, SSCmax, SSC mean, *h* index) as the three different variable types, were included in the clustering.

7.4. Results

7.4.1. Tracer accuracy and selection

After the mass balance approach performed over the artificial mixtures to check the linear additivity of colour tracers, all individual colour tracers showed very low nRMSE's between measured and predicted values (Figure 7.3). Cie x and cie y showed the lowest difference in values. The error with cie yy (brightness) was slightly larger,

with an nRMSE of 4%. Average nRMSEs ranged between 1.3% and 1.9 for Red, Green and Blue. No trend was observed between the number of sources in the mixtures (i.e. 2, 3 and 4) and the average nRMSE values (1.3% for 2 source mixtures, 2% for 3 source mixtures and 1.7% for the 4 source mixtures; Figure 7.3).

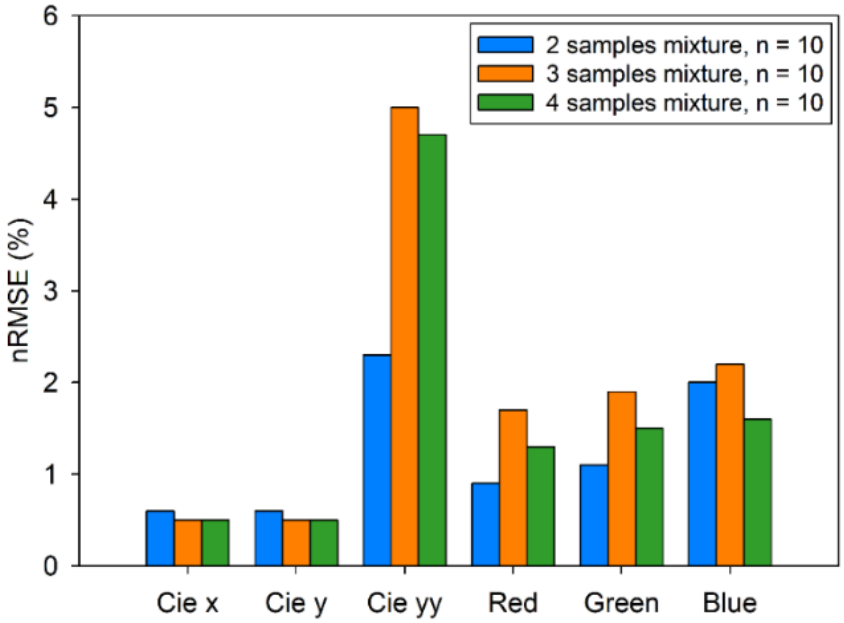

Figure 7.3. Normalized root mean square error (nRMSE) between estimated and measured colour tracers for the artificial mixtures created with 2 (blue), 3 (orange) and 4 (green) different source samples.

Cie x did not pass the Kruskal-Wallis H test ($p > 0.05$) (Figure 7.4 and Supplementary table 7.2) and was discarded. Cie y, Cie yy, Red, Green and Blue did not show significant differences between the forest soil and scrubland soil sources. In addition, results showed no significant differences in FRNs concentrations between channel bank vs crop soil, and forest soil vs scrubland soil. As a result, the number of sources was reduced to two by merging the channel bank and crop soil samples (hereafter referred to as channel-crop), and the forest soil and scrubland samples (hereafter referred to as forest-scrub). In a second stage, a source origin analysis was performed only using colour parameters to allow the discrimination between surface (i.e. crop soil and forest-scrubland) and subsurface (i.e. channel banks) source types.

After Cie x was discarded, most of the target suspended sediment values were within crop and channel bank ranges for all tracers except $^{210}Pb_{ex}$ (Figure 7.4). The $^{210}Pb_{ex}$ activities measured in the SS samples fall within the range of forest and scrubland soil.

PCA showed how two components explained 83.2% of the variance (i.e. PC1 67.2% and PC2 15.9%; see Figure 7.5). All tracers except $^{210}Pb_{ex}$ were associated with the Component 1, corroborating the unilaterality of $^{210}Pb_{ex}$. As a result, $^{210}Pb_{ex}$ was discarded.

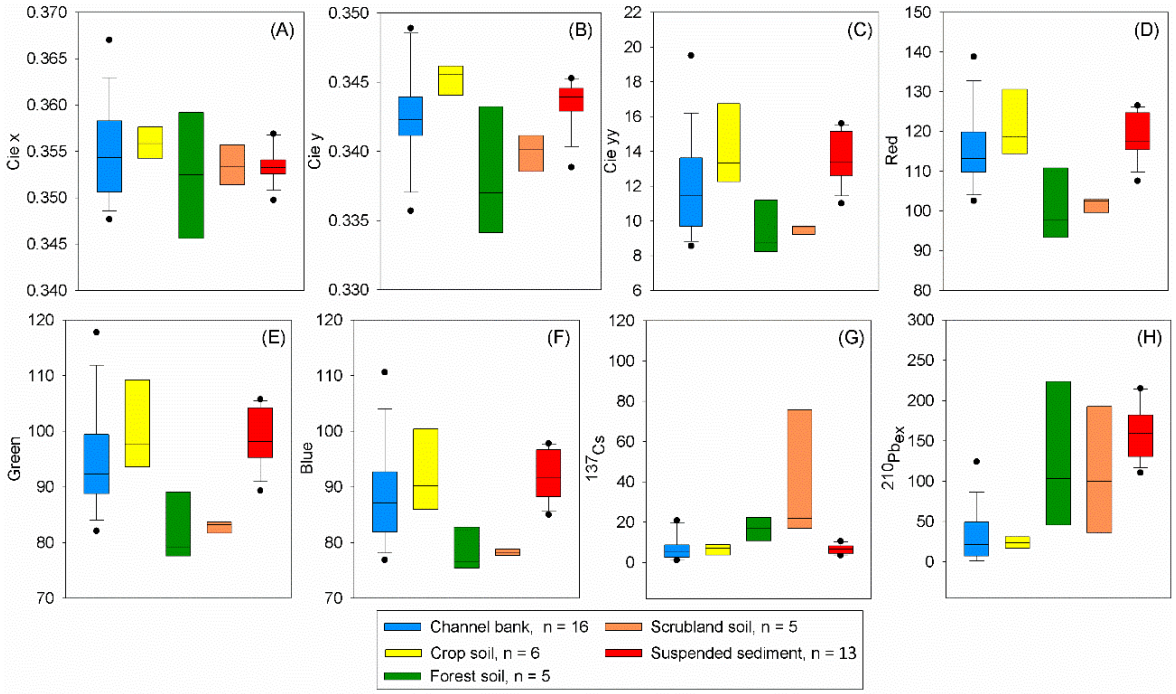

Figure 7.4. Boxplots showing the distribution of the (A) Cie x, (b) Cie y, (C) Cie yy, (D) Red, (E) Green, (F) Blue, (G) ^{137}Cs and (H) $^{210}Pbex$ values measured in the suspended sediment and source samples.

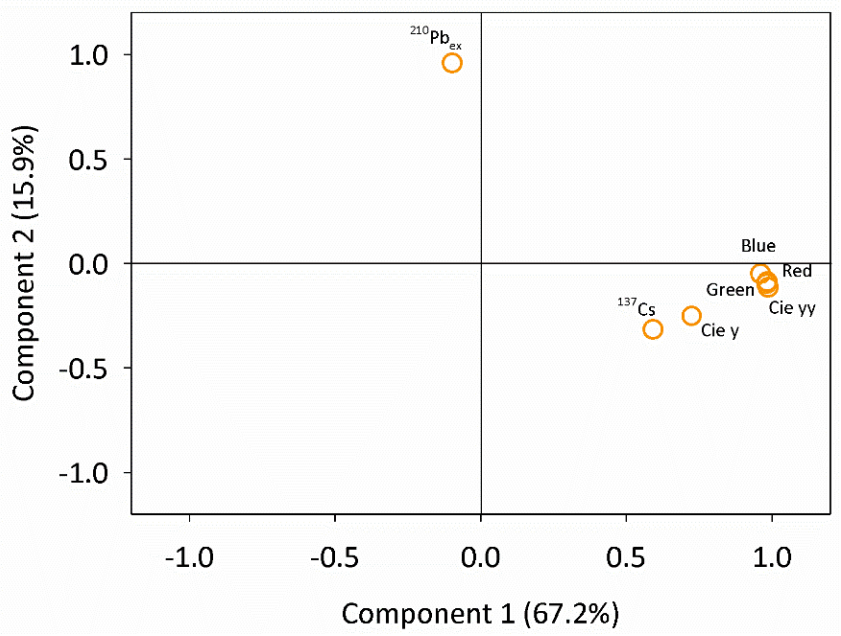

Figure 7.5. Principal Component Analysis with Varimax rotation performed with suspended sediment values of Cie y, Cie yy, Red, Green, Blue, ^{137}Cs and $^{210}Pb_{ex}$

Results of the DFA (Table 7.1) showed that 78.1% and 59.4% of the samples were correctly classified when considering two and three sources, respectively. The Blue colour parameter did not pass the tolerance threshold and was discarded.

Table 7.1. Individual efficiency of colour parameters to discriminate 2 (channel-crop and forest-scrubland) and 3 sources (i.e. channel bank, crop and forest-scrubland).

DFA	Correctly classified (%)	
Individual tracers	Two sources	Three sources
Cie y	78.1	62.5
Cie yy	75.0	56.3
Red	78.1	59.4
Green	75.0	59.4
Blue	68.8	53.1
^{137}Cs	75.0	-
Independent variables together		
Correct classification (%)	78.1	59.4
Tracers removed (*failing tolerance test. 0.001)*	Blue	Blue

7.4.2. Unmixing of the artificial mixtures

MixSIAR showed an absolute un-mixing error of 11.4 ± 10% in the 10 artificial mixtures of 2 samples, being able to identifying the dominant sample in 8 mixtures (Supplementary table 7.3). For three samples mixtures (Supplementary table 7.4) the absolute error increased up to 16.7 ± 8.1%, coinciding the main sample in 6 of the 10 mixtures. Finally, in the 4 samples mixtures (Supplementary table 7.5), the error was 13 ± 3.9%, being the sample contributing to a larger extent identified in 6 out of the 10 samples. It should be noted that when forest and scrubland samples were grouped and considered as a unique source (see section 7.4.1), the dominant samples in the mixtures were correctly identified in 23 samples instead of 20.

7.4.3. Particle size, C and N content

Source and suspended sediment particle size distribution (Supplementary figure 7.1) did not show a normal distribution (Shapiro-Wilk, $p < 0.05$). When applying the Wilkoxon signed-rank test, samples in all sources were statistically similar to

suspended sediment samples (p=0.44 for channel bank, p = 0.34 for crop soil, p = 0.63 for forest soil and p= 0.59 for scrubland soil).

Total C values of the different sample groups are showed in Figure 7.6. Suspended sediment showed the highest average total C values. However, all samples except one –collected during the event 2 and with a total C content of 16.5%– felt within the sources range values. Total N values are also shown in Figure 7.6, with the lowest values measured in the channel bank and crop soils, and the largest in the forest.

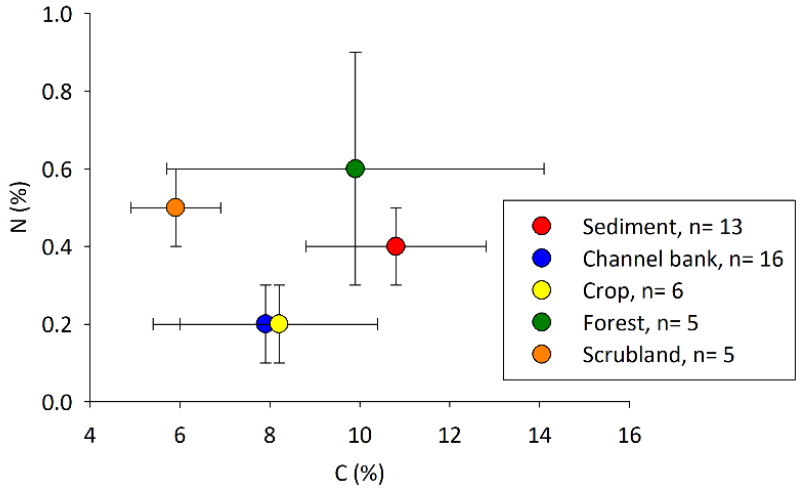

Figure 7.6. Total carbon and total nitrogen content in source and sediment samples.

7.4.4. Sediment fingerprinting

Considering two sources and using the complete set of tracers that passed the tracer accuracy and selection tests (i.e. Cie y, Cie yy, Red, Green, and ^{137}Cs; section 7.4.1), MixSIAR determined that channel-crop was the main sediment source in 12 of the 13 sediment samples, with results ranging between 74% ± 16.7 and 90.8% ± 7.1 (Figure 7.7 and Supplementary table 7.6). Source ascription for Sample 2 was 54.2% ± 21.5 for forest-scrub and 45.8% ± 21.5 for channel-crop.

The source analysis with MixSIAR using only colour parameters (three sources) showed a predominance of crop source contributions in 12 of the 13 integrated samples, ranging from 38.5% ± 18.7 to 69.9% ± 18.1 (Figure 7.8 and Supplementary table 7.7). Nevertheless, forest-scrubland was the main source for Sample 2 with 55.2% ± 17.

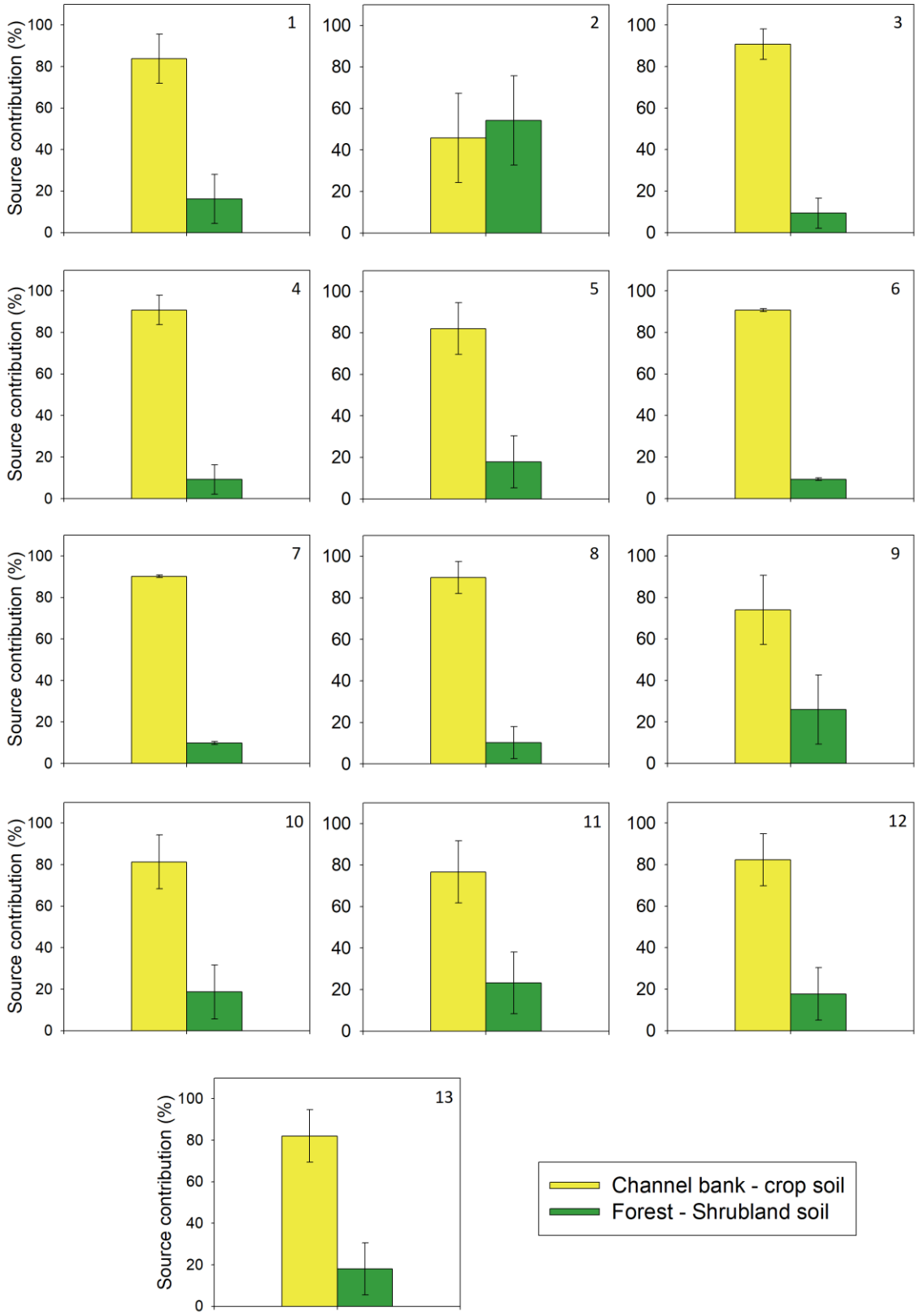

Figure 7.7. MixSIAR source apportionment predictions using colour parameters and ^{137}Cs considering two potential sources: channel-crop and forest-scrubland. The numbers in the upper right of each plot indicate the sample number (Figure 7.2).

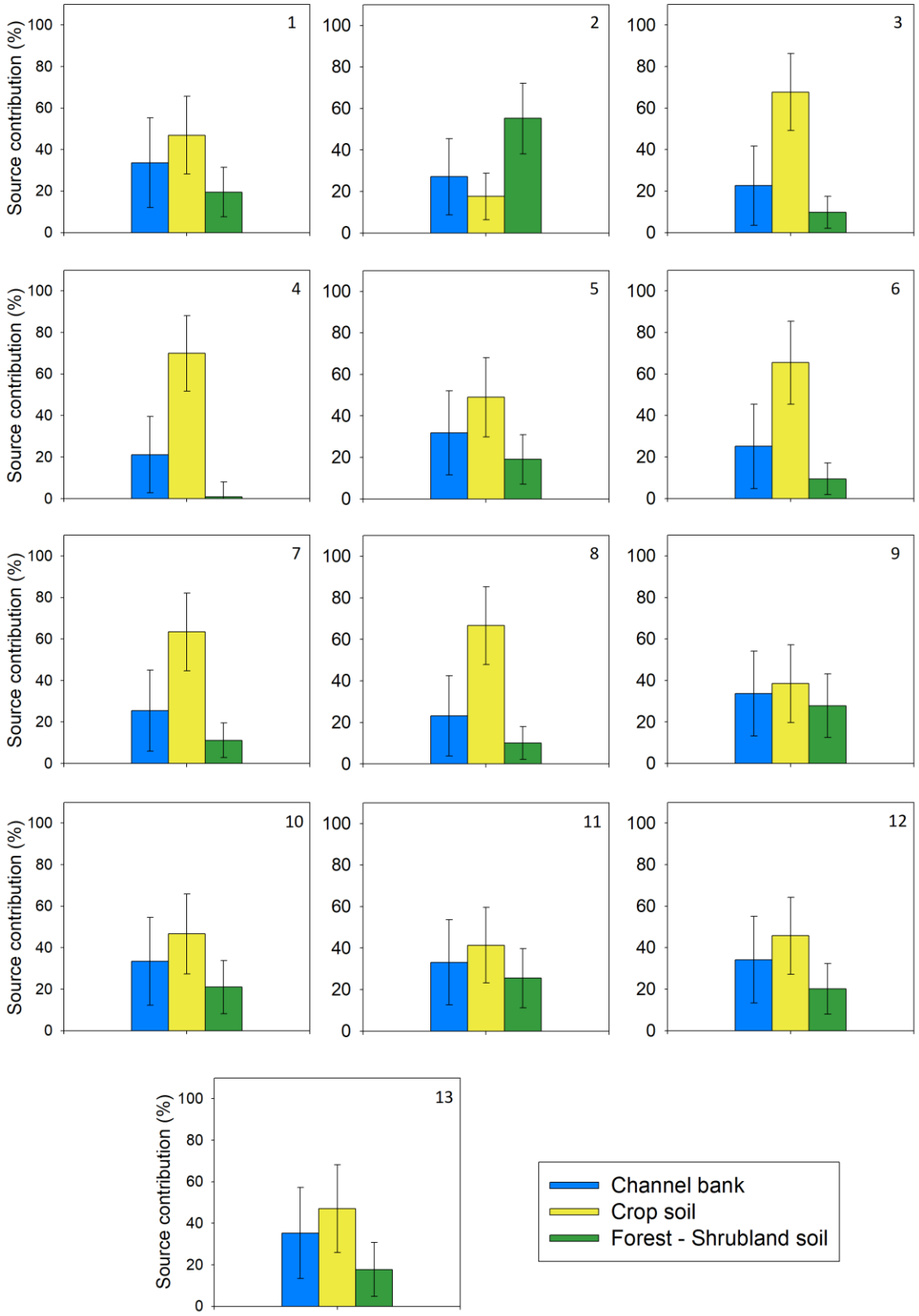

Figure 7.8. MixSIAR source apportionment predictions using colour parameters and considering three potential sources: channel bank, crops soil and forest-scrubland. The numbers in the upper right of each plot indicate the sample number (Figure 7.2).

EMMA results are displayed in Figure 7.9. Correlations with at least one other tracer (i.e. $r^2 > 0.5$, p value < 0.01) were found on all tracers except for ^{137}Cs, which was kept in the analysis for consistency with the mixing model results. Suspended sediment samples always plotted within the mixing area defined by the endmembers. When considering two sources (Figure 7.9A), sediment samples tracer data was most similar to channel-crop source data. Only Sample 2 plotted at a major distance from the rest, suggesting a contribution from the forest-scrubland source. When considering three sources (Figure 7.10B), all sediment samples clustered in the crop soil and channel bank domains but Sample 2, which plots in an intermediate position between channel bank and forest-scrubland.

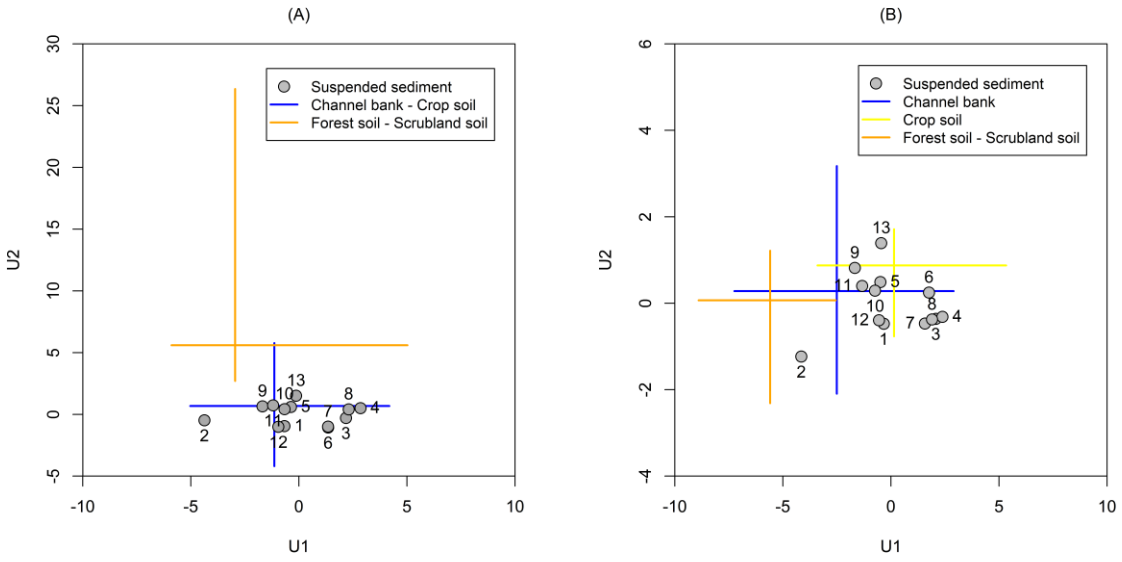

Figure 7.9. U1–U2 mixing diagram of suspended sediment tracer data (grey dots). Number identify sediment samples (Figure 7.2). Sources tracer data were grouped into two (Figure A) and three (B) end-members and the interquartile ranges of each end-member were projected into the mixing space (U space).

7.4.5. Hydro-sedimentary response

The 34 floods were classified into six hysteresis types (Table 7.2; Figure 7.2). Eighteen floods showed clockwise patterns (Class I; h index between 0.04 to 0.58). Floods 1, 13 and 18 drew eight-shaped clockwise loops (Class II; h index between 0.09 to 0.16). Seven floods were classified as eight-shaped anticlockwise loops (Class III; h index between 0.01 to 0.41). Four floods showed counter-clockwise patterns (Class IV; h index between 0.12 to 0.42), Flood 32 as eight-shaped clockwise direction complex loop (Class VI; h index 0.06) and Flood 2 as eight-shaped anticlockwise (Class VIII; h

index 0.25). The percentage distribution was 52.9% clockwise, 11.8% counter-clockwise, 11.8% clockwise eight shaped and 23.5% eight-shaped anticlockwise. No clear patterns were found between hysteretic classes and dominant suspended sediment sources (as predicted by MixSIAR; Table 7.2) due to the low temporal variability in the tracing results.

The variables Rtot, Imax-30, Wvol, Qmax, Qmean, SSload, SSCmax, SSCmean and AR_{1d} were selected to perform a clustering analysis (Supplementary table 7.8). Floods were clustered into four groups, which passed an ANOVA test (all variables, $p<0.05$; Table 7.2). Cluster 1 is the largest cluster and encloses 26 floods. Cluster 2 enclose 2 floods and clusters 3 and 4, 3 floods both. Cluster 1 showed in general lower average values for all variables in comparison with the other 3 clusters (Table 7.3). Cluster 2 showed more heterogeneous average values with the highest in Rtot, SSmean, and AR_{1d} and the lowest in Wvol and Qmax. Cluster 3 performed the highest values in Wvol, Qmax and Qmean and the lowest in SSCmean. Finally, Cluster 4 floods obtained the highest average values in Imax-30, SSload and SSCmax. Despite all floods classified in clusters 2 and 3 occurred during the wet season, no clear seasonal pattern emerged. Moreover, floods assigned to different hysteresis class were randomly distributed between clusters, and the large dispersion in loop's amplitude values did not allow a robust classification.

Finally, Supplementary table 7.9 (considering two sources) and Supplementary table 7.10 (considering three sources) show the SSload in tons ascribed to each source in relation with its percentage using MixSIAR. In the integrated suspended sediment samples that encompass more than one flood event (marked in grey), the total SSload was the sum of all events.

Table 7.2. Summary of the seasonal distribution, predicted main sediment sources (MixSIAR model), hysteretic class (h class) of each flood, and average and standard deviation h index values per flood cluster.

Clusters	Integrated samples	ID	Season	Main source (2 sources)	Main source (3 sources)	*h* class	Average *h* index absolute values and standard deviation
Cluster 1	S1	Flood 1	winter	channel-crop	Crop	II	0.24 ± 0.12
	S2	Flood 2	spring	Forest-scrub	Forest-scrub	VII	
	S3	Flood 3	spring	channel-crop	Crop	IV	
	S7	Flood 7	winter	channel-crop	Crop	I	
	S7	Flood 8	winter			IV	
	S7	Flood 9	winter			I	
	S8	Flood 10	summer	channel-crop	Crop	I	
	S9	Flood 11	autumn	channel-crop	Crop	III	
	S9	Flood 13	autumn			II	
	S9	Flood 14	winter			I	
	S9	Flood 16	winter			I	
	S9	Flood 17	winter			III	
	S9	Flood 18	winter			II	
	S9	Flood 19	winter			IV	
	S9	Flood 20	winter			I	
	S10	Flood 21	spring	channel-crop	Crop	I	
	S11	Flood 22	winter	channel-crop	Crop	I	
	S11	Flood 23	winter			I	
	S11	Flood 24	winter			I	
	S11	Flood 25	winter			I	
	S11	Flood 26	winter			I	
	S13	Flood 30	autumn	channel-crop	Crop	III	
	S13	Flood 31	autumn			III	
	S13	Flood 32	autumn			VI	
	S13	Flood 33	autumn			I	
	S13	Flood 34	autumn			III	
Cluster 2	S12	Flood 27	winter	channel-crop	Crop	I	0.31 ± 0.22
		Flood 28	winter			III	
Cluster 3	S6	Flood 6	winter	channel-crop	Crop	I	0.25 ± 0.29
	S9	Flood 12	autumn	channel-crop	Crop	I	
	S9	Flood 15	winter			I	
Cluster 4	S4	Flood 4	summer	channel-crop	Crop	I	0.17 ± 0.17
	S5	Flood 5	winter	channel-crop	Crop	IV	
	S13	Flood 29	autumn	channel-crop	Crop	III	

Table 7.3. Average and standard deviation values per cluster of the following variables: total rainfall (Rtot), rainfall maximum intensity in 30 minutes (Imax-30), total water volume (Wvol), maximum discharge peak (Qmax), average discharge (Qmean), total suspended sediment load (SSload), maximum suspended sediment concentration (SSCmax), mean suspended sediment concentration (SSCmean) and one-day antecedent rainfall (AR1d).

	Rtot (mm)	Imax-30 (mm h^{-1})	Wvol (m^3)	Qmax (m^3 s^{-1})	Qmean (m^3 s^{-1})	SSload (t)	SSCmax (mg l^{-1})	SSCmean (mg l^{-1})	AR_{1d} (mm)
Cluster 1	31.3 ± 19.4	7.9 ± 5.5	15856.8 ± 13753.9	0.8 ± 0.6	0.3 ± 0.3	1.6 ± 2	218.6 ± 203.9	86.9 ± 88.4	16.6 ± 23.9
Cluster 2	120.6 ± 31.1	9 ± 0	5955.5 ± 3850.7	0.5 ± 0.2	0.3 ± 0.1	3.8 ± 2.8	841.5 ± 34.2	570.4 ± 118.1	106.8 ± 32.2
Cluster 3	77.9 ± 36	11.5 ± 5.9	102294.9 ± 2662.4	2.9 ± 0.9	1.1 ± 0.5	10.1 ± 2.1	241.5 ± 53.1	85.5 ± 42.7	27.5 ± 6.9
Cluster 4	53.5 ± 25.5	27.4 ± 25.1	29003.6 ± 25136.6	2.1 ± 0.2	0.4 ± 0.3	15.7 ± 4.1	2026.3 ± 669.7	276.8 ± 235.6	17.2 ± 11.9

7.5. Discussion

7.5.1. Comparison between sediment fingerprinting approaches

The selection of tracers was problematic in this study. In a first attempt, sources were grouped into two sources based in the Kruskall-Wallis results (i.e. channel-crop and forest-scrub) to accommodate a larger number of tracers. This was decided because the reduction of tracers in the model may increase the probability that inappropriate or non-conservative tracers influence the results (e.g. Martínez-Carreras et al., 2010b). In this respect, MixSIAR optimally handles redundancy, so it works well with collinear tracers (i.e. colour parameters) (Blake et al., 2018). FRNs did not discriminate between channel bank and crop soils. This could be attributed to ploughing in the upper soil layers, resulting in the migration of the FRNs to deeper subsurface layers (Owens et al., 1996). On the contrary, sources less exposed to human perturbations (i.e. forest and scrubland) showed ^{137}Cs activities that allowed its differentiation from the other source categories. Similarly, colour tracers did not discriminate between forest and scrub sources (Supplementary table 7.2) and, even if channel bank and crop colour values differ (Section 7.4.1), their spectral signatures were relatively close (Figure 7.4). This may explain the errors in predicting the main sediment source in some the artificial mixtures.

In the Es Fangar catchment, MixSIAR identified channel bank-crops soil as the dominant sources in the two source analysis and crop soils in the three source analysis. Comparing MixSIAR results between the two and three sources analysis (suspended sediment samples), the mean absolute error in the source apportion percentage

prediction was relatively low (1.2%) (i.e. summing crop and channel bank % results for the three source analysis), which denotes robustness in the model using the selected tracers set in both analyses. EMMA showed similar results. When plotting the sources tracer values in the U1–U2 mixing diagram of suspended sediment tracers it was possible to observe that sediment samples clustered close to the crop and channel bank signatures (Figure 7.9). Hence, results showed that the approach is able to determine the main sediment sources. Furthermore, coinciding with the MixSIAR results, sample 2 plotted closer to the forest and channel bank signatures.

Lithology, land use, and the presence of agricultural terraces and stone walls might partially explain the low intra-annual sediment sources variability in the Es Fangar catchment. Scrubland and forest areas are located in the catchment headwaters, where the steepest slopes are covered with trees and scrubs, protecting the soil and reducing runoff and suspended sediment generation. Moreover, carbonate materials and karst features dominate in the upper part, characterized by low sediment availability and transmission losses (Calvo-Cases et al., 2003; Li et al., 2019), whereas crop fields dominate in the valley bottom, which are completely exposed during certain periods of the year (normally during the dry season). Furthermore, a large part of channel banks is constrained by dry stone walls, limiting channel bank sediment contributions. Therefore, the transference of significant amounts of sediment from the channel banks to the fluvial network only occurs when a dry stone wall collapses, what has been rarely observed in the catchment. Results highlight the relevant role of human structures in suspended sediment contributions. Check dams and terraces (Figures 7.1C and D) are located traditionally in erosion vulnerable areas laminating runoff, retaining soil particles and avoiding rill formation (Tarolli et al., 2014). And subsurface drains in flat areas reduce the soil saturation during wet season (Estrany et al., 2010).

7.5.2. Catchment hydro-sedimentary response and suspended sediment sources

The analysed flood events depicted a wide intra- and inter- annual variability. The 85.3% of events occurred during the wet season and the 14.7% during dry season,

evidencing the strong seasonal distribution and coinciding with other studies performed in the same catchment (e.g. Fortesa et al., 2020a). In addition, the wide range of hydro-sedimentary responses ensured a good representativeness of the driving forces controlling sediment transport. Floods were grouped into four clusters with differentiate characteristic. However, despite the fact that different patterns were associated to each cluster (e.g. distinct sediment loads and maximum suspended sediment concentrations), it was not possible to establish a correlation between sediment origin and hydro-sedimentary variables.

Sediment tracing results showed that in the Es Fangar catchment sediment mainly originates from crop fields all along the year (Sections 7.4.4 and 7.5.1). As in other Mediterranean catchments, no seasonal patterns or dominant source changes in function of flood patterns were observed (e.g. Uber et al., 2019). Sample 2, the only one showing fingerprints associated to forest-scrub surface soils, could not be related to any specific hydro-sedimentary variable either (Figure 7.1). Flood 2 was associated to a class VII hysteresis loop (eight-shaped anticlockwise loop; Table 7.3), suggesting contributions from various sediment sources and/or the activation of different erosion processes (Williams, 1989). However, samples 11 and 12 also drew eight-shaped anticlockwise loops and, on the contrary, were related to dominant sediment contribution from crop soils.

Fortesa et al. (2020a) investigated hysteretic patterns for 45 floods occurred between 2012 and 2017 in the same study area. Their results showed that 73% of the hysteresis responded to clockwise and linear loops. Accordingly, clockwise hysteresis loops predominated during the events analysed in this study (52.9%), what might indeed suggest that in-channel sediment remobilisation and erosion from near stream areas (i.e. crops) are the dominant processes in the catchment. Anti-clockwise or complex hysteresis patterns (47.1%) are sometimes related with the activation of different sediment sources (De Girolamo et al., 2015). However, this is not shown by the sediment fingerprinting results, suggesting that the analysis of hysteretic patterns might not always accurately inform about sediment origin (Smith and Dragovich, 2009; Vercruysse et al., 2017).

Few studies combined suspended sediment source assessment with the analysis of hydro-sedimentary response at catchments scale. Navratil et al. (2012) combined river/rainfall monitoring and sediment fingerprinting using FRNs and geochemistry in a 905 km^2 catchment located in the French Alps. The authors showed that ca. 80% of the catchment sediment load occurred during widespread and long rainfall events with low intensities, while shorter storms were associated to higher discharge peaks and suspended sediment concentrations. However, mobilized sediment did not usually reach the catchment outlet. A high intra- and inter-flood variability was detected during 7 floods monitored between 2007 and 2009, but sediment sources remained relatively stable (black marls up to 70%). Vercruysse and Grabowski (2019) found relevant source variations in function of hydro-meteorological drivers in an 879 km^2 catchment in UK. Street dust and limestone grassland sources (located in the steepest area of the catchment) were strongly correlated with suspended sediment concentration, showing similar correlations with discharge and 1-day antecedent rainfall. Millstone and coals grassland sources, located in urban or gentle slope areas, were mainly correlated to antecedent hydro-meteorological conditions (e.g. precipitation and discharge). Finally, riverbank material was poorly correlated to hydro-meteorological factors, attributing their maximum contribution when a sudden collapse of a channel bank occurred.

The area of the Es Fangar catchment is smaller, in comparison with the catchments studied in Navratil et al. (2012) and Vercruysse and Grabowski (2019). Hence, flow paths from the source areas to the catchment outlet are shorter, changing the hydro-sedimentary processes. Even if the association between sediment fingerprinting and monitoring does not always outcomes clear patterns (e.g. this study and Navratil et al. 2012), the approach helps to better understand sediment delivery processes. This is because sediment tracing results alone do not provide information on the total mass of sediment transported for each event, whereas the events exporting the largest sediment loads will influence the most the source predictions of the total load.

7.5.3. Catchment management implications

Integrated catchment management plans need to assimilate information about the complex relationships between hydrological systems, land-uses, ecosystems human health and political aspects under an interdisciplinary optic to successfully address complex problematics (Bakker, 2012; Bunch et al., 2014; Wang et al., 2016). By definition, an integrated approach needs to account for as much information as possible. We argue that to reach a comprehensive understanding about erosion and sediment transport dynamics in catchments it is essential to develop effectively integrated management approaches (McCarney-Castle et al., 2017; Owens et al., 2005). The methodology that we proposed is based on the combination of continuous monitoring of water and sediment with sediment fingerprinting (Evrard et al., 2020; Navratil et al., 2012; Vercruysse and Grabowski, 2019). The first informs about the spatiotemporal variation in suspended sediment concentrations and loads, what is relevant in highly variable environments such as the Mediterranean basin. Sampling during high and low flows throughout the year and extending the sampling over time is needed (Vercruysse and Grabowski, 2019) if we are to predict climate change impacts and account for nonstationary in management plans. Furthermore, this information is required to develop sediment transport models that integrate information on sediment origin (Owens et al., 2005; Perks et al., 2017; Vercruysse et al., 2019).

No consensus has been reached about the best mixing model to predict suspended sediment sources. In this study we have tested two different prediction models, MixSIAR Bayesian mixing model and the EMMA approach. Results showed that the EMMA approach, which is not based on a mixing model but on a PCA of the tracer values measured in the sediment samples, can provide valuable insights to determine dominant sources. We argue that precise estimation of suspended sediment sources might not be always needed when implementing sediment management plans, but rather an accurate identification of dominant sources. In this respect, EMMA (which has been extensively use in hydrograph separation (Hooper, 2003) but rarely used in sediment fingerprinting) offers advantages as based on simplified procedures compared with sediment fingerprinting (e.g. MixSIAR), what could result in a larger implementation.

This study also pays attention to the fact that it is always desirable to include different types of tracers (e.g. geochemistry, FRNs, mineral magnetics) in order to create composite signatures to reduce possible discrimination uncertainties (Walling, 2013). However, the use of a heterogeneous set of tracers often entails significant costs of time and money. Therefore, the use of low cost tracers as colour seems to be a good option in this type of studies not only because of its low cost, but also because they are easy and quick to measure (Pulley and Rowntree, 2016), being their effectiveness comparable to more classical tracers (e.g. Martínez-Carreras et al., 2010a; Pulley et al., 2018).

The results obtained indicate that in the Es Fangar, sediment sources are relatively stable through the year. This is due, in part, to human modification associated to traditional soil conservation practices (Calsamiglia et al., 2018; Estrany et al., 2010a). It has also been previously recognised that the interactions between hydro-meteorological factors and human disturbances determine the sediment origin and catchment-scale sediment flux in highly modified landscapes (Fryirs, 2017; Poeppl et al., 2020). Hence, the stability of the Es Fangar catchment geomorphic system depends to a certain extent on the maintenance and restoration of the elements that conform it, including soil conservation structures. Otherwise, a sudden change in its operation could eventually result in increased sediment yields, soil loss and degradation.

7.6. Conclusions

This study links hydro-sedimentary dynamics at event scale (n=34) with sediment fingerprinting source ascription (n=13) to better understand erosive processes in a Mediterranean catchment. Scrubland and forest sources were not differentiated using colour coefficients and ^{137}Cs was not able to discriminate between channel and crop sources. Using only colour parameters and MixSIAR, crops were the main sediment source in 12 of the 13 integrated sediment samples. The EMMA analysis showed similar results, clustering all sediment samples close to crop land and channel bank signatures except one (Sample 2), coinciding with MixSIAR results. Our analysis suggests that the EMMA approach can be a good choice to identify dominant sources

of sediment using simplified procedures in comparison with mixing models. We argue that the use of this approach in sediment tracing studies needs to be further explored.

Even if floods could be clustered in function of event-based variables (e.g. rainfall, discharge, suspended sediment concentration and hysteretic relationship between water and sediment), a clear relation with sediment source changes was not found. Lithology, land uses and the presence of agricultural terraces and dry stone walls might partially explain the low sediment source inter- and intra-annual variability in the Es Fangar catchment. Furthermore, the complexity and spatial variability of Mediterranean catchments complicates the definition of clear suspended sediment transport patterns and its link with sediment source ascription. Even if further research is necessary to reach a comprehensive understanding about erosion and sediment transport dynamics in Es Fangar catchment. The proposed approach and the results obtained can not only help managers in defining optimal intervention strategies, but also be used to create quantitative (in terms of amount) and qualitative (in terms of origin) sediment models to be integrated in catchment management plans.

Acknowledgements

This work was supported by the Spanish Ministry of Science, Innovation and Universities, the Spanish Agency of Research (AEI) and the European Regional Development Funds (ERDF) through the project CGL2017-88200-R "Functional hydrological and sediment connectivity at Mediterranean catchments: global change scenarios –MEDhyCON2". Julián García-Comendador is in receipt of a pre-doctoral contract (FPU15/05239) funded by the Spanish Ministry of Education and Culture. Núria Martínez-Carreras acknowledges funding for this study from the Luxembourg National Research Fund (PAINLESS project, C17/SR/11699372). Josep Fortesa has a contract funded by the Vice-presidency and Ministry of Innovation, Research and Tourism of the Autonomous Government of the Balearic Islands (FPI/2048/2017). Meteorological data were facilitated by the Spanish Meteorological Agency (AEMET). We would like to acknowledge support by Franz Ronellenfitsch for the set-up of the spectroradiometer.

7.7. References

Abban, B., Thanos Papanicolaou, A.N., Cowles, M.K., Wilson, C.G., Abaci, O., Wacha, K., Schilling, K., Schnoebelen, D., 2016. An enhanced Bayesian fingerprinting framework for studying sediment source dynamics in intensively managed landscapes. Water Resour. Res. 52, 4646–4673. https://doi.org/10.1002/2015WR018030

Aich, V., Zimmermann, A., Elsenbeer, H., 2014. Quantification and interpretation of suspended-sediment discharge hysteresis patterns: How much data do we need? Catena 122, 120–129. https://doi.org/10.1016/j.catena.2014.06.020

Bakker, K., 2012. Water security: Research challenges and opportunities. Science (80-.). https://doi.org/10.1126/science.1226337

Barthod, L.R.M., Liu, K., Lobb, D.A., Owens, P.N., Martínez-Carreras, N., Koiter, A.J., Petticrew, E.L., McCullough, G.K., Liu, C., Gaspar, L., 2015. Selecting Color-based Tracers and Classifying Sediment Sources in the Assessment of Sediment Dynamics Using Sediment Source Fingerprinting. J. Environ. Qual. 44, 1605–1616. https://doi.org/10.2134/jeq2015.01.0043

Blake, W.H., Boeckx, P., Stock, B.C., Smith, H.G., Bodé, S., Upadhayay, H.R., Gaspar, L., Goddard, R., Lennard, A.T., Lizaga, I., Lobb, D.A., Owens, P.N., Petticrew, E.L., Kuzyk, Z.Z.A., Gari, B.D., Munishi, L., Mtei, K., Nebiyu, A., Mabit, L., Navas, A., Semmens, B.X., 2018. A deconvolutional Bayesian mixing model approach for river basin sediment source apportionment. Sci. Rep. 8, 1–12. https://doi.org/10.1038/s41598-018-30905-9

Bu, C.F., Cai, Q.G., Ng, S.L., Chau, K.C., Ding, S.W., 2008. Effects of hedgerows on sediment erosion in Three Gorges Dam Area, China. Int. J. Sediment Res. 23, 119–129. https://doi.org/10.1016/S1001-6279(08)60011-6

Bunch, M.J., Parkes, M., Zubrycki, K., Venema, H., Hallstrom, L., Neudorffer, C., Berbés-Blázquez, M., Morrison, K., 2014. Watershed management and public health: An exploration of the intersection of two fields as reported in the literature from 2000 to 2010. Environ. Manage. 54, 240–254. https://doi.org/10.1007/s00267-014-0301-3

Calsamiglia, A., Fortesa, J., García-Comendador, J., Lucas-Borja, M.E., Calvo-Cases, A., Estrany, J., 2018. Spatial patterns of sediment connectivity in terraced lands: Anthropogenic controls of catchment sensitivity. L. Degrad. Dev. 29, 1198–1210. https://doi.org/10.1002/ldr.2840

Calvo-Cases, A., Boix-Fayos, C., Imeson, A.. C., 2003. Runoff generation, sediment movement and soil water behaviour on calcareous (limestone) slopes of some Mediterranean environments in southeast Spain. Geomorphology 50, 269–291. https://doi.org/10.1016/S0169-555X(02)00218-0

Christophersen, N., Hooper, R.P., 1992. Multivariate analysis of stream water chemical data: The use of principal components analysis for the end-member mixing problem. Water Resour. Res. 28, 99–107. https://doi.org/10.1029/91WR02518

Collins, A.L., Blackwell, M., Boeckx, P., Chivers, C.A., Emelko, M., Evrard, O., Foster, I., Gellis, A., Gholami, H., Granger, S., Harris, P., Horowitz, A.J., Laceby, J.P., Martinez-Carreras, N., Minella, J., Mol, L., Nosrati, K., Pulley, S., Silins, U., da Silva, Y.J., Stone, M., Tiecher, T., Upadhayay, H.R., Zhang, Y., 2020. Sediment source fingerprinting: benchmarking recent

outputs, remaining challenges and emerging themes. J. Soils Sediments 20, 1–34. https://doi.org/10.1007/s11368-020-02755-4

Collins, A.L.L., Pulley, S., Foster, I.D.L.D.L., Gellis, A., Porto, P., Horowitz, A.J.J., 2017. Sediment source fingerprinting as an aid to catchment management: A review of the current state of knowledge and a methodological decision-tree for end-users. J. Environ. Manage. 194, 86–108. https://doi.org/10.1016/j.jenvman.2016.09.075

Collins, A.L.L., Walling, D.E.E., Leeks, G.J.L.J.L., 1997. Source type ascription for fluvial suspended sediment based on a quantitative composite fingerprinting technique. Catena 29, 1–27. https://doi.org/10.1016/S0341-8162(96)00064-1

Cooper, R.J., Krueger, T., 2017. An extended Bayesian sediment fingerprinting mixing model for the full Bayes treatment of geochemical uncertainties. Hydrol. Process. 31, 1900–1912. https://doi.org/10.1002/hyp.11154

Cooper, R.J., Krueger, T., Hiscock, K.M., Rawlins, B.G., 2015. High-temporal resolution fluvial sediment source fingerprinting with uncertainty: a Bayesian approach. Earth Surf. Process. Landforms 40, 78–92. https://doi.org/10.1002/esp.3621

Davis, C.M., Fox, J.F., 2009. Sediment Fingerprinting: Review of the Method and Future Improvements for Allocating Nonpoint Source Pollution. J. Environ. Eng. 135, 490–504. https://doi.org/10.1061/(ASCE)0733-9372(2009)135:7(490)

de Boer, D.H., Campbell, I.A., 1989. Spatial scale dependence of sediment dynamics in a semi-arid badland drainage basin. Catena 16, 277–290. https://doi.org/10.1016/0341-8162(89)90014-3

De Girolamo, A.M., Pappagallo, G., Lo Porto, A., 2015. Temporal variability of suspended sediment transport and rating curves in a Mediterranean river basin: The Celone (SE Italy). Catena 128, 135–143. https://doi.org/10.1016/j.catena.2014.09.020

de Vente, J., Verduyn, R., Verstraeten, G., Vanmaercke, M., Poesen, J., 2011. Factors controlling sediment yield at the catchment scale in NW Mediterranean geoecosystems. J. Soils Sediments 11, 690–707. https://doi.org/10.1007/s11368-011-0346-3

Du, P., Walling, D.E., 2017. Fingerprinting surficial sediment sources: Exploring some potential problems associated with the spatial variability of source material properties. J. Environ. Manage. 194, 4–15. https://doi.org/10.1016/j.jenvman.2016.05.066

Estrany, J., Garcia, C., Batalla, R.J., 2010a. Hydrological response of a small mediterranean agricultural catchment. J. Hydrol. 380, 180–190. https://doi.org/10.1016/j.jhydrol.2009.10.035

Estrany, J., Garcia, C., Walling, D.E., 2010b. An investigation of soil erosion and redistribution in a Mediterranean lowland agricultural catchment using caesium-137. Int. J. Sediment Res. 25, 1–16. https://doi.org/10.1016/S1001-6279(10)60023-6

Evrard, O., Navratil, O., Ayrault, S., Ahmadi, M., Némery, J., Legout, C., Lefèvre, I., Poirel, A., Bonté, P., Esteves, M., 2011. Combining suspended sediment monitoring and fingerprinting to determine the spatial origin of fine sediment in a mountainous river catchment. Earth Surf. Process. Landforms 36, 1072–1089. https://doi.org/10.1002/esp.2133

Fortesa, J., Latron, J., García-Comendador, J., Company, J., Estrany, J., 2020a. Runoff and soil

moisture as driving factors in suspended sediment transport of a small mid-mountain Mediterranean catchment. Geomorphology 368, 107349. https://doi.org/10.1016/j.geomorph.2020.107349

Fortesa, J., Latron, J., García-Comendador, J., Tomàs-Burguera, M., Company, J., Calsamiglia, A., Estrany, J., 2020b. Multiple temporal scales assessment in the hydrological response of small mediterranean-climate catchments. Water 12, 299. https://doi.org/10.3390/w12010299

Fryirs, K.A., 2017. River sensitivity: a lost foundation concept in fluvial geomorphology. Earth Surf. Process. Landforms 42, 55–70. https://doi.org/10.1002/esp.3940

García-Comendador, J., Fortesa, J., Calsamiglia, A., Garcias, F., Estrany, J., 2017. Source ascription in bed sediments of a Mediterranean temporary stream after the first post-fire flush. J. Soils Sediments 17, 2582–2595. https://doi.org/10.1007/s11368-017-1806-1

García-Ruiz, J.M., Nadal-Romero, E., Lana-Renault, N., Beguería, S., 2013. Erosion in Mediterranean landscapes: Changes and future challenges. Geomorphology 198, 20–36. https://doi.org/10.1016/j.geomorph.2013.05.023

Giménez, R., Casalí, J., Grande, I., Díez, J., Campo, M.A., Álvarez-Mozos, J., Goñi, M., 2012. Factors controlling sediment export in a small agricultural watershed in Navarre (Spain). Agric. Water Manag. 110, 1–8. https://doi.org/10.1016/j.agwat.2012.03.007

Guijarro, J.A., 1986. Contribucion a la bioclimatologia de Baleares. PhD Thesis. University of the Balearic Islands, Palma, Spain.

Guzmán, G., Quinton, J.N., Nearing, M.A., Mabit, L., Gómez, J.A., 2013. Sediment tracers in water erosion studies: Current approaches and challenges. J. Soils Sediments 13, 816–833. https://doi.org/10.1007/s11368-013-0659-5

Haddadchi, A., Olley, J., Laceby, P., 2014. Accuracy of mixing models in predicting sediment source contributions. Sci. Total Environ. 497–498, 139–152. https://doi.org/10.1016/j.scitotenv.2014.07.105

Haddadchi, A., Ryder, D.S., Evrard, O., Olley, J., 2013. Sediment fingerprinting in fluvial systems: review of tracers, sediment sources and mixing models. Int. J. Sediment Res. 28, 560–578. https://doi.org/10.1016/S1001-6279(14)60013-5

Hooper, R.P., 2003. Diagnostic tools for mixing models of stream water chemistry. Water Resour. Res. 39, 1055. https://doi.org/10.1029/2002WR001528

Horowitz, A.J., Elrick, K.A., Smith, J.J., 2007. Measuring the fluxes of suspended sediment, trace elements and nutrients for the city of atlanta, USA: Insights on the global water quality impacts of increasing urbanization. IAHS-AISH Publ. 314, 57–70.

James, A.L., Roulet, N.T., 2006. Investigating the applicability of end-member mixing analysis (EMMA) across scale: A study of eight small, nested catchments in a temperate forested watershed. Water Resour. Res. 42, W08434. https://doi.org/10.1029/2005WR004419

Langlois, J.L., Johnson, D.W., Mehuys, G.R., 2005. Suspended sediment dynamics associated with snowmelt runoff in a small mountain stream of Lake Tahoe (Nevada). Hydrol. Process. 19, 3569–3580. https://doi.org/10.1002/hyp.5844

Lawler, D.M., Petts, G.E., Foster, I.D.L., Harper, S., 2006. Turbidity dynamics during spring

storm events in an urban headwater river system: The Upper Tame, West Midlands, UK. Sci. Total Environ. 360, 109–126. https://doi.org/10.1016/j.scitotenv.2005.08.032

Lees, J.A., 1997. Mineral magnetic properties of mixtures of environmental and synthetic materials: Linear additivity and interaction effects. Geophys. J. Int. 131, 335–346. https://doi.org/10.1111/j.1365-246X.1997.tb01226.x

Li, Z., Xu, X., Zhu, J., Xu, C., Wang, K., 2019. Effects of lithology and geomorphology on sediment yield in karst mountainous catchments. Geomorphology 343, 119–128. https://doi.org/10.1016/j.geomorph.2019.07.001

Lloyd, C.E.M., Freer, J.E., Johnes, P.J., Collins, A.L., 2016. Using hysteresis analysis of high-resolution water quality monitoring data, including uncertainty, to infer controls on nutrient and sediment transfer in catchments. Sci. Total Environ. 543, 388–404. https://doi.org/10.1016/j.scitotenv.2015.11.028

López-Bermúdez, F., 1990. Soil erosion by water on the desertification of a semi-arid Mediterranean fluvial basin: the Segura basin, Spain. Agric. Ecosyst. Environ. 33, 129–145. https://doi.org/10.1016/0167-8809(90)90238-9

López-Tarazón, J.A., Estrany, J., 2017. Exploring suspended sediment delivery dynamics of two Mediterranean nested catchments. Hydrol. Process. 31, 698–715. https://doi.org/10.1002/hyp.11069

Ludwig, W., Probst, J.L., 1996. Predicting the oceanic input of organic carbon by continental erosion. Global Biogeochem. Cycles 10, 23–41. https://doi.org/10.1029/95GB02925

Manjoro, M., Rowntree, K., Kakembo, V., Collins, A.L., 2017. Use of sediment source fingerprinting to assess the role of subsurface erosion in the supply of fine sediment in a degraded catchment in the Eastern Cape, South Africa. J. Environ. Manage. 194, 27–41. https://doi.org/10.1016/J.JENVMAN.2016.07.019

Martínez-Carreras, N., Krein, A., Gallart, F., Iffly, J.F., Pfister, L., Hoffmann, L., Owens, P.N., 2010a. Assessment of different colour parameters for discriminating potential suspended sediment sources and provenance: A multi-scale study in Luxembourg. Geomorphology 118, 118–129. https://doi.org/10.1016/j.geomorph.2009.12.013

Martínez-Carreras, N., Udelhoven, T., Krein, A., Gallart, F., Iffly, J.F., Ziebel, J., Hoffmann, L., Pfister, L., Walling, D.E., 2010b. The use of sediment colour measured by diffuse reflectance spectrometry to determine sediment sources: Application to the Attert River catchment (Luxembourg). J. Hydrol. 382, 49–63. https://doi.org/10.1016/j.jhydrol.2009.12.017

McCarney-Castle, K., Childress, T.M., Heaton, C.R., 2017. Sediment source identification and load prediction in a mixed-use Piedmont watershed, South Carolina. J. Environ. Manage. 185, 60–69. https://doi.org/10.1016/j.jenvman.2016.10.036

Merheb, M., Moussa, R., Abdallah, C., Colin, F., Perrin, C., Baghdadi, N., 2016. Hydrological response characteristics of Mediterranean catchments at different time scales: a meta-analysis. Hydrol. Sci. J. 61, 2520–2539. https://doi.org/10.1080/02626667.2016.1140174

Motha, J.A., Wallbrink, P.J., Hairsine, P.B., Grayson, R.B., 2003. Determining the sources of suspended sediment in a forested catchment in southeastern Australia. Water Resour. Res. 39, 1056. https://doi.org/10.1029/2001WR000794

Mukundan, R., Radcliffe, D.E., Ritchie, J.C., Risse, L.M., McKinley, R.A., 2010. Sediment Fingerprinting to Determine the Source of Suspended Sediment in a Southern Piedmont Stream. J. Environ. Qual. 39, 1328–1337. https://doi.org/10.2134/jeq2009.0405

Murtagh, F., Legendre, P., 2014. Ward's Hierarchical Agglomerative Clustering Method: Which Algorithms Implement Ward's Criterion? J. Classif. 31, 274–295. https://doi.org/10.1007/s00357-014-9161-z

Navas, A., Garcés, B.V., Machín, J., 2004. An approach to integrated assessement of reservoir siltation : the Joaquín Costa reservoir as a case study. Hydrol. Easrt Syst. Sci. 8, 1193–1199. https://doi.org/10.5194/hess-8-1193-2004

Navratil, O., Evrard, O., Esteves, M., Legout, C., Ayrault, S., Némery, J., Mate-Marin, A., Ahmadi, M., Lefèvre, I., Poirel, A., Bonté, P., 2012. Temporal variability of suspended sediment sources in an alpine catchment combining river/rainfall monitoring and sediment fingerprinting. Earth Surf. Process. Landforms 37, 828–846. https://doi.org/10.1002/esp.3201

Newcombe, C.P., Macdonald, D.D., 1991. Effects of Suspended Sediments on Aquatic Ecosystems. North Am. J. Fish. Manag. 11, 72–82. https://doi.org/10.1577/1548-8675(1991)011<0072:EOSSOA>2.3.CO;2

Nosrati, K., Govers, G., Semmens, B.X., Ward, E.J., 2014. A mixing model to incorporate uncertainty in sediment fingerprinting. Geoderma 217–218, 173–180. https://doi.org/10.1016/j.geoderma.2013.12.002

Owens, P.N., Batalla, R.J., Collins, A.J., Gomez, B., Hicks, D.M., Horowitz, A.J., Kondolf, G.M., Marden, M., Page, M.J., Peacock, D.H., Petticrew, E.L., Salomons, W., Trustrum, N.A., 2005. Fine-grained sediment in river systems: Environmental significance and management issues. River Res. Appl. 21, 693–717. https://doi.org/10.1002/rra.878

Owens, P.N., Walling, D.E., He, Q., 1996. The behaviour of bomb-derived caesium-137 fallout in catchment soils. J. Environ. Radioact. 32, 169–191. https://doi.org/10.1016/0265-931X(96)84941-1

Palazón, L., Navas, A., 2017. Variability in source sediment contributions by applying different statistic test for a Pyrenean catchment. J. Environ. Manage. 194, 42–53. https://doi.org/10.1016/j.jenvman.2016.07.058

Perks, M.T., Warburton, J., Bracken, L.J., Reaney, S.M., Emery, S.B., Hirst, S., 2017. Use of spatially distributed time-integrated sediment sampling networks and distributed fine sediment modelling to inform catchment management. J. Environ. Manage. 202, 469–478. https://doi.org/10.1016/j.jenvman.2017.01.045

Phillips, J.M., Russell, M.A., Walling, D.E., 2000. Time-integrated sampling of fluvial suspended sediment: A simple methodology for small catchments. Hydrol. Process. 14, 2589–2602. https://doi.org/10.1002/1099-1085(20001015)14:14<2589::AID-HYP94>3.0.CO;2-D

Poeppl, R.E., Fryirs, K.A., Tunnicliffe, J., Brierley, G.J., 2020. Managing sediment (dis)connectivity in fluvial systems. Sci. Total Environ. 736, 139627. https://doi.org/10.1016/j.scitotenv.2020.139627

Poulenard, J., Legout, C., Némery, J., Bramorski, J., Navratil, O., Douchin, A., Fanget, B., Perrette, Y., Evrard, O., Esteves, M., 2012. Tracing sediment sources during floods using Diffuse Reflectance Infrared Fourier Transform Spectrometry (DRIFTS): A case study in a

highly erosive mountainous catchment (Southern French Alps). J. Hydrol. 414, 452–462. https://doi.org/10.1016/j.jhydrol.2011.11.022

Pulley, S., Rowntree, K., 2016. The use of an ordinary colour scanner to fingerprint sediment sources in the South African Karoo. J. Environ. Manage. 165, 253–262. https://doi.org/10.1016/j.jenvman.2015.09.037

Pulley, S., Van der Waal, B., Rowntree, K., Collins, A.L., 2018. Colour as reliable tracer to identify the sources of historically deposited flood bench sediment in the Transkei, South Africa: A comparison with mineral magnetic tracers before and after hydrogen peroxide pre-treatment. Catena 160, 242–251. https://doi.org/10.1016/j.catena.2017.09.018

Rose, L.A., Karwan, D.L., Aufdenkampe, A.K., 2018. Sediment Fingerprinting Suggests Differential Suspended Particulate Matter Formation and Transport Processes Across Hydrologic Regimes. J. Geophys. Res. Biogeosciences 123, 1213–1229. https://doi.org/10.1002/2017JG004210

Rovira, A., Batalla, R.J., 2006. Temporal distribution of suspended sediment transport in a Mediterranean basin: The Lower Tordera (NE SPAIN). Geomorphology 79, 58–71. https://doi.org/10.1016/j.geomorph.2005.09.016

Sherriff, S.C., Rowan, J.S., Fenton, O., Jordan, P., Melland, A.R., Mellander, P.E., Huallacháin, D., 2016. Storm Event Suspended Sediment-Discharge Hysteresis and Controls in Agricultural Watersheds: Implications for Watershed Scale Sediment Management. Environ. Sci. Technol. 50, 1769–1778. https://doi.org/10.1021/acs.est.5b04573

Smith, H.G., Dragovich, D., 2009. Interpreting sediment delivery processes using suspended sediment-discharge hysteresis patterns from nested upland catchments, south-eastern Australia. Hydrol. Process. 23, 2415–2426. https://doi.org/10.1002/hyp.7357

Stock, B.C., Jackson, A.L., Ward, E.J., Parnell, A.C., Phillips, D.L., Semmens, B.X., 2018. Analyzing mixing systems using a new generation of Bayesian tracer mixing models. PeerJ 6, e5096. https://doi.org/10.7717/peerj.5096

Stock, B.C., Semmens, B.X., 2016. Unifying error structures in commonly used biotracer mixing models. Ecology 97, 2562–2569. https://doi.org/10.1002/ecy.1517

Tarolli, P., Preti, F., Romano, N., 2014. Terraced landscapes: From an old best practice to a potential hazard for soil degradation due to land abandonment. Anthropocene 6, 10–25. https://doi.org/10.1016/j.ancene.2014.03.002

Tiecher, T., Caner, L., Minella, J.P.G., Santos, D.R. dos, 2015. Combining visible-based-color parameters and geochemical tracers to improve sediment source discrimination and apportionment. Sci. Total Environ. 527–528, 135–149. https://doi.org/10.1016/j.scitotenv.2015.04.103

Uber, M., Legout, C., Nord, G., Crouzet, C., Demory, F., Poulenard, J., 2019. Comparing alternative tracing measurements and mixing models to fingerprint suspended sediment sources in a mesoscale Mediterranean catchment. J. Soils Sediments 19, 3255–3273. https://doi.org/10.1007/s11368-019-02270-1

Vercruysse, K., Dawson, D.A., Glenis, V., Bertsch, R., Wright, N., Kilsby, C., 2019. Developing spatial prioritization criteria for integrated urban flood management based on a source-to-impact flood analysis. J. Hydrol. 578, 124038. https://doi.org/10.1016/j.jhydrol.2019.124038

Vercruysse, K., Grabowski, R.C., 2019. Temporal variation in suspended sediment transport: linking sediment sources and hydro-meteorological drivers. Earth Surf. Process. Landforms 44, 2587–2599. https://doi.org/10.1002/esp.4682

Vercruysse, K., Grabowski, R.C., Rickson, R.J., 2017. Suspended sediment transport dynamics in rivers: Multi-scale drivers of temporal variation. Earth-Science Rev. 166, 38–52. https://doi.org/10.1016/j.earscirev.2016.12.016

Walling, D.E., 2013. The evolution of sediment source fingerprinting investigations in fluvial systems. J. Soils Sediments 13, 1658–1675. https://doi.org/10.1007/s11368-013-0767-2

Walling, D.E., 2006. Human impact on land-ocean sediment transfer by the world's rivers. Geomorphology 79, 192–216. https://doi.org/10.1016/j.geomorph.2006.06.019

Walling, D.E., Collins, a. L., 2008. The catchment sediment budget as a management tool. Environ. Sci. Policy 11, 136–143. https://doi.org/10.1016/j.envsci.2007.10.004

Wang, G., Mang, S., Cai, H., Liu, S., Zhang, Z., Wang, L., Innes, J.L., 2016. Integrated watershed management: evolution, development and emerging trends. J. For. Res. 27, 967–994. https://doi.org/10.1007/s11676-016-0293-3

Ward, J.H., 1963. Hierarchical Grouping to Optimize an Objective Function. J. Am. Stat. Assoc. 58, 236. https://doi.org/10.2307/2282967

Williams, G.P.G.., 1989. Sediment concentration versus water discharge during single hydrologic events in rivers. J. Hydrol. 111, 89–106. https://doi.org/10.1016/0022-1694(89)90254-0

Zuecco, G., Penna, D., Borga, M., van Meerveld, H.J., 2016. A versatile index to characterize hysteresis between hydrological variables at the runoff event timescale. Hydrol. Process. 30, 1449–1466. https://doi.org/10.1002/hyp.10681

7.8. Supplementary material

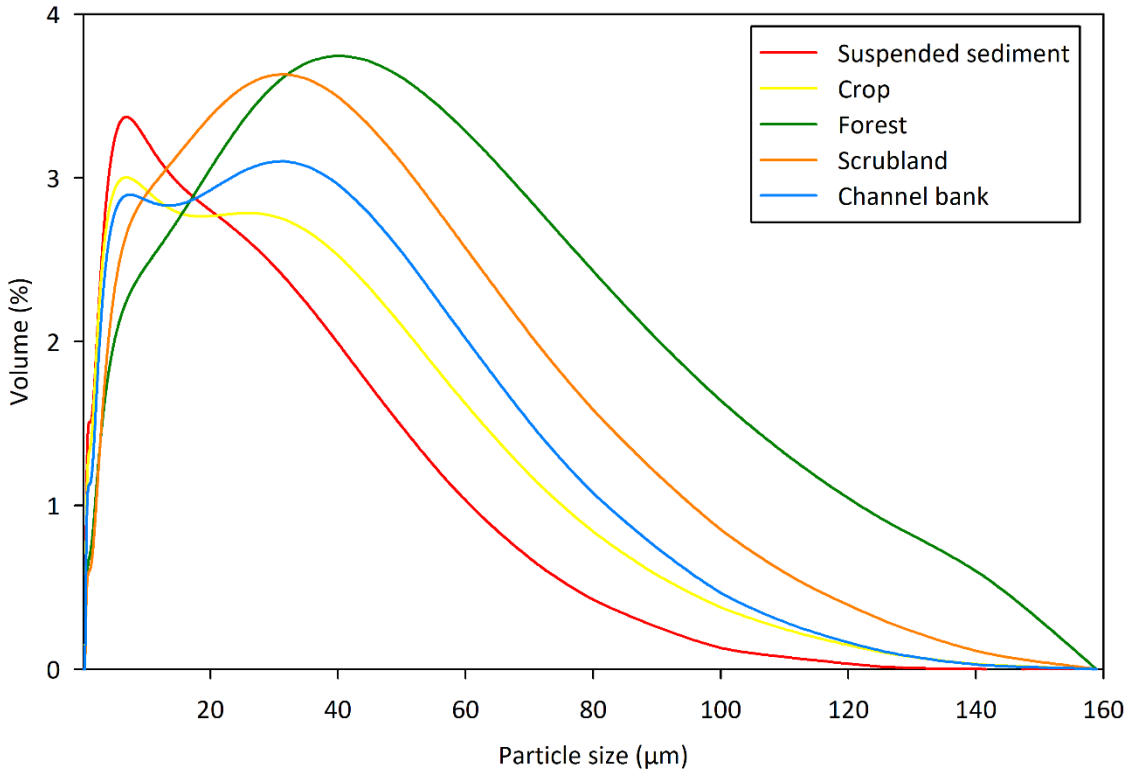

Supplementary figure 7.1. Average particle size distributions of the different source and suspended sediment samples.

Supplementary table 7.1. Artificial mixtures in different proportions of channel bank (CB), crop soil (CS), forest soil (FS) and scrubland soil (SS).

Number of sources	ID	Sources types used	% proportion (respectively)
2 sources	mix2-1	CB + CS	80 + 20
	mix2-2	CB + FS	80 + 20
	mix2-3	SS + CB	80 + 20
	mix2-4	SS + FS	80 + 20
	mix2-5	FS + CB	80 + 20
	mix2-6	FS + SS	80 + 20
	mix2-7	FS + CS	80 + 20
	mix2-8	CS + FS	80 + 20
	mix2-9	CS + SS	80 + 20
	mix2-10	CS + CB	80 + 20
3 sources	mix3-1	CB + SS + FS	70 + 20 + 10
	mix3-2	CB + CS + SS	70 + 20 + 10
	mix3-3	SS + CB + FS	70 + 20 + 10
	mix3-4	SS + FS + CS	70 + 20 + 10
	mix3-5	FS + SS + CS	70 + 20 + 10
	mix3-6	FS + SS + CB	70 + 20 + 10
	mix3-7	FS + CB + CS	70 + 20 + 10
	mix3-8	CS + FS + CB	70 + 20 + 10
	mix3-9	CS + SS + FS	70 + 20 + 10
	mix3-10	CS + CB + SS	70 + 20 + 10
4 sources	mix4-1	CB + SS + FS + CS	60 + 20 + 10 + 10
	mix4-2	CB + CS + SS + FS	60 + 20 + 10 + 10
	mix4-3	SS + CB + FS + CS	60 + 20 + 10 + 10
	mix4-4	SS + FS + CS + CB	60 + 20 + 10 + 10
	mix4-5	FS + SS + CS + CB	60 + 20 + 10 + 10
	mix4-6	FS + SS + CB + CS	60 + 20 + 10 + 10
	mix4-7	FS + CB + CS + SS	60 + 20 + 10 + 10
	mix4-8	CS + FS + CB + SS	60 + 20 + 10 + 10
	mix4-9	CS + SS + FS + CB	60 + 20 + 10 + 10
	mix4-10	CS + CB + SS + FS	60 + 20 + 10 + 10

Supplementary table 7.2. Summary statistics for each tracer and source type.

Tracers	Sources	Min.	Median	Mean	Max.	Sta.Dev.
Cie x	Channel	0.348	0.354	0.355	0.367	0.005
	Crop	0.353	0.356	0.356	0.361	0.003
	Forest	0.345	0.353	0.352	0.362	0.007
	Scrubland	0.350	0.353	0.354	0.357	0.002
Cie y	Channel	0.336	0.342	0.343	0.349	0.003
	Crop	0.343	0.346	0.345	0.346	0.001
	Forest	0.333	0.337	0.338	0.344	0.005
	Scrubland	0.338	0.340	0.340	0.341	0.001
Cie Y	Channel	8.567	11.476	12.011	19.524	2.758
	Crop	9.753	13.324	14.086	19.028	3.129
	Forest	7.973	8.728	9.522	12.398	1.768
	Scrubland	9.013	9.665	9.504	9.724	0.298
Red	Channel	95.450	111.090	112.460	138.840	10.807
	Crop	104.800	118.800	120.600	137.800	11.145
	Forest	91.690	97.780	101.200	115.140	9.530
	Scrubland	98.290	102.500	101.490	103.220	1.984
Green	Channel	78.940	90.560	92.280	117.790	10.132
	Crop	83.200	97.760	99.840	116.370	11.103
	Forest	76.290	79.210	82.510	94.230	7.119
	Scrubland	80.830	83.200	82.780	83.760	1.189
Blue	Channel	76.050	84.440	86.030	110.620	9.078
	Crop	77.500	90.200	92.000	106.980	9.905
	Forest	74.720	76.470	78.550	87.530	5.157
	Scrubland	77.380	78.220	78.260	79.110	0.636
^{137}Cs	Channel	1.200	5.450	6.831	20.800	5.765
	Crop	1.000	7.100	6.317	9.400	3.164
	Forest	9.000	17.200	16.700	26.700	6.692
	Scrubland	15.700	21.900	41.480	100.200	35.858
$^{210}Pbex$	Channel	1.000	21.480	31.820	124.240	32.728
	Crop	13.340	23.690	24.070	36.520	8.183
	Forest	19.800	103.360	128.280	252.060	94.190
	Scrubland	11.700	100.140	111.580	200.100	80.627

Supplementary table 7.3. MixSIAR source apportionment and absolute error in comparison with real proportions for the two sources artificial mixtures.

				MixSIAR		
Samples		Sources	Real proportions (%)	Estimated proportions (%)	Absolute error (%)	Average absolute error (%)
2 samples mixtures	mix2-M1	Channel	80	75 ± 6.5	5.0	5.0
		Crop	20	25 ± 6.5	5.0	
	mix2-M2	Channel	80	58.3 ± 17.3	21.7	21.7
		Forest	20	41.7 ± 17.3	21.7	
	mix2-M3	Scrubland	80	49.9 ± 25.8	30.1	30.1
		Channel	20	50.1 ± 25.8	30.1	
	mix2-M4	Scrubland	80	67.9 ± 21.4	12.1	12.1
		Forest	20	32.1 ± 21.4	12.1	
	mix2-M5	Forest	80	76.5 ± 11.1	3.5	3.5
		Channel	20	23.5 ± 11.1	3.5	
	mix2-M6	Forest	80	63.2 ± 15	16.8	16.8
		scrubland	20	36.8 ± 15	16.8	
	mix2-M7	Forest	80	83.3 ± 6.8	3.3	3.3
		Crop	20	16.7 ± 6.8	3.3	
	mix2-M8	Crop	80	61.4 ± 22.7	18.6	18.6
		Forest	20	38.6 ± 22.7	18.6	
	mix2-M9	Crop	80	80.8± 9.7	0.8	0.8
		scrubland	20	19.2 ± 9.7	0.8	
	mix2-M10	Crop	80	77.5 ± 5.5	2.5	2.5
		Channel	20	22.5 ± 5.5	2.5	

Supplementary table 7.4. MixSIAR source apportionment and absolute error in comparison with real proportions for the three sources artificial mixtures.

				MixSIAR		
Samples		Sources	Real proportions (%)	Estimated proportions (%)	Absolute error (%)	Average absolute error (%)
3 samples mixtures	mix3-M1	Channel	70	33.2 ± 21.5	36.8	24.5
		Scrubland	20	32.8 ± 21.7	12.8	
		Forest	10	34 ± 21.5	24.0	
	mix3-M2	Channel	70	42.6 ± 21.9	27.4	22.0
		Crop	20	14.3 ± 7.4	5.7	
		Scrubland	10	43 ± 22.9	33.0	
	mix3-M3	Scrubland	70	36.3 ± 21.7	33.7	22.5
		Channel	20	40.7 ± 18.1	20.7	
		Forest	10	23 ± 14.1	13.0	
	mix3-M4	Scrubland	70	40 ± 22.4	30.0	20.0
		Forest	20	40.5 ± 15.8	20.5	
		Crop	10	19.4 ± 8.9	9.4	
	mix3-M5	Forest	70	49.2 ± 21.6	20.8	16.3
		Scrubland	20	44.5 ± 23.4	24.5	
		Crop	10	6.3 ± 3.4	3.7	
	mix3-M6	Forest	70	34.8 ± 13.6	35.2	23.5
		Scrubland	20	31.6 ± 17.6	11.6	
		Channel	10	33.6 ± 19.9	23.6	
	mix3-M7	Forest	70	37.9 ± 21.6	32.1	21.4
		Channel	20	21.3 ± 11.6	1.3	
		Crop	10	40.8 ± 17.9	30.8	
	mix3-M8	Crop	70	70.2 ± 7.8	0.2	4.5
		Forest	20	13.3 ± 8.6	6.7	
		Channel	10	16.5 ±10.4	6.5	
	mix3-M9	Crop	70	65.8 ± 0.8	4.2	3.1
		Scrubland	20	19.6 ± 12	0.4	
		Forest	10	14.6 ±9.4	4.6	
	mix3-M10	Crop	70	55.9 ± 4.8	14.1	9.4
		Channel	20	20.8 ± 11.9	0.8	
		Scrubland	10	23.3 ± 13.5	13.3	

Supplementary table 7.5. MixSIAR source apportionment and absolute error in comparison with real proportions for the four sources artificial mixtures

				MixSIAR		
Samples		Sources	Real proportions (%)	Estimated proportions (%)	Absolute error (%)	Average absolute error (%)
4 samples mixtures	mix4-M1	Channel	60	28.4 ± 18.2	31.6	15.8
		Scrubland	20	26.9 ± 17.1	6.9	
		Forest	10	24.5 ± 14.2	14.5	
		Crop	10	20.3 ± 9.1	10.3	
	mix4-M2	Channel	60	33.8 ± 18.3	26.2	15.9
		Crop	20	14.4 ± 9.3	5.6	
		Scrubland	10	34.1 ± 19.5	24.1	
		Forest	10	17.7 ± 11.3	7.7	
	mix4-M3	Scrubland	60	31.5 ± 19.6	28.5	15.4
		Channel	20	29.4 ± 19	9.4	
		Forest	10	31.4 ± 17.9	21.4	
		Crop	10	7.6 ± 3.9	2.4	
	mix4-M4	Scrubland	60	27.5 ± 18.6	32.5	16.3
		Forest	20	25.1 ± 15	5.1	
		Crop	10	20.6 ± 7.7	10.6	
		Channel	10	26.8 ± 17	16.8	
	mix4-M5	Forest	60	32.3 ± 18.4	27.7	16.1
		Scrubland	20	30.9 ± 19.3	10.9	
		Crop	10	5.4 ± 2.9	4.6	
		Channel	10	31.1 ± 19.3	21.1	
	mix4-M6	Forest	60	40.4 ± 15	19.6	10.5
		Scrubland	20	25 ± 16.7	5	
		Channel	10	25.9 ± 17.6	15.9	
		Crop	10	8.7 ± 17.6	1.3	
	mix4-M7	Forest	60	30.8 ± 18.7	29.2	14.7
		Channel	20	19.9 ± 13	0.1	
		Crop	10	33.3 ± 14.9	23.3	
		Scrubland	10	16 ± 10.4	6	
	mix4-M8	Crop	60	57.3 ± .6	2.7	5.5
		Forest	20	11.8 ± 8.8	8.2	
		Channel	10	14.6 ± 10.7	4.6	
		Scrubland	10	16.3 ± 11.5	6.3	
	mix4-M9	Crop	60	47.3 ± 9.7	12.7	7.7
		Scrubland	20	17.4 ± 12.1	2.6	
		Forest	10	13 ± 9.4	3	
		Channel	10	22.4 ± 15.5	12.4	
	mix4-M10	Crop	60	39.1 ± 7.4	20.9	12.8
		Channel	20	15 ± 10.5	5	
		Scrubland	10	18.4 ± 12.2	8.4	
		Forest	10	26.7 ± 17.7	16.7	

Supplementary table 7.6. MixSIAR source apportionment considering two group sources (i.e. channel-crop and forest-scrub) using colour and ^{137}Cs.

		MixSIAR	
SS sample	Sources	Average (%)	Quantile distribution 5% - 95%
Sample1	channel-crop	**83.8 ± 11.8**	60.6 - 98.7
	Forest scrub	16.2 ± 11.8	1.3 - 39.4
Sample2	channel-crop	45.8 ± 21.5	13.5 - 86.9
	Forest scrub	**54.2 ± 21.1**	13.1 - 86.5
Sample3	channel-crop	**90.7 ± 7.3**	76.5 - 99.3
	Forest scrub	9.3 ± 7.3	0.7 - 23.5
Sample4	channel-crop	**90.8 ± 7.1**	76.9 - 99.4
	Forest scrub	9.2 ± 7.1	0.6 - 23.1
Sample5	channel-crop	**82.1 ± 12.5**	58.7 - 98.2
	Forest scrub	17.9 ± 12.5	1.8 - 41.3
Sample6	channel-crop	**90.7 ± 0.7**	75.5 - 99.4
	Forest scrub	9.3 ± 0.7	0.6 - 24.5
Sample7	channel-crop	**90.2 ± 0.7**	74.4 - 99.3
	Forest scrub	9.8 ± 0.7	0.7 - 25.6
Sample8	channel-crop	**89.8 ± 7.7**	75 - 99.2
	Forest scrub	10.2 ± 7.7	0.8 - 25
Sample9	channel-crop	**74 ± 16.7**	44.1 - 97.3
	Forest scrub	26 ± 16.7	2.7 - 61.6
Sample10	channel-crop	**81.3 ± 13**	56.9 - 98.4
	Forest scrub	18.7 ± 13	1.6 - 43.1
Sample11	channel-crop	**76.7 ± 14.9**	50.3 - 97.5
	Forest scrub	23.3 ± 14.9	2.5 - 49.7
Sample12	channel-crop	**82.3 ± 12.6**	58.5 - 92.6
	Forest scrub	17.7 ± 12.6	25.8 - 41.5
Sample13	channel-crop	**82 ± 12.6**	58 - 98.5
	Forest scrub	18 ± 12.6	1.5 - 42

Supplementary table 7.7. MIxSIAR source apportionment considering three group sources (i.e. channel bank, crop soil and forest-scrub) using colour parameters.

		MixSIAR	
SS sample	Sources	Average (%)	Quantile distribution 5% - 95%
Sample 1	Channel	33.6 ± 21.6	0.37 - 74.1
	Crop	**46.9 ± 18.7**	11.4 - 75.2
	Forest-scrub	19.5 ± 11.9	2.5 - 40.4
Sample 2	Channel	27.1 ± 18.3	2.9 - 62.4
	Crop	17.6 ± 11.2	2 - 38
	Forest-scrub	**55.2 ± 17**	22.5 - 79.8
Sample 3	Channel	22.6 ± 19.1	1.7 - 63
	Crop	**67.7 ± 18.5**	30.6 - 91.5
	Forest-scrub	**9.7 ± 7.7**	0.6 - 24.6
Sample 4	Channel	21.1 ± 18.4	1.3 - 59.6
	Crop	**69.9 ± 18.1**	32.8 - 92.7
	Forest-scrub	0.8 ± 7.2	0.6 - 22.8
Sample 5	Channel	31.8 ± 20.3	3.7 - 69.8
	Crop	**49 ± 19.1**	14.8 - 78.7
	Forest-scrub	19.1 ± 11.9	2.5 - 41
Sample 6	Channel	25.1 ± 20.3	1.8 - 67.2
	Crop	**65.4 ± 19.9**	25.5 - 91.2
	Forest-scrub	9.5 ± 7.6	0.7 - 25
Sample 7	Channel	25.4 ± 19.5	2 - 64.7
	Crop	**63.4 ± 18.7**	27.7 - 89.2
	Forest-scrub	11.2 ± 8.3	0.9 - 26.6
Sample 8	Channel	23.2 ± 19.4	1.6 - 64.3
	Crop	**66.6 ± 18.7**	28.4 - 91.1
	Forest-scrub	10.1 ± 7.8	0.7 - 25.7
Sample 9	Channel	33.7 ± 20.5	4.3 - 70.6
	Crop	**38.5 ± 18.7**	8.1 - 70.6
	Forest-scrub	27.8 ± 15.3	4.2 - 53.6
Sample 10	Channel	33.4 ± 21.2	3.6 - 72.3
	Crop	**46.5 ± 19.2**	11.7 - 75.9
	Forest-scrub	21 ± 12.8	2.7 - 43.7
Sample 11	Channel	33.1 ± 20.5	4.2 - 70
	Crop	**41.4 ± 18.1**	9.4 - 70.5
	Forest-scrub	25.5 ± 14.3	3.7 - 50.6
Sample 12	Channel	34.2 ± 20.9	4.1 - 72.6
	Crop	**45.7 ± 18.5**	12.2 - 74.6
	Forest-scrub	20.1 ± 12.2	2.3 - 42.2
Sample 13	Channel	35.3 ± 21.9	3.9 - 75
	Crop	**47 ± 21.2**	9.9 - 81.4
	Forest-scrub	17.7 ± 13	1.4 - 42.4

Supplementary table 7.8. Pearson correlation coefficients between total rainfall (Rtot), rainfall maximum intensity in 30 minutes (Imax-30), total water volume (Wvol), maximum discharge peak (Qmax), suspended sediment load (SSload), maximum suspended sediment concentration (SSCmax), one-day antecedent rainfall (AP1d), three days' antecedent rainfall (AP3d) and the hysteretic h index (h-index). p <0.01 significance in bold.

	Rtot	Imax-30	Wvol	Qmax	Qmean	SSload	SSCmax	SSCmean	AR1d	AR3d	AR7d	*h*-index
Rtot	1											
Imax-30	0.22	1										
Wvol	0.38	-0.02	1									
Qmax	0.23	0.26	**0.75**	1								
Qmean	0.21	-0.01	**0.57**	**0.83**	1							
SSload	0.38	0.36	**0.56**	**0.78**	**0.55**	1						
SSCmax	0.20	**0.67**	-0.05	0.37	0.11	**0.67**	1					
SSCmean	**0.44**	0.13	-0.12	0.11	0.20	0.37	**0.62**	1				
AR1d	**0.52**	-0.11	0.11	0.12	0.21	0.12	0.11	**0.48**	1			
AR3d	0.24	-0.25	0.06	0.15	0.36	0.09	0.01	0.30	**0.76**	1		
AR7d	0.21	-0.22	-0.01	-0.01	0.15	0.00	0.00	0.28	**0.69**	**0.83**	1	
h-index	0.05	-0.04	0.13	-0.06	-0.14	-0.20	-0.05	0.01	0.09	-0.15	-0.11	1

p<0.01 correlations in bold

Supplementary table 7.9. Total suspended sediment load ascribed to each source using MixSIAR results and considering only two sources (i.e. channel-crop and Forest-scrub).

2 sources ascription				
Integrated samples	Total Ssload (t)	Sources	Source proportion (%)	SSload (t)
Sample1	0.26	channel-crop	83.8	0.22
		forest-scrub	16.2	0.04
Sample2	0.71	channel-crop	45.8	0.33
		forest-scrub	54.2	0.38
Sample3	0.11	channel-crop	90.7	0.10
		forest-scrub	9.3	0.01
Sample4	11.56	channel-crop	90.8	10.50
		forest-scrub	9.2	1.06
Sample5	19.66	channel-crop	82.1	16.14
		forest-scrub	17.9	3.52
Sample6	8.14	channel-crop	90.7	7.38
		forest-scrub	9.3	0.76
Sample7	2.81	channel-crop	90.2	2.54
		forest-scrub	9.8	0.28
Sample8	0.96	channel-crop	89.8	0.86
		forest-scrub	10.2	0.10
Sample9	30.42	channel-crop	74	22.51
		forest-scrub	26	7.91
Sample10	0.07	channel-crop	81.3	0.06
		forest-scrub	18.7	0.01
Sample11	11.69	channel-crop	76.7	8.97
		forest-scrub	23.3	2.72
Sample12	7.59	channel-crop	82.3	6.24
		forest-scrub	17.7	1.34
Sample13	31.51	channel-crop	82	25.84
		forest-scrub	18	5.67

Supplementary table 7.10. Supp. Table 10. Total suspended sediment load ascribed to each source using MixSIAR results and considering three sources (i.e. channel, crop and Forest-scrub).

3 sources ascription				
Integrated samples	Total Ssload (t)	Sources	Source proportion (%)	SSload (t)
Sample 1	0.26	channel	33.6	0.09
		crop	46.9	0.12
		forest-scrub	19.5	0.05
Sample 2	0.71	channel	27.1	0.19
		crop	17.6	0.12
		forest-scrub	55.2	0.39
Sample 3	0.11	channel	22.6	0.02
		crop	67.7	0.07
		forest-scrub	9.7	0.01
Sample 4	11.56	channel	21.1	2.44
		crop	69.9	8.08
		forest-scrub	0.8	0.09
Sample 5	19.66	channel	31.8	6.25
		crop	49	9.63
		forest-scrub	19.1	3.76
Sample 6	8.14	channel	25.1	2.04
		crop	65.4	5.32
		forest-scrub	9.5	0.77
Sample 7	2.81	channel	25.4	0.71
		crop	63.4	1.78
		forest-scrub	11.2	0.32
Sample 8	0.96	channel	23.2	0.22
		crop	66.6	0.64
		forest-scrub	10.1	0.10
Sample 9	30.42	channel	33.7	10.25
		crop	38.5	11.71
		forest-scrub	27.8	8.46
Sample 10	0.07	channel	33.4	0.02
		crop	46.5	0.03
		forest-scrub	21	0.01
Sample 11	11.69	channel	33.1	3.87
		crop	41.4	4.84
		forest-scrub	25.5	2.98
Sample 12	7.59	channel	34.2	2.59
		crop	45.7	3.47
		forest-scrub	20.1	1.53
Sample 13	31.51	channel	35.3	11.12
		crop	47	14.81
		forest-scrub	17.7	5.58

8. In-channel alterations of soil properties used as tracers in sediment fingerprinting studies

ABSTRACT

Soil properties conservativeness is an essential requirement in sediment fingerprinting studies. Soil properties need to remain stable or vary in a predictable way on their transfer from sources to sinks in order to compare suspended sediment and soil samples with reliability and accuracy. The attention on conservative behaviour of soil properties is focused on the effects produced by the differences in the particle size and organic matter. However, in-channel biochemical alterations can occur, being these possible variations usually ignored. An experiment on the in-channel soil properties variations was performed using the most commonly soil properties used as tracers (i.e. colour, fallout radionuclides and geochemical elements) in sediment fingerprinting studies. Twenty-eight soil samples composed from different land uses were introduced in an intermittent stream channel of a small Mediterranean mountainous catchment. Samples were extracted in different time intervals (i.e. 7, 30, 60, 90, 150, 210, 270, 365 days) along one year. The experiment showed that changes on soil properties (coefficient of variation average 8.1 ± 8.8%) were generally lower than its spatial variability within the catchment (coefficient of variation average 16.3 ± 18.5%). Furthermore, the colour parameters were the most stable tracers with a coefficient of variation of 2.6 ± 2.2%. Finally, the general low variability observed in soil properties, and its strong correlations with the specific surface area and C further emphasize the role of particle size and organic matter in the conservative behaviour of soil properties.

Preliminary results

In-channel alterations of the most common soil properties used as tracers in sediment fingerprinting studies. **Paper in preparation**.

8.1. Introduction

Eroded soil particles can trigger alterations in their course over the sediment cycle in drainage catchments. These alterations can produce unknown effects on sediment tracing studies, leading to inaccurate results. Sediment fingerprinting is a standard methodology to trace suspended sediment origin (cf. Collins et al., 2020). The basis of its application is the comparison between different physical, geochemical and/or biochemical properties between soil samples collected in potential sediment source areas and sediment samples collected within the fluvial network (Collins et al., 1997; Klages and Hsieh, 1975; Wall and Wilding, 1976; Walling et al., 1979). However, the fingerprinting technique does not provide unequivocal source discrimination and results exhibit uncertainties. These uncertainties can be associated to sampling methodologies (e.g. Manjoro et al., 2017), spatial variability of source material properties (e.g. Du and Walling, 2017), statistical models (e.g. Haddadchi et al., 2014; Nosrati et al., 2014; Palazón and Navas, 2017) or due to alteration of soil properties during conveyance or temporal deposition within the river channel (e.g. Koiter et al., 2013). Accordingly, despite soil and sediment tracer values can be representative of source areas and discriminate them, are measurable and presumably remain stable or vary in a predictable way (Motha et al., 2002), alteration processes during mobilization and mixing along hydrological pathways it is known that they can occur (Koiter et al., 2013). The degree of alteration is, however, highly site-dependent, difficult to address, and often, not taken into consideration.

It is widely known that particle size and organic matter influence the concentrations of certain soil properties, preventing direct comparison between source material and suspended sediment (e.g. Crockford and Olley, 1998; Hill et al., 1998; Horowitz and Elrick, 1987; Koiter et al., 2018; Laceby et al., 2017). Sediment specific surface area (SSA) affects the reactivity of sediment particles, where smaller fractions are more chemically active than coarser particles (Foster and Charlesworth, 1996; Horowitz et al., 1993). For example, fallout radionuclide activity (e.g. $^{210}Pb_{ex}$, ^{137}Cs) is normally higher in fine particles, and usually shows a non-linear relationship with SSA in particles >1 m^2 g^{-1} (Fan et al., 2014; He and Walling, 1996) as well as with some

geochemical elements (Russell et al., 2001). Conversely, organic matter content highly correlates with several soil elements under certain conditions, enriching humic and fulvic substances (Hirner et al., 1990) or altering colour properties (Ben-Dor and Banin, 1995; Pulley and Rowntree, 2016). Differences between sources and sediment material were normally addressed by sieving to a specific particle size (e.g. He and Walling, 1996), removing the organic content (e.g. Pulley and Rowntree, 2016) or using correction factors (Collins et al., 1997; Russell et al., 2001). Limitations associated to tracer conservatism have also been solved by defining an optimal set of tracers for statistically discerning those with conservative behaviour. For instance, a widespread method is the use of a Discriminant Function Analysis (DFA) to select the optimum tracer set and range tests to exclude potentially non-conservative tracers (Collins and Walling, 2002; Collins et al., 1997; Walden et al., 1997; Wilkinson et al., 2013). However, other statistical procedures have been used in the sediment fingerprinting literature, such as Principal Component Analysis (PCA; e.g. Walling, 2005), Mann–Whitney *U* test (e.g. Carter et al., 2003), Wilcoxon rank-sum test (e.g. Juracek and Ziegler, 2009), Tukey test (e.g. Motha et al., 2003), *t* test (e.g. Hancock and Revill, 2013), linear trends between tracers using in bivariate scatterplots (James and Roulet, 2006; Rose et al., 2018), conservativeness index and a ranking based on consensus (Lizaga et al., 2020) or using tracer-particle size relationships and source mixing polygons (Smith et al., 2018).

Together with the effect of particle size and organic matter, other sediment alteration processes might occur, including chemical precipitation, diagenesis, or the addition of new atmospheric elements such as N, S and ^{210}Pb (Koiter et al., 2013; Owens et al., 2012; Wilkinson et al., 2009). Transformations can be remarkable during transport and in temporary sediment accumulation deposits (Koiter et al., 2013). Abrasion and disaggregation processes can alter the particle size and shape of sediment transferring iron oxide coats to smaller particles, influencing mineral magnetic properties (Crockford and Olley, 1998). Some sediment properties associated with highly reactive particulate carrier phases such as Fe and Mn oxyhydroxides, particulate organic matter, carbonates, and sulphides, can be dissolved reducing its concentration in the suspended load (Dabrin et al., 2021). Biochemical processes can also influence

elements like K (Withers and Jarvie, 2008). In addition, some metals and fallout radionuclides (e.g. ^{137}Cs) can be released from sediment deposits to water flow (Foster et al., 2006; Hudson-Edwards et al., 1998).

As far as we know, few studies have been specifically designed to investigate the conservative behaviour of sediment tracers. Motha et al. (2002) studied the conservativeness of fallout radionuclides (i.e. ^{137}Cs and $^{210}Pb_{ex}$), major elemental geochemistry and mineral magnetism of soil properties during the sediment generation process. These authors simulated three different rainfall conditions over five 200 m^2 plots (south-west Australian) and compared the properties of source soil and mobilized sediment. They found differences in particles size and organic matter content between the eroded sediment and the soil samples analysed, deciding to use correction factors. After their use to address differences in particle size and organic matter it was stated that the major part of mineral magnetic, geochemistry elements and fallout radionuclides remained conservative in the mobilization processes. However, concentrations of Fe_2O_3, Al_2O_3, the sum of molecular proportions of CaO** (Ca in the silicate fractions), Na_2O, K_2O and Al_2O_3 and the magnetic properties IRM_{850} and χ showed a non-conservative behaviour at least in one case. Koiter et al. (2018) studied the conservative behaviour of geochemical soil properties through the mobilisation process simulating rainfall over plots in two agricultural catchments in Canada. After the analysis of soil and mobilised material sieved at <63 µm, they found a fine-grain and organic material enrichment in the eroded samples. As a consequence, they applied particle size and organic matter correction factors to compare geochemical element concentrations between sources and eroded material. Corrections factors resulted in over-corrections for most elements, increasing the differences in concentrations between mobilized soil and source soil. In addition, they observed relations of SSA and soil organic carbon content with the concentration of different elements being specific for every individual element and catchment. To test the conservativeness of soil spectral signatures after in-channel submersion, Poulenard et al. (2012) introduced different sediment source samples sieved to <63 µm within a stream (French southern Alps). Samples were placed in microporous bags and remained submersed during different intervals of time (i.e. 1 day, 1 week and 2

weeks). After collection, samples were used for source ascription (Partial Least Square analysis). The authors concluded that differences in the results associated to different submersion times were between 5 and 15% for the dominant source, and considered that spectral signatures were sufficiently conservative to be used as tracers. The conservative experiment was replicated by Legout et al. (2013) in the same catchment in March 2009. Forty-five artificial samples sieved at <63 µm were introduced in double layer nylon porous bags with 20 µm mesh size after verifying that the double layer allowed the water renewal without the clogging by external suspended sediment with limited material loss. Samples were submersed and collected after 1, 7, 14, 35 and 63 days. After collection, samples lost a mass average of 5%. Considering all different sources and submersion intervals, all spectrometric parameters experimented low variations (<10 %), being the marls and molasses samples more sensitive to changes than the limestone material. Finally, Uber et al. (2019) –following the same methodology described by Legout et al. (2013)– assessed the potential effect of biogeochemical alterations on spectrometric tracers after submersion times of 1, 3, 7, and 22 days. Results showed variations <10% with an average < 4% for all parameters.

Simulation of hypothetical natural conditions is difficult for observing possible changes in soil and sediment properties during in-channel transport and deposition. Main constraints can be associated to the rather large spectrum of control variables and driving forces of erosion, transport and deposition, the design of appropriate sampling strategies, and the large variability in soils and sediment tracer values across different study sites. As a consequence, results might vary in different catchments and regions. Submersion experiments to investigate in-channel alterations of soil properties have never been performed in Mediterranean catchments, mostly characterized by temporary regimes. In the case of intermittent rivers, the hydrological regime exhibits large inter-annual contrasts (Fortesa et al., 2020b). This current paper is based on the studies by Motha et al. (2002), Koiter et al. (2018), Poulenard et al. (2012), Legout et al. (2013) and Uber et al. (2019) with the aim to investigate eventual in-channel transformation of soil properties in a Mediterranean catchment. Special attention was paid to the fact that many Mediterranean streams are ephemeral and have an

intermittent regime (Estrany et al., 2011). Under this context, different soil samples were introduced in an intermittent stream channel of a small Mediterranean mountainous catchment (Es Fangar, Mallorca, Spain) during one year (i.e. November 2018– 2019). Samples were exposed to natural and contrasted hydro-meteorological conditions to discern soil properties more prone to biochemical in-channel alteration. Tracers in-channel variability was compared with its spatial variability within the catchment, and variations were correlated with SSA and C content to evaluate the influence of particle size and organic matter.

8.2. Study area

The Es Fangar Creek catchment (3.4 km^2; Figure 8.1A and B) is located at the northern part of the Mallorca Island (Western Mediterranean Sea, Spain), in the mountainous area of the Serra de Tramuntana. Climate is classified as Mediterranean temperate sub-humid according to the Emberger classification (Guijarro, 1986). Mean annual rainfall is 926 mm yr^{-1} (1964-2017; Biniatró AEMET station, located 1.1 km west from the study area) with a coefficient of variation ca. 23%. The average annual temperature is 15.7°C. The hydrological regime is intermittent flashy (49% of zero-flow days; Fortesa et al., 2020b). Annual runoff coefficients ranged from 2.9% to 14.2% (average of 10.4%) and quickflow from 9.9% to 45% (average of 33%). The 80% of the sediment load is exported during autumn and winter, with an annual average sediment yield of 5.38 t km^{-2} y^{-1} (Fortesa et al., 2020a). The lithology is mainly composed by massive calcareous and dolomite materials from the Lower Jurassic. Dolomite and marls formations from the Triassic (Rhaetian) dominate in the upper parts, whereas Jurassic limestones and Cretaceous marls are found in the valley bottoms. Altitudes range between 72 and 404 m.a.s.l., with an average slope of 26%. Land use occupation is forest (47%), rainfed herbaceous crops fields (36%) and scrubland (17%). In addition, 16% of the catchment is covered by dry-stone agricultural terraces (Figure 8.1C).

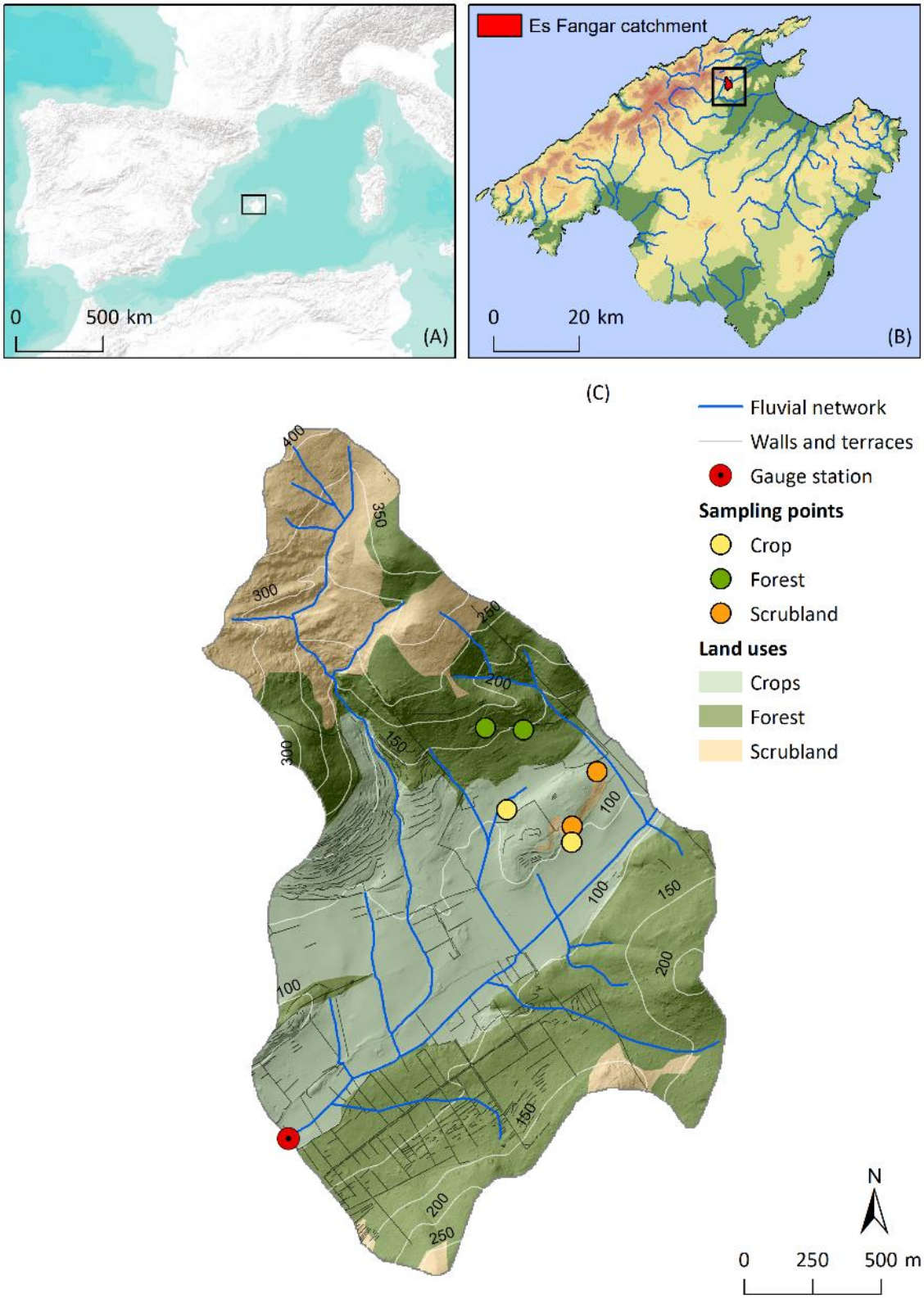

Figure 8.1. (A) Map showing the location of Mallorca in the Western Mediterranean. (B) Location of Es Fangar creek catchment within Mallorca island. (C) Sampling points, gauge station, drainage network and terraced areas over land uses map.

8.3. Material and methods

8.3.1. Hydrological monitoring

A gauging station to continuously monitor water and suspended sediment fluxes was installed in 2012 in the Es Fangar Creek (i.e. Figure. 8.1C). The station was equipped with a Campbell CS451 pressure probe and an OBS-3+ turbidimeter with a double measurement range (0-1,000 / 1,000-4,000 NTU) and a wipe system. A Campbell CR200X logger stored 15-minutes average values of water stage and turbidity (based on 1-minute readings). In addition, a tipping bucket pluviometer was installed in October 2014 at 500 m.a.s.l. and at ca. 2.5 km away from the Es Fangar gauging station (Figure 8.1C). It was positioned at 1 m above the ground and connected to a HOBO Pendant G Data Logger - UA-004-64 recording rainfall at 0.2 mm resolution.

8.3.2. Soil sampling, pre-treatment and field experiment

The sampling strategy was designed considering the three main catchment land use types (i.e. forest, crop fields and scrubland; Figure 8.1C) as potential surficial sediment sources. Vegetation cover and land uses are the most important driven factors in erosion hillslope processes (García-Ruiz, 2010; Kosmas et al., 1997; Thornes, 1990) being an optimal grouping for catchment management. Soil bulk samples were collected in March 2018 from 0 to 2 cm depth in six different plots (3 m^2 each) encompassing every land use category. Sampling points (Figure 8.1C) were selected according to accessibility and soil availability on hillslopes with an active sediment slope-to-channel connectivity. Note that a first attempt was made to collect overland flow during rainfall simulation experiments (Garcia-Comendador et al., 2018). However, despite simulating >50 mm h^{-1} rainfall intensities, the amount of mobilised soil was insufficient to collect enough material to meet analytical requirements. Therefore, it was decided to collect surface soil samples, which are hereafter referred to as ‘in-channel samples’.

Results of in-channel variations for each soil property were compared with tracer spatial variability within the catchment - as to address eventual impacts on suspended sediment fingerprinting results. Consequently, source tracer data collected across the

catchment (hereafter referred as 'catchment source samples') and presented in Chapter 7 was used.

Bulk samples were oven dried at <40 °C and disaggregated using a pestle and a mortar. Samples were then homogenised per land use type and sieved to <63 µm fraction (ca. 1 kg for every land use). The latest as to be able to compare results with the catchment source samples used in Chapter 7), which were sieved to <63 µm. In addition to the fact that sieving to this fraction size is widely used in sediment fingerprinting studies (e.g. Koiter et al., 2018), sieving to different fractions was discarded due to the large amount of soil used in the experiment. Thirty-one in-channel samples were generated in total: nine for each land use (60 g each), which were positioned in the stream channel, and four extra samples from the crop plots that were introduced inside a time-integrated sediment sampler (referred as 'TIS samples'; Table 8.1).

Each soil sample was split into three 20 g subsamples introduced in 5x7 cm white polyamide bags with a 25 µm mesh Ø, and sealed using cable ties (Figure 8.2A). Subsamples were placed inside a larger sealed bag of the same mesh (Figure 8.2B).

Samples were then introduced into the stream channel ca. 2 m downstream the Es Fangar gauging station (Figure 8.1D), where a cross-section with a rectangular broad-crested concrete weir was built for measuring low water stages (see dimensions in Figure 8.2E, F). Samples were located 70 cm downstream from the weir Eight 70 cm steel corrugated bars were nailed into the channel bed and sample bags were fixed to the metal bars using cable ties. Water height had to reach 17 cm at the pressure probe location to completely cover the samples. The TIS samples were introduced inside a time-integrated sediment sampler (Phillips et al., 2000) fixed at 5 cm from the channel bed (Figure 8.2C). The water flow reached the inlet hole at ca. 10 cm high. Therefore, TIS samples were not only in different conditions of moisture, temperature and insolation, but also affected by partial mobility inside the sampler.

Table 8.1. List of samples used in the conservativeness experiment. Highlighted in green the samples extracted during the wet period, and in yellow samples extracted during the dry period. TIS refers to the fact that samplers were introduced inside a time-integrated sediment sampler. 'Days submersed' and 'Days dry' refer to the total number of days that the samples were immersed and outside the water, respectively.

Sample type	ID	Days in channel	Days submersed	Days dry	Baseflow index (%)	Initial mass (g)	Mass at collection (g)
Forest	Forest 0	0	0	0	0	60	-
	Forest 1	7	7	0	89	60	58.14
	Forest 2	30	22	8	24	60	57.75
	Forest 3	60	29	31	12	60	57.54
	Forest 4	90	35	55	9	60	57.93
	Forest 5	150	35	115	8	60	58.3
	Forest 6	210	35	175	8	60	58.22
	Forest 7	270	35	235	8	60	59.01
	Forest 8	365	37	328	8	60	57.05
Crop	Crop 0	0	0	0	0	60	-
	Crop 1	7	7	0	89	60	57.18
	Crop 2	30	22	8	24	60	57.79
	Crop 3	60	29	31	12	60	57.17
	Crop 4	90	35	55	9	60	58
	Crop 5	150	35	115	8	60	57.55
	Crop 6	210	35	175	8	60	58.1
	Crop 7	270	35	235	8	60	57.23
	Crop 8	365	37	328	8	60	57.69
Scrubland	Scrubland 0	0	0	0	0	60	-
	Scrubland 1	7	7	0	89	60	58.17
	Scrubland 2	30	22	8	24	60	58.24
	Scrubland 3	60	29	31	12	60	57.76
	Scrubland 4	90	35	55	9	60	57.85
	Scrubland 5	150	35	115	8	60	58.14
	Scrubland 6	210	35	175	8	60	57.05
	Scrubland 7	270	35	235	8	60	57.87
	Scrubland 8	365	37	328	8	60	57.22
TIS samples	TIS 1	60	60	0	58	18.86	16.76
	TIS 2	210	108	102	60	31.73	29.83
	TIS 3	270	108	162	60	47.49	45.29
	TIS 4	365	111	254	58	59.48	57.48

Eight time intervals were selected to extract the samples after starting the experiment at t=0 (i.e. 7, 30, 60, 90, 150, 210, 270, 365 days). Number of days within the channel and also submersion days for each sample are listed in Table 8.1.

Total rainfall during the study period was 316.8 mm. Total water volume ca. 175,000 m^3, with a mean discharge of 0.01 m^3 s^{-1}, and a maximum peak of 1.31 m^3 s^{-1} (Figure 8.3). Total sediment load was 2.06 t, mean suspended sediment concentration of 1.19 mg l^{-1} with a maximum peak of 321 mg l^{-1}. Runoff was present 38% of the time. Soil samples were submerged between 7 to 37 days. The baseflow index (i.e. proportion of groundwater in relation to discharge; (Sear et al., 1999)) ranged between 89 to 8%,

whilst TIS samples were submersed between 60 to 111 days with a baseflow index ranging between 58 to 60% (Table 8.1).

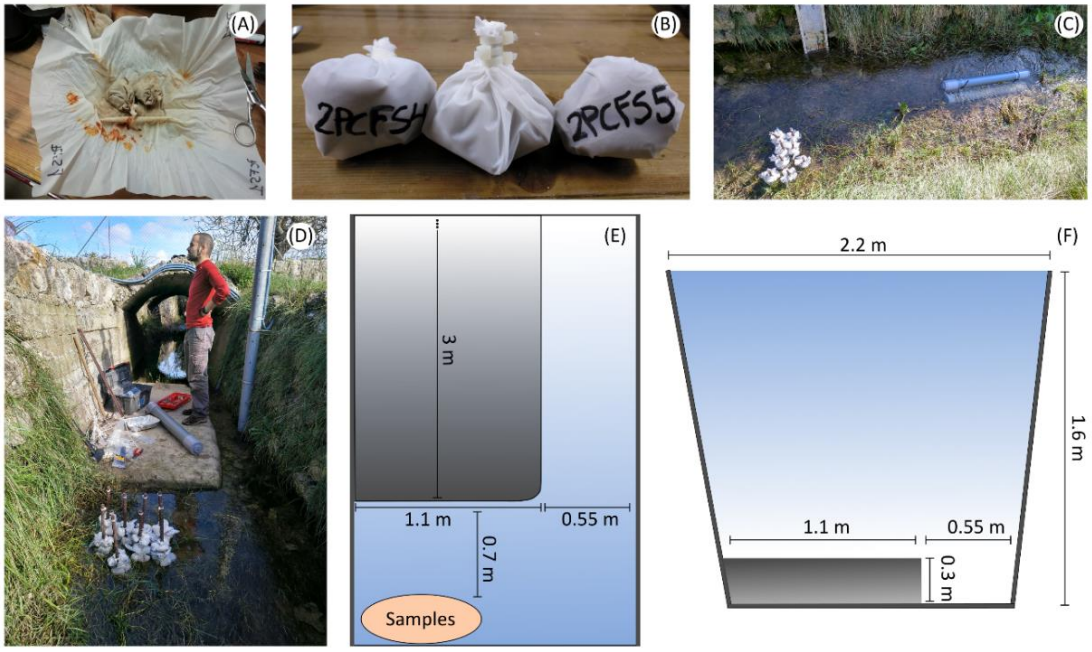

Figure 8.2. Pictures of (A) 20 g subsamples bags over the larger piece of mesh, (B) sealed samples with the three subsamples bags inside, (C) location inside the channel and distance between samples and time-integrated sediment samplers, (D) upstream view of Es Fangar stream with the samples nailed to the bed channel and diagram of the plan (E) and transverse (F) proportions of the cross section in the Es Fangar outlet

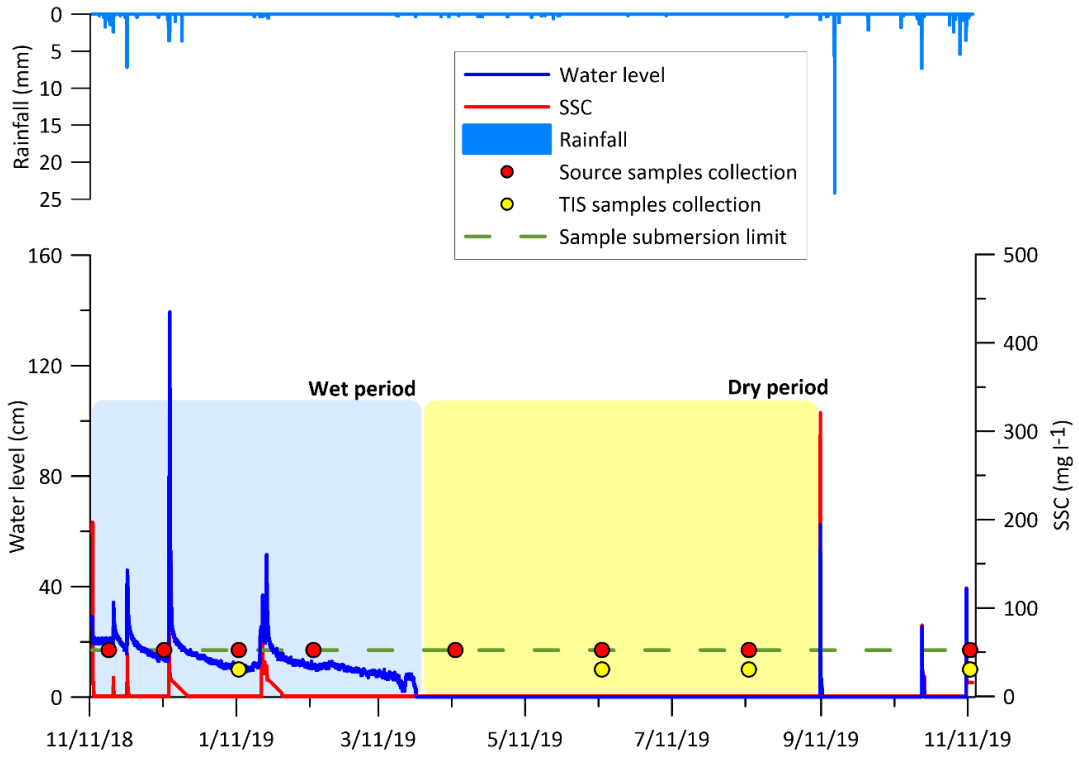

Figure 8.3. Water level, hyetograph and sedigraph at the Es Fangar station during the study period, November 2018-November 2019. Points indicate sample collection dates (in-channel samples in red, TIS samples in yellow) and the green discontinued line the submersion limit of the in-channel samples.

8.3.3. Laboratory analysis

Particle size distribution and the SSA for all samples were measured using a Malvern Mastersizer 3000 (Malvern instruments, Ltd.) at the Luxembourg Institute of Science and Technology (LIST, Luxembourg). Total C and N were measured by high-temperature combustion (Elementar vario MACRO cube, Hanau, Germany) at LIST. Using gamma spectrometry, $^{210}Pb_{ex}$ and ^{137}Cs activity ($Bq \cdot kg^{-1}$) was measured at the Environmental Radioactivity Laboratory of the University of the Balearic Islands (Spain) using a high-purity coaxial intrinsic germanium (HPGe) detector.

Diffuse reflectance was measured with an ASD FieldSpect-II spectroradiometer in a dark room at 1 nm steps over the 400-2500 nm range. The soil and sediment samples were placed in transparent PVC round petri dishes (4.7 cm diameter; Pall Corporation) and smoothed with a spatula to homogenize the surface roughness avoiding micro shadow effects. The spectrometer optical lens was installed in a tripod perpendicularly over a flat surface, at 10 cm of the reference standard panel of known reflectivity (Spectralon). The samples and the spectralon were illuminated in an angle of 30° using a 50-w quartz halogen lamp placed at c.a. 30 cm of distance. Following the International Commission on Illumination (CIE, 1931), we computed the CIE xyY colour coefficients (i.e. cie x, cie y and cie yy) from the spectra reflectance measurements as well as the RGB colour values (i.e. red, green and blue). We then used the ColoSol software, developed by Viscarra Rossel (Viscarra Rossel et al., 2006), to estimate the Munsell HVC (i.e. Munsell H, Munsell V and Munsell C), CIE XYZ (i.e. cie X, cie Y and cie Z), CIE LAB (cie L, cie a* and cie b*), CIELUB (i.e. cie L, cie u* and cie v*), CIELHC (i.e. cie L, cie H and cie C), and decorrelated RGB (i.e. HRGB, IRGB and SRGB) colour parameters, as well as the redness index (hereinafter RI) and Helmoltz chromaticity coordinates (i.e. DW nm, Pe %).

Samples were digested according to the microwave digestion USEPA 3051A method, as follows. Initially, pulverized soil samples (0.5 g) were transferred into polytetrafluoroethylene tubes, where 9 ml of HNO_3 and 3 ml of HCl (i.e. aqua regia), of high analytical purity, were added. Samples were placed in a microwave oven (Multiwave GO, Anton Paar, Austria) for 5 min on a temperature ramp, the necessary

time to reach 175 °C. Then, the temperature was maintained for an additional 10 minutes. After digestion, all extracts were transferred to 100 ml flasks, filling with ultrapure water (Millipore Direct-Q System) and filtered through 0,45 µm nylon filters (Labbox Labware, S.L). High-purity acids were used in the analyses (PamReac ApplyChem, SLU). Glassware was cleaned and decontaminated in a 10% nitric acid solution for 24 hours and then rinsed with distilled water. Calibration curves for metals determination were prepared from standard 1,000 mg l^{-1} (Sharlau, Spain). The concentrations of metals in the extracts were determined by ICP-AES (DV Optima5300, Perkin Elmer®, Inc.) equipped with a GemCone pneumatic nebulizer for viscous solutions and solutions with high content of dissolved solids (Waltham, MA, USA). Following the recommendations by the United States Environmental Protection Agency (2000), values below the detection limits were assigned the detection limit value for each element.

8.3.4. Evaluation of changes in sediment properties

The Shapiro-Wilk ($p < 0.05$) normality test was performed to check the particle size distribution data. The Wilcoxon signed-rank test was used to check if particle size distributions changed during the experiment, by comparing original samples (t=0) and the samples deployed in the channel, for every source category. Coefficients of variation (CV) expressed in % were calculated for all soil properties. Data was also divided in four time intervals to identify when major changes occurred: initial submersion (i.e. 0-7 days), constant flow (wet period, 7-90 days), the period without flow (dry period, 150-270 days) and the whole year (Figure 8.3 and Table 8.1). In addition, catchment source tracer data from forest (n= 6), crop (n= 5) and scrubland (n= 5) (Chapter 7) were used to calculate the spatial variability of the investigated soil properties within the catchment. Pearson's and Spearman's correlation coefficients were computed to identify eventual linear or monotonic correlations between the different soil properties and (i) grain size (expressed as SSA; $m^2\ kg^{-1}$), and (ii) C content in percentage as an approximation to organic matter content.

8.4. Results

8.4.1. Variability of soil properties in submersed samples

A mass loss was detected in all submerged samples (average of 2 ± 0.4 g, Table 8.1). However, no significant differences in particle size distribution were observed between the original samples (i.e. not submerged) and the rest (i.e. source and TIS samples; Figure 8.4). SSA CVs are < 10% for all samples during all the study period (Figure 8.4E and Figure 8.5D). On the other hand, the average spatial variability observed in the catchment source samples was of 19.8 ± 11.7% for the tree source types (Figure 8.6A).

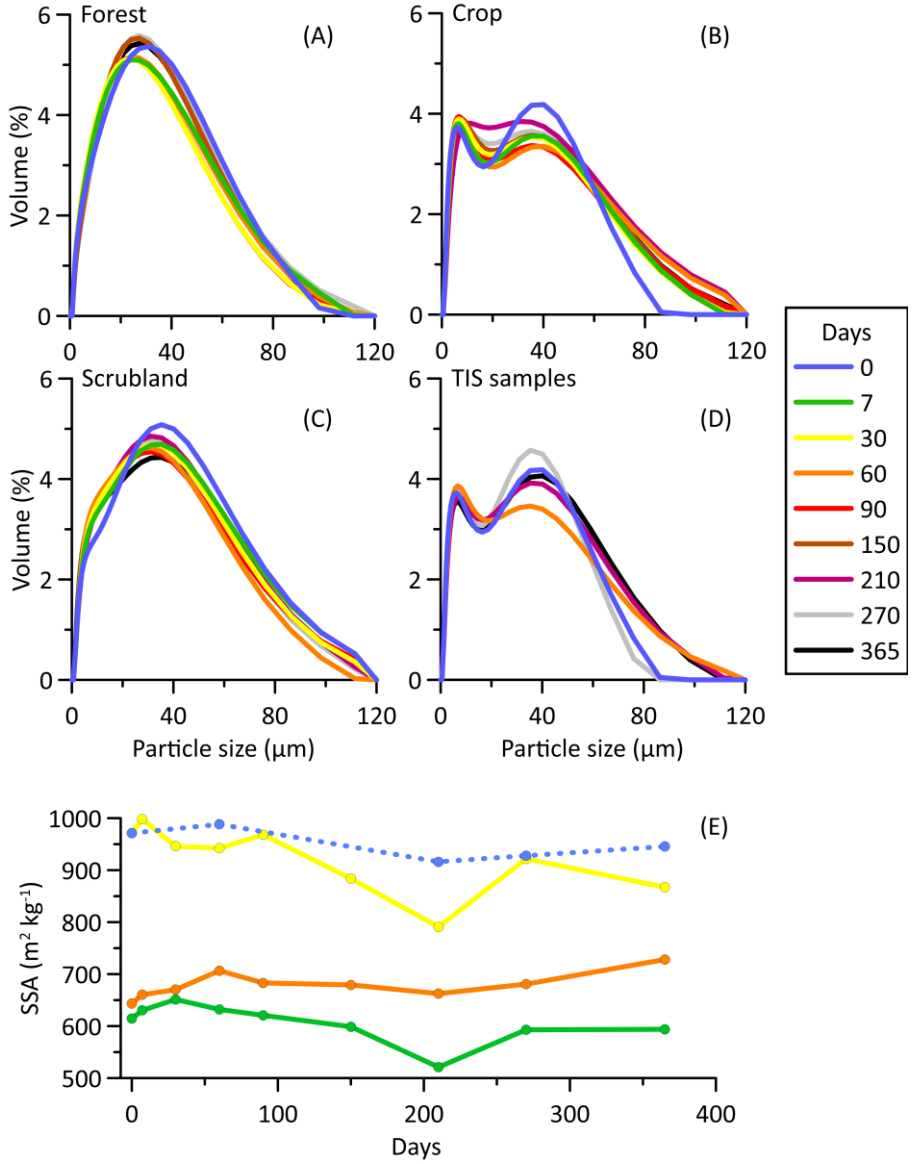

Figure 8.4. Particle size distribution of (A) forest, (B) crop, (C) scrubland, (D) TIS samples and (E) SSA at the different sampling times (E).

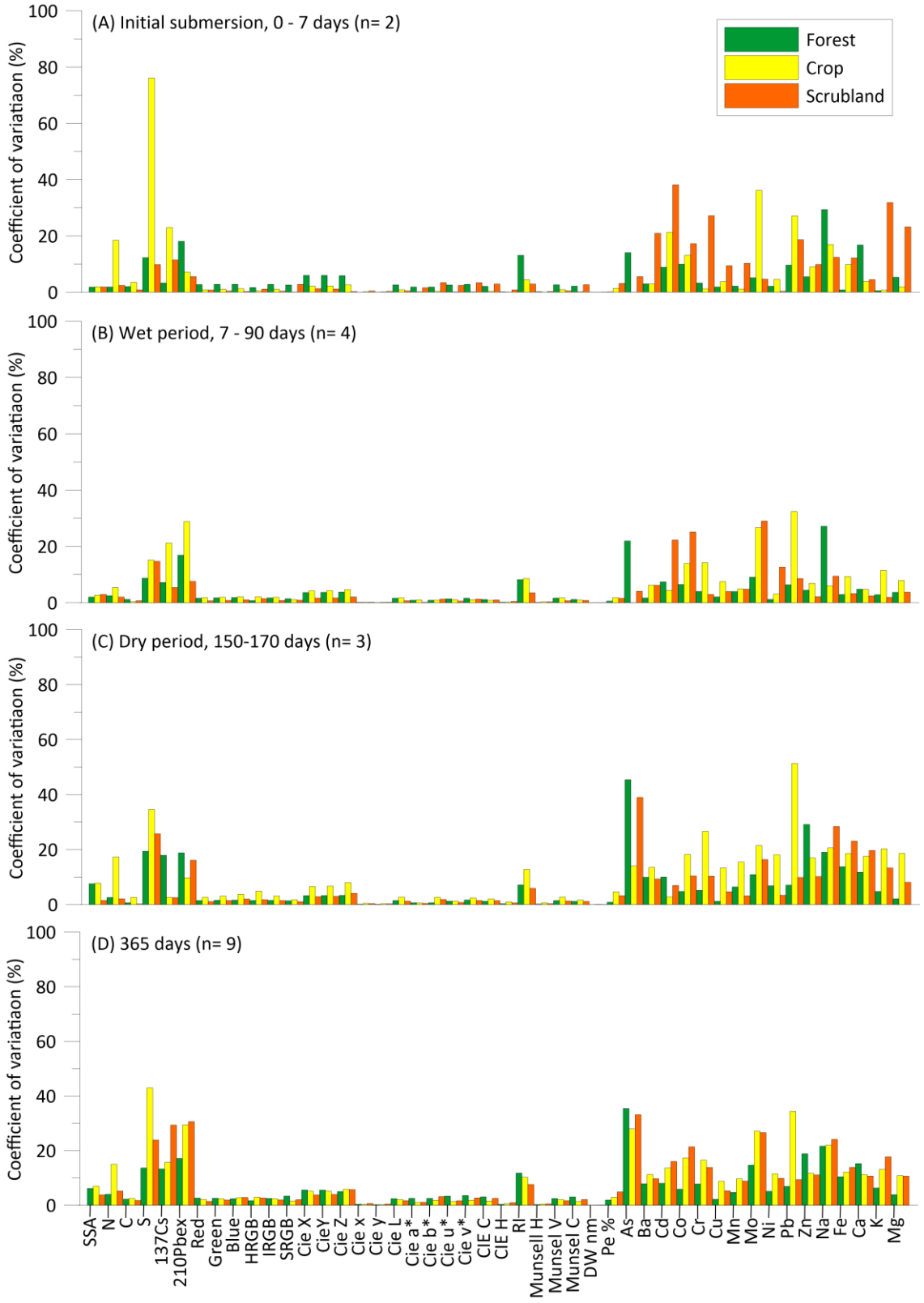

Figure 8.5. Coefficient of variation of soil properties measured on the in-channel samples during four different periods: (A) the seven first days of submersion, (B) the wet period, (C) the dry period and (D) the whole year.

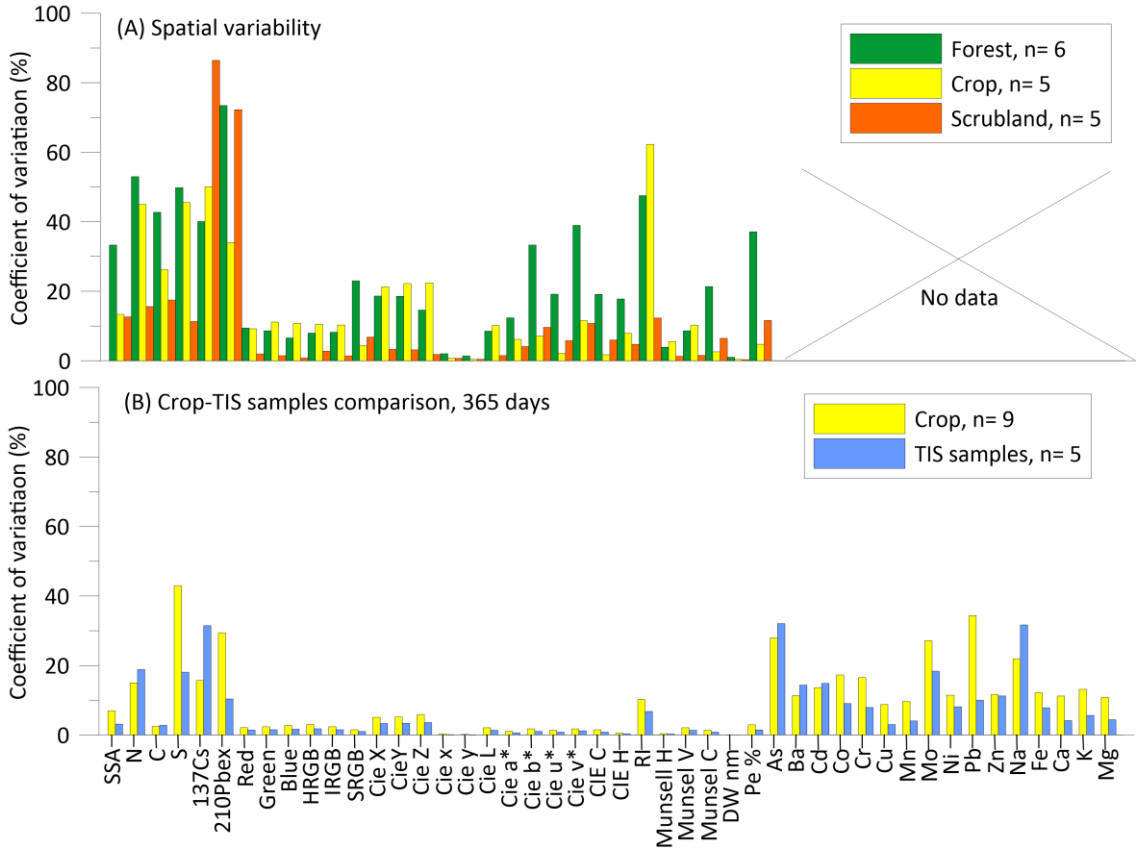

Figure 8.6. (A) Coefficient of variation of FRNs activity and colour properties measured in the catchment source samples (Chapter 7), and (B) coefficient of variation of soil properties measured on the in-channel samples collected in crop fields and TIS samples.

Nitrogen (N) and Carbon (C) CVs for all in-channel samples and the TIS samples were < 20% (Figure 8.5D and Figure 8.7). Sulphur (S experimented a higher variability, especially in crop samples (Figure 8.5D). Changes occurred principally in the first 7 days, with a crop CV of 76.1% between the original material and the first sample collection (Figure 8.5A and Figure 8.7). In addition, the crop CV of S when looking at all the study period (i.e. 43%) was higher in comparison with the CV observed in the TIS samples (18%, Figure 8.6B). S variability of in-channel crop samples was similar to spatial variability measured in the catchment source samples from crop lands (CV of 45.5%, Figure 8.6A).

^{137}Cs and $^{210}Pb_{ex}$ CVs measured on the in-channel samples for all the study period ranged between 10.4 and 31.4% (Figure 8.5D and Figure 8.7), being slightly higher in $^{210}Pb_{ex}$. The variability was lower in comparison with the spatial variability measured on the catchment source samples for the three source types, with CVs ranging from 40.1 to 86.5 % for ^{137}Cs, and from 33.9 to 73.4% for $^{210}Pb_{ex}$ (Figure 8.6A).

All colour parameters presented CVs <10% when looking at all the study period except Redness Index (RI) in forest (CV = 11.8%) and crop samples (CV = 10.2%, Figure 8.5, 8.7 and Supplementary figure 8.1). Colour spatial variability within the catchment was also low, with an average CV of 10.3 ± 11.5% reaching a CV >40% only in the RI measurements for forest and crop samples (Figure 8.6A).

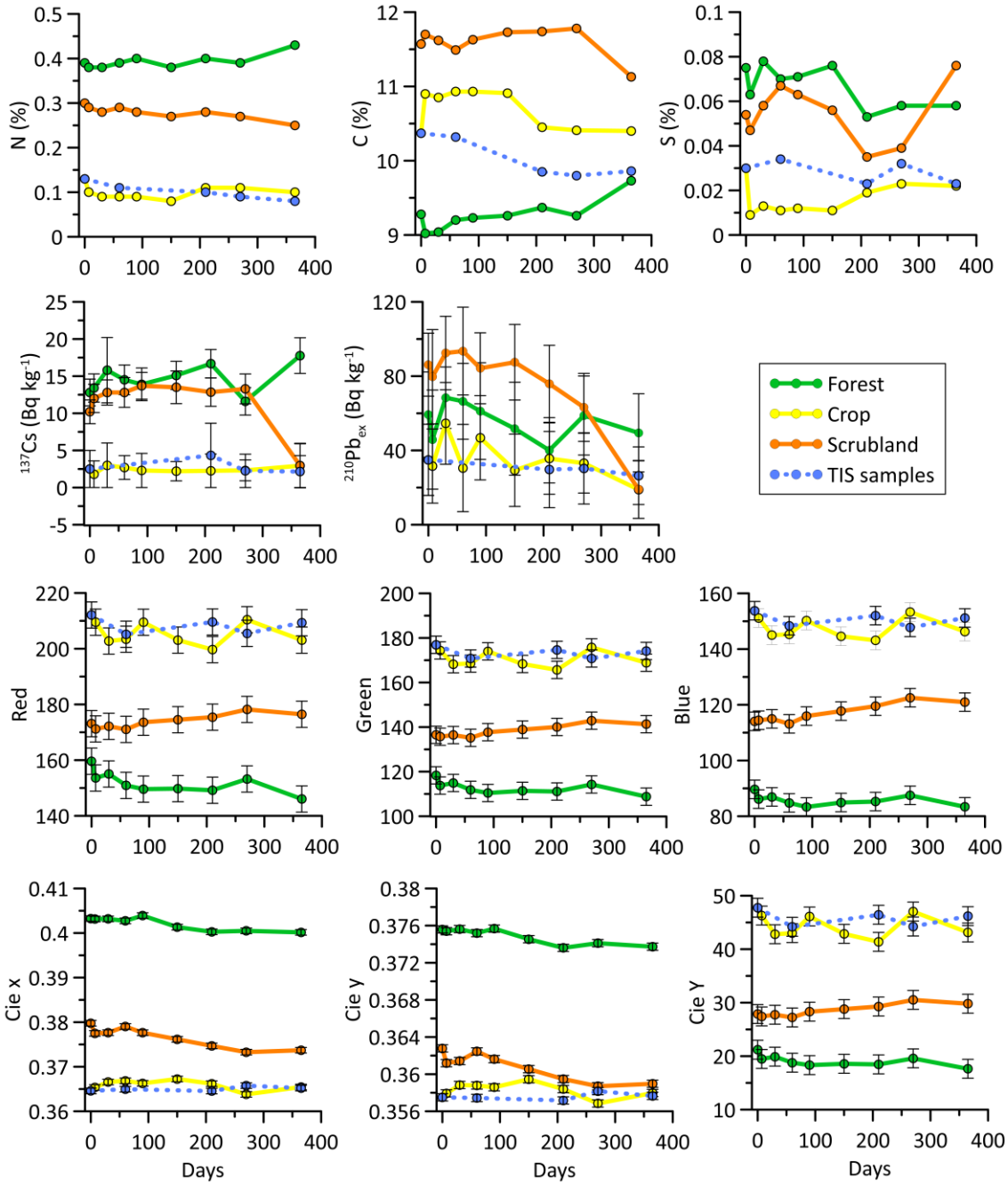

Figure 8.7. Temporal variability of N, C, S (%), ^{137}Cs, $^{210}Pb_{ex}$ (Bq kg^{-1}) red, green, blue, cie x, cie y and cie Y tracer values measured on the in-channel samples.

Geochemical properties showed more variability than colour properties. For all the study period, Ba, Cd, Co, Cr, Cu, Mn, Ni, Zn, Fe, Ca, K and Mg CVs of the in-channel samples were < 25% (Figure 8.5D and 8.8). However, As, Mo, Pb and Na showed CVs ranging between 25 and 40% at least in one of the in-channel source categories or TIS samples (Figure 8.5D and 8.8).

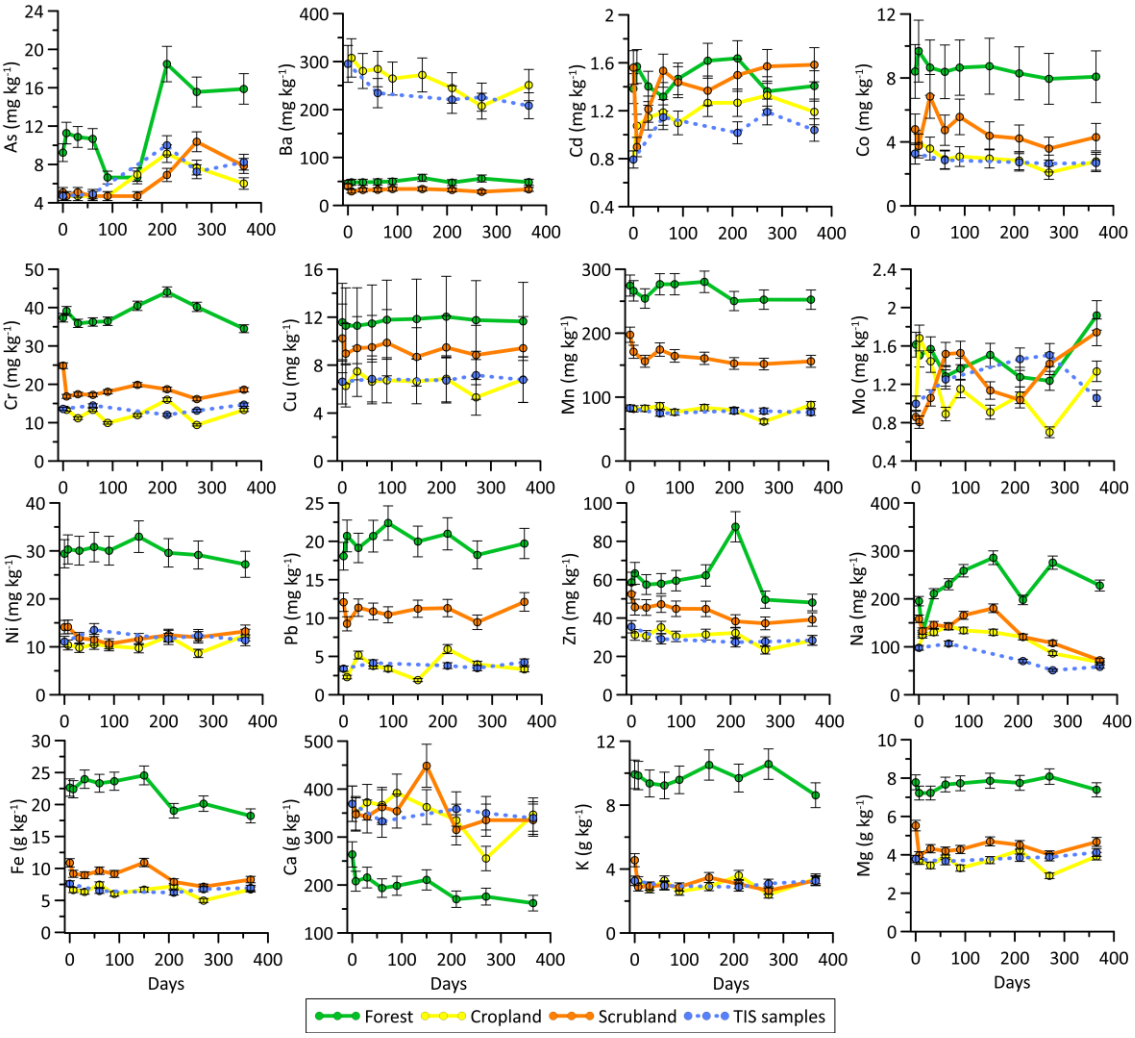

Figure 8.8. In-channel temporal variability of As, Ba, Cd, Co, Cr, Cu, Mn, Mo, Na Fe, Ca, K, Mg measured on the in-channel samples

No significant changes were observed in the variability of most of the soil properties depending on the channel conditions (i.e. wet and dry period; Figure 8.5). During the initial submersion (i.e. 0-7 days) S showed the highest CV (76% for crop samples), followed by Cd, Cr, Mo, Pb, Na and K with CVs between 25 and 40% in different in-channel source categories (Figure 8.5A). Regarding the wet period, CVs between 25 and 40% only were detected in Na for forest samples, $^{210}Pb_{ex}$, Mo and Pb for crop

samples and Co and Ni for scrubland samples (Figure 8.5B). Finally, during the dry period (Figure 8.5C), the highest CVs were detected in forest samples for AS (45%) and crop samples for Pb (51%). Looking at the overall period (i.e. 365 days), the highest average CVs considering all in-channel source types (i.e. forest, crop and scrubland) were measured in S (27 ± 15%), $^{210}Pb_{ex}$ (26 ± 7%), As (32 ± 4%) and Mo (23 ± 7%).

8.4.2. Correlation of soil properties with grain size and carbon content

Pearson's correlation coefficient showed a $p<0.01$ positive or negative C correlations with 10 and 24 parameters respectively (Figure 8.9A). The positive correlations $R\geq 0.8$ were detected only with two parameters (i.e. Cie b* and DW nm). However, 10 soil parameters showed inverse correlations $R\geq -0.8$ with C (i.e. SRGB, Cie y, Cie v*, Cie C, Munsell C, Ni, Fe, Ca, K and Mg.

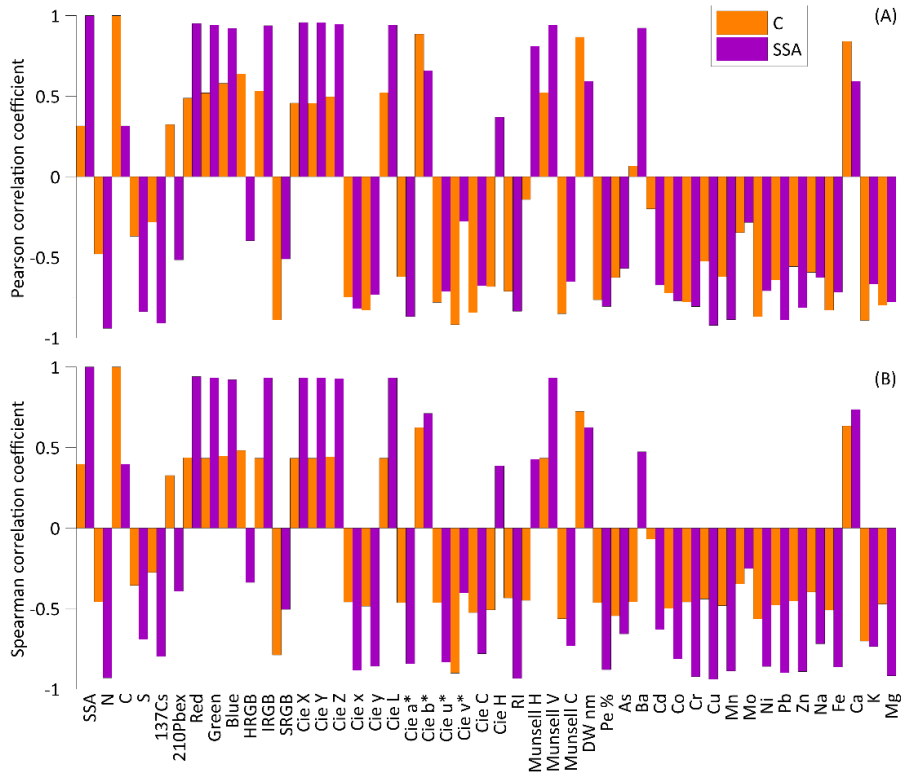

Figure 8.9. (A) Pearson correlation coefficient between C (orange) and SSA (purple) and the rest of soil parameters analysed. (B) Spearman correlation coefficient between C (orange) and SSA (purple) and the rest of soil parameters analysed

No significate correlations were detected between C and SSA, S, ^{137}Cs, $^{210}Pb_{ex}$, Munsell H, Ba, CD and Mo. Moreover, SSA is correlated positively and negatively ($p<0.01$) with 40 of the 46 soil parameters considered (Figure 8.9A). The positive correlations were

R≥ 0.8 with 11 soil parameters (i.e. Red, green, Blue, IRGB, Cie X, Cie Y, Cie Z, Cie L, Munsell H, Munsell V and Ba) and negative R≥ -0.8 with 12 (i.e. N, S, ^{137}Cs, Cie x, Cie a*, RI, Pe%, Cr, Cu, Mn, Pb and Zn). No significate correlations were detected between SSA and C, Cie v*, Cie H and Mo. Applying the Spearman's correlation coefficient, C had positive $p<0.01$ correlations with 10 soil parameters and negative with 24 (Figure 8.9B). No positive correlations R≥ 0.8 were detected, and only cie V had a R≥ -0.8 negative correlation with C. Regarding SSA, 12 parameters showed positive $p<0.01$ correlations (9 with R≥ 0.8) and 25 parameters negative correlations (16 with R≥ -0.8; Figure 8.9B).

8.5. Discussion

8.5.1. Conservative behaviour of soil properties

The low changes in particle size distributions and C content (average CV for all land uses and TIS samples of 2.1 ± 0.3%) allowed the direct comparison of in-channel soil properties without interferences of differential absorbance or organic matter. Similarly, most of the soil properties presented a low degree of alteration during the experiment, independently of source type (i.e. forest, crop and scrubland; average CV = 8.1 ± 8.8%). Variability values were lower than the average spatial variability measured on the catchment source soil properties (Figure 6A; average CV = 16.3 ± 18.5%). For instance, the spatial variability of C, N and S content within the Es Fangar catchment was higher (average CV of 28.8 ± 12.8%, 37.9 ± 19.7% and 35.5 ± 21.1, respectively, for all land use types) than the in-channel variability (average in channel CVs for all land use types of 2.1 ± 0.4%, 8.1 ± 6% and 26.8 ± 14.9% for C, N and S, respectively). C and N content in sediment can suffer transformations in streams or riparian areas, which are often considered as hot spots of biochemical processes (Koiter et al., 2013). In this way, microbial transformations can cause denitrification, decomposition of organic matter or the release of organic C and N to stream waters (Vidon et al., 2010) or even transform inorganic elements in to organic forms (Thayer, 2002). Despite not being able to decipher to which extent these processes occurred in the Es Fangar catchment, temporal changes observed were slightly different than the variability measured in top soil samples (0-2 cm) between June and July 2015 in a 1.8

ha SW England pasture field (Collins et al., 2019). The authors collected soil samples 4 times and observed average CVs for C and N of 14.9 and 4.5%.

Fallout radionuclides in-channel average CVs for all land use types were 19.4 ± 8.7 for ^{137}Cs and 25.7 ± 7.5 for $^{210}Pb_{ex}$. Here, a constant downward trend in $^{210}Pb_{ex}$ activity in the scrubland samples was observed, which was more evident during the dry period. This trend could eventually be explained by losses towards the water column (Foster et al., 2006; Koiter et al., 2013). Radioactivity decay was discarded as a cause of soil $^{210}Pb_{ex}$ activity reduction due its long half live (22.3 years). Another cause could be important analytical errors. Measurements of $^{210}Pb_{ex}$ activities are technically complicated. Estimated uncertainties for $^{210}Pb_{ex}$ may be as high as ±30–50% (Mabit et al., 2008). This can generate errors in the determination of ^{210}Pb supported in equilibrium with ^{226}Ra, and these equilibrium differences will inevitably spread to the determination of $^{210}Pb_{ex}$ (Mabit et al., 2014). However, the high decrease in activity registered in the last scrubland sample (i.e. 365 days) is also reflected in other parameters such as ^{137}Cs, C or N (Figure 8.7). In addition, despite SSA and $^{210}Pb_{ex}$ showed a negative linear correlation, these abrupt changes were not detected for the other land use types despite its higher SSA variability. We cannot be firmly state the cause of the variability in scrubland samples.

Colour demonstrated to be the more stable tracers with in-channel average CVs of 2.6 ± 2.2%, with CVs above 10% only detected in forest and crop redness index (11.8 and 10.2% respectively). This low variability in colour parameters coincides with Poulenard et al. (2012), Legout et al. (2013), and Uber et al. (2019). Poulenard et al. (2012), only detected errors ranging between 5% - 15% using submersed samples (1 day, 1 week and 2 weeks) to calculate the real proportions of the same samples before submersion using a Partial Least Square model. Legout et al. (2013) considering all submersion intervals from its experiment (i.e. 1, 7, 14, 35 and 63 days) describes changes in colour parameters <10%. Finally, Uber et al. (2019) detected changes <10% in all cases with average changes <4% after 1, 3, 7, and 22 days.

Geochemical elements showed a more heterogeneous behaviour. The more stable elements during the study period were Ba, Cd, Co, Cr, Cu, Mn, Ni, Pb, Zn, Fe, Ca, K and

Mg with in-channel average CVs for all land uses ranging from 5.4 to 16.9%. On the contrary, As, Mo and Na presented higher variability (average CVs from 22.6 to 32.2%). The results obtained can be seem unusual in some elements. For example, Ca, K and Mg are often considered non-conservative tracers because of its water solubility potential (Kraushaar et al., 2015), but they showed low variability in the Es Fangar catchment, even during the wet period (Figure 8.5). Na, is also usually considered a non-conservative tracer (Négrel et al., 2015). However, some studies have considered it as conservative because of its low reactivity to hydrochloric acid extraction as well as Ti, Al, Li, V, Cr, Ba, and As (Dabrin et al., 2021). On the contrary, here As showed the highest variability.

In general, the three land use type showed similar variability in soil properties, although was slightly higher in crop samples (Figure 8.5). Comparing crop and TIS samples (average in-channel CV for all properties of 9.3 ± 0.1% and 8.6 ± 9.2% respectively) it can be stated that direct insolation deprivation and presumable differentiated humidity and temperature conditions did not have significant effects on soil properties in this specific case.

The general low variability observed in soil properties, and its strongest correlations with SSA and C (Figure 8.9) further emphasize the role of particle size and organic matter in the conservative behaviour of soil properties (Koiter et al., 2018).

8.5.2. Limitations of the experiment and implications for sediment fingerprinting

Replication of the natural transport and deposition processes that sediment is difficult due to transport is affected by high variability in time and space from the catchment sources to the outlet. In this field experiment, soil samples were exposed to the hydro-meteorological variability of a Mediterranean intermittent river (e.g. temperature, pH, moisture) as samples were in the channel during one year. Nonetheless, results must be carefully considered. In-channel samples were not affected by transport and deposition processes, but remaining in suspension due to the steadiness of the sample bags. The samples were placed in nylon bags to reduce the loss of particles with the aim of being able to decipher variations mainly associated with biochemical changes.

The nylon bags and the steel bars fixed into the bed channel were two external elements that could influence soil properties. The extension of this impact has not been addressed. However, the stability of Fe and C concentrations suggest a low influence on the soil property values. Similarly, the effect of temporary compaction of the sieved soil within the nylon bags remain unknown.

Mediterranean fluvial systems have a singular complexity. Their heterogeneous hydrological regimes promote significant temporal and spatial differences in the hydrological response, accentuated by the relationships between natural and human-induced variables (Fortesa et al., 2020b). The conjunction of these features can promote unique abiotic and biotic conditions on their streams –even in different points of the same channel– which might lead to distinctive alteration of sediment properties. In this study, samples were exposed to contrasting environmental conditions (i.e. dry and wet periods) where different processes (e.g. diagenesis, organic matter additions, loss of properties due to solubility) (Koiter et al., 2013) influencing sediment properties could occur. Furthermore, sediment transport is highly influenced by high intensity torrential floods triggering that > 80% of annual suspended sediment load is exported in <10% of the time (Estrany et al., 2009; Rovira and Batalla, 2006). In the Es Fangar catchment, previous research spanning 5 hydrological years, showed that 91% of the suspended sediment load was exported during 5% of the time (Fortesa et al., 2020a). Together with the small size of the catchment, this process suggests a rapid suspended sediment transit from sources to the catchment outlet, which could decrease the influence of biochemical changes on sediment properties. However, in-channel discontinuities in the sediment conveyor belt generating reservoirs during prolonged time intervals can be produced. In addition, in-channel transformations only represent a part of the potential changes in properties during erosion and sediment delivery processes. Therefore, on-site processes (at hillslopes) that may alter soil properties should also be considered (Koiter et al., 2018; Motha et al., 2002).

Notwithstanding the aforementioned challenges, results may be useful when assessing uncertainties associated with tracer selection and alteration in suspended sediment fingerprinting studies conducted in Mediterranean fluvial systems. In addition, alteration of emerging tracers in sediment fingerprinting studies –as compound-

specific stable isotope (Mabit et al., 2018) or biomarkers (Collins et al., 2020)– during transport in Mediterranean environments should be further explored.

8.6. Conclusions

Most investigated soil properties in sediment fingerprinting studies showed a low variability during the experiment. The catchment spatial source variability was always higher than in-channel variability. In addition, no significate differences were observed between the different land use samples or collection intervals. SSA and C content also presented low variability over time, allowing the direct comparison between the original and the submerged samples. No differences were found either with crop and TIS samples, indicating low variability in soil properties even in different environmental conditions. Soil properties that showed higher in-channel CVs were S, ^{137}Cs, $^{210}Pb_{ex}$, As, Mo and Na. Conversely, C and colour parameters were the most stable in time. Despite its limitations, this study can be basic for performing future suspended sediment fingerprinting studies in Mediterranean catchments as to better understand which sediment properties are more sensitive to in-channel biochemical transformation.

Acknowledgments

This work was supported by the research project CGL2017-88200-R "Functional hydrological and sediment connectivity at Mediterranean catchments: global change scenarios –MEDhyCON2" funded by the Spanish Ministry of Science, Innovation and Universities, the Spanish Agency of Research (AEI) and the European Regional Development Funds (ERDF). Julián García-Comendador is in receipt of a pre-doctoral contract [FPU15/05239] funded by the Spanish Ministry of Education, Culture and Sport. Josep Fortesa has a contract funded by Ministry of Innovation, Research and Tourism of the Autonomous Government of the Balearic Islands [FPI/2048/2017]. Jaume Company is in receipt of Young Qualified Program fund by Employment Service of the Balearic Islands and European Social Fund (SJ-QSP 48/19). Núria Martínez-Carreras acknowledges funding for this study from the Luxembourg National Research Fund (PAINLESS project, C17/SR/11699372). We would like to acknowledge support by Franz Ronellenfitsch for the set-up of the spectroradiometer.

8.7. References

Ben-Dor, E., Banin, A., 1995. Near-Infrared Analysis as a Rapid Method to Simultaneously Evaluate Several Soil Properties. Soil Sci. Soc. Am. J. 59, 364–372. https://doi.org/10.2136/sssaj1995.03615995005900020014x

Carter, J., Owens, P.N., Walling, D.E., Leeks, G.J.L., 2003. Fingerprinting suspended sediment sources in a large urban river system, in: Science of the Total Environment. Elsevier, pp. 513–534. https://doi.org/10.1016/S0048-9697(03)00071-8

Collins, A.. L., Walling, D.. E., 2002. Selecting fingerprint properties for discriminating potential suspended sediment sources in river basins. J. Hydrol. 261, 218–244. https://doi.org/10.1016/S0022-1694(02)00011-2

Collins, A.L., Blackwell, M., Boeckx, P., Chivers, C.A., Emelko, M., Evrard, O., Foster, I., Gellis, A., Gholami, H., Granger, S., Harris, P., Horowitz, A.J., Laceby, J.P., Martinez-Carreras, N., Minella, J., Mol, L., Nosrati, K., Pulley, S., Silins, U., da Silva, Y.J., Stone, M., Tiecher, T., Upadhayay, H.R., Zhang, Y., 2020. Sediment source fingerprinting: benchmarking recent outputs, remaining challenges and emerging themes. J. Soils Sediments 20, 1–34. https://doi.org/10.1007/s11368-020-02755-4

Collins, A.L., Burak, E., Harris, P., Pulley, S., Cardenas, L., Tang, Q., 2019. Field scale temporal and spatial variability of δ13C, δ15N, TC and TN soil properties: Implications for sediment source tracing. Geoderma 333, 108–122. https://doi.org/10.1016/j.geoderma.2018.07.019

Collins, A.L., Walling, D.E., Leeks, G.J.L., 1997. Source type ascription for fluvial suspended sediment based on a quantitative composite fingerprinting technique. Catena 29, 1–27. https://doi.org/10.1016/S0341-8162(96)00064-1

Crockford, R.H., Olley, J.M., 1998. The effects of particle breakage and abrasion on the magnetic properties of two soils. Hydrol. Process. 12, 1495–1505. https://doi.org/10.1002/(SICI)1099-1085(199807)12:9<1495::AID-HYP652>3.0.CO;2-M

Dabrin, A., Bégorre, C., Bretier, M., Dugué, V., Masson, M., Le Bescond, C., Le Coz, J., Coquery, M., 2021. Reactivity of particulate element concentrations: apportionment assessment of suspended particulate matter sources in the Upper Rhône River, France. J. Soils Sediments 1–19. https://doi.org/10.1007/s11368-020-02856-0

Du, P., Walling, D.E., 2017. Fingerprinting surficial sediment sources: Exploring some potential problems associated with the spatial variability of source material properties. J. Environ. Manage. 194, 4–15. https://doi.org/10.1016/j.jenvman.2016.05.066

Estrany, J., Garcia, C., Batalla, R.J., 2009. Suspended sediment transport in a small Mediterranean agricultural catchment. Earth Surf. Process. Landforms 34, 929–940. https://doi.org/10.1002/esp.1777

Estrany, J., Garcia, C., Walling, D.E., Ferrer, L., 2011. Fluxes and storage of fine-grained sediment and associated contaminants in the Na Borges River (Mallorca, Spain). Catena 87, 291–305. https://doi.org/10.1016/j.catena.2011.06.009

Fan, Q., Yamaguchi, N., Tanaka, M., Tsukada, H., Takahashi, Y., 2014. Relationship between the adsorption species of cesium and radiocesium interception potential in soils and

minerals: An EXAFS study. J. Environ. Radioact. 138, 92–100. https://doi.org/10.1016/j.jenvrad.2014.08.009

Fortesa, J., Latron, J., García-Comendador, J., Company, J., Estrany, J., 2020a. Runoff and soil moisture as driving factors in suspended sediment transport of a small mid-mountain Mediterranean catchment. Geomorphology 368, 107349. https://doi.org/10.1016/j.geomorph.2020.107349

Fortesa, J., Latron, J., García-Comendador, J., Tomàs-Burguera, M., Company, J., Calsamiglia, A., Estrany, J., 2020b. Multiple temporal scales assessment in the hydrological response of small mediterranean-climate catchments. Water 12, 299. https://doi.org/10.3390/w12010299

Foster, I.D.L., Charlesworth, S.M., 1996. Heavy metals in the hydrological cycle: Trends and explanation. Hydrol. Process. 10, 227–261. https://doi.org/10.1002/(SICI)1099-1085(199602)10:2<227::AID-HYP357>3.0.CO;2-X

Foster, I.D.L., Mighall, T.M., Proffitt, H., Walling, D.E., Owens, P.N., 2006. Post-depositional ^{137}Cs mobility in the sediments of three shallow coastal lagoons, SW England. J. Paleolimnol. 35, 881–895. https://doi.org/10.1007/s10933-005-6187-6

Garcia-Comendador, J., Palacio, E., Andres Lopez-Tarazón, J., Martínez-Carreras, N., Calsamiglia, A., Fortesa, J., Calvo-Cases, A., Ferrer, L., Estrany, J., 2018. A methodological approach to collect representative source sediment fingerprinting samples using an ad hoc rainfall simulator. Geophys. Res. Abstr. 20, 16790.

García-Ruiz, J.M., 2010. The effects of land uses on soil erosion in Spain: A review. Catena 81, 1–11. https://doi.org/10.1016/j.catena.2010.01.001

Guijarro, J.A., 1986. Contribucion a la bioclimatologia de Baleares. PhD Thesis. University of the Balearic Islands, Palma, Spain.

Haddadchi, A., Olley, J., Laceby, P., 2014. Accuracy of mixing models in predicting sediment source contributions. Sci. Total Environ. 497–498, 139–152. https://doi.org/10.1016/j.scitotenv.2014.07.105

Hancock, G.J., Revill, A.T., 2013. Erosion source discrimination in a rural Australian catchment using compound-specific isotope analysis (CSIA). Hydrol. Process. 27, 923–932. https://doi.org/10.1002/hyp.9466

He, Q., Walling, D.E., 1996. Interpreting particle size effects in the adsorption of ^{137}Cs and unsupported ^{210}Pb by mineral soils and sediments. J. Environ. Radioact. 30, 117–137. https://doi.org/10.1016/0265-931X(96)89275-7

Hill, B.R., DeCarlo, E.H., Fuller, C.C., Wong, M.F., 1998. Using sediment 'fingerprints' to assess sediment-budget errors, North Halawa Valley, Oahu, Hawaii, 1991–92. Earth Surf. Process. Landforms 23, 493–508. https://doi.org/10.1002/(SICI)1096-9837(199806)23:6<493::AID-ESP862>3.0.CO;2-V

Hirner, A. V., Kritsotakis, K., Tobschall, H.J., 1990. Metal-organic associations in sediments-I. Comparison of unpolluted recent and ancient sediments and sediments affected by anthropogenic pollution. Appl. Geochemistry 5, 491–505. https://doi.org/10.1016/0883-2927(90)90023-X

Horowitz, A.J., Elrick, K.A., 1987. The relation of stream sediment surface area, grain size and

composition to trace element chemistry. Appl. Geochemistry 2, 437–451. https://doi.org/10.1016/0883-2927(87)90027-8

Horowitz, A.J., Elrick, K.A., Cook, R.B., 1993. Effect of mining and related activities on the sediment trace element geochemistry of lake coeur D'Alene, idaho, USA. Part I: Surface sediments. Hydrol. Process. 7, 403–423. https://doi.org/10.1002/hyp.3360070406

Hudson-Edwards, K.A., Macklin, M.G., Curtis, C.D., Vaughan, D.J., 1998. Chemical remobilization of contaminant metals within floodplain sediments in an incising river system: implications for dating and chemostratigraphy. Earth Surf. Process. Landforms 23, 671–684. https://doi.org/10.1002/(SICI)1096-9837(199808)23:8<671::AID-ESP871>3.0.CO;2-R

James, A.L., Roulet, N.T., 2006. Investigating the applicability of end-member mixing analysis (EMMA) across scale: A study of eight small, nested catchments in a temperate forested watershed. Water Resour. Res. 42, W08434. https://doi.org/10.1029/2005WR004419

Juracek, K.E., Ziegler, A.C., 2009. Estimation of sediment sources using selected chemical tracers in the Perry lake basin, Kansas, USA. Int. J. Sediment Res. 24, 108–125. https://doi.org/10.1016/S1001-6279(09)60020-2

Klages, M.G., Hsieh, Y.P., 1975. Suspended Solids Carried by the Gallatin River of Southwestern Montana: II. Using Mineralogy for Inferring Sources. J. Environ. Qual. 4, 68–73. https://doi.org/10.2134/jeq1975.00472425000400010016x

Koiter, A.J., Owens, P.N., Petticrew, E.L., Lobb, D.A., 2018. Assessment of particle size and organic matter correction factors in sediment source fingerprinting investigations: An example of two contrasting watersheds in Canada. Geoderma 325, 195–207. https://doi.org/10.1016/j.geoderma.2018.02.044

Koiter, A.J.J., Owens, P.N.N., Petticrew, E.L.L., Lobb, D.A.A., 2013. The behavioural characteristics of sediment properties and their implications for sediment fingerprinting as an approach for identifying sediment sources in river basins. Earth-Science Rev. 125, 24–42. https://doi.org/10.1016/j.earscirev.2013.05.009

Kosmas, C., Danalatos, N., Cammeraat, L.H., Chabart, M., Diamantopoulos, J., Farand, R., Gutierrez, L., Jacob, A., Marques, H., Martinez-Fernandez, J., Mizara, A., Moustakas, N., Nicolau, J.M., Oliveros, C., Pinna, G., Puddu, R., Puigdefabregas, J., Roxo, M., Simao, A., Stamou, G., Tomasi, N., Usai, D., Vacca, A., 1997. The effect of land use on runoff and soil erosion rates under Mediterranean conditions. Catena 29, 45–59. https://doi.org/10.1016/S0341-8162(96)00062-8

Kraushaar, S., Schumann, T., Ollesch, G., Schubert, M., Vogel, H.J., Siebert, C., 2015. Sediment fingerprinting in northern Jordan: element-specific correction factors in a carbonatic setting. J. Soils Sediments 15, 2155–2173. https://doi.org/10.1007/s11368-015-1179-2

Laceby, J.P., Evrard, O., Smith, H.G., Blake, W.H., Olley, J.M., Minella, J.P.G., Owens, P.N., 2017. The challenges and opportunities of addressing particle size effects in sediment source fingerprinting: A review, Earth-Science Reviews. Elsevier. https://doi.org/10.1016/j.earscirev.2017.04.009

Legout, C., Poulenard, J., Nemery, J., Navratil, O., Grangeon, T., Evrard, O., Esteves, M., 2013. Quantifying suspended sediment sources during runoff events in headwater catchments using spectrocolorimetry. J. Soils Sediments 13, 1478–1492.

https://doi.org/10.1007/s11368-013-0728-9

Lizaga, I., Latorre, B., Gaspar, L., Navas, A., 2020. Consensus ranking as a method to identify non-conservative and dissenting tracers in fingerprinting studies. Sci. Total Environ. 720, 137537. https://doi.org/10.1016/j.scitotenv.2020.137537

Mabit, L., Benmansour, M., Abril, J.M., Walling, D.E., Meusburger, K., Iurian, A.R., Bernard, C., Tarján, S., Owens, P.N., Blake, W.H., Alewell, C., 2014. Fallout ^{210}Pb as a soil and sediment tracer in catchment sediment budget investigations: A review. Earth-Science Rev. https://doi.org/10.1016/j.earscirev.2014.06.007

Mabit, L., Benmansour, M., Walling, D.E., 2008. Comparative advantages and limitations of the fallout radionuclides ^{137}Cs, ^{210}Pb$_{ex}$ and ^{7}Be for assessing soil erosion and sedimentation. J. Environ. Radioact. https://doi.org/10.1016/j.jenvrad.2008.08.009

Mabit, L., Gibbs, M., Mbaye, M., Meusburger, K., Toloza, A., Resch, C., Klik, A., Swales, A., Alewell, C., 2018. Novel application of Compound Specific Stable Isotope (CSSI) techniques to investigate on-site sediment origins across arable fields. Geoderma 316, 19–26. https://doi.org/10.1016/j.geoderma.2017.12.008

Manjoro, M., Rowntree, K., Kakembo, V., Collins, A.L., 2017. Use of sediment source fingerprinting to assess the role of subsurface erosion in the supply of fine sediment in a degraded catchment in the Eastern Cape, South Africa. J. Environ. Manage. 194, 27–41. https://doi.org/10.1016/J.JENVMAN.2016.07.019

Motha, J.A., Wallbrink, P.J., Hairsine, P.B., Grayson, R.B., 2003. Determining the sources of suspended sediment in a forested catchment in southeastern Australia. Water Resour. Res. 39, 1056. https://doi.org/10.1029/2001WR000794

Motha, J.A., Wallbrink, P.J., Hairsine, P.B., Grayson, R.B., 2002. Tracer properties of eroded sediment and source material. Hydrol. Process. 16, 1983–2000. https://doi.org/10.1002/hyp.397

Négrel, P., Sadeghi, M., Ladenberger, A., Reimann, C., Birke, M., Albanese, S., Andersson, M., Baritz, R., Batista, M.J., Bel-lan, A., Cicchella, D., Demetriades, A., De Vivo, B., De Vos, W., Dinelli, E., Duriš, M., Dusza-Dobek, A., Eggen, O.A., Eklund, M., Ernstsen, V., Filzmoser, P., Flight, D.M.A., Forrester, S., Fuchs, M., Fügedi, U., Gilucis, A., Gosar, M., Gregorauskiene, V., De Groot, W., Gulan, A., Halamic, J., Haslinger, E., Hayoz, P., Hoffmann, R., Hoogewerff, J., Hrvatovic, H., Husnjak, S., Janik, L., Jordan, G., Kaminari, M., Kirby, J., Kivisilla, J., Klos, V., Krone, F., Kwecko, P., Kuti, L., Lima, A., Locutura, J., Lucivjansky, D.P., Mann, A., Mackovych, D., McLaughlin, M., Malyuk, B.I., Maquil, R., Meuli, R.G., Mol, G., O'Connor, P., Oorts, R.K., Ottesen, R.T., Pasieczna, A., Petersell, W., Pfleiderer, S., Ponavic, M., Pramuka, S., Prazeres, C., Rauch, U., Radusinovic, S., Salpeteur, I., Scanlon, R., Schedl, A., Scheib, A.J., Schoeters, I., Šefcik, P., Sellersjö, E., Skopljak, F., Slaninka, I., Šorša, A., Srvkota, R., Stafilov, T., Tarvainen, T., Trendavilov, V., Valera, P., Verougstraete, V., Vidojevic, D., Zissimos, A., Zomeni., Z., 2015. Geochemical fingerprinting and source discrimination of agricultural soils at continental scale. Chem. Geol. 396, 1–15. https://doi.org/10.1016/j.chemgeo.2014.12.004

Nosrati, K., Govers, G., Semmens, B.X., Ward, E.J., 2014. A mixing model to incorporate uncertainty in sediment fingerprinting. Geoderma 217–218, 173–180. https://doi.org/10.1016/j.geoderma.2013.12.002

Owens, P.N., Blake, W.H., Giles, T.R., Williams, N.D., 2012. Determining the effects of wildfire

on sediment sources using ^{137}Cs and unsupported ^{210}Pb: The role of landscape disturbances and driving forces. J. Soils Sediments 12, 982–994. https://doi.org/10.1007/s11368-012-0497-x

Palazón, L., Navas, A., 2017. Variability in source sediment contributions by applying different statistic test for a Pyrenean catchment. J. Environ. Manage. 194, 42–53. https://doi.org/10.1016/j.jenvman.2016.07.058

Phillips, J.M., Russell, M.A., Walling, D.E., 2000. Time-integrated sampling of fluvial suspended sediment: A simple methodology for small catchments. Hydrol. Process. 14, 2589–2602. https://doi.org/10.1002/1099-1085(20001015)14:14<2589::AID-HYP94>3.0.CO;2-D

Poulenard, J., Legout, C., Némery, J., Bramorski, J., Navratil, O., Douchin, A., Fanget, B., Perrette, Y., Evrard, O., Esteves, M., 2012. Tracing sediment sources during floods using Diffuse Reflectance Infrared Fourier Transform Spectrometry (DRIFTS): A case study in a highly erosive mountainous catchment (Southern French Alps). J. Hydrol. 414, 452–462. https://doi.org/10.1016/j.jhydrol.2011.11.022

Pulley, S., Rowntree, K., 2016. The use of an ordinary colour scanner to fingerprint sediment sources in the South African Karoo. J. Environ. Manage. 165, 253–262. https://doi.org/10.1016/j.jenvman.2015.09.037

Rose, L.A., Karwan, D.L., Aufdenkampe, A.K., 2018. Sediment Fingerprinting Suggests Differential Suspended Particulate Matter Formation and Transport Processes Across Hydrologic Regimes. J. Geophys. Res. Biogeosciences 123, 1213–1229. https://doi.org/10.1002/2017JG004210

Rovira, A., Batalla, R.J., 2006. Temporal distribution of suspended sediment transport in a Mediterranean basin: The Lower Tordera (NE SPAIN). Geomorphology 79, 58–71. https://doi.org/10.1016/j.geomorph.2005.09.016

Russell, M.. A., Walling, D.. E., Hodgkinson, R.. A., 2001. Suspended sediment sources in two small lowland agricultural catchments in the UK. J. Hydrol. 252, 1–24. https://doi.org/10.1016/S0022-1694(01)00388-2

Sear, D.A., Armitage, P.D., Dawson, F.H., 1999. Groundwater dominated rivers. Hydrol. Process. 13, 255–276. https://doi.org/10.1002/(SICI)1099-1085(19990228)13:3<255::AID-HYP737>3.0.CO;2-Y

Smith, H.G., Karam, D.S., Lennard, A.T., 2018. Evaluating tracer selection for catchment sediment fingerprinting. J. Soils Sediments 18, 3005–3019. https://doi.org/10.1007/s11368-018-1990-7

Thayer, J.S., 2002. Review: Biological methylation of less-studied elements. Appl. Organomet. Chem. 16, 677–691. https://doi.org/10.1002/aoc.375

Thornes, J.B., 1990. The interaction of erosional and vegetational dynamics in land degradation: spatial outcomes., in: Vegetation and Erosion. Processes and Environments. John Wiley and Sons Ltd., Chichester, UK, pp. 41–53.

Uber, M., Legout, C., Nord, G., Crouzet, C., Demory, F., Poulenard, J., 2019. Comparing alternative tracing measurements and mixing models to fingerprint suspended sediment sources in a mesoscale Mediterranean catchment. J. Soils Sediments 19, 3255–3273. https://doi.org/10.1007/s11368-019-02270-1

United States Environmental Protection Agency, 2000. Guidance for Data Quality Assessment., Guidance for data quality assessment.

Vidon, P., Allan, C., Burns, D., Duval, T.P., Gurwick, N., Inamdar, S., Lowrance, R., Okay, J., Scott, D., Sebestyen, S., 2010. Hot spots and hot moments in riparian zones: Potential for improved water quality management. J. Am. Water Resour. Assoc. 46, 278–298. https://doi.org/10.1111/j.1752-1688.2010.00420.x

Viscarra Rossel, R.A., Minasny, B., Roudier, P., McBratney, A.B., 2006. Colour space models for soil science. Geoderma 133, 320–337. https://doi.org/10.1016/J.GEODERMA.2005.07.017

Walden, J., Slattery, M.C., Burt, T.P., 1997. Use of mineral magnetic measurements to fingerprint suspended sediment sources: Approaches and techniques for data analysis. J. Hydrol. 202, 353–372. https://doi.org/10.1016/S0022-1694(97)00078-4

Wall, G.J., Wilding, L.P., 1976. Mineralogy and Related Parameters of Fluvial Suspended Sediments in Northwestern Ohio. J. Environ. Qual. 5, 168–173. https://doi.org/10.2134/jeq1976.00472425000500020012x

Walling, D.E., Peart, M.R., Oldfield, F., Thompson, R., 1979. Suspended sediment sources identified by magnetic measurements. Nature 281, 110–113. https://doi.org/10.1038/281110a0

Walling, D.E.E., 2005. Tracing suspended sediment sources in catchments and river systems 344, 159–184.

Wilkinson, S.N., Hancock, G.J., Bartley, R., Hawdon, A.A., Keen, R.J., 2013. Using sediment tracing to assess processes and spatial patterns of erosion in grazed rangelands, Burdekin River basin, Australia. Agric. Ecosyst. Environ. 180, 90–102. https://doi.org/10.1016/j.agee.2012.02.002

Wilkinson, S.N.N., Wallbrink, P.J.J., Hancock, G.J.J., Blake, W.H.H., Shakesby, R.A.A., Doerr, S.H.H., 2009. Fallout radionuclide tracers identify a switch in sediment sources and transport-limited sediment yield following wildfire in a eucalypt forest. Geomorphology 110, 140–151. https://doi.org/10.1016/J.GEOMORPH.2009.04.001

Withers, P.J.A., Jarvie, H.P., 2008. Delivery and cycling of phosphorus in rivers: A review. Sci. Total Environ. 400, 379–395. https://doi.org/10.1016/j.scitotenv.2008.08.002

8.8. Supplementary material

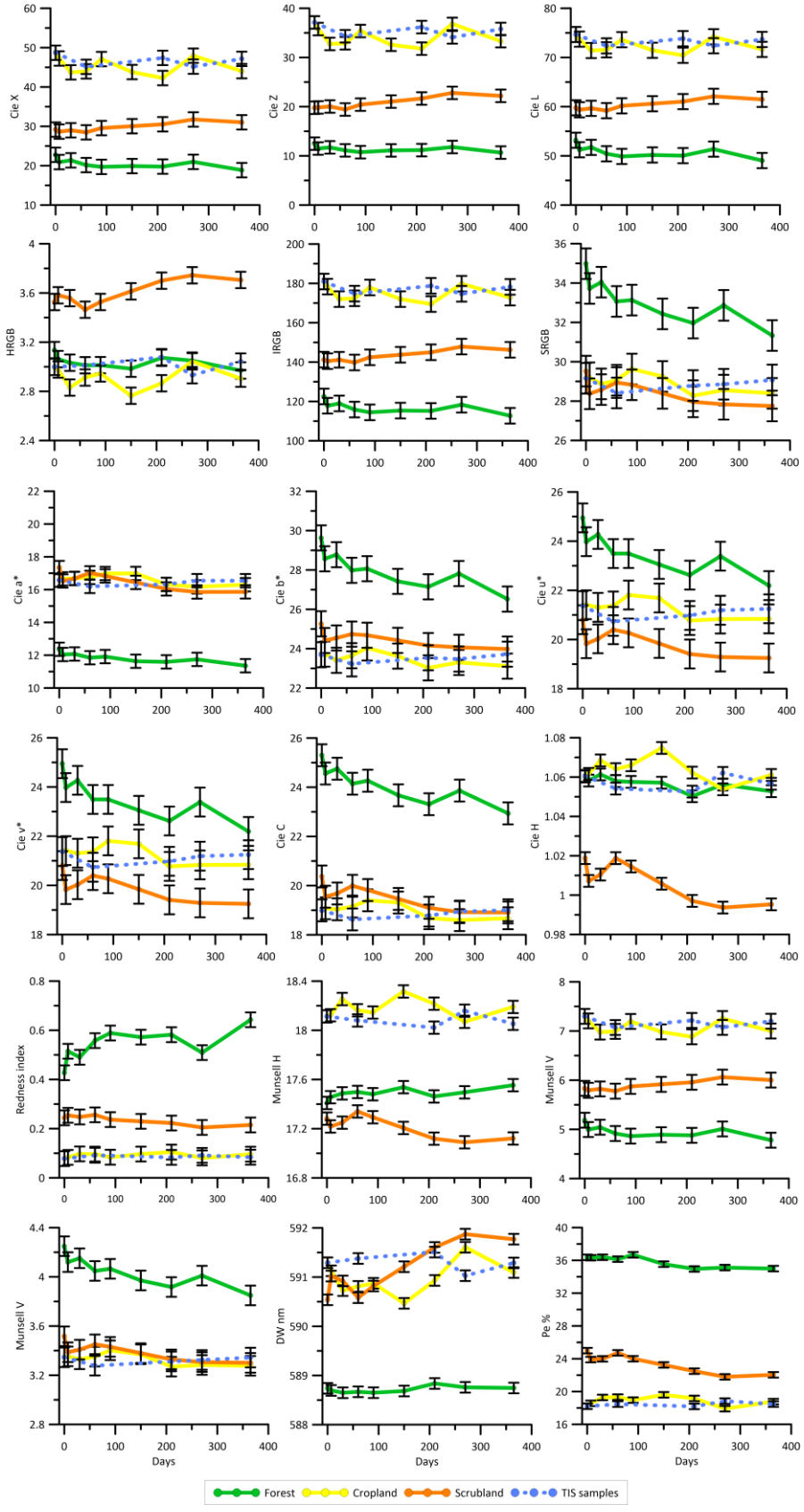

Supplementary figure 8.1. In-channel colour parameters evolution for forest, crop, scrubland and TIS samples.

9. Discussion and conclusions

The preceding chapters of this thesis assessed the hydro-sedimentary dynamics in two Mediterranean catchments affected by Global Change processes, especially sediment transport and sediment source variability at different spatiotemporal scales. In this chapter, a brief synthesis is presented of the most relevant results of the thesis, which are then discussed as a whole with a view to presenting a comprehensive interpretation of (i) the assessment of the hydro-sedimentary dynamics in the study areas (i.e. Sa Font the la Vila and Es Fangar), (ii) the sediment source fingerprinting results, in terms of improving applicability and reducing uncertainties, and (iii) estimating the role of hydro-sedimentary monitoring combined with sediment fingerprinting as tools for catchment management. Thus, the final objective of the overall analysis of the thesis body will serve to refute or validate the two hypotheses presented in Chapter 1.

9.1. Sa Font de la Vila and Es Fangar hydro-sedimentary dynamics

Chapters 4, 5 and 6 focus on the fire-affected catchment Sa Font de la Vila (4.8 km^2). A nested catchment approach was used covering the 1.2 km^2 Sa Murtera sub-catchment, and water and sediment yields were measured at the outlet of both sites. Sediment origin was investigated using sediment fingerprinting and ^{137}Cs, $^{210}Pb_{ex}$ and colour parameters as tracers.

During the first three post-fire hydrological years (i.e. 2013-14 to 2015-16) the average sediment yields were 1.6 and 6.3 t km^{-2} yr^{-1} for Sa Murtera and Sa Font de la Vila respectively. These values can be considered rather low in comparison with other burned catchments (see Table 4.1 in Chapter 4). However, they are higher than those obtained in other non-burned terraced catchments of the island of Mallorca (Estrany et al., 2009; Fortesa et al., 2021). Water yield in Sa Font the la Vila was also extremely low, despite the fact that the annual precipitation totals did not significantly deviate from the long-term average totals (see section 4.4.1. in Chapter 4). Counter-clockwise hysteretic loops between suspended sediment concentration and discharge dominated

in Sa Font the la Vila (60%) during the study period. Normally, this kind of loop shape is ascribed to relatively distanced sediment sources (Oeurng et al., 2010; Williams, 1989), which could be fire-affected hillslopes in the study area. The percentage of counter-clockwise loops was higher during the first post-fire year (67%) coinciding with the highest annual sediment yield. Both values decreased over the following years. The percentage of counter-clockwise loops percentage can be considered high in comparison with other non-burned Mediterranean catchments (López-Tarazón and Estrany, 2017; Oeurng et al., 2010; Rovira and Batalla, 2006; Seeger et al., 2004), probably due to the wildfire perturbation. This hypothesis is reinforced by the results presented in Chapters 5 and 6. In the former, ^{137}Cs and $^{210}Pb_{ex}$ were used as tracers to evaluate bed sediments' source ascription during the first post-fire flush in Sa Coma Freda creek (the east sub-catchment of Sa Font de la Vila catchment; see figure 5.2A). Results showed an average source contribution from burned hillslopes in the upstream part of 67%, reaching 75% in the downstream part (see the different parts of the stream in Figure 5.2B). In addition, in Chapter 6 we analysed suspended sediment origin during 4 floods which occurred between 2013 and 2015, including the first post-fire flush, in the Sa Murtera sub-catchment and the Sa Font de la Vila catchment. In general, tracing results using ^{137}Cs, $^{210}Pb_{ex}$ and colour parameters showed a larger relative contribution from burned hillslopes during the first flood events. A contribution that gradually decreased with time (see Chapter 6). This results coincide with the observed decrease in the relative contribution of sediment originating in burned sources in Chapters 4 and 5.

As regards the prospect of increased erosion rates, runoff coefficients and sediment delivery in burned areas as documented by several authors (e.g. Shakesby and Doerr, 2006; Vieira et al., 2015), the results presented in Chapters 4, 5 and 6 appear to be reliable. However, other studies showed remarkable divergences in landscape response after a wildfire (Estrany et al., 2016; Owens et al., 2012; Smith et al., 2011; Wilkinson et al., 2009) (see section 6.5.2. of Chapter 6). Here it is hypothesized that the gradual decrease in sediment contribution from burned areas was not only due to a partial vegetation recovery, but also to the fact that the rainfall intensity thresholds generating effective slope-to-channel connectivity were not reached during the second

post-fire hydrological year (Calvo-Cases et al., 2003; Li et al., 2019), resulting in partial sediment disconnexion of burned hillslopes.

In the Chapter 7 hydro-sedimentary continuous monitoring was combined with sediment fingerprinting (using ^{137}Cs, $^{210}Pb_{ex}$ and colour parameters as tracers) to investigate suspended sediment origin in the Es Fangar catchment. Previous investigations determined that during the period 2012-2017 the annual runoff coefficient in the catchment ranged from 2.9% to 14.2% (average of 10.4%), whereas the quickflow contribution ranged from 9.9% to 45% (average of 33%), illustrating a huge inter-annual variability in the rainfall-runoff relationship (Fortesa et al., 2020b). During the same period, 80% of the sediment load was exported during autumn and winter, with an annual average sediment yield of 5.38 t km^{-2} y^{-1}. Flood events depicted a wide intra- and inter-annual variability and a marked seasonality with 85.3% of events occurring during the wet season. Sediment tracing results from the MixSIAR unmixing model showed that sediment mainly originated from crop fields all along the study period (Sections 7.4.4 and 7.5.1 of Chapter 7), with no seasonal patterns or major source changes regarding flood hydro-sedimentary characteristics. A similar low variability in sediment origin was observed in other Mediterranean catchments (e.g. Uber et al., 2019). Clockwise hysteresis loops predominated in the Es Fangar (occurring during 52.9% of the monitored events), coinciding with the results by Fortesa et al. (2020a), what suggested in-channel sediment remobilisation and erosion from near stream areas (i.e. crops). On the contrary, anti-clockwise or complex hysteresis patterns (47.1% of the monitored events) are sometimes related with the activation of different sediment sources (De Girolamo et al., 2015). Nevertheless, the sediment fingerprinting results did not provide information about different sediment origin regarding hysteretic type, suggesting that the analysis of hysteretic patterns might not always accurately provide information about sediment origin (Smith and Dragovich, 2009; Vercruysse et al., 2017). In the Es Fangar catchment, the lithology, land uses and the presence of agricultural terraces and dry stone walls could partially explain the low sediment source variability during the studied period (Calsamiglia et al., 2018; Estrany et al., 2010). Scrubland and forest areas are located in the catchment headwaters, where vegetation protects the soils of the steepest hillslopes, reducing runoff and

suspended sediment generation. Moreover, carbonate materials characterized by low sediment availability and transmission losses (Calvo-Cases et al., 2003; Li et al., 2019) dominate in the upper parts of the catchment, whereas crop fields dominate in the valley bottom, which are completely exposed during certain periods of the year. Furthermore, a large part of the channel banks is constrained by dry stone walls, limiting channel bank sediment contributions. Therefore, the transference of significant amounts of sediment from the channel banks to the fluvial network would only occur when a dry stone wall collapses, which has been observed only rarely in the catchment.

Climatic, geological, topographical and land cover features regulate the sediment delivery in catchments (Walling, 1983). Mediterranean catchments are characterized by high inter- and intra-annual rainfall variability, heterogeneous lithology and highly human modified land uses and landscape topographic features (Calsamiglia et al., 2018; García-Ruiz and Lana-Renault, 2011; Yair, 1983; Zdruli, 2014). Mediterranean catchments show the highest sediment yields in Europe. Vanmaercke et al. (2011) reviewed suspended sediment concentrations across Europe and concluded that concentrations exceeded 40 t km^2 yr^{-1} in 85% of the revised data, and exceeded 200 t km^2 yr^{-1}in more than 50% of the values considered. In this context, Sa Font de la Vila and Es Fangar catchment average sediment yields, 6.3 t km^2 yr^{-1} and 4.5 t km^2 yr^{-1} respectively, can be considered as low. This can be explained, in part, given the (dis)connectivity concept within the sediment connectivity framework, as "*the degree to which any limiting factor constrains the efficiency of sediment transfer relationships*" (Fryirs, 2013; Fryirs et al., 2007). The (dis)connectivity framework defines a conceptual model of relationships between sediment linkages -categorized as lateral, longitudinal or vertical linkages- and blockages -barriers, buffers and blankets (cf. Fryirs, 2013). The effectivity between the different linkages is generally determined by its spatial configuration, or the presence of disrupting blockages. The increase of landscape connectivity depends on the breaching of blockages. Here, Fryirs et al. (2013) interpret the blockages as switches that can be activated depending on the magnitude of the driving forces, which have to exceed the thresholds established for every blockage before connecting different landscape compartments. In the Sa Font de la Vila and Es

Fangar catchments, agricultural terraces are considered to be blockages, that disconnect the different catchment compartments even when the window of disturbance tends to be more open (Prosser and Williams, 1998), i.e. after a wildfire perturbation. Agricultural terraces are water and sediment decoupling structures that dramatically increase the activation thresholds. Therefore, terrace status and its spatial configuration are key factors that control the (dis)connectivity. This could explain the low sediment yields and source stability in Sa Font the la Vila and Es Fangar catchments. However, these thresholds can also be exceeded. This happened on 29th October 2013 in Sa Font de la Vila, when a high intensity storm generated a suspended sediment yield of 17 t km^2 yr^{-1} in only 15 minutes, 92% of the sediment load measured during the first three post-fire hydrological years. Therefore, interactions between hydro-meteorological factors and human disturbances determine the sediment origin and catchment-scale sediment flux in highly modified landscapes (Fryirs, 2017; Poeppl et al., 2020). The results obtained are associated to human modifications through traditional soil conservation practices (Calsamiglia et al., 2018; Estrany et al., 2010). Thus, the Sa Font de la Vila and Es Fangar geomorphic systems depend to a certain extent on the maintenance and restoration of the human structures that configure it, especially soil conservation structures. Otherwise, a rapid change in its operation could eventually result in increased sediment yields, soil loss and degradation, promoting a sediment cascade effect (Burt and Allison, 2009).

9.2. Thesis contributions to the sediment fingerprinting framework

In a recent review of the state of the art of the sediment sources fingerprinting technique, Collins et al. (2020) highlighted some emerging topics and outstanding issues related to the sediment fingerprinting research and application. Some of the most relevant issues have been discussed in this thesis, such as (I) the application of sediment fingerprinting to wildfire impacted landscapes (Chapters 5 and 6), (II) the combination of sediment fingerprinting with other approaches for catchment management (Chapter 7) and (III) the tracer conservatism issue (Chapter 8).

I. Application of sediment fingerprinting to wildfire impacted landscapes

In Chapter 5, fallout radionuclides (^{137}Cs and $^{210}Pb_{ex}$) were used as tracers in the eastern sub-catchment of the Sa Font de la Vila catchment (Sa Coma Freda) to determine the relative contributions of sediment sources in terms of spatial provenance (burned vs. unburned) and source type (soil surface vs. channel bank) in bed sediments. As regards this first approach, looking at the post-fire sediment source determination, results indicated that 67% of the upstream bed sediment contribution was generated from burned hillslopes, reaching 75% in the downstream part of the catchment due to the propagation of sediment delivered from burned areas (see figure 5.2B to observe the stream different parts).

In Chapter 6, the sediment origin in Sa Font de la Vila was further studied. Colour soil parameters measured with a spectrometer and a standard office scanner were used for the first time as tracers to effectively discriminate between burned and unburned sediment sources in the Sa Font de la Vila catchment and the Sa Murtera sub-catchment. The main advantage of colour parameters is that they can be measured quickly, are cheap and the method is non-destructive. Hence, they might be used to take quick decisions on post-fire management, as well as to evaluate the success of these measures since they make it possible to follow up. The efficiency of soil colour parameters was evaluated by using unmixing artificial laboratory mixtures when applying the MixSIAR Bayesian tracer mixing model framework (Stock et al., 2018). The results showed average absolute errors of 12.3% ± 9.1, 12.3% ± 4.2 and 10.1% ± 4.2 for 2-, 3- and 4-source mixtures, respectively. Errors were of the same order of magnitude as errors obtained by other authors using other types of tracers (Brosinsky et al., 2014; Gaspar et al., 2019; Haddadchi et al., 2014). However, when the colour signatures were similar (e.g. mix 4-m4, mix4-m5, Supplementary Table 6.5), colour tracer measurements are not reliable enough to quantify source contributions. The changes in the soil's visible reflectance (Lentile et al., 2006) and its carbon content (Bodí et al., 2014) caused by the presence of ash, triggered the change of the upper soil layer colour. As a result, colour parameters estimated from diffuse reflectance laboratory measurements were able to discriminate between burned surface soil, unburned surface soil and channel bank sources. Artificial mixtures showed that most colour parameters were linear additive and, individually, were able to predict the colour of

the mixtures by using a mass balance approach and, again, the errors were comparable with values reported in other studies (Gaspar et al., 2019; Martínez-Carreras et al., 2010b; Uber et al., 2019). Chromatic parameters calculated from the spectrometer in the laboratory and scanner-based colour parameters correlated closely ($p < 0.01$), confirming that colour parameters obtained with an office scanner can be as reliable as colour tracers from a spectrophotometer. Scanner measured colour parameters were used in other fingerprinting research by Pulley et al. (2016). They compared colour and mineral magnetic signatures to trace bed and suspended sediment in the South African Karoo. The discriminatory efficiency of colour signatures ranged between 92.2% and 96.7% and were comparable to the results obtained using mineral magnetic signatures (i.e. 94%). In the Sa Font de la Vila catchment, colour parameters were compared with ^{137}Cs and $^{210}Pb_{ex}$ as tracers. Estimated source ascriptions with both methods matched when it came to predicting the dominant source in 7 of the 9 samples measured. Thus, colour tracers proved to be useful in discriminating between burned and unburned sources. Therefore, it can be considered suitable for suspended sediment source ascription and monitoring as part of post-fire management strategies.

After a wildfire, the hydro-sedimentary response in affected landscapes can be drastically altered (Moody et al., 2013; Shakesby, 2011; Shakesby and Doerr, 2006). In general, surface runoff and sediment yield from hillslopes is increased (Candela et al., 2005; Scott et al., 1998), promoting erosion and a higher slope-to-channel sediment transfer that may generate downstream impacts related to fine sediment transport and its associated pollutants (Collins et al., 2017). Wildfires are one of the disturbances that can be increased as a result of global change processes (Huang et al., 2014) such as increased temperatures, variations in rainfall patterns and land use changes. The potential risks associated with wildfires can seriously impact the ecological status of the environment, and therefore are attracting increasing interest from researchers and landscape managers (Robinne et al., 2020; Smith et al., 2011; Wohl, 2018). Chapters 5 and 6 are focused on research into the effects of wildfires on soil properties and hydrological and geomorphological processes by using the sediment fingerprinting technique. There are not many studies that discriminate between burned and unburned sources (e.g. Estrany et al., 2016), so the contributions in these chapters are

valuable in their own right. However, the greater novelty lies in the development of the use of colour coefficients to investigate changes in soil properties (i.e. incorporation of ash) and sediment sources following a wildfire. These colour fingerprints, in combination with fallout radionuclides, were used to understand geomorphological processes following the 2013 wildfire which occurred in the Sa Font de la Vila catchment. The results obtained may be relevant for future studies that use sediment fingerprinting to understand how catchments respond to natural and anthropogenic disturbances, especially wildfires. However, further investigation needs to be done on the application of sediment fingerprinting in fire affected landscapes, particularly in relation to the differential effects of fire on sediment properties (Collins et al., 2020) and its evolution over time.

II. Combination of sediment fingerprinting with other approaches

In Chapter 7, the hydro-sedimentary dynamics in Es Fangar Creek were linked with the uses of soil colour parameters and fallout radionuclides as tracers within an integrated approach to predict dominant suspended sediment sources. A Bayesian mixing model (MixSIAR; Stock et al., 2018) and an End Member Mixing Analysis (EMMA; Christophersen and Hooper, 1992) were applied. The selection of tracers was problematic. Fallout radionuclides did not discriminate between channel bank and crop soils, and colour parameters did not discriminate between forest and scrub sources. In addition, even though colour parameters discriminated between channel bank and crops their spectral signatures were relatively close (Figure 7.4).

To combine fallout radionuclides and colour parameters in the same tracer set, sources were grouped into only two categories (i.e. channel-crop and forest-scrub) in a first un-mix to accommodate a larger number of tracers. The unmixing process was repeated using only colour parameters so as to be able to discriminate between three sources (i.e. channel bank, crop soil and forest-scrubland as a single source). MixSIAR identified channel bank-crops soil as the dominant sources in the two source analysis and crop soils in the three source analysis. In addition, comparing MixSIAR results between the two and three sources analysis, the mean absolute error in the source apportion percentage prediction was relatively low (1.2%) (i.e. adding up crop and channel bank % results for the three source analysis), which shows that the model is

robust using the selected tracers set in both analyses. EMMA showed similar results. The source tracer values plotted in the U1–U2 mixing diagram of suspended sediment tracers showed that it was possible to observe that sediment samples were clustered close to the crop and channel bank signatures (Figure 7.10). Hence, results revealed that the approach is able to determine the main sediment sources. Furthermore, as in the MixSIAR results, sample 2 was plotted closer to the forest and channel bank signatures. Our analysis suggests that the EMMA approach can be a good choice when it comes to identifying dominant sources of sediment using simplified procedures, in comparison with standard mixing models.

In this Chapter 7, it was found that EMMA, a statistically simpler model compared to MixSIAR and rarely used in sediment fingerprinting (Munkundan et al., 2010; Rose et al., 2018), can robustly identify the main sediment sources. Therefore, its use may be appropriate in sediment fingerprinting analysis alone or as a complementary model to check the robustness of results obtained with other models. However, the main purpose was to combine hydro-sedimentary monitoring with sediment fingerprinting to determine the main factors regulating sediment source contributions. Although floods were grouped into four clusters based on its hydro-sedimentary characteristics and hysteretic loops analysis, it was not possible to establish a correlation between sediment origin and hydro-sedimentary variables, because sediment sources showed a low variability in the Es Fangar catchment during the study period.

Few studies combined suspended sediment source assessment with the analysis of hydro-sedimentary response at the catchments scale. Navratil et al. (2012) combined river/rainfall monitoring and sediment fingerprinting using fallout radionuclides and geochemistry in a 905 km^2 catchment located in the French Alps. They observed how the ca. 80% sediment load occurred during widespread and long rainfall events with low intensities, while shorter storms were associated with higher discharge peaks and suspended sediment concentrations. However, and despite the high intra- and inter-flood variability of the analysed flood sediment sources remained relatively stable. On the contrary, Vercruysse and Grabowski (2019) found interesting source variations regarding hydro-meteorological drivers in an 879 km^2 catchment in UK. On the one hand, street dust and limestone grassland sources were strongly correlated

with suspended sediment concentration, discharge and 1-day antecedent rainfall. On the other hand, millstone and coals grassland sources were mainly correlated to antecedent hydro-meteorological conditions (e.g. precipitation and discharge).

In the Es Fangar catchment, the association between fingerprinting and sediment monitoring did not show any pattern because the agroforestry terraced landscape mosaic over carbonate rocks combined with the lack of extreme flood events during the study period, avoided the activation of remote or inaccessible sediment sources during frequent floods. However, the combination of these different approaches could provide information on the activation thresholds for each of the sediment sources considered. A good knowledge of the relationships between hydro-sedimentary dynamics and the activation of different sediment sources can help managers to define optimal intervention strategies, but can also be used to create optimized quantitative (in terms of amount) and qualitative (in terms of origin) sediment models to be integrated in catchment management plans. Thus, further research is necessary to reach a comprehensive understanding about erosion and sediment transport dynamics in the Es Fangar catchment.

III. Tracer conservatism

Finally, in Chapter 8 an experiment was performed to investigate eventual in-channel changes occurring to the most common soil properties used as tracers in sediment fingerprinting studies. Preliminary results in the Es Fangar Creek catchment showed a low variability in sediment properties during the study period with an average in-channel coefficient of variation of 8.1 ± 8.8% for all properties in different land uses (i.e. forest, crop and scrubland). The average spatial variability of sediment properties (16.3 ± 18.5) was higher in comparison with in-channel variation in the 90% of the comparable observations (i.e. all parameters for every land use except S, green, blue, cie X, cie Y, cie Z and cie L in scrubland samples). Colour properties were the most stable tracers with in-channel average CVs for 365 days of 2.6 ± 2.2%. This low variability in colour parameters was similar to that in other studies of shorter duration (Legout et al., 2013; Poulenard et al., 2012; Uber et al., 2019), confirming that colour parameters can be used as stable tracers (i.e. conservative) in sediment fingerprinting. Geochemical elements showed a more heterogeneous behaviour. The more stable

elements during the study period were Ba, Cd, Co, Cr, Cu, Mn, Ni, Pb, Zn, Fe, Ca, K and Mg with in-channel average CVs for all land uses in 365 days ranging from 5.4 to 16.9%. On the contrary, As, Mo and Na presented higher variability (CVs 22.6 to 32.2%). C, N and S showed less in-channel variability (average in channel CVs for all land uses in 365 days of 2.1 ± 0.4% and 8.1 ± 6% and 26.8 ± 14.9% for C, N and S respectively) in comparison with its spatial variability (average CV of 28.8 ± 12.8% and 37.9 ± 19.7% and 35.5 ± 21.1 respectively for all three land uses). Finally, fallout radionuclides in-channel average CVs for all land uses were 19.4 ± 8.7 for ^{137}Cs and 25.7 ± 7.5 for $^{210}Pb_{ex}$. In general, the three land use types showed similar variability in soil properties, being slightly higher in crop samples. Comparing crop and TIS samples (i.e. samples within time integrated suspended sediment traps; average in-channel CV for all properties for 365 days of 9.3 ± 0.1% and 8.6 ± 9.2% respectively), it can be stated that lack of direct insolation and likely differentiated humidity and temperature conditions did not have significant effects on soil properties. The general low variability observed in soil properties, and its strongest correlations with SSA and C further emphasizes the role of particle size and organic matter in the conservative behaviour of soil properties (Koiter et al., 2018).

An increase in our knowledge of tracer conservativeness is one of the main issues as regards sediment fingerprinting (Collins et al., 2020; Koiter et al., 2013; Lizaga et al., 2020). To use a soil property as a tracer it should be representative of main erosion sources, it must be able to differentiate between them, must be measurable and remain stable or vary in a predictable way over time and space (Motha et al., 2002). However, some alteration processes are known to occur during mobilization and mixing along hydrologic pathways. The degree of alteration depends on the stability of the marker and is highly site dependent. Therefore, this is difficult to address and is not often considered beyond defining the set of tracers with conservative behaviour by performing statistical analysis (e.g. Collins and Walling, 2002; Collins et al., 1997; Smith et al., 2018; Walden et al., 1997; Walling, 2005; Wilkinson et al., 2013).

Few studies have investigated the conservative behaviour of soil properties (Koiter et al., 2018; Legout et al., 2013; Motha et al., 2002; Poulenard et al., 2012; Uber et al., 2019). In Chapter 8 an investigation was conducted into eventual in-channel changes

occurring to the most common soil properties used as tracers in sediment fingerprinting studies. The novelty relies (I) in the characteristics of the study area (i.e. Es Fangar), a Mediterranean catchment with an intermittent flow regime with marked dry and wet seasons and (II) the duration of the experiment exposing the sediment over large time periods (i.e. one year) with different hydro-meteorological conditions. In the experiment, soil samples were exposed to natural variables (e.g. temperature, pH, moisture), covering the intra-annual hydro-meteorological variability in Mediterranean environments. Therefore, the conditions can be considered optimal when it comes to assessing possible changes over time in Mediterranean catchments or temporary rivers.

Despite its limitations (Chapter 8, section 8.5.2), such a study under this time scale may be useful for evaluating the application of certain tracers in fingerprinting studies, especially in Mediterranean environments where hydro-meteorological conditions exhibit a great contrast throughout the year. However, it is necessary to continue iterating as regards the study of the tracers' conservativeness, considering the possible transformations which occurred in hillslopes and channels, so as to reduce the uncertainties in sediment fingerprinting.

9.3. Sediment fingerprinting and hydro-sedimentary monitoring as tools for catchment management in Mediterranean environments

One of the most relevant aspects of scientific knowledge for society is its applicability. In this regard, applied geomorphology could be defined as the "branch of science within the broader discipline of geomorphology that focuses on geomorphological landforms and processes of societal concern" (Meitzen, 2017). Therefore, it is the usefulness of geomorphological scientific knowledge when it comes to solving socially relevant problems by helping, among others, landscape managers with decision-making on numerous issues of social relevance. The general objective of the present thesis was "*To identify erosion and sediment transport processes (functional connectivity) in two Mediterranean catchments affected by different global change processes at different spatio-temporal scales, by improving current techniques for*

sediment origin determination (i.e., reducing uncertainties, time and cost) for its better implementation in catchment management plans". Therefore, apart from a better hydro-sedimentary dynamic understanding of the study areas and the optimization of the sediment fingerprinting technique, results had to be useful for catchment management.

Integrated catchment management plans need to reach a comprehensive understanding about erosion and sediment transport dynamics to effectively develop integrated management approaches (McCarney-Castle et al., 2017; Owens et al., 2005). Therefore, one needs to assess the sediment cascade between upstream erosive processes, sediment mobilization through hillslopes and within the channel, and downstream sediment yields to mitigate its possible negative effects. Sediment fingerprinting and river hydro-sedimentary monitoring and analysis were useful approaches to monitoring and controlling sources of soil and sediment erosion for a variety of different land uses and environments. Here it is argued that the combination of sediment fingerprinting and river hydro-sedimentary monitoring improves our knowledge about all these processes and, therefore, are essential tools in management plans.

Sediment source fingerprinting has been widely used in recent decades to detect fine sediment sources at catchment scale (Collins et al., 2020; Davis and Fox, 2009; Guzmán et al., 2013). Interesting methodological guides have been published aimed at end-users as a basis for correctly applying the technique (Collins et al., 2017). During the development of this thesis, the use of economic tracers –in terms of time and economic cost– has been emphasized to simplify the application process of sediment fingerprinting technique. As in previous studies (e.g. Barthod et al., 2015; Martínez-Carreras et al., 2010a), colour parameters have been shown to have a comparable efficacy in contrast with more established tracers (i.e. ^{137}Cs and $^{210}Pb_{ex}$), even in wildfire affected landscapes (Chapter 6). In addition, there is the possibility of performing the measurements using a standard office scanner with good results (Pulley and Rowntree, 2016; Chapter 6) obtaining, on this occasion, correlations of $p<0.01$ with the measurements made with a laboratory spectroradiometer. Sediment tracing by using colour parameters allows rapid samplings and pre-treatments,

because of the low mass required to perform the measurements (ca. 1-2 g) and the possibility of using an office scanner to measure the samples. In addition, the probably low in-channel variability of colour tracers detected in comparison with the rest of the tracers evaluated in Chapter 8, highlighted colour parameters as a remarkable tracer for use in catchment management plans. Another interesting point investigated during the development of the thesis was the use of the EMMA approach, which is not based on a mixing model but on a principal component analysis of the data set (PCA). It is argued that a quantitative estimation of the sediment apportion of the different suspended sediment sources in a catchment might not always be needed when implementing sediment management plans, but rather an accurate identification of dominant sources. EMMA offers advantages based on simplified procedures in comparison with the more extended mixing models, what could result in easier implementation.

Finally, the combination of sediment fingerprinting and continuous hydro-sedimentary monitoring was proposed, to assess the factors that control suspended sediment transport as a surrogate of erosion problems in river catchments. Despite being complementary, the integration of these approaches to detect activation patterns for different sediment sources or disconnected catchment compartments is not usual (Evrard et al., 2011; Navratil et al., 2012; Vercruysse and Grabowski, 2019). A detailed study about hydro-sedimentary characteristics of flood events, linked to the spatiotemporal variation of suspended sediment sources can allow the detection of the predominant sediment sources based on the flood hydro-sedimentary dynamics, as well as the (dis)connectivity thresholds that can activate it. The acquisition of this knowledge could be relevant to develop sediment transport models that integrate information on sediment origin (Owens et al., 2005; Perks et al., 2017; Vercruysse et al., 2019), and useful for detecting drastic changes in catchment geomorphological processes as well as predicting Global Change impacts.

In Chapter 7, sediment fingerprinting and hydro-sedimentary monitoring were combined to determine the main factors regulating sediment source contributions, and evaluate the potential of hydro-sedimentary monitoring combined with sediment fingerprinting as a sediment management tool in Mediterranean catchments. The

stability of the Es Fangar catchment in terms of sediment source contributions made it impossible to find correlations between sediment origin and hydro-sedimentary variables. However, in other study areas it has been possible to establish correlation patterns (Vercruysse and Grabowski, 2019). Throughout, it is desirable to continue research into this issue, especially in highly variable environments such as the Mediterranean basin.

9.4. Limitations and future perspectives

Research in geomorphology encompasses a series of difficulties, which can sometimes turn into limitations. In this type of science, the laboratory is the field, so there are numerous factors that can interact, varying the initial planning of the research proposal. The methodological development of any experiment in catchment geomorphology involves considerable effort in an environment that cannot be controlled.

The main limitations of the thesis are listed below, as well as some proposals for future work:

Chapter 4: One of the most evident limitations was the lack of data for the first post-fire year in the Sa Murtera sub-catchment caused by technical problems with the turbidity probe into the gauging station. This problem did not make it possible to monitor the hydro-sedimentary processes in a part of the Sa Font de la Vila headwaters where the hillslope-channel coupling is higher and when the landscape was more vulnerable to erosion. In addition, a multivariate correlation analysis, a principal component analysis to group variables and the application of a quantitative hysteresis index (e.g. Zuecco et al., 2016) could have been carried out to achieve a better understanding of the hydro-sedimentary response of Sa Font de la Vila. Opportunely, the continuous water and sediment monitoring has continued over time. This will allow an exhaustive analysis of the evolution of a Mediterranean catchment after a fire for more than 7 years. These data, in conjunction with sediment origin analysis (i.e. sediment fingerprinting), could provide valuable information during the

medium and long-term for assessing geomorphological processes in fire-affected catchments.

Chapter 5: The limitations in this chapter are mainly due to the lack of a larger set of tracers, the lack of artificial samples to check the reliability of the tracers when predicting source proportions in sediment samples, and not applying a complementary mixing model to contrast the results and the reduced number of samples from unburned sources compared to burned sources. However, all these limitations have been solved in later works as reflected in Chapter 6.

Chapter 6: The main limitations were the absence of an annual source resampling, to check tracer evolution and the use of ash from another catchment for an experiment on its influence on the colour tracers. However, these limitations were solved in part by using soil samples collected in a headwater micro-catchment in 2016 and by using the above-mentioned ash samples collected in a catchment with similar characteristics. Future work can involve the use of novel tracers (e.g. compound specific stable isotopes, biomarkers) in other sediment fingerprinting research, the combination of hydro-sedimentary data with sediment origin to identify the activation patterns for different sediment sources, the use of a different source categorization (e.g. land uses) or even by performing a tracer conservativeness experiment as in Chapter 8.

Chapter 7: It was not possible to establish patterns between flood event hydro-sedimentary characteristics and sediment origin. Here a larger set of tracers might have helped to discriminate more robustly between source types. In addition, a resampling of the sources could have been proposed or a larger number of samples could have been included for each type of land use. Future work can be focused on solving the previously explained limitations by carrying out a source resampling or by including novel tracers in the sediment origin analysis. In addition, the continuous monitoring of water and sediment fluxes in the gauge station installed in Es Fangar, will make it possible to repeat the study and, perhaps, observe the activation of the different sediment sources in Es Fangar and link it with flood characteristics.

Chapter 8: The limitations were associated with the difficulty of conducting the experiment in natural conditions, as well as the large amount of time and resources that is required. The main limitations were the inability to integrate the physical effects on sediment particles derived from the transport in suspension (e.g. abrasion, aggregation), the possible influence of nylon bags and the steel bars on some soil properties, the absence of samples sieved to different particle sizes or the lack of different replicas for each sample. In addition, in-channel transformations only represent a part of the potential property changes during the erosion and sediment delivery processes. Therefore, in the evaluation of the conservative behaviour of a tracer, the processes generated on hillslopes should also be considered (Koiter et al., 2018; Motha et al., 2002). Here, for future works on tracer conservativeness we will work with 15 artificial source mixtures with different known proportions generated and submerged during the experiment. The possibility of performing an analysis of the proportions of the artificial mixtures by using "sources" such as the original soil material exposed to different in-channel intervals with different hydrological conditions, will verify the reliability of the variability/stability results for all the tracers analysed.

9.5. Conclusions

The hydro-sedimentary dynamics and suspended sediment origin has been investigated in two Mediterranean catchments affected by different Global Change processes. Despite the limitations explained in section 9.4, the combination of sediment fingerprinting with continuous hydro-sedimentary monitoring made it possible to assess its hydro-sedimentary dynamics during the study period. In Sa Font de la Vila, results showed a gradual decrease from burned source contributions over time, while in Es Fangar the contributions from crops sources dominated throughout the study period without substantial changes. Sediment yields were 6.3 t km^{-2} yr^{-1} and 4.5 t km^{-2} yr^{-1} for Sa Font de la Vila and Es Fangar respectively, being low in comparison with other Mediterranean catchments. This was mainly attributed to catchment lithology, land uses (in Es Fangar), vegetation recovery (in Sa Font de la Vila) and the presence of agricultural terraces and dry stone walls.

The use of soil colour parameters as tracers has been successfully proven in the two catchments, confirming its suitability for use in sediment fingerprinting as a rapid and economic tracer, even in fire-affected catchments. In addition, the strong correlations between the measures made with a laboratory spectroradiometer and a standard office scanner make colour parameters even easier to use in research and management plans. Moreover, the long duration tracer conservativeness experiment which was carried out, despite its limitations, confirmed that in-channel changes suffered by all the analysed tracers were generally lower than their own spatial variability within the catchment. Additionally, colour parameters were the most stable tracers. These statements contribute to the improvement of the sediment fingerprinting technique, so it can be said that **hypothesis 1**: *"optimization of the sediment fingerprinting technique through research on the conservative behaviour of soil parameters and the use of low-cost and fast-to-measure tracers allowing evaluation of some of the assumptions underlying the technique, improvement of its applicability and the reduction of uncertainties"* is **confirmed**.

It was not possible to identify the activation patterns of different sediment sources by using a combination of hydro-sedimentary monitoring and sediment fingerprinting. This was caused mainly due to the Es Fangar catchment stability in terms of suspended sediment origin (mainly from crop sources). Like the low sediment yields recorded, the sediment source stability is attributed to lithological characteristics, land uses and the presence of agricultural terraces in the study area. However, events of higher magnitude could exceed the sedimentary (dis)connectivity thresholds of the rest of the sources considered, and activate them. Therefore, and despite the fact that in other similar studies it has been possible to establish links between the hydro-sedimentary behaviour and the origin of the sediment, in this case **hypothesis 2**: "*hydro-sedimentary monitoring combined with sediment fingerprinting makes possible a better identification of the activation patterns of the different sediment sources within a catchment, resulting in a useful tool for catchment management*" is **partially refuted**. The links between flood events characteristics and sediment origin could not be established. However, it has been proven that hydro-sedimentary monitoring and

sediment fingerprinting are useful tools for integrated catchment management plans in Mediterranean environments.

9.6. References

Barthod, L.R.M., Liu, K., Lobb, D.A., Owens, P.N., Martínez-Carreras, N., Koiter, A.J., Petticrew, E.L., McCullough, G.K., Liu, C., Gaspar, L., 2015. Selecting Color-based Tracers and Classifying Sediment Sources in the Assessment of Sediment Dynamics Using Sediment Source Fingerprinting. J. Environ. Qual. 44, 1605–1616. https://doi.org/10.2134/jeq2015.01.0043

Bodí, M.B., Martin, D.A., Balfour, V.N., Santín, C., Doerr, S.H., Pereira, P., Cerdà, A., Mataix-Solera, J., 2014. Wildland fire ash: Production, composition and eco-hydro-geomorphic effects. Earth-Science Rev. 130, 103–127. https://doi.org/10.1016/j.earscirev.2013.12.007

Brosinsky, A., Foerster, S., Segl, K., Kaufmann, H., 2014. Spectral fingerprinting: sediment source discrimination and contribution modelling of artificial mixtures based on VNIR-SWIR spectral properties. J. Soils Sediments 14, 1949–1964. https://doi.org/10.1007/s11368-014-0925-1

Burt, T.P., Allison, R.J., 2009. Sediment Cascades: An Integrated Approach, Sediment Cascades: An Integrated Approach. https://doi.org/10.1002/9780470682876

Calsamiglia, A., Fortesa, J., García-Comendador, J., Lucas-Borja, M.E., Calvo-Cases, A., Estrany, J., 2018. Spatial patterns of sediment connectivity in terraced lands: Anthropogenic controls of catchment sensitivity. L. Degrad. Dev. 29, 1198–1210. https://doi.org/10.1002/ldr.2840

Calvo-Cases, A., Boix-Fayos, C., Imeson, A.. C., 2003. Runoff generation, sediment movement and soil water behaviour on calcareous (limestone) slopes of some Mediterranean environments in southeast Spain. Geomorphology 50, 269–291. https://doi.org/10.1016/S0169-555X(02)00218-0

Candela, A., Aronica, G., Santoro, M., 2005. Effects of Forest Fires on Flood Frequency Curves in a Mediterranean Catchment/Effets d'incendies de forêt sur les courbes de fréquence de crue dans un bassin versant Méditerranéen. Hydrol. Sci. J. 50, 206. https://doi.org/10.1623/hysj.50.2.193.61795

Christophersen, N., Hooper, R.P., 1992. Multivariate analysis of stream water chemical data: The use of principal components analysis for the end-member mixing problem. Water Resour. Res. 28, 99–107. https://doi.org/10.1029/91WR02518

Collins, A.. L., Walling, D.. E., 2002. Selecting fingerprint properties for discriminating potential suspended sediment sources in river basins. J. Hydrol. 261, 218–244. https://doi.org/10.1016/S0022-1694(02)00011-2

Collins, A.L., Blackwell, M., Boeckx, P., Chivers, C.A., Emelko, M., Evrard, O., Foster, I., Gellis, A., Gholami, H., Granger, S., Harris, P., Horowitz, A.J., Laceby, J.P., Martinez-Carreras, N., Minella, J., Mol, L., Nosrati, K., Pulley, S., Silins, U., da Silva, Y.J., Stone, M., Tiecher, T., Upadhayay, H.R., Zhang, Y., 2020. Sediment source fingerprinting: benchmarking recent outputs, remaining challenges and emerging themes. J. Soils Sediments 20, 1–34. https://doi.org/10.1007/s11368-020-02755-4

Collins, A.L.L., Pulley, S., Foster, I.D.L.D.L., Gellis, A., Porto, P., Horowitz, A.J.J., 2017. Sediment source fingerprinting as an aid to catchment management: A review of the current state of knowledge and a methodological decision-tree for end-users. J. Environ. Manage. 194,

86–108. https://doi.org/10.1016/j.jenvman.2016.09.075

Davis, C.M., Fox, J.F., 2009. Sediment Fingerprinting: Review of the Method and Future Improvements for Allocating Nonpoint Source Pollution. J. Environ. Eng. 135, 490–504. https://doi.org/10.1061/(ASCE)0733-9372(2009)135:7(490)

De Girolamo, A.M., Pappagallo, G., Lo Porto, A., 2015. Temporal variability of suspended sediment transport and rating curves in a Mediterranean river basin: The Celone (SE Italy). Catena 128, 135–143. https://doi.org/10.1016/j.catena.2014.09.020

Estrany, J., Garcia, C., Batalla, R.J., 2010. Hydrological response of a small mediterranean agricultural catchment. J. Hydrol. 380, 180–190. https://doi.org/10.1016/j.jhydrol.2009.10.035

Estrany, J., Garcia, C., Batalla, R.J., 2009. Groundwater control on the suspended sediment load in the Na Borges River, Mallorca, Spain. Geomorphology 106, 292–303. https://doi.org/10.1016/j.geomorph.2008.11.008

Estrany, J., López-Tarazón, J.A., Smith, H.G., 2016. Wildfire Effects on Suspended Sediment Delivery Quantified Using Fallout Radionuclide Tracers in a Mediterranean Catchment. L. Degrad. Dev. 27, 1501–1512. https://doi.org/10.1002/ldr.2462

Evrard, O., Navratil, O., Ayrault, S., Ahmadi, M., Némery, J., Legout, C., Lefèvre, I., Poirel, A., Bonté, P., Esteves, M., 2011. Combining suspended sediment monitoring and fingerprinting to determine the spatial origin of fine sediment in a mountainous river catchment. Earth Surf. Process. Landforms 36, 1072–1089. https://doi.org/10.1002/esp.2133

Fortesa, J., Latron, J., García-Comendador, J., Company, J., Estrany, J., 2020a. Runoff and soil moisture as driving factors in suspended sediment transport of a small mid-mountain Mediterranean catchment. Geomorphology 368, 107349. https://doi.org/10.1016/j.geomorph.2020.107349

Fortesa, J., Latron, J., García-Comendador, J., Tomàs-Burguera, M., Company, J., Calsamiglia, A., Estrany, J., 2020b. Multiple temporal scales assessment in the hydrological response of small mediterranean-climate catchments. Water 12, 299. https://doi.org/10.3390/w12010299

Fortesa, J., Ricci, G.F., García-Comendador, J., Gentile, F., Estrany, J., Sauquet, E., Datry, T., De Girolamo, A.M., 2021. Analysing hydrological and sediment transport regime in two Mediterranean intermittent rivers. Catena 196, 104865. https://doi.org/10.1016/j.catena.2020.104865

Fryirs, K., 2013. (Dis)Connectivity in catchment sediment cascades: A fresh look at the sediment delivery problem. Earth Surf. Process. Landforms 38, 30–46. https://doi.org/10.1002/esp.3242

Fryirs, K.A., 2017. River sensitivity: a lost foundation concept in fluvial geomorphology. Earth Surf. Process. Landforms 42, 55–70. https://doi.org/10.1002/esp.3940

Fryirs, K.A., Brierley, G.J., Preston, N.J., Kasai, M., 2007. Buffers, barriers and blankets: The (dis)connectivity of catchment-scale sediment cascades. Catena 70, 49–67. https://doi.org/10.1016/j.catena.2006.07.007

García-Ruiz, J.M., Lana-Renault, N., 2011. Hydrological and erosive consequences of farmland abandonment in Europe, with special reference to the Mediterranean region - A review. Agric. Ecosyst. Environ. https://doi.org/10.1016/j.agee.2011.01.003

Gaspar, L., Blake, W.H., Smith, H.G., Lizaga, I., Navas, A., 2019. Testing the sensitivity of a multivariate mixing model using geochemical fingerprints with artificial mixtures. Geoderma 337, 498–510. https://doi.org/10.1016/j.geoderma.2018.10.005

Guzmán, G., Quinton, J.N., Nearing, M.A., Mabit, L., Gómez, J.A., 2013. Sediment tracers in water erosion studies: Current approaches and challenges. J. Soils Sediments 13, 816–833. https://doi.org/10.1007/s11368-013-0659-5

Haddadchi, A., Olley, J., Laceby, P., 2014. Accuracy of mixing models in predicting sediment source contributions. Sci. Total Environ. 497–498, 139–152. https://doi.org/10.1016/j.scitotenv.2014.07.105

Huang, Y., Wu, S., Kaplan, J.O., 2014. Sensitivity of global wildfire occurrences to various factors in thecontext of global change. Atmos. Environ. 121, 86–92. https://doi.org/10.1016/j.atmosenv.2015.06.002

Koiter, A.J., Owens, P.N., Petticrew, E.L., Lobb, D.A., 2018. Assessment of particle size and organic matter correction factors in sediment source fingerprinting investigations: An example of two contrasting watersheds in Canada. Geoderma 325, 195–207. https://doi.org/10.1016/j.geoderma.2018.02.044

Koiter, A.J.J., Owens, P.N.N., Petticrew, E.L.L., Lobb, D.A.A., 2013. The behavioural characteristics of sediment properties and their implications for sediment fingerprinting as an approach for identifying sediment sources in river basins. Earth-Science Rev. 125, 24–42. https://doi.org/10.1016/j.earscirev.2013.05.009

Legout, C., Poulenard, J., Nemery, J., Navratil, O., Grangeon, T., Evrard, O., Esteves, M., 2013. Quantifying suspended sediment sources during runoff events in headwater catchments using spectrocolorimetry. J. Soils Sediments 13, 1478–1492. https://doi.org/10.1007/s11368-013-0728-9

Lentile, L.B., Holden, Z.A., Smith, A.M.S., Falkowski, M.J., Hudak, A.T., Morgan, P., Lewis, S.A., Gessler, P.E., Benson, N.C., 2006. Remote sensing techniques to assess active fire characteristics and post-fire effects. Int. J. Wildl. Fire 15, 319–345. https://doi.org/10.1071/WF05097

Li, Z., Xu, X., Zhu, J., Xu, C., Wang, K., 2019. Effects of lithology and geomorphology on sediment yield in karst mountainous catchments. Geomorphology 343, 119–128. https://doi.org/10.1016/j.geomorph.2019.07.001

Lizaga, I., Latorre, B., Gaspar, L., Navas, A., 2020. Consensus ranking as a method to identify non-conservative and dissenting tracers in fingerprinting studies. Sci. Total Environ. 720, 137537. https://doi.org/10.1016/j.scitotenv.2020.137537

López-Tarazón, J.A., Estrany, J., 2017. Exploring suspended sediment delivery dynamics of two Mediterranean nested catchments. Hydrol. Process. 31, 698–715. https://doi.org/10.1002/hyp.11069

Martínez-Carreras, N., Krein, A., Gallart, F., Iffly, J.F., Pfister, L., Hoffmann, L., Owens, P.N., 2010a. Assessment of different colour parameters for discriminating potential suspended sediment sources and provenance: A multi-scale study in Luxembourg. Geomorphology 118, 118–129. https://doi.org/10.1016/j.geomorph.2009.12.013

Martínez-Carreras, N., Udelhoven, T., Krein, A., Gallart, F., Iffly, J.F., Ziebel, J., Hoffmann, L., Pfister, L., Walling, D.E., 2010b. The use of sediment colour measured by diffuse reflectance spectrometry to determine sediment sources: Application to the Attert River

catchment (Luxembourg). J. Hydrol. 382, 49–63. https://doi.org/10.1016/j.jhydrol.2009.12.017

Meitzen, K.M., 2017. Applied Geomorphology, in: International Encyclopedia of Geography: People, the Earth, Environment and Technology. John Wiley & Sons, Ltd, Oxford, UK, pp. 1–7. https://doi.org/10.1002/9781118786352.wbieg0144

Moody, J.A., Shakesby, R.A., Robichaud, P.R., Cannon, S.H., Martin, D. a., 2013. Current research issues related to post-wildfire runoff and erosion processes. Earth-Science Rev. 122, 10–37. https://doi.org/10.1016/j.earscirev.2013.03.004

Motha, J.A., Wallbrink, P.J., Hairsine, P.B., Grayson, R.B., 2002. Tracer properties of eroded sediment and source material. Hydrol. Process. 16, 1983–2000. https://doi.org/10.1002/hyp.397

Mukundan, R., Radcliffe, D.E., Ritchie, J.C., Risse, L.M., McKinley, R.A., 2010. Sediment Fingerprinting to Determine the Source of Suspended Sediment in a Southern Piedmont Stream. J. Environ. Qual. 39, 1328–1337. https://doi.org/10.2134/jeq2009.0405

Navratil, O., Evrard, O., Esteves, M., Legout, C., Ayrault, S., Némery, J., Mate-Marin, A., Ahmadi, M., Lefèvre, I., Poirel, A., Bonté, P., 2012. Temporal variability of suspended sediment sources in an alpine catchment combining river/rainfall monitoring and sediment fingerprinting. Earth Surf. Process. Landforms 37, 828–846. https://doi.org/10.1002/esp.3201

Oeurng, C., Sauvage, S., Sánchez-Pérez, J.M., 2010. Dynamics of suspended sediment transport and yield in a large agricultural catchment, southwest France. Earth Surf. Process. Landforms 35, 1289–1301. https://doi.org/10.1002/esp.1971

Owens, P.N., Blake, W.H., Giles, T.R., Williams, N.D., 2012. Determining the effects of wildfire on sediment sources using ^{137}Cs and unsupported ^{210}Pb: The role of landscape disturbances and driving forces. J. Soils Sediments 12, 982–994. https://doi.org/10.1007/s11368-012-0497-x

Poeppl, R.E., Fryirs, K.A., Tunnicliffe, J., Brierley, G.J., 2020. Managing sediment (dis)connectivity in fluvial systems. Sci. Total Environ. 736, 139627. https://doi.org/10.1016/j.scitotenv.2020.139627

Poulenard, J., Legout, C., Némery, J., Bramorski, J., Navratil, O., Douchin, A., Fanget, B., Perrette, Y., Evrard, O., Esteves, M., 2012. Tracing sediment sources during floods using Diffuse Reflectance Infrared Fourier Transform Spectrometry (DRIFTS): A case study in a highly erosive mountainous catchment (Southern French Alps). J. Hydrol. 414, 452–462. https://doi.org/10.1016/j.jhydrol.2011.11.022

Prosser, I.P., Williams, L., 1998. The effect of wildfire on runoff and erosion in native Eucalyptus forest. Hydrol. Process. 12, 251–265. https://doi.org/10.1002/(SICI)1099-1085(199802)12:2<251::AID-HYP574>3.0.CO;2-4

Pulley, S., Rowntree, K., 2016. The use of an ordinary colour scanner to fingerprint sediment sources in the South African Karoo. J. Environ. Manage. 165, 253–262. https://doi.org/10.1016/j.jenvman.2015.09.037

Robinne, F.N., Hallema, D.W., Bladon, K.D., Buttle, J.M., 2020. Wildfire impacts on hydrologic ecosystem services in North American high-latitude forests: A scoping review. J. Hydrol. https://doi.org/10.1016/j.jhydrol.2019.124360

Rose, L.A., Karwan, D.L., Aufdenkampe, A.K., 2018. Sediment Fingerprinting Suggests

Differential Suspended Particulate Matter Formation and Transport Processes Across Hydrologic Regimes. J. Geophys. Res. Biogeosciences 123, 1213–1229. https://doi.org/10.1002/2017JG004210

Rovira, A., Batalla, R.J., 2006. Temporal distribution of suspended sediment transport in a Mediterranean basin: The Lower Tordera (NE SPAIN). Geomorphology 79, 58–71. https://doi.org/10.1016/j.geomorph.2005.09.016

Scott, D., Versfeld, D.B., Lesch, W., 1998. Erosion and sediment yield in relation to afforestation and fire in the mountains of the western cape province, south africa. South African Geogr. J. 80, 52–59. https://doi.org/10.1080/03736245.1998.9713644

Seeger, M., Errea, M.P., Beguería, S., Arnáez, J., Martí, C., García-Ruiz, J.M., 2004. Catchment soil moisture and rainfall characteristics as determinant factors for discharge/suspended sediment hysteretic loops in a small headwater catchment in the Spanish pyrenees. J. Hydrol. 288, 299–311. https://doi.org/10.1016/j.jhydrol.2003.10.012

Shakesby, R.A. a., 2011. Post-wildfire soil erosion in the Mediterranean: Review and future research directions. Earth-Science Rev. 105, 71–100. https://doi.org/10.1016/j.earscirev.2011.01.001

Shakesby, R.A. a., Doerr, S.H.H., 2006. Wildfire as a hydrological and geomorphological agent. Earth-Science Rev. 74, 269–307. https://doi.org/10.1016/j.earscirev.2005.10.006

Smith, H.G., Dragovich, D., 2009. Interpreting sediment delivery processes using suspended sediment-discharge hysteresis patterns from nested upland catchments, south-eastern Australia. Hydrol. Process. 23, 2415–2426. https://doi.org/10.1002/hyp.7357

Smith, H.G., Karam, D.S., Lennard, A.T., 2018. Evaluating tracer selection for catchment sediment fingerprinting. J. Soils Sediments 18, 3005–3019. https://doi.org/10.1007/s11368-018-1990-7

Smith, H.G., Sheridan, G.J., Lane, P.N.J.J., Noske, P.J., Heijnis, H., 2011. Changes to sediment sources following wildfire in a forested upland catchment, southeastern Australia. Hydrol. Process. 25, 2878–2889. https://doi.org/10.1002/hyp.8050

Stock, B.C., Jackson, A.L., Ward, E.J., Parnell, A.C., Phillips, D.L., Semmens, B.X., 2018. Analyzing mixing systems using a new generation of Bayesian tracer mixing models. PeerJ 6, e5096. https://doi.org/10.7717/peerj.5096

Uber, M., Legout, C., Nord, G., Crouzet, C., Demory, F., Poulenard, J., 2019. Comparing alternative tracing measurements and mixing models to fingerprint suspended sediment sources in a mesoscale Mediterranean catchment. J. Soils Sediments 19, 3255–3273. https://doi.org/10.1007/s11368-019-02270-1

Vanmaercke, M., Poesen, J., Verstraeten, G., de Vente, J., Ocakoglu, F., 2011. Sediment yield in Europe: Spatial patterns and scale dependency. Geomorphology 130, 142–161. https://doi.org/10.1016/j.geomorph.2011.03.010

Vercruysse, K., Grabowski, R.C., 2019. Temporal variation in suspended sediment transport: linking sediment sources and hydro-meteorological drivers. Earth Surf. Process. Landforms 44, 2587–2599. https://doi.org/10.1002/esp.4682

Vercruysse, K., Grabowski, R.C., Rickson, R.J., 2017. Suspended sediment transport dynamics in rivers: Multi-scale drivers of temporal variation. Earth-Science Rev. 166, 38–52. https://doi.org/10.1016/j.earscirev.2016.12.016

Vieira, D.C.S., Fernández, C., Vega, J. a., Keizer, J.J., 2015. Does soil burn severity affect the post-fire runoff and interrill erosion response? A review based on meta-analysis of field rainfall simulation data. J. Hydrol. 523, 452–464. https://doi.org/10.1016/j.jhydrol.2015.01.071

Walden, J., Slattery, M.C., Burt, T.P., 1997. Use of mineral magnetic measurements to fingerprint suspended sediment sources: Approaches and techniques for data analysis. J. Hydrol. 202, 353–372. https://doi.org/10.1016/S0022-1694(97)00078-4

Walling, D.E., 1983. The sediment delivery problem. J. Hydrol. 65, 209–237. https://doi.org/10.1016/0022-1694(83)90217-2

Walling, D.E.E., 2005. Tracing suspended sediment sources in catchments and river systems 344, 159–184.

Wilkinson, S.N., Hancock, G.J., Bartley, R., Hawdon, A.A., Keen, R.J., 2013. Using sediment tracing to assess processes and spatial patterns of erosion in grazed rangelands, Burdekin River basin, Australia. Agric. Ecosyst. Environ. 180, 90–102. https://doi.org/10.1016/j.agee.2012.02.002

Wilkinson, S.N.N., Wallbrink, P.J.J., Hancock, G.J.J., Blake, W.H.H., Shakesby, R.A.A., Doerr, S.H.H., 2009. Fallout radionuclide tracers identify a switch in sediment sources and transport-limited sediment yield following wildfire in a eucalypt forest. Geomorphology 110, 140–151. https://doi.org/10.1016/J.GEOMORPH.2009.04.001

Williams, G.P.G.., 1989. Sediment concentration versus water discharge during single hydrologic events in rivers. J. Hydrol. 111, 89–106. https://doi.org/10.1016/0022-1694(89)90254-0

Wohl, E., 2018. Introduction to the themed issue: Wildfire and Geomorphic Systems. Earth Surf. Process. Landforms 43, 1542–1546. https://doi.org/10.1002/esp.4325

Yair, A., 1983. Hillslope hydrology water harvesting and areal distribution of some ancient agricultural systems in the northern Negev desert. J. Arid Environ. 6, 283–301. https://doi.org/10.1016/s0140-1963(18)31514-3

Zdruli, P., 2014. Land resources of the Mediterranean: Status, pressures, trends and impacts on future regional development. L. Degrad. Dev. 25, 373–384. https://doi.org/10.1002/ldr.2150

Zuecco, G., Penna, D., Borga, M., van Meerveld, H.J., 2016. A versatile index to characterize hysteresis between hydrological variables at the runoff event timescale. Hydrol. Process. 30, 1449–1466. https://doi.org/10.1002/hyp.10681